DISSIPATIVE NANOPATTERNING OF SURFACES

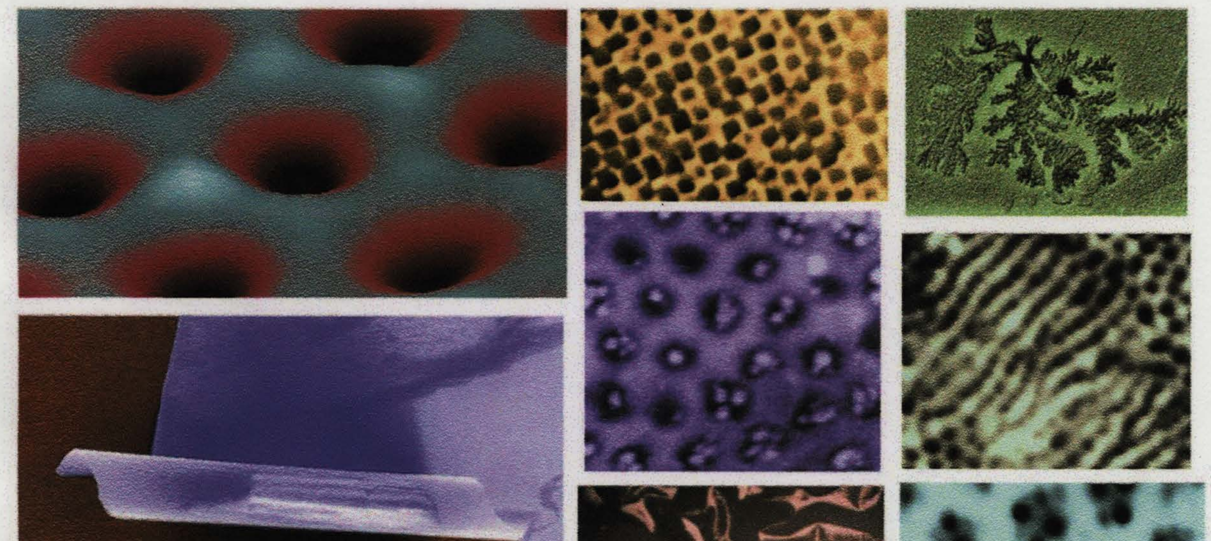

ENGINEERING NANOSTRUCTURES USING DISSIPATIVE ELECTROCHEMICAL PROCESSES.

By

SHERDEEP SINGH, M.S.

A Thesis
Submitted to the School of Graduate Studies
in Partial Fulfillment of the Requirements
for the Degree
Doctor of Philosophy

McMaster University

DOCTOR OF PHILOSOPHY (2008) McMaster University
(CHEMISTRY) Hamilton, Ontario, Canada

TITLE: Engineering Nanostructures Using Dissipative Electrochemical Processes

AUTHOR: Sherdeep Singh, M.S.

SUPERVISOR: Dr. Peter Kruse

NUMBER OF PAGES: xix, 224

Committee in charge:

Dr. Peter Kruse, Department of Chemistry, McMaster University

Dr. Alex Bain, Department of Chemistry, McMaster University

Dr. Gillian Goward, Department of Chemistry, McMaster University

To my Parents, Friends and to Late Ustad Nusrat Fateh Ali Khan.

Abstract

The realm of the nano-world begins when things start getting smaller in size than one thousandth of the thickness of the human hair. Surface patterning at the nanoscale has started to find applications in information storage, self-cleaning of surfaces due to the "lotus effect", biocompatible materials based on surface roughness and many more. Several methods such as particle-beam writing, optical lithography, stamping and various kinds of self-assembly are widely used to serve the purpose of patterning smaller surface structures. However, globally much research is going into developing more efficient, reproducible and simple methods of patterning surfaces and in better controlling the order of these nanostructures. Researchers have always looked upon Nature to get inspiration and to mimic its model in engineering novel architectures. One of the methods used by this greatest artist (Nature) to make beautiful patterns around is through reaction-diffusion based non-linear processes. Non-linear systems driven away from equilibrium sustain pattern only during the continuous dissipation of a regular flow of energy and are different from equilibrium processes that are converging towards a minimum in free energy (a. k. a. self-assembly). Dissipative pattern formation from micrometer to kilometers scale has been known but ordered patterns at nanoscale have never been achieved.

In the process of thoroughly characterizing suitable substrates for nanoelectronics applications, we came across a remarkable process leading to the formation of highly ordered arrays of dimples on tantalum. The pattern formation happens in a narrow

electrochemical windows which are functions of many parameters such as concentration, external applied voltage, temperature etc. After investigating the formation of dimples by performing spatio-temporal studies, we found that the underlying principles behind this unique way of engineering nano-structures have their roots in nonlinear interaction/reaction electro-hydrodynamics. We then have demonstrated the generality of this process by extending it to titanium, tungsten and zirconium surfaces. The pattern similar to Rayleigh-Bernard convection cells originates inside the electrochemical solution due to coupling among electrolyte ions during their migration across the electrochemical double layer (Helmholtz layer) and simultaneously imprints on the surface due to dissolution of metal oxide via etching. Based on these results we further postulate that, given appropriate electropolishing chemistry; these patterns can be formed on virtually any metal or semiconductor surface. The application of these nanostructures as nanobeakers for placing metal nanoparticles is also elucidated.

Highly porous materials such as mesoporous oxides are of technological interest for catalytic, sensing, optical and filtration applications: the mesoporous materials (with pores of size 2–50 nm) in the form of thin films can be used as membranes due large surface area. In the second part of this thesis, a new technique of making detachable ultrathin membranes of transition metal oxides is presented. The underlying concepts behind the detachment of membranes from the underlying substrate surface are discussed. The control on the size of the pores by modulating the voltage and concentration is also elucidated. The method is generalized by showing the similar detachment behavior on other metal oxide membranes.

Thus, the results of this work introduces new techniques of engineering nanostructures on surfaces based on reaction-diffusion adaptive systems and contribute to the better understanding of electrochemical self-organization phenomena due to migration coupling induced electro-hydrodynamics.

Acknowledgements

I wish to express my genuine gratitude to a number of people whose support and moral encouragement lead to this important scientific piece of work. I could only mention a few by name, but the support of others is not less important. I pay heartfelt tribute to all who have shared part of their scientific lives with me.

I am deeply grateful to my thesis advisor; Dr. Peter Kruse, for his continuous encouragement, for providing me with the necessary means to do the present research and for his strong belief in my own individual work style. He proposed many new ideas full of excitement and challenges.

I am very much obliged to Dr. Alex Bain and Dr. Gillian Goward for being my committee members and for initiating stimulating discussions during my committee meetings.

Thanks go also to my two undergraduate students, Warren Barden and Miguel Festin, for their contribution to my work.

Moreover, I particularly wish to thank Dr. Ferdinand Gongaza and Mark Greiner for their continuous motivation and inspiration during tiring times both in and outside the lab and for making every moment cheerful. I will never forget the impact of the informal refreshing chats especially in front of JHE Building with Ferdinand, Mark, Kevin, Subir, Warren, Miguel, and Renita during our long coffee breaks.

I am also deeply indebted to those whose research I used as referential ladder to reach the scientific goals of my thesis. I express my special thanks to Electron

Spectroscopy facility McMaster University and Surface Science Western for help in collecting extremely valuable data.

Financial support from the McMaster University is gratefully acknowledged. Financial support by the 'Natural Science and Engineering Research Council of Canada' and an 'Ontario Premier's Research Excellence Award' is gratefully acknowledged.

Nomenclature

AFM	Atomic Force Microscope
BZ	Belousov Zhabotinsky
CVD	Chemical Vapor Deposition
DBL	Diffusive Boundary Layer
EDL	Electrochemical Double layer
EDS	Energy Dispersive X-ray Spectroscopy
LOFO	Lift-Off-Float-On
LB	Langmuir Blodgett
NRA	Nuclear Reaction Analysis
PAA	Porous Anodic Alumina
RB	Rayleigh Benard
SEM	Scanning electron microscope
TEM	Transmission electron microscope
ToF-SIMS	Time-of-flight secondary ion mass spectrometry
XPS	X-ray photoelectron spectroscopy
XRD	X-ray diffraction

Contents

1 Introduction

2 Formation of Highly Ordered Arrays of Dimples on Tantalum at the Nanoscale

3 **Nanopatterning of transition metal surfaces via electrochemical dimple array formation.**

4 **Dissipative Nanopatterning on Electropolished Surfaces as an Alternative to Self-assembly**

5 **Robust Inorganic Membranes from Detachable Ultrathin Tantalum Oxide Film**

9 Appendix B

10 Appendix C

List of Figures

List of Tables

Chapter-1

Introduction

One of the senses known as "Sight" or "Vision" of mankind and of almost every living organism gets very pleased on perceiving beautiful patterns around. The natural patterns which exist in everyday life are either highly periodic having varying degrees of symmetry or are totally random in space with their size ranging between infinite and zero. Also the rate of change in their shape and size ranges from the speed of light (patterns of light) to ultra slow (patterns in Cosmological objects).

Humans have always been tempted to create some new patterns with their imagination or by getting some inspiration from nature. Although enormous advances have recently been made in forming complex spontaneous spatio-temporal patterns in the laboratory, nature is still far superior and obviously the greatest artist. Stripes, triangles, squares and many other polygons fall under the category of symmetric shapes whereas spirals and dendrites are among the asymmetric shapes. From this variety of different patterns, the hexagonal shape is a simple recurring symmetric pattern nature constructs at different length scales such as from the astrophysical scale in the distributions of galaxies, of stars within galaxies to the millimeter scale of the honeycomb and further to the micrometer scale of the ommatidium found in the compound eyes of certain insects.[1,2]

The hexagonal packing on the surface lowers the surface energy and is known to be the most economical way of organizing structures in two dimensions.

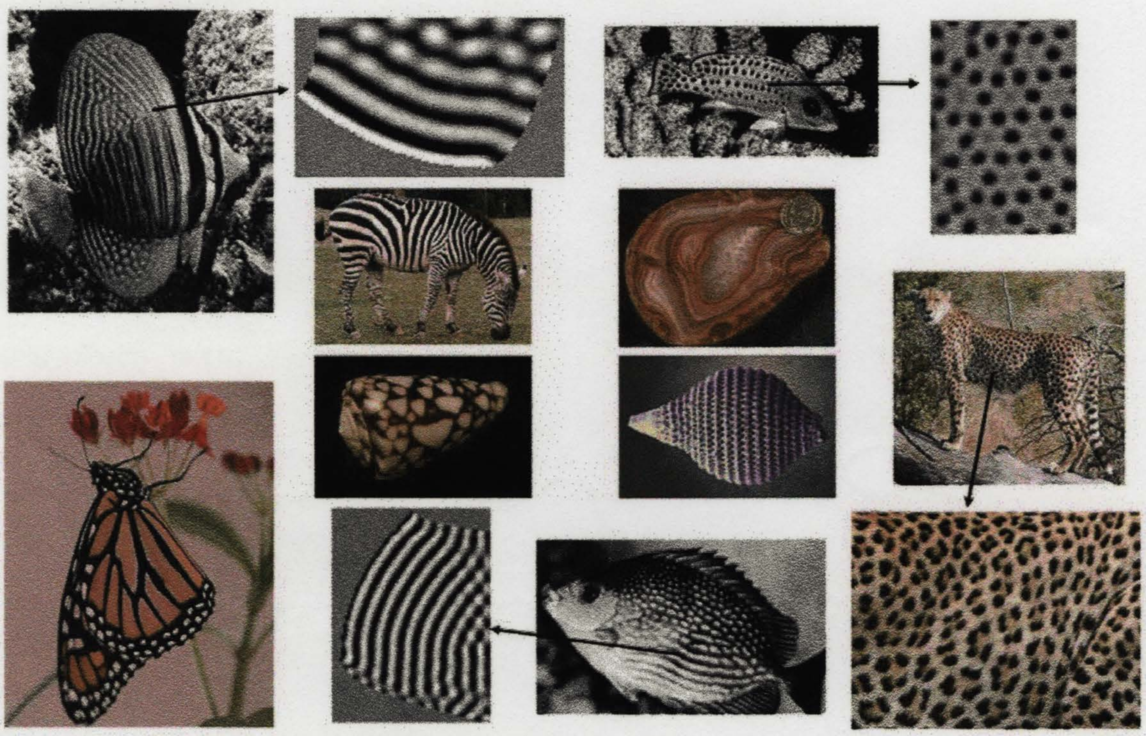

Figure 1.1. Pattern formation in Nature.[3,4,5,6]

With the help of modern scientific instruments ordered patterns can be drawn on surfaces by "bottom-up" or "top-down" approaches. These well established techniques are approaching the point where fundamental issues, fabrication speed (serial in nature) and high production costs are expected to limit their use in microelectronics and for many other applications. Self-organized patterns are also observed in autonomous systems in which the individual components form ordered structures while attaining the equilibrium state without any human intervention. But the most interesting process is when highly ordered patterns evolve from completely disordered states without using any sculpting tools. These kinds of self organizing patterns are mostly found in highly complex systems that are sustained far from equilibrium. Some of the self-organizing systems are non-teleological, i.e. they do not have a specific function except their own existence and therefore self-maintenance is the only important motive for them. The underlying mechanisms behind their formation are so complicated that the whole process seems to be dictated by some magical powers. Even after seeking a little insight into these processes, it is hard to predict and extend their principles to make similar structures on other closely related systems as the pattern selection and formation becomes highly probable. This is acceptable because there are forces which exist for reasons that are well beyond our understanding.

1.1 Background

1.1.1 Pattern Formation in Biological Systems

In biological systems, pattern formation arises from the presence of various chemicals in embryonic tissue that influence the movement and organization of cells during the development of structural features of an organism by forming a concentration gradient. Alan Turing in his landmark paper in 1952 referred to these chemicals behind the pattern formation as morphogens, and a proposed mathematical model for pattern formation.[7] Turing showed that, in a chemical system that starts off as spatially homogeneous, a diffusing short-range activator and a long-range inhibitor could give rise to stationary-wave like concentration profiles of chemicals. His mathematical models of long-range inhibition and localized activation predicted the emergence of two kinds of spontaneous patterns: spots and stripes. The difference between these two patterns comes from the limit in the rate of production of the activator and inhibitor. Stripes are less common and have the tendency to break into hexagonally arranged spots.

However, even after more than 50 years it has not been easy to create Turing-type structures artificially in lab due to the difficulty involved in creating stringent conditions for the generation of highly ordered patterns. A simple example of using a diffusion limited process for pattern generation is the dye industry. Folding and binding fabric in a systematic way prevents dye from entering the folds and surprisingly generates beautiful patterns. The resulting work does not appear to be handmade, but rather as if created by some natural processes. Complex results can occur from quite simple manipulations.

Researchers have discovered that the principle of life is also closely related to the generation of periodic patterns inside the body. The beating of the heart in humans and many other organisms can give rise to countless rhythmic patterns but life exists only in a very small subset of these patterns (regular heart beats of one per second in humans). The fundamental principles behind these rhythms of life have their origin in electrical waves which are triggered by the development of a potential across cell walls due to the concentration gradient of ions. The electrical waves (nerve impulses) activate muscle contraction and hence trigger the heart to pump blood at regular intervals of time.[8] The leading cause of death due to heart attack happens when the tissues of heart leads to an uncoordinated motion. This behavior is called as cardiac arrhythmia.

1.1.2 Pattern Formation in Chemical Systems

The pioneering work by Russian chemist Boris P. Belousov in the 1950s at the Institute for Theoretical and Experimental Biophysics (Puschino) demonstrated that spatiotemporal colorful patterns can be formed inside a beaker full of appropriate chemicals. His intentions during these attempts were to find an inorganic reaction analog to the Krebs cycle. He observed beautiful patterns of periodically changing colours, they started off from green color, which turns blue, purple, and red, and then cycles back to green and repeat. However, as society always repels new ideas, his results were also rejected from publication in a chemical journal on the grounds that "it is impossible" and they are evidence of non-serious scientific work. The scientific reason given for the rejection was that the whole cyclic process of formation of periodic colors inside the solution disobeys the second law of thermodynamics. Later, he was left with no choice but to publish his results in the institute's 1957 annual assay of radiobiology.[9] Zhabotinsky was the graduate student of Schnoll who was one of the close friends of Belousov and was a Professor of biochemistry at the same Institute. Actually, Belousov left science forever after being offended by the rejection of his paper and handed the recipe of his mystifying reaction to Schnoll. It was Zhabotinsky who revived the interest in these systems in the 1960s and started serious research in his laboratory about this system.[10] Over time, these kinds of chemical reactions gained popularity after finding them in many other chemical systems and are known as "Belousov-Zhabotinsky" (BZ) reactions. They exhibit an astonishing range of chemical behavior.

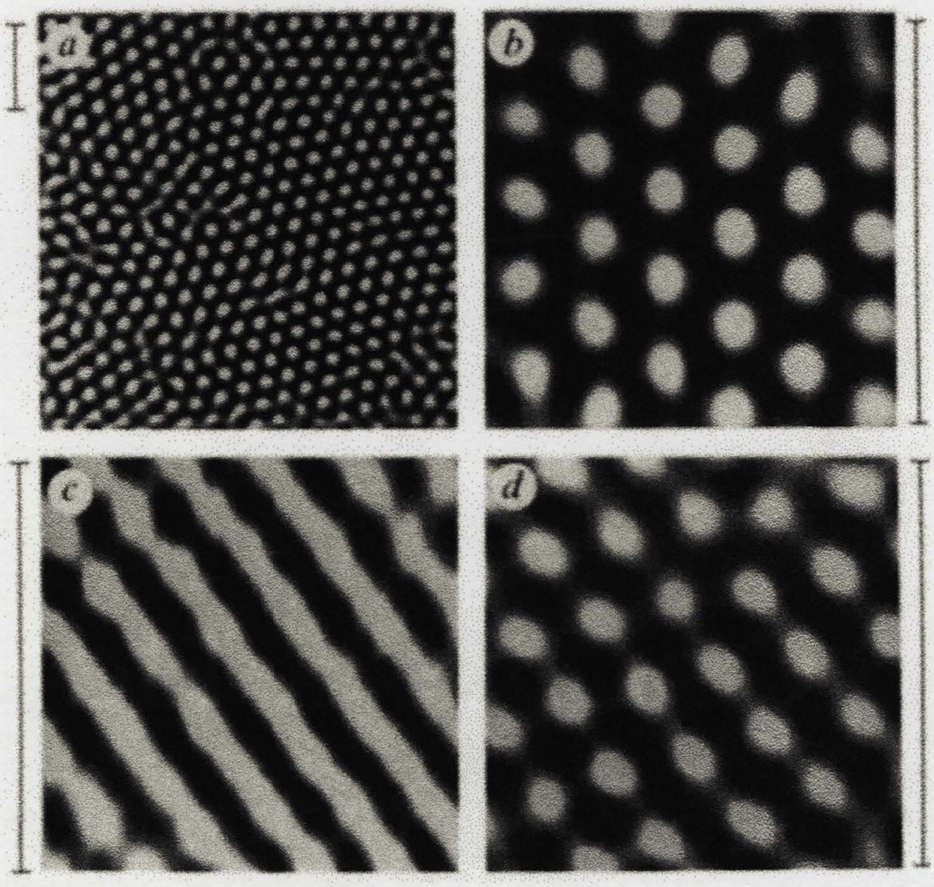

Figure 1.2. Stationary Patterns of (a) and(b) Spots (c) Stripes (d) mixed state showing the breakup of stripes into spots. The results were obtained in a continuously fed laboratory reactor containing $CH_2(COOH)_2$, NaOH, Na_2SO_4, H_2SO_4 and ClO_2^- and maintained at a temperature of 5.6 °C. The scale bar besides each picture represents 1 mm.[23]

A little later, after the recognition of BZ reactions, the research in the field of "chemical pattern formation" entered into a number of physico-chemical disciplines such as catalysis, liquid-phase reactions, combustion chemistry, surface science and electrochemistry. The efforts of De Groot and Glansdorff[11,12] with many others helped to loosen the tight grip of the second law of thermodynamics, by introducing new knowledge of thermodynamics for far-from-equilibrium processes. In the 1970s and 1980s, many scientists working in various disciplines such as computer science and engineering, hydrodynamics, laser physics, bifurcation theory and theoretical physics started to realize the similarity of the nonlinear phenomena in their systems. This gave birth to a new interdisciplinary branch of science called "Nonlinear-Dynamics". The objective of this field was to model the various complex natural phenomena using mathematical tools.

1.1.3 Pattern Formation in Electrochemical Systems

Electrochemical systems were not considered as part of nonlinear dynamics until recent advancements. However, the first reports of oscillations in electrochemical systems by Fechner date back to 1828.[13] The inhomogeneous spatial structures were observed long before they were explained.[14] In 1922, E. Muller discovered the kinetic oscillations in electrocatalytic systems during the oxidation of various small organic compounds and the reduction of certain anions like $S_2O_8^{2-}$.[15] A lot of interest was later developed in the study of the reduction of $S_2O_8^{2-}$ under both stationary and oscillatory conditions owing to its use for technical application such as direct methanol fuel cells. Among others, Frumkin thoroughly studied these reactions and did a lot of work in this application driven research field.[16] In the mid 1980's, the experimental self-organization during electrochemical dissolution was reported.[17] But the patterns were not highly ordered and there was no significant understanding behind this kind of complex pattern formations. A better understanding behind these kinds of patterns came with Koper in 1996.[18] He experimentally showed that the rate of change of the applied potential gives rise to oscillations during the anodic nickel dissolution in aqueous sulfuric acid solutions. All of these achievements set the stage for investigations into the pattern formation in electrochemical system. This tremendous increase in the systematic research behind pattern formation in electrochemical systems is mostly because of the progress and development in suitable experimental techniques during the past few decades.[19,20,21] Even Turing-type quasipatterns due to the difference in activation-inhibition were found in electrochemical systems.[22,23] Stationary, far from equilibrium Turing-type patterns, resembling those of biological systems have also been observed on electrode surfaces in 2001 by Li *et al* (see Figure 1.3).[24] The patterns emerge in a dissipative manner owing to the interplay between interfacial kinetics and transport processes parallel to the electrode surface. The important variable for the dynamics of the electrochemical systems is the voltage drop over the solid-liquid interface, the so called *double layer potential.* This variable differentiates electrochemical processes from other reaction-diffusion processes as the associated ion transport mechanism is migration rather than diffusion.

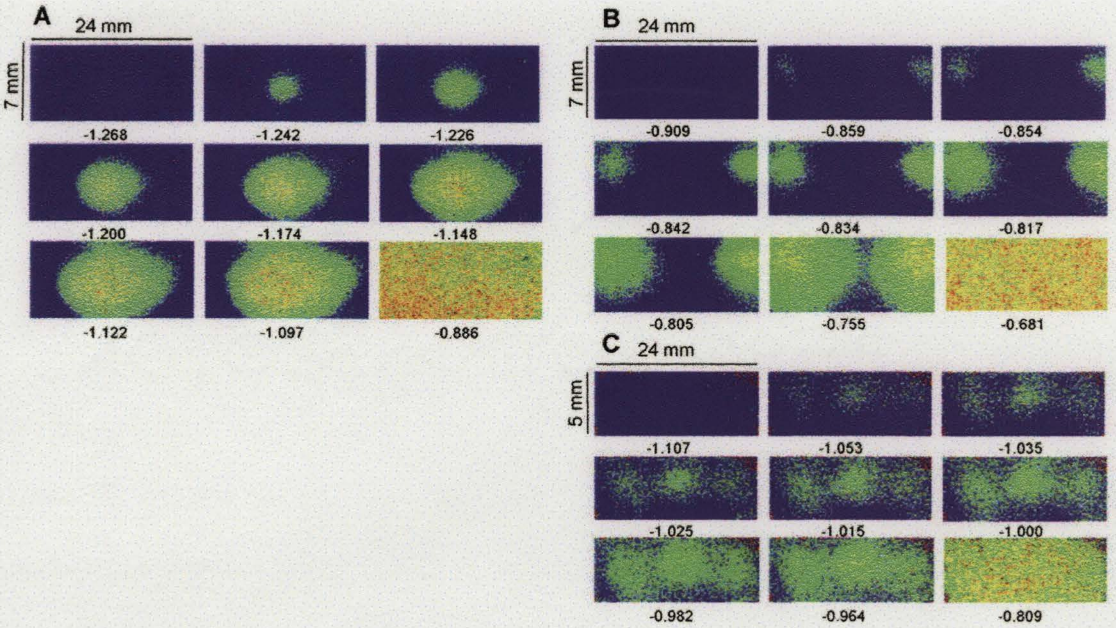

Figure 1.3. “Patterns emerging in different electrolyte compositions: (a) 5 mM camphor, 0.5 mM NaClO4, and 0.5 mM NaIO4; (b) 5 mM camphor, 1 mM NaClO4, and 1 mM NaIO4; and (c) 5 mM camphor, 0 mM NaClO4, and 1 mM NaIO4. The numbers given below the images are the potential values at which the images were obtained during a potential scan. When holding the potential at those values, the patterns did not change with time, i.e., under these conditions, stationary patterns existed on the electrode. Blue colors indicate a nearly camphor-free electrode; orange and yellow colors indicate a high camphor coverage. (The measured intensities are normalized at each point.)”[24]

We have come pretty far in understanding pattern formation in electrochemical systems. Nevertheless, major questions in the field are still controversial and do not lead to a general theory behind their formation. This might be due to the divergent nature of the different results. Today, pattern formation in electrochemical systems is still at a stage where we find frequently different patterns first and then try to find models to explain them. However, each system shows something new which can only be explained by introducing or changing most of the parameters of the previous model system.

1.2 Parameters Dictating Pattern Formation

Conceptually, the basic mechanism behind all these pattern forming processes on the most abstract (and simplistic) level can be due to a chemical 'program' comprising the details of the chemical reactions involved. The common and most important set of functions/instructions which dictate the execution of these chemical programs to fabricate beautiful architectures are rate constants, concentration/potential gradients, diffusion constants and initial/boundary conditions. Other parameters such as surface tension and adsorption coefficient of species are also important.

Three concepts are central for pattern formation in any nonlinear systems including electrochemical processes — feedback, limit-cycle oscillations and coupling. By the functioning of three factors together, the most significant patterns displayed are homogeneous oscillations, chaos, stationary spatially periodic patterns, spirals, traveling waves, target patterns, and turbulence.[25] However, spots and stripes are the most common periodic patterns observed in these far from equilibrium systems. Here, I have provided a general overview and meaning of these different factors. The in-depth explanation and mathematical models for these terms can be found in some excellent textbooks and reviews.[25,26,27]

Feedback is a process, in which part of the output signal is looped-back (fed back) into the system to drive the next output. In all the far from equilibrium processes, internal feedback loops of the system are necessary to control and drive an oscillatory or fluctuating system. The feedback loops are mathematically described by nonlinear evolution equations and they generally change at least one parameter of the system to drive it in a particular direction. However, the internal feedback loop and other typical components of a self-sustained oscillator are not always easily identifiable in a particular system. The feedback of a system can be negative or positive. They are also referred to as stabilizing and destabilizing loops of a system. A positive feedback tends to increase the output signal and accelerates a process whereas negative feedback reduces the output signal and slows it down. However, it is quite hard to predict beforehand whether a specific feedback loop will be able to correct the perturbations and give a desired final effect in a chaotic system.

Periodic or aperiodic oscillations form a large part of the dynamics of the nonlinear systems and are commonly sustained by an external force. Oscillations in the nonlinear systems originate from the presence of both negative and positive feedback loops. The general feature of oscillators is the slow growth (linear or not) of some quantity and its resetting at the threshold. There can be many small oscillators present in the nonlinear system which are coupled among each other at the spatially extended scale.

Oscillations can further give rise to bifurcation in the system where a small smooth change in the dynamical variables can lead to a sudden qualitative change. However, it is impossible to predict the fate of the system at the bifurcation point. The chances of the system going in any of the possible states are equal. However, the mechanisms of self-oscillations are universal and distinct electrochemical oscillatory phenomena have been reported in literature.[28,29]

The term "Coupling" defines the synchronization between the transport of ions in electrochemical systems. Nearly all of the nonlinear systems exhibiting self-organization employ some kind of coupling between different parameters. Coupling can be local or global in nature. In case of electrochemical systems coupling is mostly global in nature. This means that the interaction between individually reacting elements due to an electric field happens on a large spatially extended range. Recently, the concept of remote coupling has been demonstrated by Ertl and coworkers but these kinds of cases have rarely been observed and reported in the literature.[30]

1.3 Kinetics of the Electrochemical Interface

This section discusses some of the basic electrochemical principles of the electrified interfaces, which are crucial to understand the pattern formation on electrode surfaces. In an electrochemical system, when the metal electrode is brought into contact with an electrolyte solution, the reorganization of the charge distribution takes place due to the different properties of the two phases. However, the distribution of hydrated electrolyte ions is considered to be spatially homogeneous (except for a very thin ordered mono-layer at the metal surface) all over before applying the external potential bias to the electrodes. The applied potential provides the external stimulus for the formation of a proper electrical double layer adjacent to the substrate surface. The double layer is further divided into various distinct phase boundary layers which subsequently play a crucial role behind the pattern formation on the electrode surface.

The most common model defines two layers: the Helmholtz layer and a diffuse layer. The Helmholtz layer can be conceived of as having an inner (adjacent to electrode surface) and outer part. The inner Helmholtz layer is comprised of highly oriented dipoles of water, ions or other molecules and is given by the distance of specifically adsorbed ions to the metal surface. The outer Helmholtz layer is defined by the distance of the solvated ions to the working electrode (WE) (Figure 1.4). The diffuse layer connects the outer Helmholtz layer to the bulk solution. The thickness of the diffuse layer depends on the concentration of the solution and the DC voltage being applied and is supposed to be large in our case except for zirconium. The more intricate processes taking place in the double layer are beyond our ability to be considered in this work.

The electrochemical system with the existence of phase boundaries after applying the external potential can be well described by an electrical circuit with capacitive and Faradaic currents placed in series with the ohmic resistance R (Figure 1.4).The double layer is like a leaky capacitor, represented by an impedance Z_f in parallel with a capacitor C_{DL}. The R represents the bulk electrolyte resistance which changes by changing the electrolyte concentration and is spread between the two electrodes.

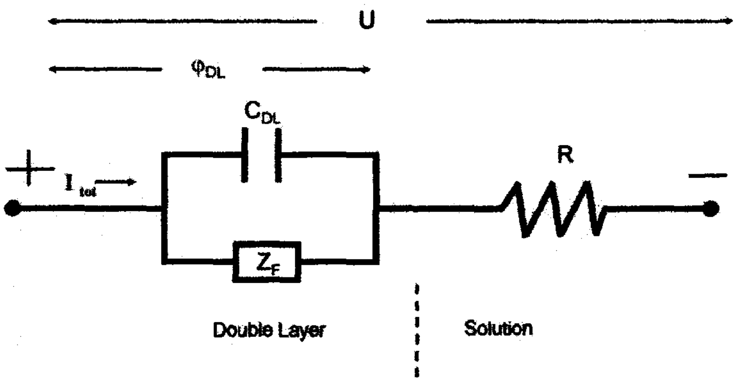

Figure 1.4. Equivalent circuit of an electrochemical cell.

The charged unsolvated and solvated ions which are adsorbed close to the electrode (inner and outer Helmholtz layer) shields some of the electric field which extends into the solution. The external voltage U is composed of the potential drop φ_{DL} across the double layer (DL) which is responsible for the interfacial process, plus the ohmic resistance R in the electrolyte between the working and reference electrode multiplied by the current I_{tot},

$$U = \varphi_{DL} + I_{tot} R.$$

I_{tot} represents the total current flowing between the working electrode and the counter electrode. Furthermore, the current I_{tot} can be split into two parts: Capacitive current (I_{cap}) and Faradaic current (I_{far}). I_{far} is charge transfer due to the chemical reactions and I_{cap} is the charge flowing to charge-up the double layer.

$I_{tot} = I_{cap} + I_{far}$

The rates of the electrochemical reactions are exponentially dependent on the potential drop in the double layer. Thus, the potential drop across the double layer is the main driving force of the electrochemical processes and hence the central variable in pattern formation dynamics.[24, 31] The potential drop across the double layer can be further subdivided into a portion across the inner Helmholtz layer up to the outer Helmholtz plane and the portion which drops across the diffuse part, called φ_2. Therefore, the effective electrode potential driving the reactions at the electrode surface is not φ_{DL}, but instead $\varphi = (\varphi_{DL} - \varphi_2)$.

The presence of convection in the electrochemical double layer due to electromigration of ions makes the calculation of concentration near the interface nontrivial. However, the distribution of ions in the diffuse layer which is some distance away from the electrode surface can be calculated by the Boltzmann distribution equation. The solution beyond the diffuse layer is considered to be electro-neutral with the ionic concentration the same as the bulk concentration. A small change in φ_{DL} at some particular point on the electrode due to some disturbance in the medium can change the potential across the whole electrode area to maintain the electro-neutrality. The changes of the electric potential are predominant near the electrode surface and abruptly decrease in magnitude as one goes away from it. Therefore a local fluctuation in the double layer potential changes the potential of the entire electrode surface leading to the spatial symmetry breaking and subsequently to pattern formation.

Christoph *et al*[30] recently suggested that the migration current due to cross diffusion of ions under the electric field is composed of a local part and a coupling part as given in equation (1). They observed a nonlocal nature of migration coupling due to the remote triggering of electrochemical reactions.

$$C\frac{\partial \varphi}{\partial t} = -i_{reac}(\varphi) + \frac{(U - \varphi_{DL})}{R} + f(\varphi, \theta) \tag{1}$$

where C is the specific double layer capacitance, $f(\varphi,\theta)$ represents the spatial coupling function between different locations on the electrode surface due to an inhomogeneous potential/concentration distribution.

1.4 Migration Coupling

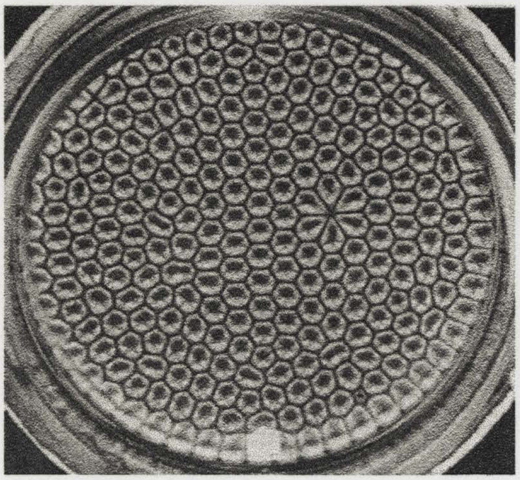

Figure 1.5. "Honeycomb" pattern in Rayleigh-Benard convection cells during the heating of fluid between two plates. Aluminum flakes were added to visualize the moment of fluid.[32]

The term coupling has a very vague meaning unless it is related to some physical process. One of the closest cases for visualizing coupling are the Rayleigh-Benard (RB) convection cycles in fluid dynamics. The pattern forms to facilitate the migration due to an appropriate temperature gradient between the top and bottom surface of the fluid. RB convection - often studied through carefully designed lab experiments - has been known to generate stripes (convection rolls), squares or honeycomb (hexagonal packing) patterns at various length scales ranging from earth's mantle for transportation of heat from the core to the surface; atmosphere to generate thunderclouds; oil in the frying-pan etc. The type of the pattern generated depends on the boundary conditions. However, nothing has ever been noticed at the nanometer length scale. The common reason behind this was that people always thought that the convection cycles at that very small-scale will be affected by thermal noise, bulk turbulence and eddies.

We believe that the migration coupling in our case due to dissolution of metal is long range and gives rise to electromigration cycles similar to RB convective cycles at the nanometer scale under a narrow set of electrochemical parameters. The pattern forms because of cross diffusion of ions which gives rise to convection currents. The electromigration coupling gives rise to convention cycles at the nanometer length scale. The oscillatory nature of the dissolution of metal oxide forms the pattern on the surface. The pattern gets amplified due to positive feedback due to the inhomogeneous distribution of electric field on the surface. The formation and dissolution of oxide becomes stronger at the bottom of the dimple than at the top of the ridge due to the convergent nature of the electric field lines. Later the dissolution and formation equilibrates at the crest and the bottom of the dimple due to diffusion limited transport of the final product from the reactions sites. This kind of engineering of nanostructures by migration coupling during versatile electrochemical reactions may provide new avenues for nanotechnology. In our case, it is the long range migration coupling between the ions which give rise to ionic convection cells similar to Rayleigh-Bernard convection cells. Regarding oscillatory dynamics, it is hard to say if it is present in our system. We did not observe it after the process attains a constant rate but there are few evidences indicating its presence in the initial stages (less than 2 seconds) of dissolution and formation of oxide during electropolishing.

1.5 Overview of This Thesis

Despite there being so much research already done on understanding the principles of pattern formation, only few works deal in presenting the use of entropically controlled dissipative processes for technical advancements. In this thesis, we have demonstrated the practical leverage of dissipative pattern formation by showing its application in fabrication of highly ordered nanostructures on hard metal surfaces which can be used to serve a variety of purposes. We have shown an elegant way of imprinting ordered hexagon and semi-ordered stripes morphology on hard surfaces. The results are important not only because they introduce a new kind of pattern formation but because the phenomenon launches a new technique of surface patterning as well. Along with devising a new technique of making patterns on hard surfaces, we also explored the reason behind their formation. At the same time this research has broken two conventional wisdoms. First, the electropolishing which was known to give nice and smooth surfaces actually produces a highly ordered surface roughness in our case. Secondly, the Rayleigh-Bernard convection was assumed not to happen at the nanoscale but we showed that it is possible under appropriate electrochemical conditions. Building on these new discoveries, we have developed a new technique of "dissipative" nanopatterning. This kind of self driven spontaneous pattern formation on electrode surfaces will have great technical implications because it will allow the fast fabrication of large surface areas in a very short time. We have shown that the pattern can only form in a narrow electrochemical regime.

The other important and interesting thing about electrochemical systems is that a significant shift in the electrochemical window (consisting mainly of applied potential and electrolyte concentration) leads to a different kind of phenomenon and hence different kind of nanostructures. Similar to electropolishing, anodization of a material's surface in appropriate electrolyte solutions is an age old and easy method. It should be noted that anodization is not very different from electropolishing except that it happens at a slightly different electrochemical regime of system parameters, especially the concentration of the electrolyte solution. Anodization is used to grow oxide in aqueous electrolyte solution under normal applied potential conditions whereas electropolishing is done in aqueous as well as non-aqueous electrolytes containing an etchant. This method permits precise, nanometer-scale control over the thicknesses and compositions of covalently cross-linked thin films. To the best of our knowledge, the oxide films formed by anodization have been known to adhere strongly to the surface and were very difficult to separate. While growing anodic tantalum oxide films in fluorine containing electrolyte solutions we got surprising results as the films did not adhere very well to the underlying metal surface.

Thin films are important two-dimensional nanostructures and microstructures that combine at the same time the properties of macroscopic material and individual molecules. However, the full potential of the thin film technology has not been exploited because free standing, purely inorganic films are very difficult to fabricate. In this part of my thesis work, we presented a very simple and versatile method of making robust, purely inorganic, detachable and stable metal oxide membranes. New concepts were discovered during the fabrication of these membranes, one of which is the fast migration of fluoride ions compared to oxygen ions. We concentrated on three fundamental issues related to the fabrication of detachable transition metal oxide films. Differential migration leading to fast transport of fluoride ions inside the oxide film; effect of concentration and voltage on controlling the porosity inside these membranes; and the function of oxyfluoride species as a sacrificial layer for the detachment of the oxide film from the surface. We performed depth profiling studies using SIMS to understand the reasons behind their detachment. This investigation elucidates the chemical mechanisms responsible for the detachment of the oxide membranes from the underlying metal surface. By systematically altering the etchant concentration, combined with modulating the applied potential in the electrolyte solutions, the pore size and density was controlled and assessed. We later extended this concept of differential migration of fluoride ions to make detachable ultra-thin oxide films of niobium, titanium and tungsten. Thin metal oxide films are important for catalysis, micro-optics and micro-electronics (in designing multilayer structures for optical resonators, photonic crystals, gate layers and so on). Finally, I also discussed the physical properties of these films.

1.6 Structure of This Thesis

As described in the previous paragraphs, the aim of this work is twofold. (a) Introduction, investigation and generalization of the dissipative pattern formation technique on metal surfaces in electrochemical systems, and (b) Demonstrating the use of the highly ordered nanostructured metal surfaces as templates for placing nanoparticles as well as their application to fabricate ultrathin porous membranes in the field of thin film fabrication. From a more general point of view, this thesis concerns the nanostructuring of material using dissipative processes. In terms of fundamental studies and technological innovation this study offers a stimulating model system to mathematicians, physicists and material scientists for further study.

The detailed outline of this thesis is as follows. In the next chapter (chapter 2) the concept of the formation of highly ordered arrays of dimples on tantalum surfaces at the nanoscale is introduced. After the description of the electrochemical processes involved in the fabrication of these ordered nanostructures, the physical methods used to characterize the surface are discussed. Finally, the applications of these nanostructures as nanobeakers for the deposition of gold and nickel nanoparticles and also the smooth coverage of dimples by thin platinum film are demonstrated.

In chapter 3 the concept of pattern formation on a tantalum electrodes is extended to other transition metal electrode surfaces. The similarities and differences between the patterns on different surfaces are discussed. The study proves that the pattern formation is not specific to a particular material and is due to a physical phenomenon which can possibly be used to nanostructure any kind of surface. The other kinds of pattern observed on the surfaces such as stripes are also reported in this chapter. The work opens the field of dissipative nanopatterning and emphasizes the need to further study these systems at the molecular level and to mimic them on other materials.

The dynamics of pattern formation is explored in chapter 4. A study, well resolved in space and time, was performed. Fundamental principles behind the formation of dimples on the tantalum surface are investigated. An alternative, explicit formulation of the global coupling term governing the evolution of the double layer potential in terms of experimentally easily measurable quantities is derived. The result has far reaching implications. It is demonstrated that the hexagonal pattern imprints on the surface in the first few milliseconds after turning on the external power supply, however the order and depth increase in time before reaching a constant value. The origin of patterns due to ion migration coupling in the electrochemical double layer is also shown. Along with the formation of the pattern, a way to erase the pattern is also demonstrated. Thus, the results of this work contribute to the understanding of emergent structures in systems subject to global coupling in general as well as to the detailed understanding of electrochemical self-organization phenomena. In the end, the work has been brought to an interdisciplinary stage where there is a close connection between results of different non-linear dynamical systems.

A new concept describing the fabrication of free-standing, ultrathin and porous tantalum oxide membranes by anodic oxidation of tantalum metal surface is introduced in chapter 5. The fundamental concepts behind the detachment of these films are investigated. Porosity is tuned by varying the concentration of the etching solution. The physical properties of these films are characterized by various techniques.

Chapter 6 is about the extension of the concept developed in previous chapter for the fabrication of detachable membranes of other metal oxide films. Herewith, the mechanism of differential fluorine ion migration under the applied potential is elaborated. The peculiarities related to the controlled etching to modulate the pore size by tuning the voltage are also explained.

Finally, the results given in this thesis are summarized with a discussion about the possible future work in chapter 7.

1.7 Bibliography

(1) Haeckel, E. *Art Forms in Nature;* Dover : New York, 2003.

(2) Redman, M. P., Al-Mostafa, Z. A., Meaburn, J., Bryce, M. & Dyson, J. E. The structure and dynamics of the unique Honeycomb Nebula in the halo of 30 Doradus. *Astron. Astrophys.* **1999**, *345*, 943–948.

(3) Barrio, R. A. *Bulletin of Mathematical Biology* **1999**, *61*, 483-505.

(4) Grzybowski et al. *Materials Today* **2007**, *10*, 38-46.

(5) http://cache.virtualtourist.com/1894345-Leopard_spots-Kruger_National_Park.jpg

(6) http://keetsa.com/blog/wp-content/uploads/2007/10/adult-monarch-butterfly-on-its-ay-to mexico-for-warmth.jpg.

(7) Turing, A. M. The chemical basis of morphogenesis. *Philos. Trans. R. Soc. London* **1952**, 237, 37-72.

(8) Glass, L. Synchronization and rhythmic processes in physiology. *Nature* **2001**, *410*, 277-284.

(9) Belousov, B. P. A periodic reaction and its mechanism. *Compilation of Abstracts on Radiation Medicine* **1959**, *147*, 145.

(10) Zhabotinsky, A. M. Periodic processes of malonic acid oxidation in a liquid phase. *Biofizika* **1964**, *9*, 306–311.

(11) DeGroot, S. R. & Mazur, P. *Grundlagen der thermodynamic Irreversibler Prozesse*; BI: Mannheim, 1969.

(12) Glansdorff, P. & Prigogine, I. *Thermodynamic theory of structure, stability and fluctuations*; Wiley-Interscience: London, 1971.

(13) Fechner. G. T. Uber Umkehrungen der Polaritat in der einfachen Kette. *Schweigg J. fur Chemie und Physik* **1828,** *53,* 129.

(14) Ostwald, W. Z. *Phys. Chem.* **1900,** *35,* 204.

(15) Mueller, E. Z. *Elektrochem.* **1922,** *28,* 101.

(16) Gokhstein, A. Frumkin, A. Dokl. Akad. Nauk. SSSR, **1960,** *132,* 388.

(17) Hackwood. S. & Beni, G. J. *Appl. Electrochem.* **1984,** *14,* 673.

(18) Koper, M. T. M. *Adv. Chem. Phys.* **1996,** *92,* 161.

(19) Lev, O., Sheintuch, M., Pismen, L. M. & Yarnitzky, C. Standing and propagating wave oscillations in the anodic dissolution of nickel. *Nature* **1998,** *336,* 458.

(20) Flatgen, G., Krischer, K., Pettinger, B., Dobelhofer, K., Junkes, H. & Ertl, G. 2d-imaging of potential waves in electrochemical systems by means of surfaceplasmon microscopy. *Science* **1995,** *269,* 668.

(21) Flatgen, G.; Krischer, K. Accelerating fronts in an electrochemical system due to global coupling. *Phys. Rev. E* **1995,** *51,* 3997.

(22) V. Castets, V., Dulos, E., Boissonade, J. & deKepper, P. Experimental evidence of a sustained standing Turing-type nonequilibrium chemical pattern. *Phys. Rev. Lett.* **1990,** *64*, 2953.

(23) Ouyang, Q. & Swinney, H. L. Transition from a uniform state to hexagonal and striped Turing patterns. *Nature* **1991,** *352*,610.

(24) Li, Y.J., Oslonovitch, J., Mazouz, N., Plenge, F., Krischer, K. & Ertl, G. Turing-type patterns on electrode surfaces. *Science* **2001,** *291,* 2395.

(25) Cross, M. C. & Hohenberg, P. C. Pattern formation outside of equilibrium. *Rev. Mod. Phys.* **1993,** *65*, 851.

(26) Chirikov, B., Cvitanovic, P., Moss, F. & Swinney, H. *Synchronization: A universal concept in nonlinear sciences.* Nonlinear Science Series 12: Cambridge, 2001.

(27) Jensen, H. J. *Self-organized criticality.* Cambridge University Press, 1998.

(28) Li Z., Cai J., & Zhou, S. J. *Chem. Soc. Faraday Trans.* **1997**, *97*, 3519.

(29) Hudson, J. L. & Tsotsis, T. T. *Chem. Eng. Sci.* **1994,** *49*, 1493.

(30) Christoph, J., Strasser, P., Eiswirth, M. & Ertl, G. Remote Triggering of Waves in an Electrochemical System. *Science* **1999,** *284*, 291-293.

(31) Plenge, F. Theory of Electrochemical Pattern Formation under Global Coupling. Thesis: Fritz-Haber-Institute, Berlin, 2003.

(32) http://www.meta-synthesis.com/webbook/24_complexity/BenardConvection.gif

Chapter-2

Formation of Highly Ordered Arrays of Dimples on Tantalum at the Nanoscale

This chapter demonstrates the electrochemical pattern formation of highly ordered dimples on tantalum surface via electropolishing as well as the methods employed to characterize the dimpled morphology. The application of these dimples as substrates for depositing nanoparticles is also demonstrated and concluded with a discussion of opportunities and challenges.

2.1 Introduction

Given the current interest in nanostructured materials and nanoparticles,[1,2] templates with monodispersed and highly ordered regular features are in high demand.[3,4] As a result, researchers are studying systems such as porous metal oxides with the goal of developing new self-assembly techniques.[5,6,7] Due to its outstanding properties, tantalum is an important material for mechanical, electronic[8, 9] and medical[10] applications, but the ability to control its surface properties at the nanoscale has been largely limited to the growth of dense anodic oxides[11] and, recently, porous oxides[7] of poor order. Here we show that electropolishing of tantalum in concentrated acid mixtures can reproducibly lead to dimples tens of nanometers in diameter, regular in shape, monodispersed in size and arranged in highly ordered arrays, which even traverse grain boundaries. After a single polishing step of less than ten minutes, dimples of 30 nm to 50 nm in diameter (a function of polishing voltage) and around 10 nm deep form a 2-dimensional structure consisting of tantalum metal covered in native oxide. Dimpled tantalum is ductile, high-melting, chemically inert and easily prepared. It can be safely used for nanostructure synthesis under extreme conditions, as demonstrated with a simple sputter coating and flame annealing procedure for gold nanoparticles. Due to their exceptional properties, we anticipate that these nanostructured tantalum surfaces will be suitable for a wide variety of applications in catalysis, combinatorial materials science, nanoparticle synthesis, biomedical devices, etc.

Nanomaterials are of significant interest for the biomedical sciences, catalysis and chemistry, electronics and semiconductors, photonics, energy and information storage as well as functional materials. Nanoparticle synthesis and nanostructuring of materials alike often rely on the availability of suitable templates.[1, 2] UV and X-ray optical as well as nanoimprint lithography can reach the nanoscale, but are limited to mass production of planar surfaces. Sequential writing techniques for making templates such as electron beam lithography, focused ion beam and scanning probe nanolithography are slow and expensive. Alternative methods create templates with repetitive patterns in parallel by self-assembly (e.g. optical interference[3], polymer spheres[4], ion-track etching[5]). Above all, anodically grown porous alumina templates have come to prominence due to their high regularity, monodispersity and tuneability. Nanochannels of uniform diameter and tunable dimensions are formed normal to the surface of aluminum as a result of the anodic oxidation process in acid solutions.[6,7,8] However, porous alumina suffers from brittleness[9] and a fairly complex fabrication process, which has led researchers to look for alternatives in other porous metal oxides,[10,11,12] none of which have been able to achieve sufficiently high order or monodispersity.

Tantalum has many outstanding properties such as chemical resistance (except to hydrofluoric acid), good conductivity, a high melting point, ductility, mechanical strength and biocompatibility.[13] It is an important material for the construction of furnaces, chemical reactors, surgical instruments, capacitors,[14] barrier layers in integrated circuits[15] and more. However, the ability to control its surface properties at the nanoscale has been largely limited to the growth of dense anodic oxides[16,17] and, recently, porous oxides.[12,18,19] During anodic oxide growth, the electrostatic field causes metal ions to enter the oxide film and travel to the electrolyte where they react to produce more oxide. Oxygen from the electrolyte also migrates through the oxide film to the metal interface where more oxide is formed. A compact oxide film is formed and remains on the tantalum surface, with a final thickness determined by the anodization voltage. Electropolishing of tantalum on the other hand is a process where the oxide layer is dissolved as soon as it is formed, not allowing the oxide film to build up. The purpose of polishing is to smoothen and clean the surface.[20, 21] It has been reported that the rates of dissolution in HF of the films formed in concentrated sulfuric or phosphoric acid solutions are much faster than those for the films grown in dilute solutions. This difference is due to the incorporation of electrolyte anions into the oxide film formed in concentrated solutions.[22]

2.2 Formation of Dimples

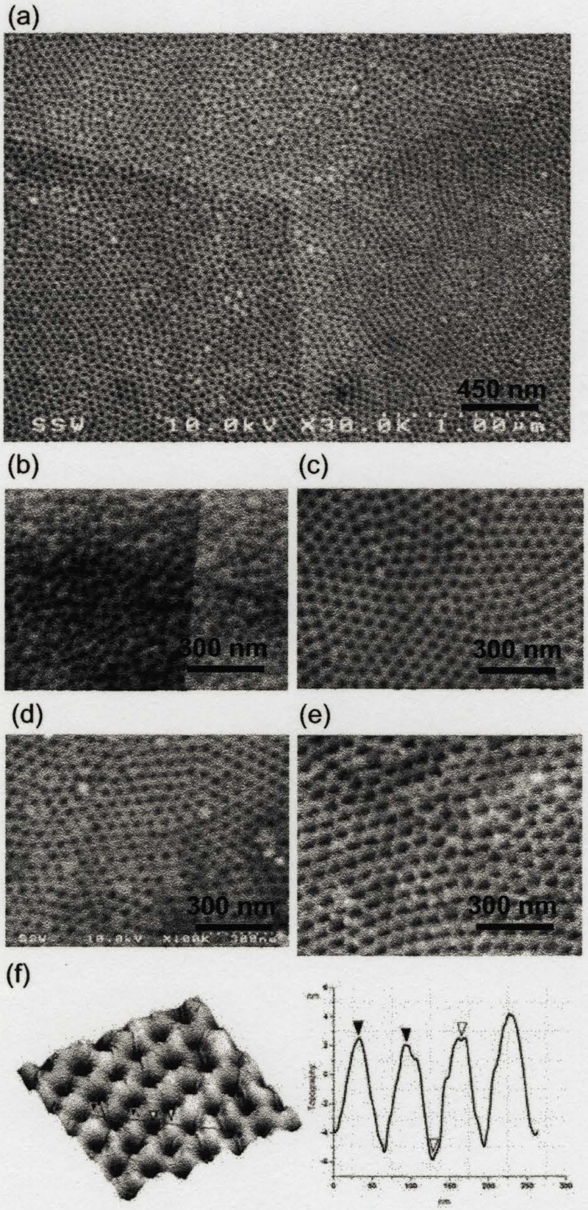

Figure 2.1. SEM images of dimpled tantalum. (a) 15 V, 5 min, showing the long-range order of pores across grain boundaries. (b) 10 V, 10 min, (c) 12 V, 10 min, 2 months old (d) 18V, 10 min (e) 20 V, 10 min, (f) 3D view AFM image 12 min, 15 V and its corresponding cross section.

Electropolishing of tantalum using a 1:9 volumetric mixture of concentrated hydrofluoric acid and concentrated sulfuric acid at room temperature leads to the formation of highly regular arrays of fairly monodispersed dimples (Figure 2.1). The degree of regularity is comparable to well-prepared porous anodic alumina and superior to other porous oxide films. At 15V (Figure 2.1a), the arrays have a periodicity of about 55 nm and traverse grain boundaries in the bulk tantalum metal without noticeable distortion, indicating isotropic etching. The periodicity is a function of the etch voltage within a useful range of about 10 V to 20 V (Figs. 1b, c, d and e). For 10, 12, 18 and 20 V, resulting periodicities are about 40, 50, 60 and 75 nm, respectively. The best monodispersity and long range order are obtained at around 15 V, although no statistical analysis was performed. The robustness of the array formation is remarkable and due to the inertness and stability of tantalum the dimple arrays are long-term stable as well. An image (Figure 2.1c) taken 2 months after sample preparation showed no visible deterioration of the array structure.

2.3 Properties of Dimples

What is the nature of the observed features? Are they an indication of a 3-dimensional porous structure of tantalum oxide or dimples (i.e. etch pits) at the surface of the tantalum metal? Atomic force microscopy (AFM) indicates that the features are on average at least around 8 to 10 nm deep on a sample polished at 15V for 10 min (Figure 2.1f), but a deeper structure cannot be excluded due to the tip geometry. In contrast to previous reports about brittle porous tantalum oxide films,[12,18] attempts to cut or bend our samples for cross-sectional SEM resulted in the layer of dimples simply stretching around the sheared-off edge. Sample-preparation of tantalum for cross-sectional TEM is non-trivial, and the question of artifacts would remain. We therefore turned to nuclear reaction analysis (NRA) and x-ray photoelectron spectroscopy (XPS) for conclusive evidence.

NRA determines the total number of oxygen atoms in a given sample area within 0.5 microns of the surface as compared to a known standard. Oxygen concentrations well below the surface would manifest themselves as a tail in the NRA peak, which was not observed, indicating that the vast majority of the measured oxygen was present in the near-surface region. NRA measurements on dimpled tantalum samples polished at 15V for 10, 20, 30, 40, 50 and 60 minutes indicate average oxide thicknesses of 3.82, 3.46, 3.71, 3.52, 3.81 and 3.69 nm (all measurements ±0.08 nm) respectively. The actual oxide coverage in our case will be somewhat less due to the higher surface area of the dimples as compared to a flat surface for which the NRA measurement is calibrated. These values are within the range of what would be expected for a native oxide film[24,25] on a flat surface, albeit slightly on the high side. The thicknesses for the different times are very close to each other and clearly demonstrate that no oxide is grown.

XPS was used to further clarify the nature of the dimpled tantalum surface. Survey spectra of cleaned samples before and after the dimpling process are virtually identical, except for slight incorporation of fluorine and sulfur into the dimpled samples

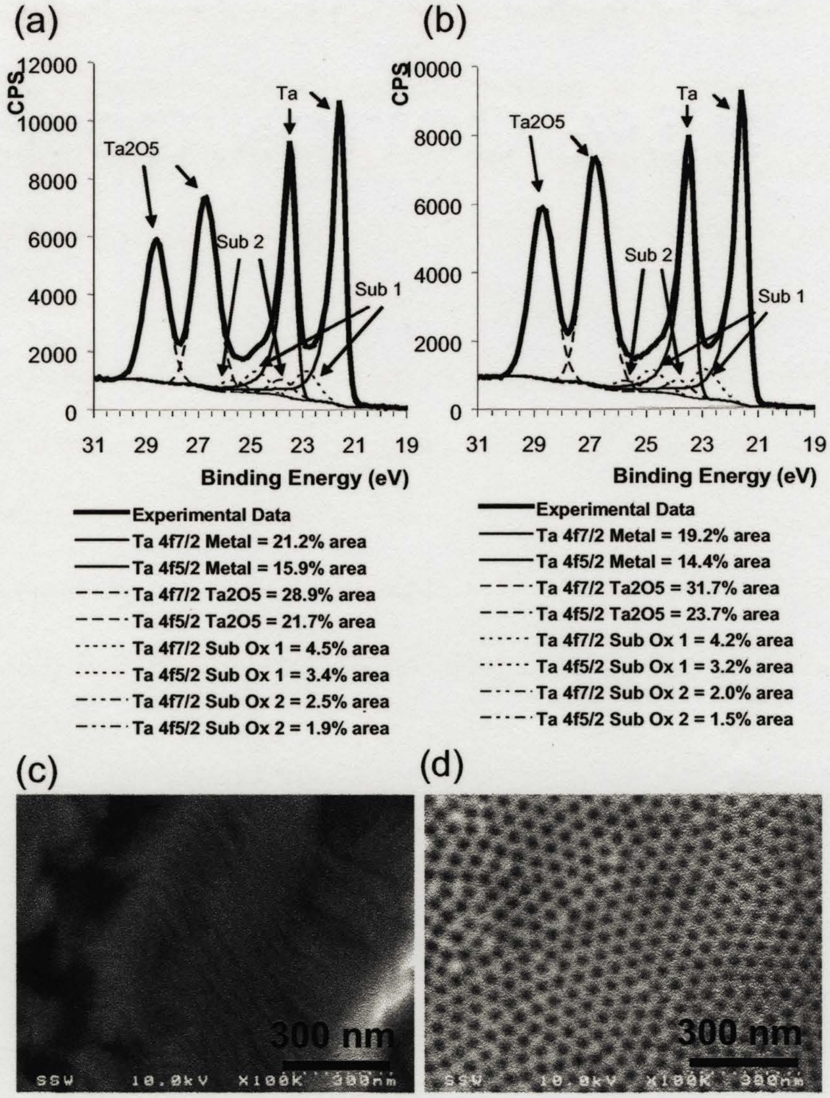

Figure 2.2. High resolution XPS spectra of tantalum (a) before and (b) after dimpling showing the Ta 4f peak with the fit for four sets of characteristic 5/2 and 7/2 duplets assigned to tantalum oxide, interfacial tantalum suboxides (two species) and underlying tantalum metal. The two spectra are virtually identical, confirming that we are dealing with dimpled metal rather than porous oxide. (c) and (d) are characteristic SEM images of the surfaces of the two samples respectively taken approx. one week after XPS analysis was performed.

(15V, 10 min). This is expected, because tantalum oxide grown in concentrated sulfuric acid (95-98%) is known to incorporate electrolyte anions (SO_4^{2-}) in the whole depth of the film[22]. More significant is the similarity of the tantalum 4f peaks in the high resolution spectrum (Figs. 2a and b). Peaks for both samples were fitted allowing for tantalum metal, two different tantalum species due to suboxide at the interface and tantalum pentoxide for the bulk of the oxide film. Calculated percentage contributions of each species to the peaks are almost identical between both samples. It should be noted, however, that the oxide film on the dimpled substrate is again measured to be slightly thicker than the native oxide. The subsequently taken SEM images of both samples (Figs. 2c and d) clearly show the differences in sample topography.

The formation of dimpled tantalum rather than porous tantalum oxide can be attributed to our use of concentrated sulfuric acid in the etching electrolyte. In 1954 Vermilyea[22] reported a difference in reactivity towards HF between tantalum oxide films formed in concentrated and dilute sulfuric acid solutions due to the incorporation of electrolyte anions into the oxide film. The incorporation is not effective when dilute acids are used for anodization. Tantalum oxide films formed in concentrated solutions were found to dissolve more rapidly than those formed in dilute solutions.[26] Thus most of the tantalum oxide formed by anodic oxidation is susceptible to dissolution in HF solution.

The chronoamperometric curve (Figure 2.3a) obtained during the electropolishing of a sample (Fig 2.3d) at 15V for 20 minutes further clarifies the dimple array formation process. Initially, a compact layer of tantalum oxide is formed through hydrolysis of tantalum at the electrolyte-metal interface. This oxide layer leads to a dramatic decrease in the recorded current density due to its poor electrical conductivity[5]. Due to the high solubility of the formed tantalum oxide in HF-containing solutions, dimples start to grow and the current density increases gradually as the surface area increases. The behavior is similar to that of porous oxide formation on Al[27] and Ti.[28,29] The dimples originate at random defect locations and continue to grow horizontally on the surface until they reach the biggest possible diameter. At the same time, they are rapidly progressing into the bulk of the tantalum. We estimate etch rates to be rather high, in the range between 20 to 50 nm/s. Due to the strong interaction between the dimples, dimple diameters equalize until the system reaches a steady state. Equilibrium is essentially reached after 2 minutes, as further illustrated by SEM images of samples that have been etched at 15 V for 5, 10 and 20 minutes without any significant changes in morphology (Figs. 2.3b, c and d). The final spacing of the dimples is likely dictated by the number of defects on the original surface that survive the selection process to develop into etch pits during the first stage of the dimpling process, followed by some sort of an equilibration process. The underlying mechanisms are unknown at this point and will require a study well-resolved in time and space to elucidate. A rapid dynamic equilibrium is likely to be key to the formation of regular dimple arrays. Dimpling recipes for other substrates may be possible if similarly high rates of dissolution can be achieved.

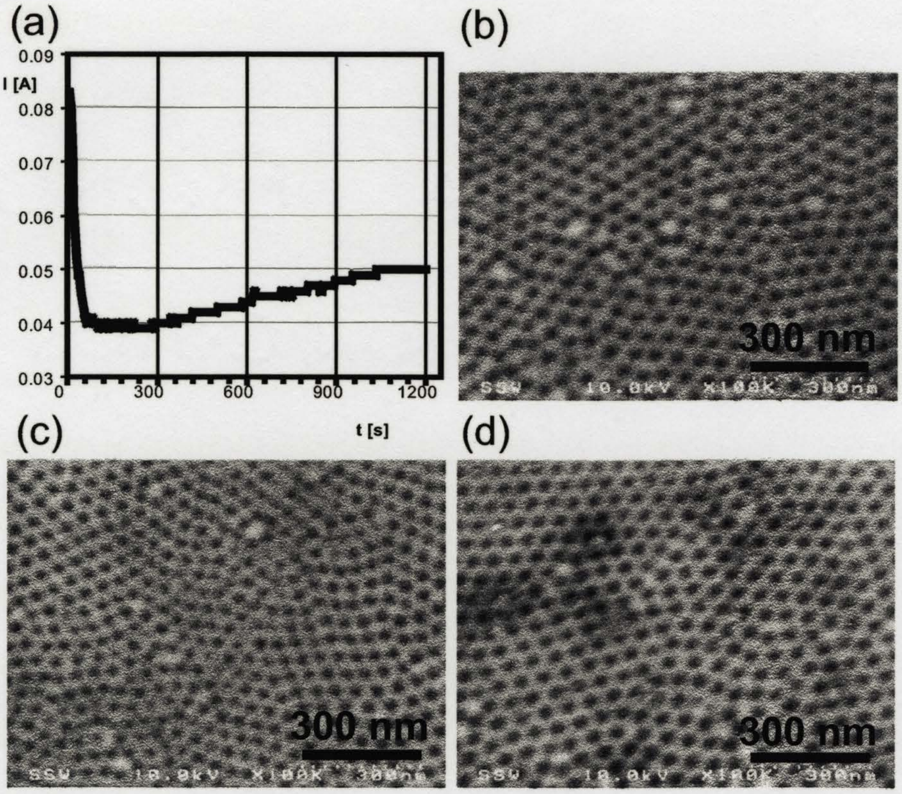

Figure 2.3. Time-dependence of dimple size and density. (a) Chronoamperometric curve recorded while dimpling a tantalum sample for 20 minutes at 15 V. (b) SEM image of a different sample dimpled for 5 minutes at 15 V. (c) SEM image of a different sample dimpled for 10 minutes at 15 V. (d) SEM image of sample for which chronoamperometric curve (a) was taken (20 min, 15 V). No significant differences are observed, indicating that the ordering process was completed in less than 5 minutes and the number and size of dimples remained constant after that.

2.4 Dimples as Ordered Template

The use of similar structures as "nanobeakers" has previously been suggested,[29] but the robustness and inertness of dimpled tantalum make it particularly suitable as a template for nanostructure synthesis. For example, thin metal films can be deposited onto the dimpled surfaces and annealed without damage to the dimple arrays or the substrate, which is of relevance to applications in catalysis and combinatorial chemistry. Here we simply illustrate the possibility of these applications without presenting any optimised procedures. Using a basic sputter coater, a thin gold film of approx. 2 to 5 nm is deposited onto a dimpled tantalum sample which is half covered by pressing a clean tantalum sheet onto it. A small butane torch is then used, with the flame in direct contact with the sample, to anneal the gold film four times for 5 seconds each. De-wetting leads to a break-up of the film into gold nanoparticles (Figure 2.4a). Due to the inhomogeneity of our flame annealing process, different areas of the surface display different de-wetting behaviour. In one area (Figure 2.4b), gold nanoparticles were partitioned into the pores. Under different conditions (Figure 2.4c), very small (less than 10 nm) nanoparticles exclusively decorate the ridges. A controlled annealing process can be used to select one of these scenarios to fit particular applications. Most remarkably, the uncoated area survived with perfectly intact dimples (Figure 2.4d) despite having been mechanically impacted by the mask and then being exposed to a hot flame during annealing. We also performed metalisation and annealing experiments under better controlled conditions (see methods section) using platinum (Figures 2.4e, f and g) and nickel (Figure 2.4h). Platinum does not de-wet the surface under those conditions and continues to form a smooth film, which under the SEM is almost indistinguishable in appearance from the uncoated areas, although the border between coated and uncoated regions is clearly visible on the sample. No nanoparticles are observed anywhere in the coated region (Figure 2.4g). In contrast, nickel forms nanoparticles that are evenly distributed inside the pores (Figure 2.4h).

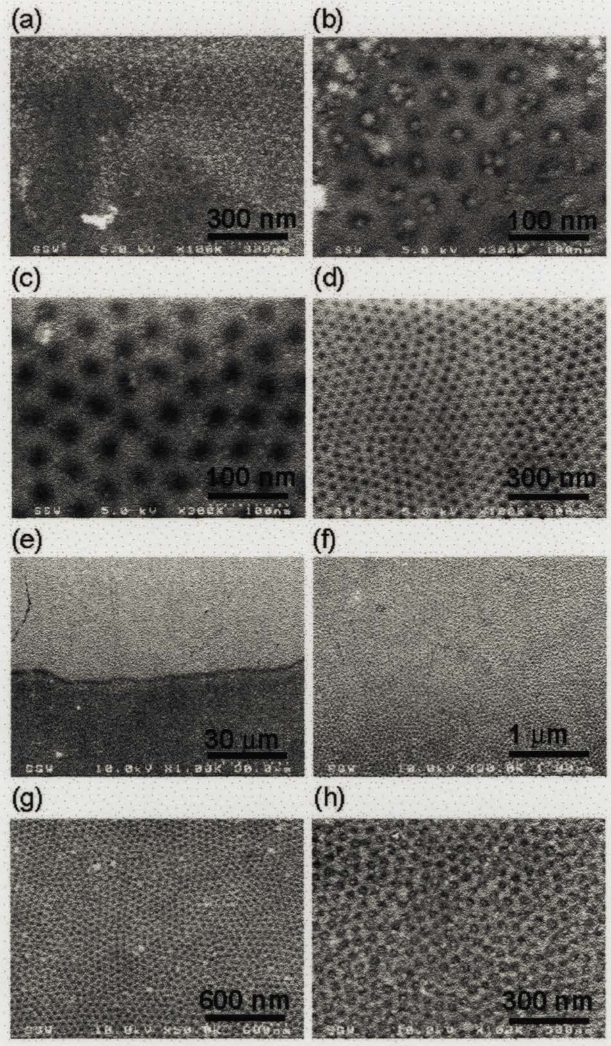

Figure 2.4. Applications to metal deposition: Au sputter-coated (a), (b), (c) and uncoated (d) regions of a dimpled tantalum sample (10 min, 15V) after flame-annealing. (e) Border between coated and uncoated regions of another dimpled tantalum sample with nominally 2 nm of Pt coated by e-beam evaporation after rapid thermal anneal to 650 Celsius, (f) close-up of border (coated region slightly darker at bottom), (g) coated region, showing a continuous film of Pt. (h) Coated and annealed region of another dimpled tantalum sample with nominally 2 nm of Ni coated by e-beam evaporation after rapid thermal annealing to 650 Celsius, showing Ni nanoparticles largely located in the pores.

2.5 Conclusions

A highly regular dimpled tantalum surface with tuneable periodicity was fabricated by electrochemical oxidation of tantalum, within the anodization potential range of 10-20 V. The ordering is complete after just a few minutes, and only a single step process is required. We have shown that the resulting dimples consist of solid tantalum metal covered with an oxide film only slightly thicker than the native oxide. The dimple array templates therefore retain many of the properties of bulk tantalum, such as ductility, high melting point and chemical inertness. This surface is a suitable template for nanoparticle fabrication under a wide range of conditions, as we have demonstrated by metal deposition and annealing to form nanoparticles with many potential applications.

2.6 Experimental Section

Prior to dimpling, tantalum foil (Alfa-Aesar, 99.95%, 0.127 mm) was carefully rinsed in acetone, isopropanol, and Millipore water (18.2 MΩ/cm resistivity). Dimpling was carried out in a stirred solution of concentrated H_2SO_4 (95-98%) and HF (48%) in a volumetric ratio of 9:1 using a conventional two-electrode system connected to a power supply (Agilent E3615A). A Pt/Ir wire was used as the counter-electrode (cathode). The working electrode (anode) was a tantalum foil substrate connected with a copper wire to the power supply. The distance between the working and counter-electrodes was kept at approx. 1.5 cm. During the entire dimpling process, the solution was stirred using a magnetic bar. Immediately after dimpling, the sample was rinsed with deionised water.

The preparation method as described here has been successfully reproduced by several different researchers within the group. The relevance of the purity of the chemicals is not entirely clear at this point since the process appears to work even with aged solutions. Freshly mixed polishing solutions typically need to settle for a few hours before the first sample is processed. All experiments were performed at room temperature (approximately 20°C).

The samples were characterized with a Hitachi S-4500 FE-SEM at Surface Science Western, except for Figs. 2.1b, c and e which were taken with a Jeol 7000F FE-SEM at the Brockhouse Institute of Materials Research. Atomic force microscopy was performed in tapping mode on a Veeco Enviroscope with a Nanoscope IIIa controller and Veeco RTESP p-doped Si tips with a nominal radius of less than 10 nm.

For the nuclear reaction analysis (NRA), the $^{16}O(d,p)^{17}O$ nuclear reaction with a 972 keV deuterium primary beam ($1 mm^2$) was used to determine the absolute oxygen content of the anodised samples within ~0.5 μm of the surface. The deuterium beam was incident on the samples along the surface normal and the detector was placed at 135° in the scattering plane which included the incident beam. The tantalum oxide thickness was estimated by comparing the number of protons emitted from the sample to those emitted from a calibration target of 70.7 nm (± 2%) Ta_2O_5/Ta in an identical geometry. More about the experimental setup of the NRA system at Interface Science Western can be found elsewhere.[30]

XPS was performed at Surface Science Western using a Kratos AXIS Ultra X-ray photoelectron spectrometer employing a monochromatic AlK_α X-ray source (1486.71

eV) and charge neutralizer system. The instrument work function was calibrated to give a binding energy (BE) of 83.96 eV for the Au $4f_{7/2}$ line for metallic gold, and the spectrometer dispersion was adjusted to give a BE of 932.62 eV for the Cu 2p3/2 line of metallic copper. Survey scan and high resolution analyses were carried out in an area 300 x 700 microns in size, using pass energies of 160 eV and 20 eV and step sizes of 0.7 eV and 0.1 eV respectively.

For the metal deposition studies, several Ta samples were dimpled at 15 V for 10 min. Half of each sample was masked by spot-welding a piece of clean tantalum across the top, touching the dimpled surface. Approximately 2 to 5 nm of gold were sputter coated onto two of the samples at a rate of 15 nm/min. The mask was removed and the sample was then flame annealed four times for about 5 seconds each using a butane torch. The flame (approx 1000 to 1300° Celsius) was in direct contact with the sample. 2nm each of nickel and platinum were separately electron beam evaporated in a vacuum chamber at a rate of 0.1 nm/s onto several other masked samples. These samples underwent rapid thermal annealing at 650° C for 5 minutes in a nitrogen environment. The e-beam evaporator and rapid thermal annealer are located in the Centre for Emerging Device Technologies at McMaster.

Author Contributions:

This chapter is based on a paper published in Nano Letters. (Sayed, H. E.; Singh, S.; Greiner, M. T.; Kruse, P. *Nano Lett.* **2006**, *6*, 2995-2999). The author contribution for this paper is as follows. H.E.S. discovered the dimpled morphology on tantalum surface and conducted the electrochemical experiments. S.S. designed and performed the XPS, AFM and particle deposition experiments which are shown in of Figure 2.1, 2.2 and 2.4. S.S. also repeated all the electrochemical experiments which led to all the figures except Figure 2.1a and 2.1b. M.T.G. helped with the NRA experiments. Overall data analyses were conducted by the P.K., S.S. and H.E.S. P.K., S.S. and H.E.S. contributed in writing the manuscript.

2.7 Bibliography

(1) Henzie, J., Barton, J. E., Stender, C. L. & Odom, T. W. Large-area nanoscale patterning: Chemistry meets fabrication. *Accounts of Chemical Research* **2006**, *39*, 249-257.

(2) Moriarty, P. Nanostructured materials. *Rep. Prog. Physics* **2001**, *64*, 297-381.

(3) Thompson, G. E., Furneaux, R. C., Wood, G. C., Richardson, J. A. & Goode, J. S. Nucleation and growth of porous anodic films on aluminum. *Nature* **1978**, *272*, 433-435.

(4) Masuda, H. & Fukuda, K. Ordered metal nanohole arrays made by a 2-step replication of honeycomb structures of anodic alumina. *Science* **1995**, ***268***, 1466-1468.

(5) Sieber, I., Hildebrand, H., Friedrich, A. & Schmuki, P. Formation of self-organized niobium porous oxide on niobium. *Electrochem. Comm.* **2005**, *7*, 97-100.

(6) Ghicov, A., Tsuchiya, H., Macak, J. M. & Schmuki, P., Titanium oxide nanotubes prepared in phosphate electrolytes. *Electrochemistry Communications* **2005**, *7*, 505-509.

(7) Sieber, I., Kannan, B. & Schmuki, P. Self-assembled porous tantalum oxide prepared in H_2SO_4/HF electrolytes. *Electrochemical and Solid State Letters* **2005**, *8*, J10-J12.

(8) Chaneliere, C., Autran, J. L., Devine, R. A. B. & Balland, B. Tantalum pentoxide (Ta2O5) thin films for advanced dielectric applications. *Materials Science & Engineering R* **1998**, *22*, 269-322.

(9) Kuiry, S. C., Seal, S., Fei, W., Ramsdell, J., Desai, V. H., Li, Y., Babu, S. V. & Wood, B. Effect of pH and H_2O_2 on Ta chemical mechanical planarization. *Journal of the Electrochemical Society* **2003**, *150*, C36-C43.

(10) Findlay, D. M., Welldon, K., Atkins, G. J., Howie, D. W., Zannettino, A. C. W. & Bobyn, D. The proliferation and phenotypic expression of human osteoblasts on tantalum metal, *Biomaterials* **2004**, *25*, 2215-2227.

(11) Young, L. Anodization constants for tantalum. *Journal of the Electrochemical Society* **1977**, *124*, 528-529.

(12) Yang, Y., Zhang, S. H. & Wang, G. P. Fabrication of two-dimensional metallodielectric quasicrystals by single-beam holography. *Applied Physics Letters* **2006**, *88*, 251104.

(13) Bullen, H. A. & Garret, S. J. TiO2 nanoparticle arrays prepared using a nanosphere lithography technique. *Nano Letters* **2002**, *2*, 739-745.

(14) Chakarvarti, S. K. & Vetter, J. Template synthesis – A membrane based technology for generation of nano-/micro materials: A review. *Radiation Measurements* **1998**, *29*, 149-159.

(15) Asoh, H., Nishio, K., Nakao, M., Tamamura, T. & Masuda, H. Conditions for fabrication of ideally ordered anodic porous alumina using pretextured Al. *Journal of the Electrochemical Society* **2001**, *148*, B152-B156.

(16) Xia, Z., Riester, L., Sheldon, B. W., Curtin, W. A., Liang, J., Yin, A. & Xu, J. M. Mechanical properties of highly ordered nanoporous anodic alumina membranes. *Reviews on Advanced Materials Science* **2004**, *6*, 131-139.

(17) Lu, Q., Mato, S., Skeldon, P., Thompson, G. E., Masheder, D., Habazaki, H. & Shimizu, K. Anodic film growth on tantalum in dilute phosphoric acid solution at 20 and 85 degrees C. *Electrochimica Acta* **2002**, *47*, 2761-2767.

(18) Sieber, I. & Schmuki, P. Porous tantalum oxide prepared by electrochemical anodic oxidation. *Journal of the Electrochemical Society* **2005**, *152*, C639-C644.

(19) Sieber, I., Hildebrand, H., Friedrich, A. & Schmuki, P. Initiation of tantalum oxide pores grown on tantalum by potentiodynamic oxidation. *Journal of Electroceramics* **2006**, *16*, 35-39.

(20) Piotrowski, O., Madore, C. & Landolt, D., Electropolishing of tantalum in sulfuric acid-methanol electrolytes. *Electrochimica Acta* **1999**, *44*, 3389-3399.

(21) Ueno, K., Abe, S., Onoki, R. & Saiki, K. Anodization of electrolytically polished Ta surfaces for enhancement of carrier injection into organic field-effect transistors. *Journal of Applied Physics* **2005**, *98*, 114503.

(22) Vermilyea, D. A. Formation of anodic oxide films on tantalum in non-aqueous solutions. *Acta Met.* **1954**, *2*, 483-486.

(23) Kerrec, O., Devilliers, D., Groult, H. & Chemla, M., Dielectric properties of anodic oxide films on tantalum. *Electrochimica Acta* **1995**, *40*, 719-724.

(24) Macagno, V. & Schultze, J. W. The growth and properties of thin oxide layers on tantalum electrodes. *Journal of Electroanalytical Chemistry* **1984**, *180*, 157-170.

(25) Shimizu, K., Brown, G. M., Habazaki, H., Kobayashi, K., Skeldon, P., Thompson, G. E. & Wood, G. C. Direct observation of anodic films formed on tantalum in concentrated phosphoric and sulphuric acid solutions. *Corrosion Science* **1998**, *40*, 963-973.

(26) Parkhutik, V. P. & Shershulsky, V. I. Theoretical Modeling of Porous Oxide-Growth on Aluminum. *Journal of Physics D-Applied Physics* **1992**, *25*, 1258-1263.

(27) Zwilling, V., Darque-Ceretti, E., Boutry-Forveille, A., David, D., Perrin, M. Y. & Aucouturier, M. Structure and physicochemistry of anodic oxide films on titanium and TA6V alloy, *Surface and Interface Analysis* **1999**, *27*, 629-637.

(28) Cai, Q. Y., Paulose, M., Varghese, O. K. & Grimes, C. A. The effect of electrolyte composition on the fabrication of self-organized titanium oxide nanotube arrays by anodic oxidation. *Journal of Materials Research* **2005**, *20*, 230-236.

(29) Barton, J. E. & Odom, T. W. Mass-limited growth in zeptoliter beakers: A general approach for the synthesis of nanocrystals. *Nano Letters* **2004**, *4*, 1525-1528.

(30) Davies, J. A. & Norton, P. R. Absolute coverage measurement of adsorbed CO and D2 on platinum. *Nuclear Instruments and Methods* **1980**, *168*, 611-615.

Chapter-3

Nanopatterning of transition metal surfaces via electrochemical dimple array formation.

Nanoscale surface patterning is of great importance for applications ranging from catalysts to biomaterials. We show the formation of highly ordered nanoscale dimple arrays on titanium, tungsten and zirconium during electropolishing, demonstrating versatility of a process previously only reported for tantalum. While conditions for titanium and tungsten resemble those for tantalum, zirconium requires a different type of electrolyte. Given the appropriate electropolishing chemistry, formation of these patterns should be possible on any metal surface.

3.1 Introduction

The preparation of surfaces with uniform nanoscale patterns is a challenge that has been addressed in a variety of ways,[1,2,3,4,5,6,7] because their applications are wide-ranging, from electronic (e. g. memory devices) and electrophotonic (e. g. solid state lighting and solar cells) materials over catalysts to bio-compatible surfaces. The quest continues, because each patterning method comes with its own set of challenges and limitations. Optical lithography, for example, has hit its resolution limits; Electron beam, ion beam or scanning probe lithographies are slow; Imprint lithography, just as the previously mentioned methods, requires expensive equipment and is then still limited to reasonably flat surfaces. Self-organization strategies have been explored as alternatives, in many cases relying on the formation of an ordered mask which is then used to imprint structure onto the substrate.[6,7] The reason for this approach is that self-organizing systems tend to be very material specific, which is why for each proposed strategy a particular mask material is chosen based on its ability to be driven into an ordered state. Direct processes for surface pattern formation are harder to come by, but examples exist.

Porous anodic oxide formation and electropolishing are two electrochemical approaches to surface patterning. Anodic oxidation involves oxidation of the anode surface in an electrolyte that is unable to attack (dissolve) the formed oxide. If the electrolyte is able to dissolve only the electrode material or a thin oxide film in the presence of a strong electric field, while a thicker oxide film is rendered inert, a porous anodic oxide may be formed. If the oxide is dissolved rapidly, while the unoxidized electrode material is either inert or only dissolved at a much lower rate, the anode surface will be electropolished, with no anodic oxide remaining. So far, only porous anodic oxide formation has been explored in more detail for a variety of materials, including aluminum,[8,9,10] titanium,[11] tantalum[12,13] and niobium.[14] Pores in these oxides are always disordered, unless the surface is pre-patterned prior to oxide formation.[9,10,13] In contrast, electropolishing of tantalum surfaces has been reported to result in highly ordered surface structures,[15,16,17,18,19] which were recently revealed to be arrays of shallow dimples.[18] A number of different ordered nanostructures have also been reported for aluminum surfaces.[20,21,22,23] However, the mechanism behind their formation was never fully understood and nobody has ever succeeded in translating them to other surfaces.

Here we show that the previously reported formation of highly ordered arrays of dimples on tantalum at the nanoscale is also applicable to titanium, tungsten and zirconium and postulate that, given an appropriate electropolishing chemistry, these patterns can be formed on virtually any metal or semiconductor surface. While pattern formation during electropolishing has been observed before, this is the first time that such a process has been extended beyond the material on which it was originally observed. Scanning electron microscopy (SEM), atomic force microscopy (AFM) and x-ray photoelectron spectroscopy (XPS) were used to confirm the metallic nature of the highly ordered dimple structure.

3.2 Formation of Dimples on Ti, W, Ta and Zr

Tantalum (99.95%), titanium (99.95%) and zirconium foil (99.5%, all 0.127 mm thick) as well as tungsten ribbon (99.95%, 0.125 mm thick) and tungsten wire (d = 0.25 mm, 99.95%, all Alfa-Aesar) were mechanically cut and rinsed with acetone, methanol and Millipore water (18.2 MΩ.cm resistivity) and then dried under argon flow before use. The Ta, Ti, W and Zr surfaces were electropolished using a two-electrode system (Figure 3.1a) connected to an Agilent E3615A power supply. A Pt/Ir wire (0.25 mm diameter) was used as a cathode. Both electrodes were kept vertical, parallel to each other with an distance of approximately 1.5 cm. No attempt was made to moderate or control the temperature of the set-up, even though the electropolishing reaction produced a significant amount of heat and the electrochemical cell warmed up to well above room temperature. Ta, Ti and W were dimpled in a stirred mixture of concentrated H_2SO_4 (95-98%) and HF (48%) in volumetric ratios of 9:1 (Ta), 8:2 (Ti) and 93:7 (W) by applying a constant DC voltage of 15 V for 2 min (Ti) and 10 min (W) respectively. Zr foil was dimpled in 0.5 M NH_4F at 20V for 5 min. The typical sample size was 5 mm wide and 30 mm long, with one third of the length immersed in the electrolyte. The solutions were stirred using a magnetic stir-bar. All samples were thoroughly rinsed with Millipore water (18.2 MΩ.cm resistivity) and then dried under argon flow after electropolishing. Freshly mixed electrolytic solutions typically needed to settle for 16-20 hours before the first sample is processed.

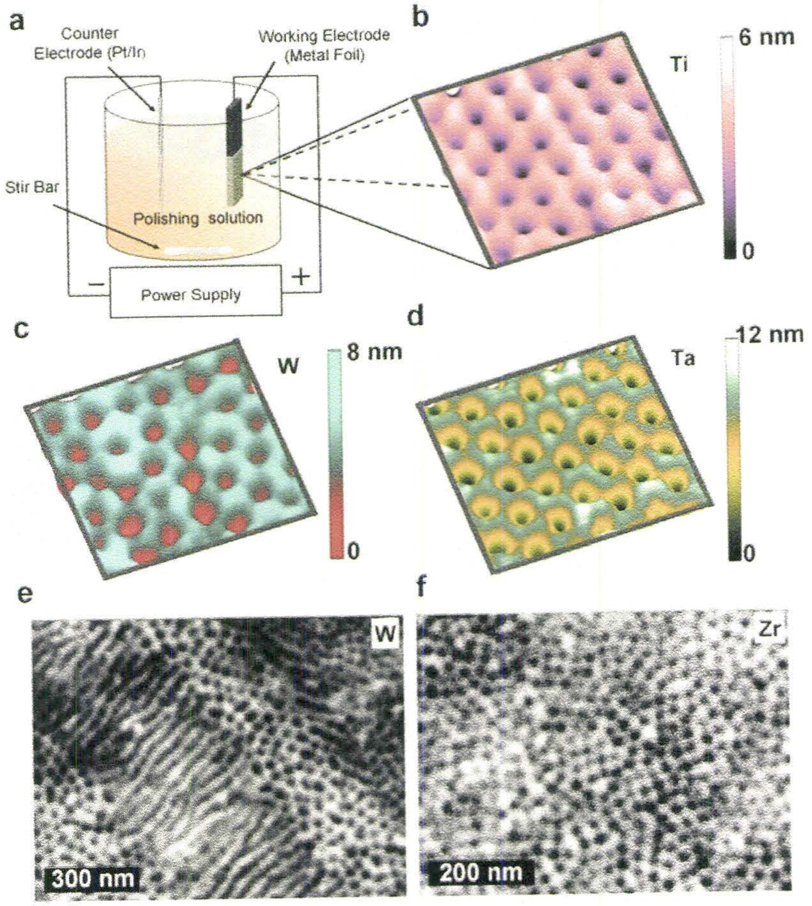

Figure 3.1. Formation of hexagonal and striped patterns on titanium, tantalum, tungsten and zirconium surfaces. a, Illustration of electrochemical set-up. b, Tapping-mode topographic (3D) AFM image of titanium after electropolishing in 8:2 c.H_2SO_4/c.HF solution for 2 minutes at 15V. c, Tapping-mode topographic (3D) AFM image of tungsten after electropolishing in 93:7 c.H_2SO_4/c.HF solution for 5 minutes at 15V. d, Tapping-mode topographic (3D) AFM image of tantalum after electropolishing in 9:1 c.H_2SO_4/c.HF solution for 5 minutes at 15V. Image dimensions for figures b, c, d are (300 x 300) nm^2. e, SEM image of hexagonal and striped patterns on the tungsten surface. f, SEM image of hexagonal patterns on the zirconium surface after electropolishing in 0.5M NH_4F solution for 5 minutes at 20V.

Highly ordered arrays of dimples can be generated reproducibly on titanium (Figure 3.1b), tungsten (Figure 3.1c, e), tantalum (Figure 3.1d) and zirconium (Figure 3.1f) (also see Figures 3.3, 3.4, 3.5, 3.6, 3.7 and 3.14 for additional SEM data on data on all metals). AFM measurements indicate that tantalum dimples are on average 8...10 nm deep (Figure 3.1d), tungsten dimples are 5...6 nm deep (Figure 3.1c) and titanium dimples are 2.5...4 nm deep (Figure 1b). Atomic force microscopy was performed in the tapping mode on a Veeco Enviroscope with a Nanoscope IIIa controller and Veeco RTESP n-doped Si tips with a nominal radius of less than 10 nm. Typical scan rates were 2 micrometers per second and the images were constructed with 512 scan lines. Care was taken to ensure that the tip was not modifying the surface during the scan. A large number of images of the same sample were obtained with different tips to pinpoint the exact depth of dimples by eliminating tip convolution effects. The data was analyzed using DI V5.30r3.sr3 software. SEM imaging was performed with a JEOL JSM-7000F Scanning Electron Microscope, equipped with a Schottky type Field Emission Gun (FEG) filament. The ordered dimple patters were uniform across the entire surface for titanium, whereas for tungsten impurities played a role and under certain circumstances stripes were also observed (Figure 3.1e). Zirconium is the exception in this study in that a very different electrolyte had to be used, with the result of somewhat smaller dimples (40 nm compared to 55 nm in the cases of Ta, Ti and W) and some oxidized areas remaining at the surface. The details of each system are described below.

Figure 3.2 shows a large area SEM image of a dimpled titanium surface, demonstrating the reproducibility of the process over large surface areas. It can be seen that grain boundaries and residual surface roughness do not impact the dimple pattern. In fact, this image is representative of a large number of images taken by us on several samples. Both tantalum[18] and titanium show highly ordered dimple patterns with excellent reproducibility (see Figures 3.3, 3.4, 3.5 and 3.6).

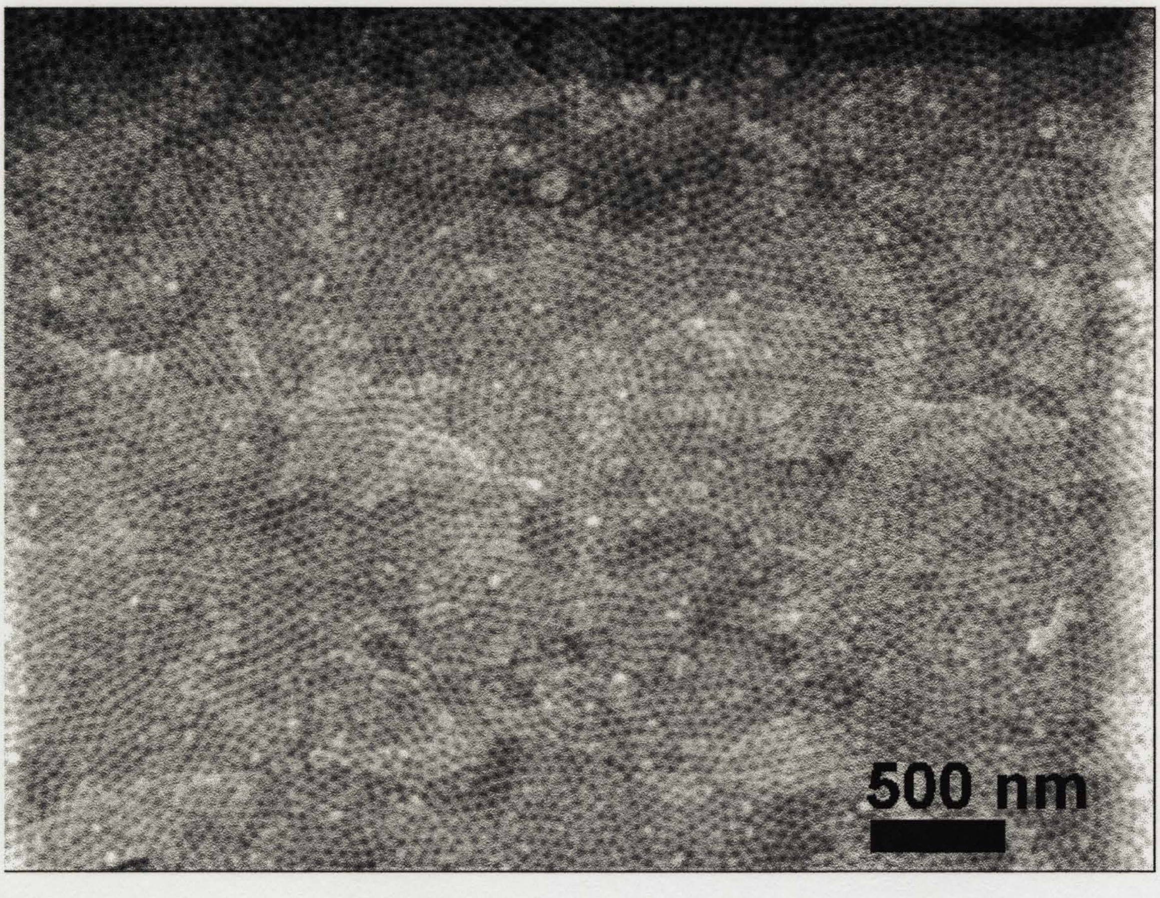

Figure 3.2. Characteristic SEM micrograph of a larger area of a Ti surface after dimpling (electropolishing).

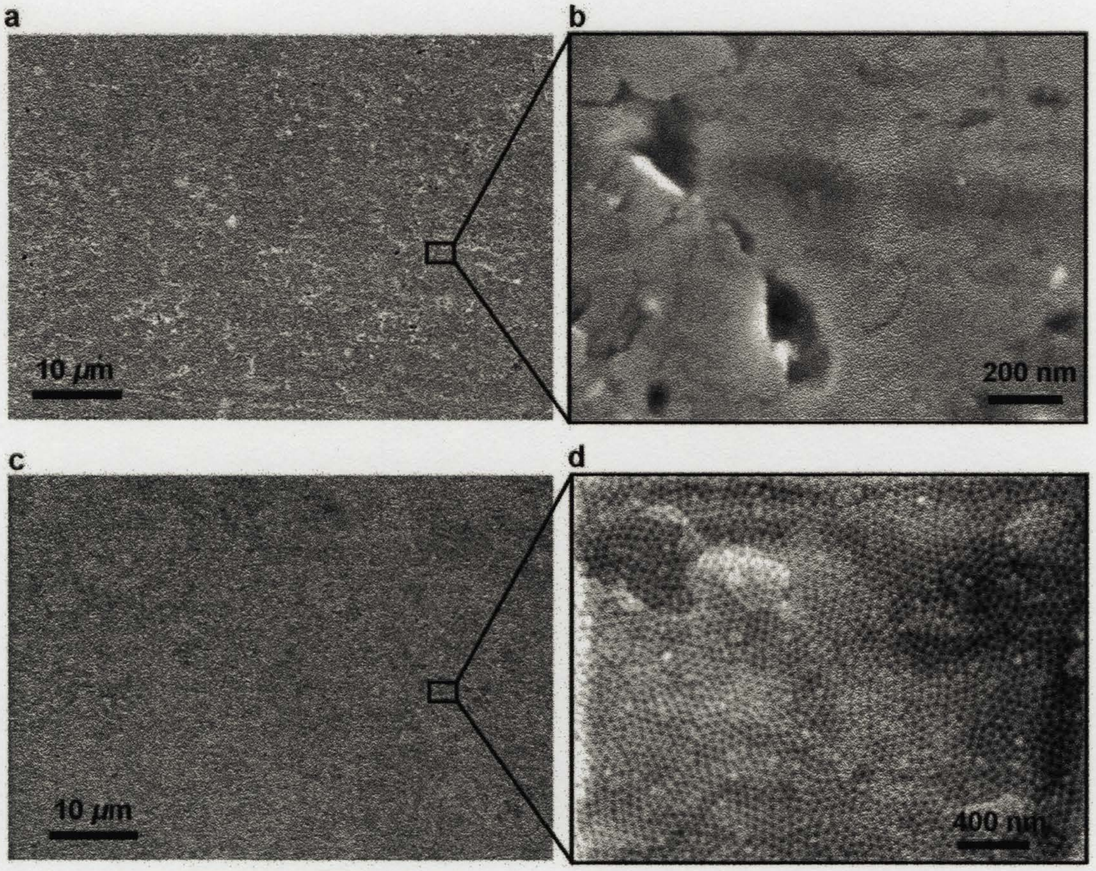

Figure 3.3. Characteristic SEM micrographs of Ti surface before and after dimpling (electropolishing). a, b, SEM micrographs of as-received (untreated) Ti sample surface. c, d, SEM micrographs of electropolished Ti sample showing the long-range order of dimples all over the surface.

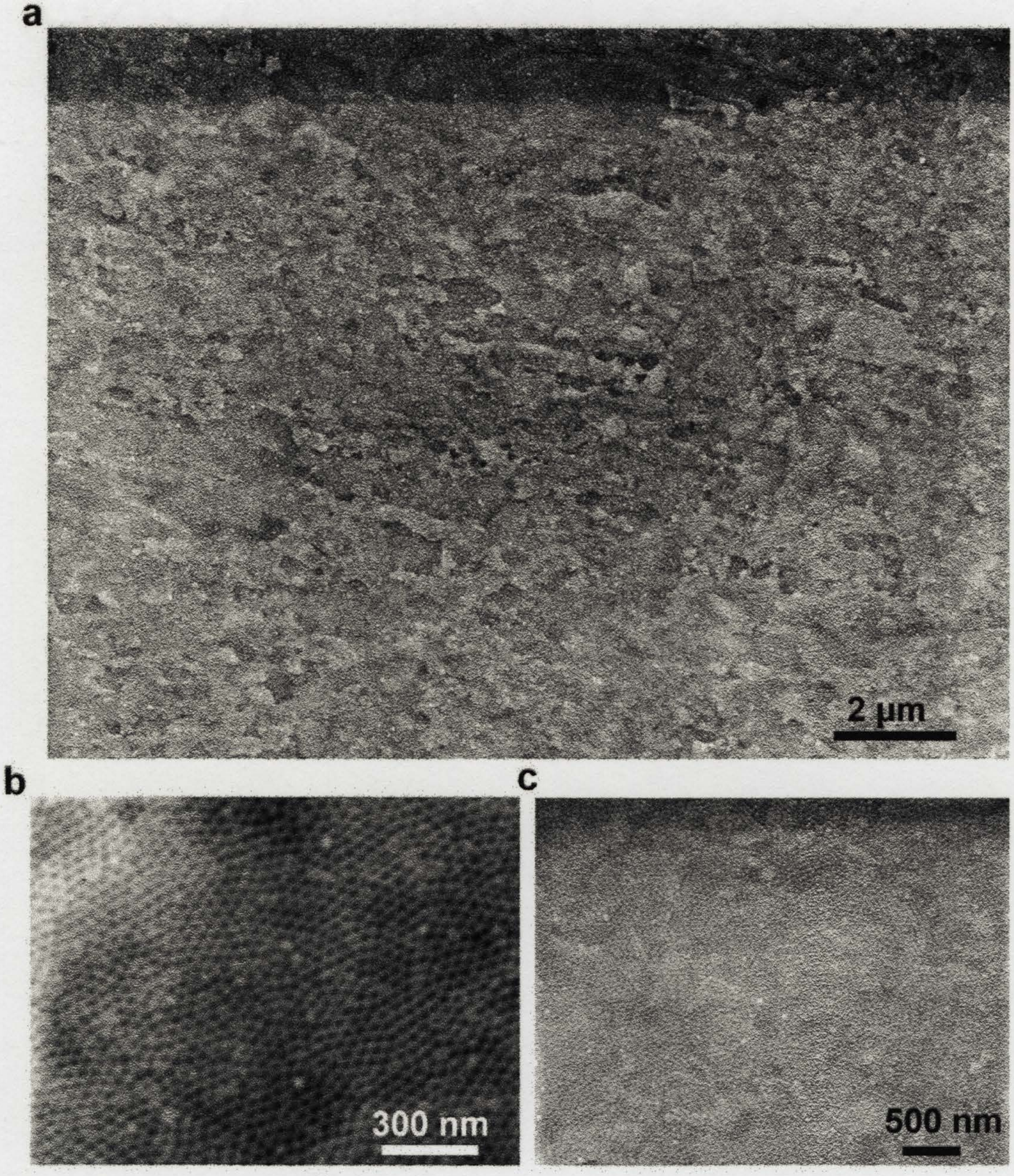

Figure 3.4. More characteristic SEM micrographs from different areas of Ti surface after dimpling (electropolishing) showing the long-range order of dimples all over the surface and hence demonstrating the versatility of the process.

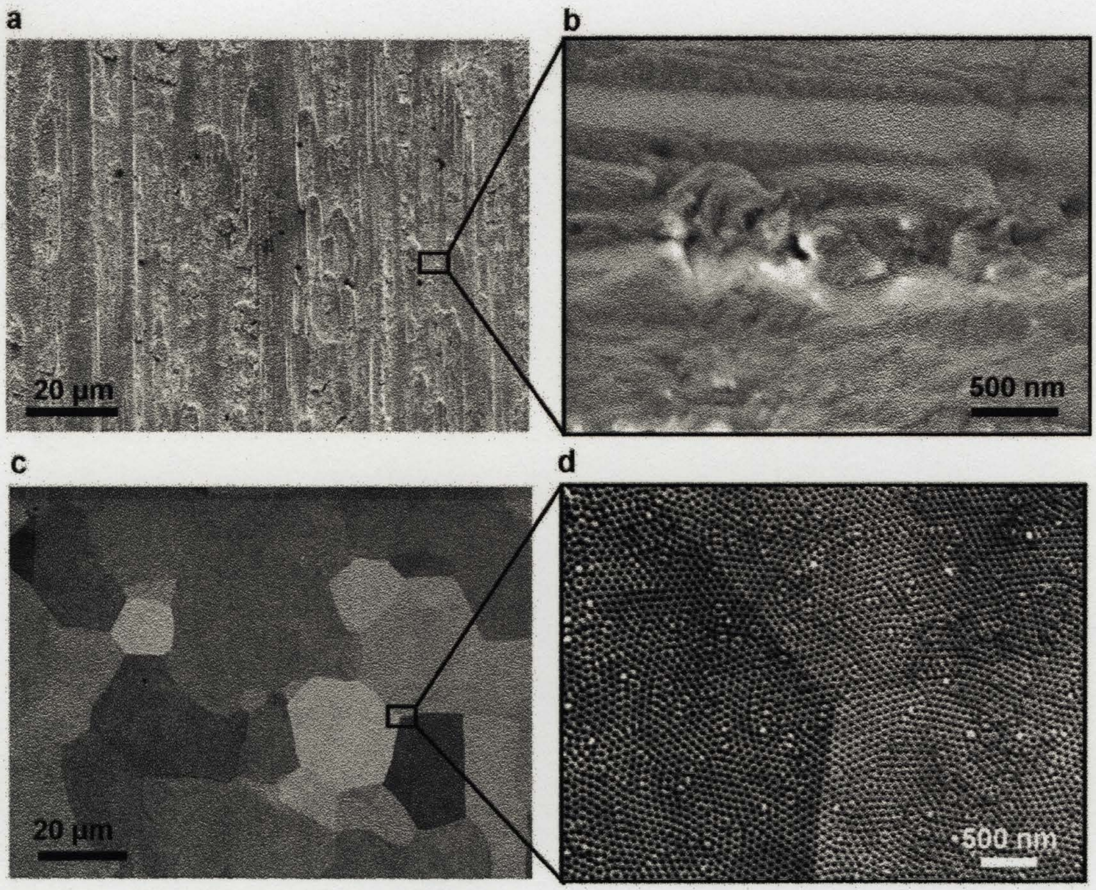

Figure 3.5. Characteristic SEM micrographs of Ta surface before and after dimpling (electropolishing). a, b, SEM micrographs of as-received (untreated) Ta sample surface. c, d, SEM micrographs of electropolished Ta sample surface showing the long-range order of dimples across grain boundaries.

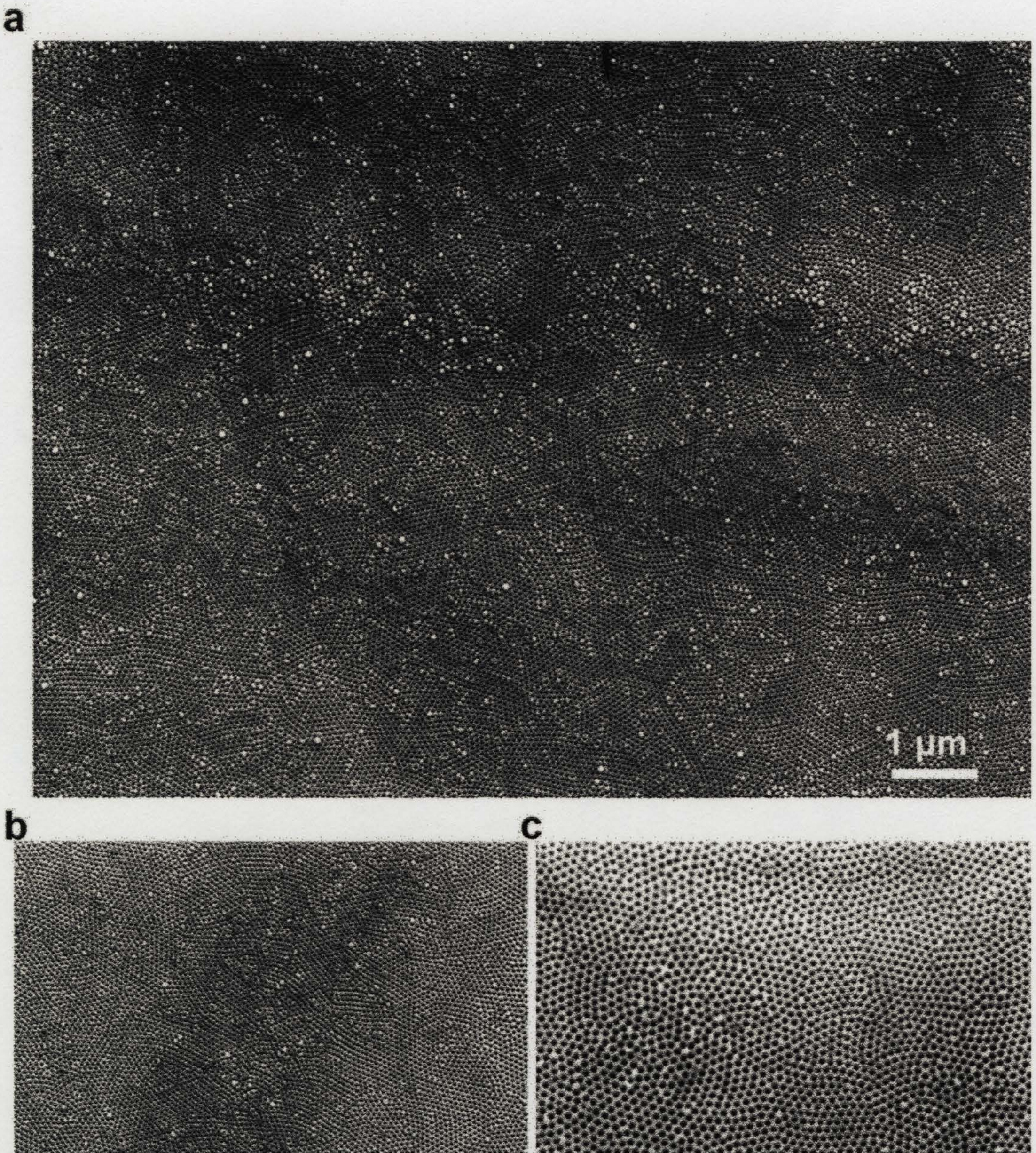

Figure 3.6. More characteristic SEM micrographs from different areas of Ta surface after dimpling (electropolishing) showing the long-range order of dimples all over the surface and hence demonstrating the versatility of the process.

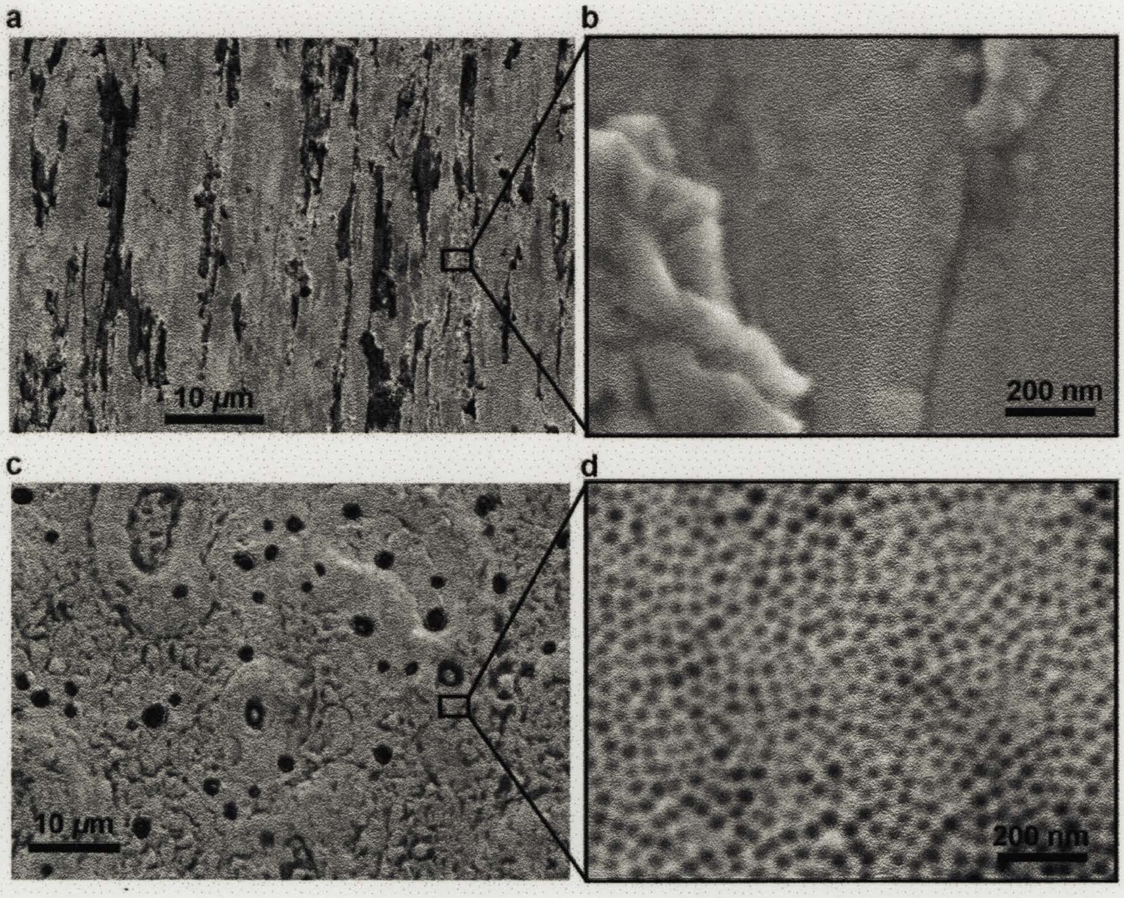

Figure 3.7. Characteristic SEM micrographs of a W surface before and after dimpling (electropolishing). a, b, SEM micrographs of the as-received (untreated) W sample surface. c, d, SEM micrographs of the electropolished W sample surface showing areas with dimples.

3.3 Characteristics of Native Surface Oxide

XPS proves that the dimpled titanium surfaces are also metallic, with only a native oxide cover (Figure 3.8b, d), when compared to unpolished surfaces (Figure 3.8a, c). X-ray photoelectron spectra were measured using a Kratos Axis Ultra X-ray photoelectron spectrometer. Survey scan analyses were carried out with an analysis area of 300 μm x 700 μm and pass energy of 160 eV. High resolution analyses were carried out with an analysis area of (300 x 700) microns^2 and pass energy of 20 eV. Survey spectra of polished samples show slight incorporation of fluorine and sulfur into the dimpled samples (see Figure 3.9). This is expected, because metal oxides grown in concentrated acids are known to incorporate electrolyte anions (F^- and SO_4^{2-}) in the entire depth of the native oxide film and even in the metal part adjacent to the metal/oxide interface. In addition to characteristic SEM images of the untreated and dimpled surfaces, Figure 3.8 also shows deconvoluted Ti 2p peaks of both surfaces. In both cases, the tantalum signal from tantalum oxide dominates the peak. Together with suboxides, over 90% of the signal comes from titanium in the superficial oxide film. Since the inelastic mean free path of the photoelectrons amounts to several nanometers in most solids, however, the metallic titanium signal from the bulk metal can be picked up. The untreated surface is essentially covered by a passive native oxide with a self-limiting thickness upon prolonged exposure to air. The ratio of oxide to metal signal decreases slightly for the dimpled surface, indicating that the dimple structure is metallic in nature, with only a minimal oxide cover as it is to be expected after exposure to air.

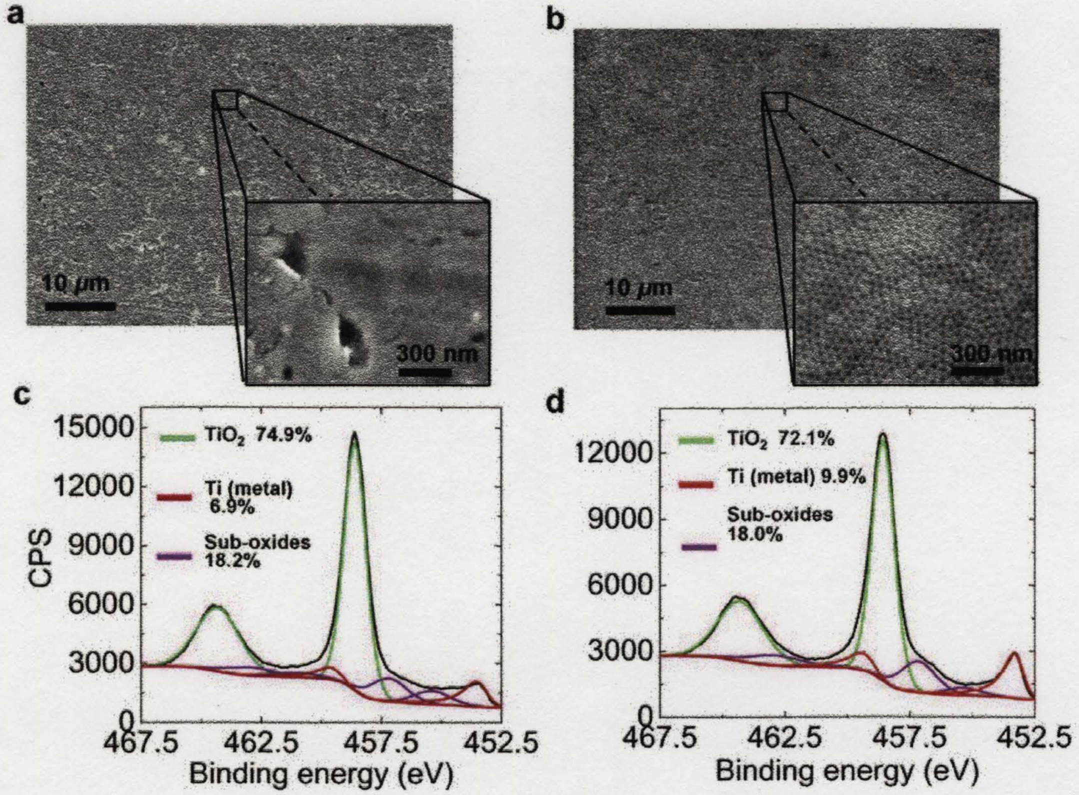

Figure 3.8. Comparison of SEM images and XPS spectra of titanium foil before and after dimpling **(a)** SEM image of the untreated titanium surface. **(b)** SEM image of the dimpled titanium surface. **(c)** Deconvoluted Ti 2p peak of the untreated titanium surface. **(d)** Deconvoluted Ti 2p peak of the dimpled titanium surface.

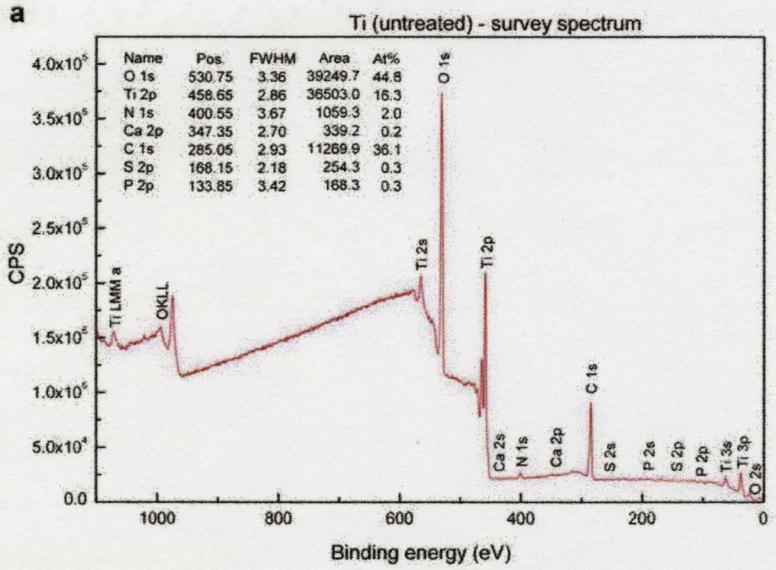

Name	Pos.	FWHM	Area	At%
O 1s	530.75	3.36	39249.7	44.8
Ti 2p	458.65	2.86	36503.0	16.3
N 1s	400.55	3.67	1059.3	2.0
Ca 2p	347.35	2.70	339.2	0.2
C 1s	285.05	2.93	11269.9	36.1
S 2p	168.15	2.18	254.3	0.3
P 2p	133.85	3.42	168.3	0.3

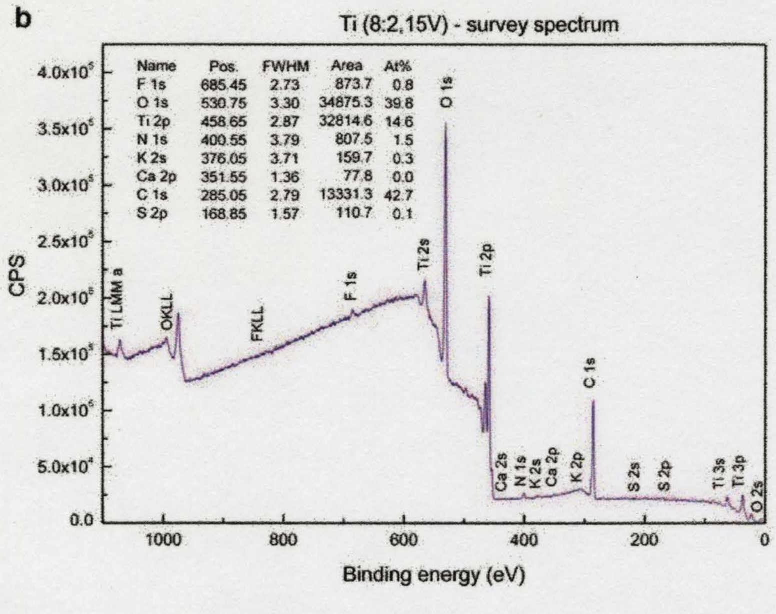

Name	Pos.	FWHM	Area	At%
F 1s	685.45	2.73	873.7	0.8
O 1s	530.75	3.30	34875.3	39.8
Ti 2p	458.65	2.87	32814.6	14.6
N 1s	400.55	3.79	807.5	1.5
K 2s	376.05	3.71	159.7	0.3
Ca 2p	351.55	1.36	77.8	0.0
C 1s	285.05	2.79	13331.3	42.7
S 2p	168.85	1.57	110.7	0.1

Figure 3.9. Core-level spectra of Ti surface before (as received) and after dimpling (electropolishing). a, Survey XPS scan from untreated (as received) Ti sample show Ti, O, C and N peaks. b, whereas Survey XPS scan from electropolished Ti sample show small F core-level band along with other Ti, O, C and N signature peaks. Both the sample surfaces were carefully rinsed in acetone, methanol, and Millipore water (18.2 MΩ cm resistivity) before taking the spectra.

The dimple structures on tungsten are of similar periodicity and regularity. XPS once again shows that they are also clearly metallic in nature. Figure 3.10 shows SEM and XPS data comparing the untreated to the dimpled surface. In this case in fact, since electropolishing leads to a smoother surface, the corresponding spectrum of the dimpled surface (W 3f peak, Figure 3.10d) shows less oxide than the spectrum of the untreated surface (W 3f peak, Figure 3.10c). Survey spectra of W also show presence of Ni on the W surface (see Figure 3.11).

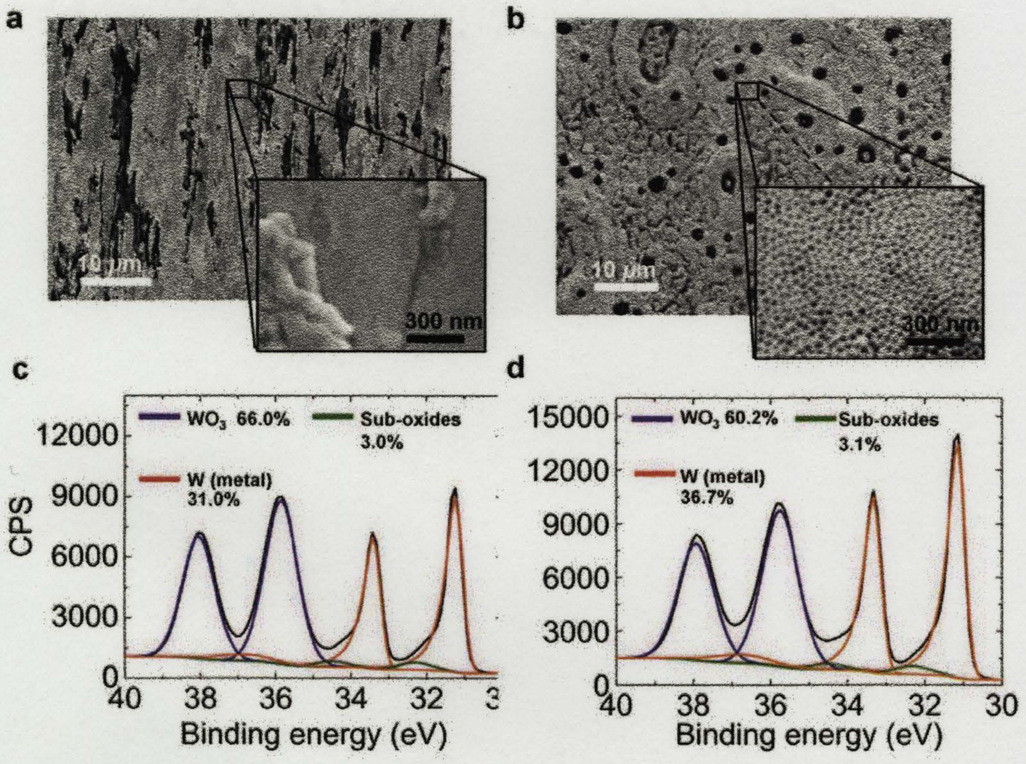

Figure 3.10. Comparison of SEM images and XPS spectra of tungsten ribbon before and after dimpling **(a)** SEM image of the untreated tungsten surface. **(b)** SEM image of the dimpled tungsten surface. **(c)** Deconvoluted W 4f peak of the untreated tungsten surface. **(d)** Deconvoluted W 4f peak of the dimpled tungsten surface.

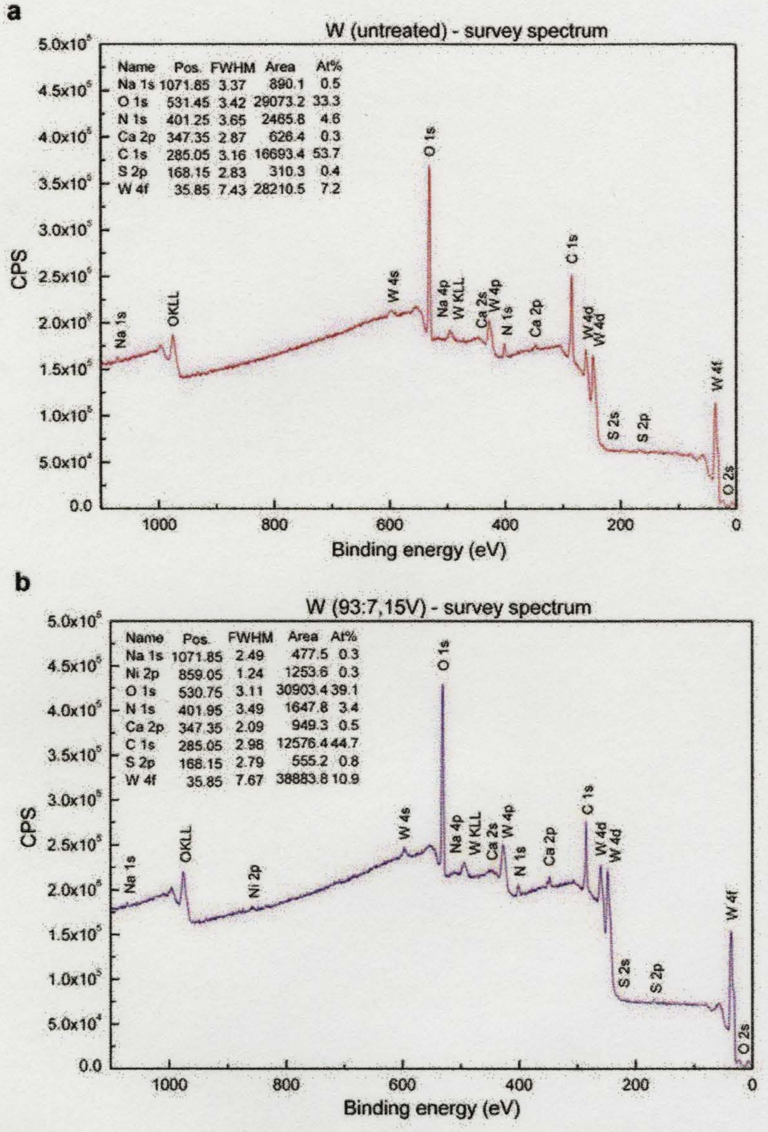

Name	Pos.	FWHM	Area	At%
Na 1s	1071.85	3.37	890.1	0.5
O 1s	531.45	3.42	29073.2	33.3
N 1s	401.25	3.65	2465.8	4.6
Ca 2p	347.35	2.87	626.4	0.3
C 1s	285.05	3.16	16693.4	53.7
S 2p	168.15	2.83	310.3	0.4
W 4f	35.85	7.43	28210.5	7.2

Name	Pos.	FWHM	Area	At%
Na 1s	1071.85	2.49	477.5	0.3
Ni 2p	859.05	1.24	1253.6	0.3
O 1s	530.75	3.11	30903.4	39.1
N 1s	401.95	3.49	1647.8	3.4
Ca 2p	347.35	2.09	949.3	0.5
C 1s	285.05	2.98	12576.4	44.7
S 2p	168.15	2.79	555.2	0.8
W 4f	35.85	7.67	38883.8	10.9

Figure 3.11. Core-level spectra of W surface before (as received) and after dimpling (electropolishing). a, Survey XPS scan from untreated (as received) W sample show W, O, Na, Ca, C and N peaks. b, whereas Survey XPS scans from electropolished W sample show small Ni and S core-level bands along with other W, O, Na, Ca, C and N signature peaks. Both the sample surfaces were carefully rinsed in acetone, methanol, and Millipore water (18.2 MΩ cm resistivity) before taking the spectra.

3.4 Effect of Impurities on Pattern Formation

It was observed in the case of tungsten that the presence of trace amount of impurities gives rise to deterioration of order of dimples but not in case of tantalum and titanium. The certificates of analysis of Ti, Ta and W showing the presence of different impurities are provided in the (Appendix B) data. To examine the spatial effect of other metal impurities on pattern formation over the W surface we mapped the elemental distribution using energy-dispersive X-ray spectroscopy (EDX) over part of the electropolished tungsten (99.95 % pure) surface. A compositional SEM image of the metal surface is shown in Figure 3.12a and corresponding W, Ni and O maps are displayed in color in Figure 3.12b, c and d. The darker regions in the SEM micrograph have higher concentrations of Ni and O and exhibit either no dimples or poorly ordered dimples. SEM imaging was performed with a JEOL JSM-7000F Scanning Electron Microscope, equipped with a Schottky type Field Emission Gun (FEG) filament. Energy dispersive X-ray (EDX) mapping was carried out using a 10 kV electron beam to obtain the distribution of O, Ni and W on the electropolished W surface. INCA 300 (EDX System, Oxford, UK) software was used for data acquisition and analysis. High resolution XPS spectra of tungsten before and after dimpling (Figure 3.13) shows no noticeable peaks corresponding to Ni or NiO in case of untreated sample but clear peaks of Ni, NiO and Ni_2O_3 in case of dimpled surface.

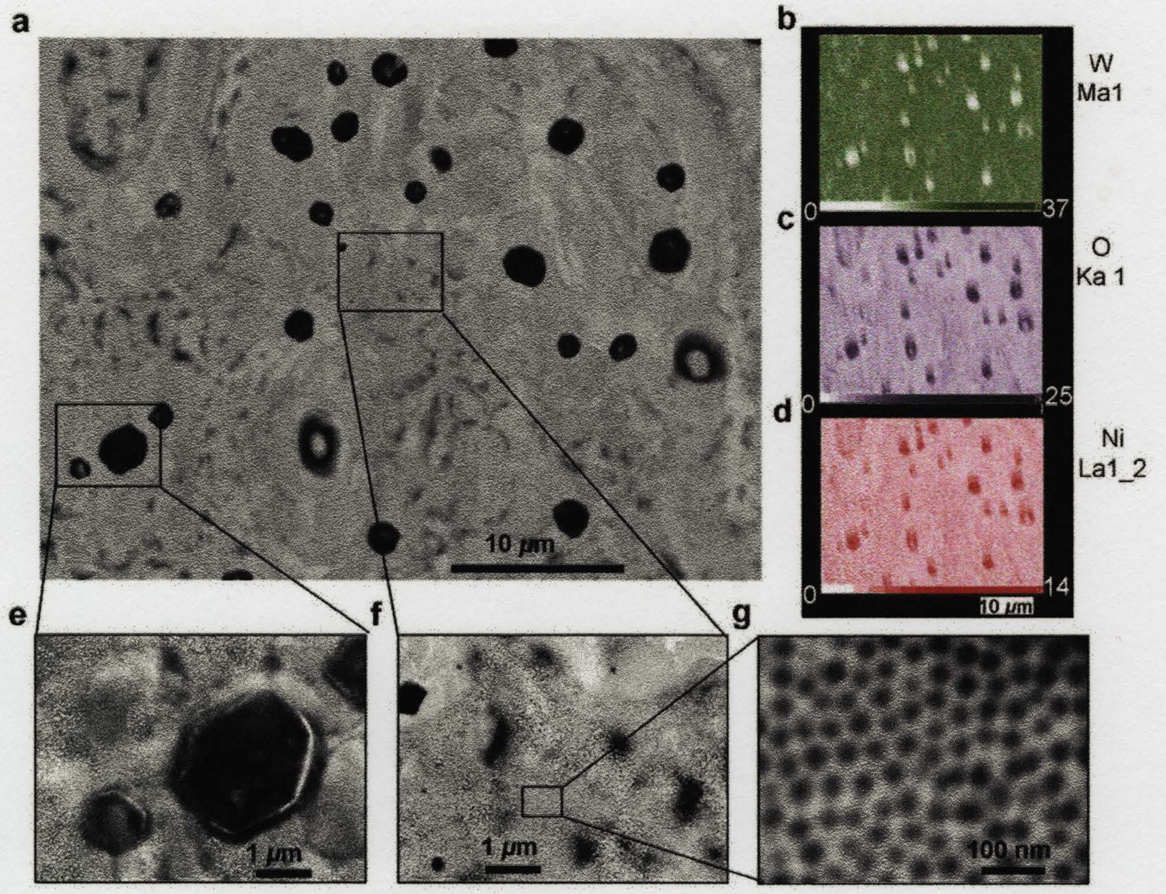

Figure 3.12. The presence of Ni as an impurity among other impurities in ppm amounts in W sample affects the order and quality of dimples. **(a)** SEM micrograph of electropolished W surface in compositional mode. **(b)** Elemental composition map of the same area as in (a) of W **(c)** O and **(d)** Ni obtained by EDX mapping . The intensity of the elements W, O, and Ni are shown on the map images itself with respect to the zero energy loss peak. **(e)** SEM micrograph in compositional mode showing the area having the NiO debris surrounded by irregular dimples. **(f)** SEM micrograph demonstrating that the regularity and order of dimples is high away from NiO rich areas. **(g)** Regular dimples in the area having no Ni present.

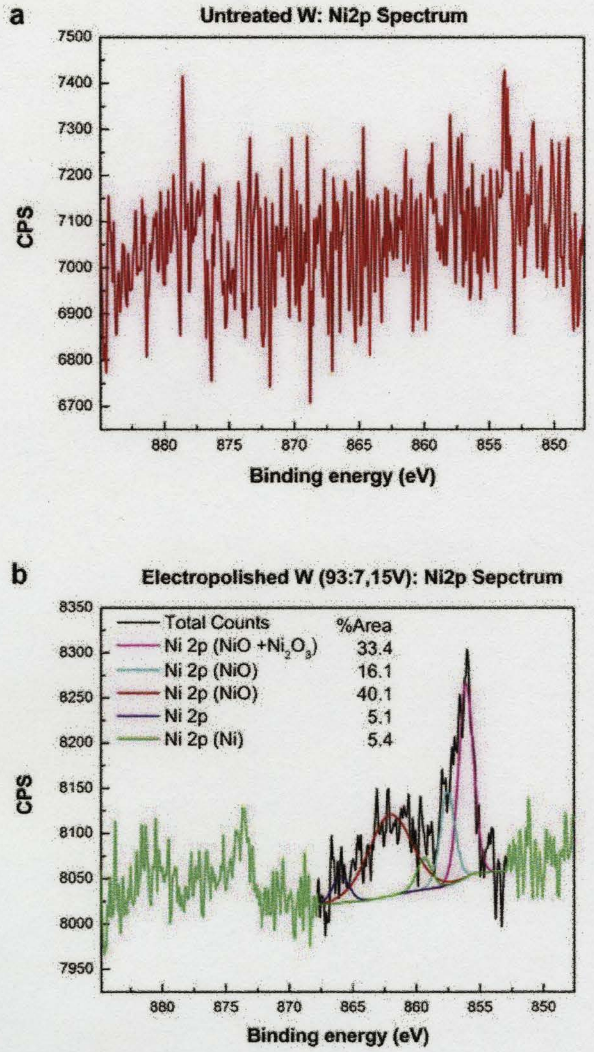

Figure 3.13. High resolution XPS spectra of W surface **a,** before and **b,** after dimpling (electropolishing). HR-XPS spectra from electropolished W sample **(b)** show the emergence of Ni, NiO and Ni_2O_3 signature peaks.

The combined analysis of EDX mapping and XPS data of unpolished and electropolished W surfaces leads to several conclusions. The electropolishing of 99.95% pure W surface either leads to a huge migration of Nickel (Ni) to the substrate surface or the process leaves the Ni behind on the surface of the metal without dissolving it; Ni sits on the surface as Nickel oxide. However there were no traces of iron (Fe) and other metals present in the tungsten foil as trace amounts left on the surface showing that they dissolve or do not migrate to the surface. The oxygen concentration is higher at areas where there is more nickel and the order of dimples on the surface is worse at these places. The results also suggest that deliberate introduction of some other ions may also introduce some changes in the size and shape of these nanostructures.

The electrolyte composition has to be varied in each case in order to achieve reaction speeds that ensure ordering. A mixture of concentrated HF (48%) and concentrated H_2SO_4 (95-98%) was used for titanium (20:80) and tungsten (7:93), comparable to the previously reported conditions for tantalum (10:90).[19] As it has been established earlier, the role of the concentrated sulfuric acid in the case of tantalum chiefly consists in degrading the quality of the formed oxide, hence increasing its solubility.[24] Because zirconium is much more soluble in hydrofluoric acid than the other metals, a dilute aqueous ammonium fluoride solution (0.5 M NH_4F) was found to be more appropriate for it. F^- ions are still required in order to sustain the strong driving force required for ordered dimple formation, while bulk composition and viscosity of the electrolyte solution only play a minor role in the process. Whether fluorine ions are essential for the pattern formation or merely a part of the etching chemistry for selected metals may only be speculated at this point, although it should be noted that nanoscale patterns with a comparable appearance and length scale have previously been observed as a result of electropolishing of aluminum in a fluoride-free solution.[22] Figure 3.14a shows

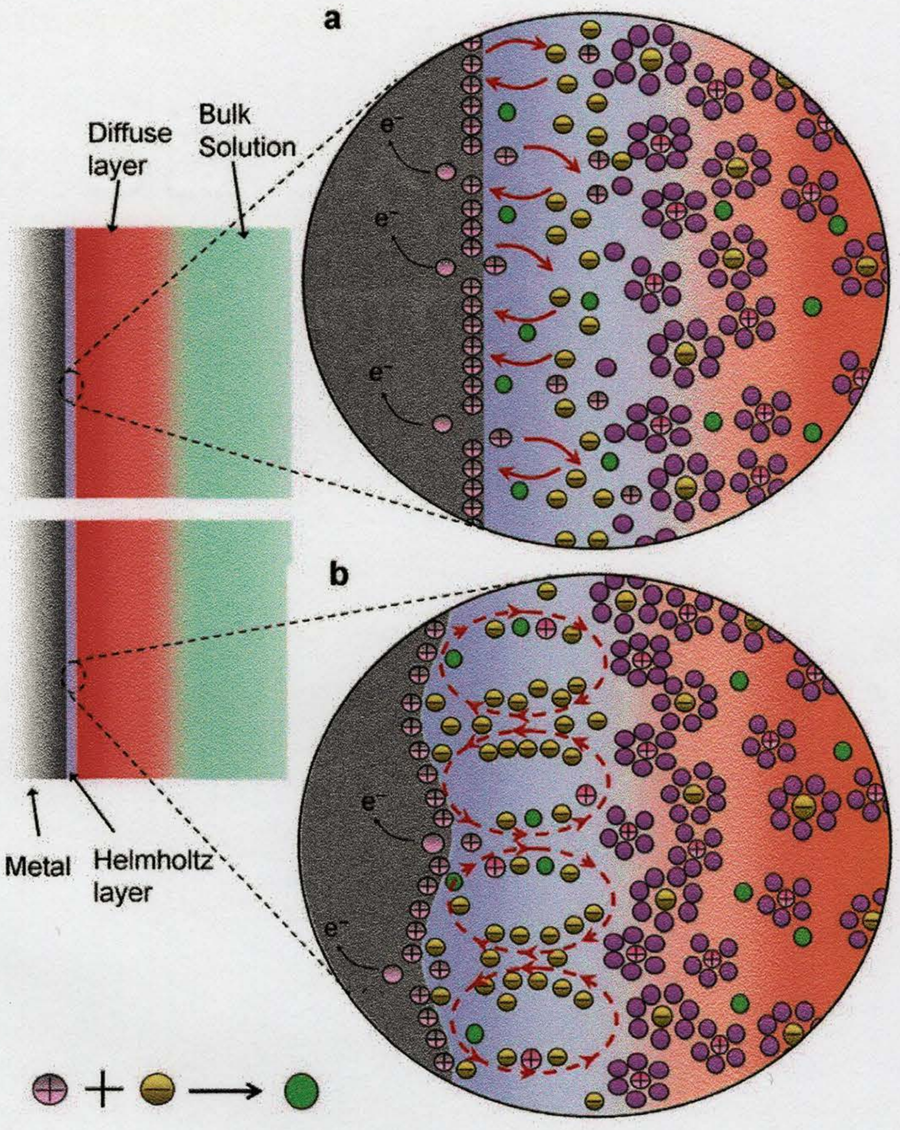

Figure 4.1. Mechanistic illustration of the Helmholtz layer under equilibrium and non-equilibrium conditions (not to scale) during the etching of the metal surface. **(a)** Undisturbed Helmholtz layer with minimal diffusion in the case of a very slow reaction. **(b)** Under vigorous reaction conditions, the layer may break up into convection cells to allow for fast electromigration of large amounts of reactants and products which leads to the dimpled morphology of the metal surface.

a partially dimpled zirconium surface. SEM images of dimpled zirconium reveal that the comparatively high speed of oxidation resulted in a mixture of dimpled regions (Figures 3.1f and 3.14b) and undissolved porous oxide (Figure 3.14c), making it difficult to determine the oxide layer thickness at the dimpled spots by XPS.

	Ta	Ti	W	Zr
Dimple Depth [nm]	10	3	6	n/a
Periodicity of Dimple Pattern [nm]	55-60	55-60	55-60	40-45
Optimal Voltage [V]	15	15	15	20
Etch Mixture c.H_2SO_4: c.HF	9:1	8:2	93:7	0.5 M NH_4F

Table 1. Comparison between etching conditions and dimple properties on different metal surfaces.

A comparison between the different metals reveals many commonalities, but also some significant differences. (Table 1) The optimal voltage stayed the same for all metals etched under non-aqueous conditions, so did the periodicity of the pattern. Larger voltages for these systems typically lead to slightly larger dimples (see ref. 18). In the case of zirconium it was necessary to switch to a dilute aqueous ammonium fluoride solution. Here, the required optimum voltage was higher, but the resulting dimple size was smaller, clearly due to resulting changes at the electrolyte-anode interface, e.g. properties of the electrochemical double layer. The regular pattern formation on metals etched under non-aqueous conditions was highly sensitive to the composition of the solution. In contrast to the constant periodicity of the dimple pattern for these systems, the depth of the dimples varied significantly between metals, but never came close to fulfilling the IUPAC definition of a pore (depth equal or greater than radius).

3.5 Conclusions

Dimple formation has now been demonstrated with a high level of uniformity on tantalum, titanium, tungsten and zirconium. As we have demonstrated in this work, electrochemical dimple array formation is an astonishingly robust process. We are currently working on expanding it to other materials, such as titanium alloys for biomedical applications. In that context it will need to be considered that on chemically heterogeneous surfaces, pattern formation will occur selectively. A good example for that are nickel impurities on a tungsten surface, because nickel oxide is formed and not readily dissolved under the optimal conditions for dimple formation on tungsten. A perturbation in the dimple pattern can be observed near the nickel islands. Heterogeneous surface compositions will allow for area-selective pattern formation. The process is self-limiting and results in uniformly shallow features, which can then provide templates for subsequent processing[13] if higher aspect ratio features are desired for applications such as the formation of biocompatible surfaces for which the 50 nm length scale is very important[25] or as a template for catalyst nanoparticle formation.[18,26] Since the process is not tied to a specific chemistry, highly ordered dimple patterns can likely be formed on any conducting or semiconducting surface amenable to electropolishing, leading to a range of potential applications in sensor array fabrication,[27] combinatorial synthesis,[28] templated nanostructure growth, composite materials, electronics, catalysis, photovoltaics and biomaterials.

3.6 Experimental Section

H_2SO_4 (95-98%, reagent grade) , HF (48%), acetone and methanol (both semiconductor grade) were purchased from Fisher Scientific. NH_4F (40%, semiconductor grade) was purchased from Sigma Aldrich. All chemicals were used as received. Tantalum (99.95%), titanium (99.95%) and zirconium foil (99.5%, all 0.127 mm thick) as well as tungsten ribbon (99.95%, 0.125 mm thick, all Alfa-Aesar) were mechanically cut and rinsed with acetone, methanol and then with Millipore water (18.2 MΩ.cm resistivity) and then dried under argon flow before use.

Ti, W, Zr and Ta surfaces were electropolishing using a conventional two-electrode system connected to a power supply (Agilent E3615A). A Pt/Ir wire (0.25 mm diameter) was used as the counter-electrode (cathode). The working electrode (anode) was a tantalum, titanium, zirconium or tungsten foil substrate connected with an alligator clip and copper wire to the power supply. The distance between the working and counter-electrodes was kept at approximately 1.5 cm. Ta, Ti and W were dimpled in a stirred mixture of concentrated H_2SO_4 (95-98%) and HF (48%) in volumetric ratios of 9:1 (Ta), 93:7 (Ti) and 8:2 (W) by applying a constant DC voltage of 15 V for 5 min (Ta), 2 min

(Ti) and 10 min (W) respectively. Zr foil was dimpled in 0.5 M NH_4F at 20V for 5 min. The typical sample size was 5 mm wide and 30 mm long, with one third of the length immersed in the electrolyte. The solution was stirred using a magnetic stir-bar. All samples were thoroughly rinsed with Millipore water (18.2 MΩ.cm resistivity) and then dried under argon flow after electropolishing. Freshly mixed electrolytic solutions typically need to settle for a 16-20 hours before the first sample is processed. All experiments were performed at room temperature (approximately 20 °C).

X-ray photoelectron spectra were measured using a Kratos Axis Ultra X-ray photoelectron spectrometer. XPS can detect all elements except hydrogen and helium, probes the surface of the sample to a depth of 7-10 nanometres, and has detection limits ranging from 0.1 to 0.5 atomic percent depending on the element. Survey scan analyses were carried out with an analysis area of (300 x 700) microns and pass energy of 160 eV. High resolution analyses were carried out with an analysis area of (300 x 700) microns and pass energy of 20 eV.

Atomic force microscopy was performed in tapping mode on a Veeco Enviroscope with a Nanoscope IIIa controller and Veeco RTESP p-doped Si tips with a nominal radius of less than 10 nm. Typical scan rates were 2 micrometer per second and the images were constructed with 512 scan lines. Care was taken to ensure that the tip was not modifying the surface during the scan. A large number of images of the same sample were obtained with different tips to pinpoint the exact depth of dimples by eliminating tip convolution effects. The data was analysed using DI V5.30r3.sr3 software.

SEM imaging was performed with a JEOL JSM-7000F Scanning Electron Microscope, equipped with a Schottky type Field Emission Gun (FEG) filament. Energy dispersive X-ray (EDX) mapping was carried out using a 10 kV electron beam to obtain the distribution of O, Ni and W on the electropolished W surface. INCA 300 (EDX System, Oxford, UK) software was used for data acquisition and analysis.

Author Contributions:

This chapter is based on a manuscript which has been submitted for publication. The author contributions for the work presented in this chapter are as follows. S. S. participated in the experimental design, performed the experiments, analyzed the data, put together the figures and contributed to the manuscript. W.R.T.B. assisted in the experiments and contributed to the figures. P.K. participated in the experimental design and contributed to the manuscript. All authors discussed the results and commented on the manuscript.

3.7 Bibliography

(1) Stewart, M. E., Motola, M. J., Yao, J., Thompson, L. B. & Nuzzo, R. G. Unconventional methods for forming nanopatterns. *Proc. IMechE Part N* **2007**, *220*, 81-138.

(2) Whitesides, G. M. & Grzbowski, B. Self assembly at all scales. *Science* **2002**, *295*, 2418-2421.

(3) Stupp, S. I., LeBohneur, V., Walker, K., Li, L. S., Huggins, K. E., Keser, M. & Amstutz, A., Supramolecular materials: Self-organized nanostructures. *Science* **1997**, *276*, 384-389.

(4) Henzie, J., Barton, J. E., Stender, C. L. & Odom, T. W. Large-area nanoscale patterning: Chemistry meets fabrication. *Acc. Chem. Res.* **2006**, *39*, 249-257.

(5) Pawin, G., Wong, K. L., Kwon, K. Y. & Bartels, L. A homomolecular porous network at a Cu(111) surface. *Science* **2006**, *313*, 961-962.

(6) Qiao, Y., Wang, D. & Buriak, J. M. Block Copolymer Templated Etching on Silicon. *Nano Lett.* **2007**, *7*, 464-469.

(7) Bullen, H. A. & Garrett, S. J. TiO_2 nanoparticle arrays prepared using a nanosphere lithography technique. *Nano Lett.* **2002**, *2*, 739-745.

(8) Thompson, G. E., Furneaux, R. C., Wood, G. C., Richardson, J. A. & Goode, J. S. Nucleation and growth of porous anodic films on aluminum. *Nature* **1978**, *272*, 433-435.

(9) Masuda, H. & Fukuda, K. Ordered metal nanohole arrays made by a 2-step replication of honeycomb structures of anodic alumina. *Science* **1995**, *268*, 1466-1468.

(10) Lee, W., Ji, R., Gosele, U. & Nielsch, K. Fast fabrication of long-range ordered porous alumina membranes by hard anodization. *Nature Mater.* **2006**, *5*, 741-747.

(11) Cai, Q. Y., Paulose, M., Varghese, O. K. & Grimes, C. A. The effect of electrolyte composition on the fabrication of self-organized titanium oxide nanotube arrays by anodic oxidation. *J. Mater. Res.* **2005**, *20*, 230-236.

(12) Sieber, I., Kannan, B. & Schmuki, P. Self-assembled porous tantalum oxide prepared in H_2SO_4/HF electrolytes. *Electrochem. Solid State Lett.* **2005**, *8*, J10-J12.

(13) Singh, S., Greiner, M. T. & Kruse, P. Robust inorganic membranes from detachable ultra-thin tantalum oxide films. *Nano Lett.* **2007**, *7*, 2676-2683.

(14) Sieber, I., Hildebrand, H., Friedrich, A. & Schmuki, P. Formation of self-organized niobium porous oxide on niobium. *Electrochem. Commun.* **2005**, *7*, 97-100.

(15) Cathcart, J. V., Bakish, R. & Norton, D. R. Oxidation Properties of Tantalum Between 400° and 530°C. *J. Electrochem. Soc.* **1960**, *107*, 668-670.

(16) Pawel, R. E. & Lundy, T. S. A submicron sectioning technique for analyzing diffusion specimens of tantalum and niobium. *J. Appl. Phys.* **1964**, *35*, 435-438.

(17) Ueno, K., Abe, S., Onoki, R. & Saiki, K. Anodization of electrolytically polished Ta surfaces for enhancement of carrier injection into organic field-effect transistors. *J. Appl. Phys.* **2005**, *98*, 114503.

(18) El-Sayed, H., Singh, S., Greiner, M. T. & Kruse, P. Formation of Highly Ordered Arrays of Dimples on Tantalum at the Nanoscale. *Nano Lett.* **2006**, *6*, 2995-2999.

(19) El-Sayed, H., Singh, S. & Kruse, P. Formation of Dimpled Tantalum Surfaces from Electropolishing. *J. Electrochem. Soc.* **2007**, *154*, C728-C732.

(20) Yuzhakov, V. V., Chang, H. C. & Miller, A. E. Pattern formation during electropolishing. *Phys. Rev. B* **1997**, *56*, 12608.

(21) Konovalov, V. V., Zangari, G. & Metzger, R. M. Highly ordered nanotopographies on electropolished aluminum single crystals, *Chem. Mater.* **1999**, *11*, 1949-1951.

(22) Caicedo-Martinez, C. E., Koroleva, E. V., Thompson, G. E., Skeldon, P., Shimizu, K., Habazaki, H. & Hoellrig, G. Surface nanotextures on aluminium. *Surf. Interface Anal.* **2002**, *34*, 405–408.

(23) Zhao, G.-Y., Xu, C. L., Guo, D. J., Li, H. & Li, H.-L. Patterning polycrystalline aluminum by electropolishing at low voltages. *J. Solid State Electrochem.* **2006**, *10*, 266–269.

(24) Vermilyea, D. A. Formation of anodic oxide films on tantalum on non-aqueous solutions. *Acta Metall.* **1954**, *2*, 483-486.

(25) Cavalcanti-Adam, E. A., Volberg, T., Micoulet, A., Kessler, H., Geiger, B. & Spatz, J. Cell spreading and focal adhesion dynamics are regulated by spacing of integrin ligands. *Biophys. J.* **2007**, *92*, 2964-2974.

(26) Wu, Z. H., Mei, X. Y., Kim, D., Blumin, M. & Ruda, H. E. Growth of Au-catalyzed ordered GaAs nanowire arrays by molecular-beam epitaxy. *Appl. Phys. Lett.* **2002**, *81*, 5177-5179.

(27) Furhop, J.-H. Molecular interactions in solvent-filled yoctowells (10^{-24} L) and zeptowells (10^{-21} L). *Curr. Opin. Coll. Interf. Sci.* **2008**, *13*, 81-85.

(28) Barton, J. E. & Odom, T. W. Mass-limited growth in zeptoliter beakers: A general approach for the synthesis of nanocrystals. *Nano Lett.* **2004**, *4*, 1525-1528.

Chapter-4

Dissipative Nanopatterning on Electropolished Surfaces as an Alternative to Self-assembly.

Dissipative pattern formation is a dynamic process far from equilibrium which is driven by the dissipation of energy, in contrast to equilibrium processes known as self-assembly which converge towards a minimum in free energy. We report the first nanoscale example of a dissipative pattern formation process, during which the electrochemical double layer breaks up into ordered electrohydrodynamic convection cells due to strong concentration gradients near the surface. We predict that these patterns can be formed on any conducting or semiconducting substrate.

4.1 Introduction

Nature has a number of intriguing ways of forming functional and beautiful patterns.[1] We can distinguish between equilibrium processes that converge towards a minimum in free energy (a. k. a. self-assembly)[2] and dynamic processes far from equilibrium which sustain a pattern only as long as they are driven by the dissipation of energy.[3,4] Ordered patterns may form during a dissipative process if the ordering allows for a speed-up in energy dissipation (steepest gradient). These dynamic patterns may be made permanent if there is a mechanism for imprinting them onto a substrate. Dissipative processes with characteristic length scales between kilometers and micrometers are well-known and have been intensely studied.[3,4,5,6,7,8,9,10] Even though self-assembly processes are well-established for the nanostructuring of materials,[2,11,12,13] no examples of dissipative processes are documented at the nanoscale. Here we show that the previously reported formation of highly ordered arrays of nanoscale dimples on tantalum,[14,15,16,17] titanium,[18] tungsten[18] and zirconium[18] is due to a electrohydrodynamic convection in solution, which imprints itself onto the metal surface. This dissipative process is driven by the concentration gradient of fresh etchant and etching products near the surface, leading to a break-up of the electrochemical double layer into ordered migration cells. We postulate that, given an appropriate electropolishing chemistry, these patterns can be formed on virtually any metal or semiconductor surface. The fundamentally different mechanism also explains why the order of the dimples is significantly higher than in the cases of porous silicon[19] or anodic porous oxides.[20,21,22,23,24]

Unlike in the case of self-assembly, dissipative processes (e. g. formation of sand dunes or stripes of a zebra) are typically associated with large length scales, much larger than the individual particles involved. Self-assembly processes are based on the tendency of a near-equilibrium system to strive towards a minimum in free energy, for example during reconstruction and monolayer formation on surfaces, dewetting, block-copolymer or surfactant assembly as well as macromolecular assembly due to hydrogen bond formation. A well-studied example of a dissipative process is Rayleigh-Benard convection in a thin layer such as that in the case of oil that is heated in a frying pan.[3]

The oil closest to the pan is heated first and expands thermally. It now has a lower density than the oil layer above, and gravity causes it to rise to the top while the heavier, colder oil sinks to the bottom. When the hot oil reaches the top, it cools down, increasing its density whereas the cold oil that had sunk to the bottom is heated up. This process is repeated many times, driven by the temperature gradient across the liquid layer. If it is driven hard enough, very regular striped or hexagonal convection cells emerge in order to facilitate efficient circulation of the oil. If it is driven too hard, the system becomes turbulent. If the pan is removed from the heat, the convection stops and the patterns disappear without a trace. Until now, a dissipative process with a characteristic length scale in the nanometer regime had not been identified.

Rayleigh-Benard style convection in particular is difficult to sustain at the nanoscale because the Rayleigh number R of the system must remain above a critical value R_c = 1707.76 in order for pattern formation to occur.[3] R is proportional to the third power of the characteristic length scale, which is comparable to the thickness of the convection layer. For theorists conducting molecular dynamics simulations, it is possible to initiate Rayleigh-Benard convection at the nanoscale by increasing gravity by factors of 2.7×10^{12} (ref. 25) or larger[26] compared to the surface of the earth. For the experimentalist, this approach is rather impractical. Instead, we can overcome this limitation by adding a stronger driving force than buoyancy, namely an electric field. Nematic liquid crystals driven by an electric field have been shown to exhibit Rayleigh-Benard style migration patterns at a smaller-than-usual length scale down to about 5 μm.[27] Rayleigh-Benard style convection between electrodes has been observed to facilitate ionic transport in electrochemical systems in cases where the distance between the electrodes was reduced to values less than 1 mm, thus imprinting a characteristic length scale in the millimeter or micrometer range onto the system.[28,29] Electrohydrodynamically driven convection in the outer boundary layer above an individual electrode has also been described recently, but once again only for micrometer scale systems.[29] If one was to desire a characteristic length in the nanometer regime, a suitably thin layer needs to be selected, such as the electrochemical double layer itself, that forms at an electrode in an electrochemical system.

Patterns arising from electrohydrodynamic convection have to be carefully distinguished from the more common chemical oscillations and patterns observed in electrochemical systems.[4,30,31] Temporal oscillations[32] and spatial periodicities[9] have been observed in a vast variety of electrochemical systems over the past 180 years. The case of spatial ordering due to Turing patterns resulting from chemical waves deserves consideration, in which dissipative pattern formation due to lateral concentration gradients in chemical reactions at electrode surfaces has been theoretically predicted[30] and practically observed.[8] However, the minimum characteristic length scale achievable in such a system was predicted to be around 1 μm,[30] well above the size of the phenomena discussed in this paper.

Here we show that nanoscale migration patterns can be induced using electromigration as a strong driving force leading to the breakup of an electrochemical double-layer. (Figure 4.1) At or near equilibrium, an electrochemical double layer forms at a metal electrode in contact with an electrolyte. (Figure 4.1a) Let us consider the example of a tantalum anode in an fluoride-containing electrolyte. As fluoride ions from the electrochemical double layer are consumed due to a reaction such as for example

$$Ta^{5+} + 7\ F^{-} \rightarrow TaF_7^{2-} \quad (1)$$

they are replaced by electromigration of F^- from the diffuse layer and then the bulk solution, displacing the reaction product in the process. The reactive F^- ions have a much higher charge to size ratio than the resulting TaF_7^{2-} complex and are therefore much more strongly attracted to the anode. This results in a lively exchange of species at the anode surface. At high reaction rates, the number of migrating ions becomes very large and they start to interact strongly, eventually leading to pattern formation as a means of facilitating migration (Fig 4.1b). If the system is driven too hard (e. g. at higher potentials), it becomes turbulent.[17] If the potential is removed, the electromigration stops and the patterns in solution disappear, leaving behind an etch pattern on the surface due to a slightly faster reaction rate at the bottom of the dimples where the fresh bulk solution hits the surface. Since the oxide is etched faster than the metal (a precondition for electropolishing as opposed to anodic oxide formation), the dissolution can keep up even at the ridges where the 'used' solution leaves the surface, leading to shallow dimples at the surface rather than leading to the formation of pores. The chemistry has to be optimized individually for each surface because a balance needs to be achieved between the speeds of oxide formation (rate determining), oxide dissolution (very fast) and metal dissolution (very slow) in order for ordering to occur.

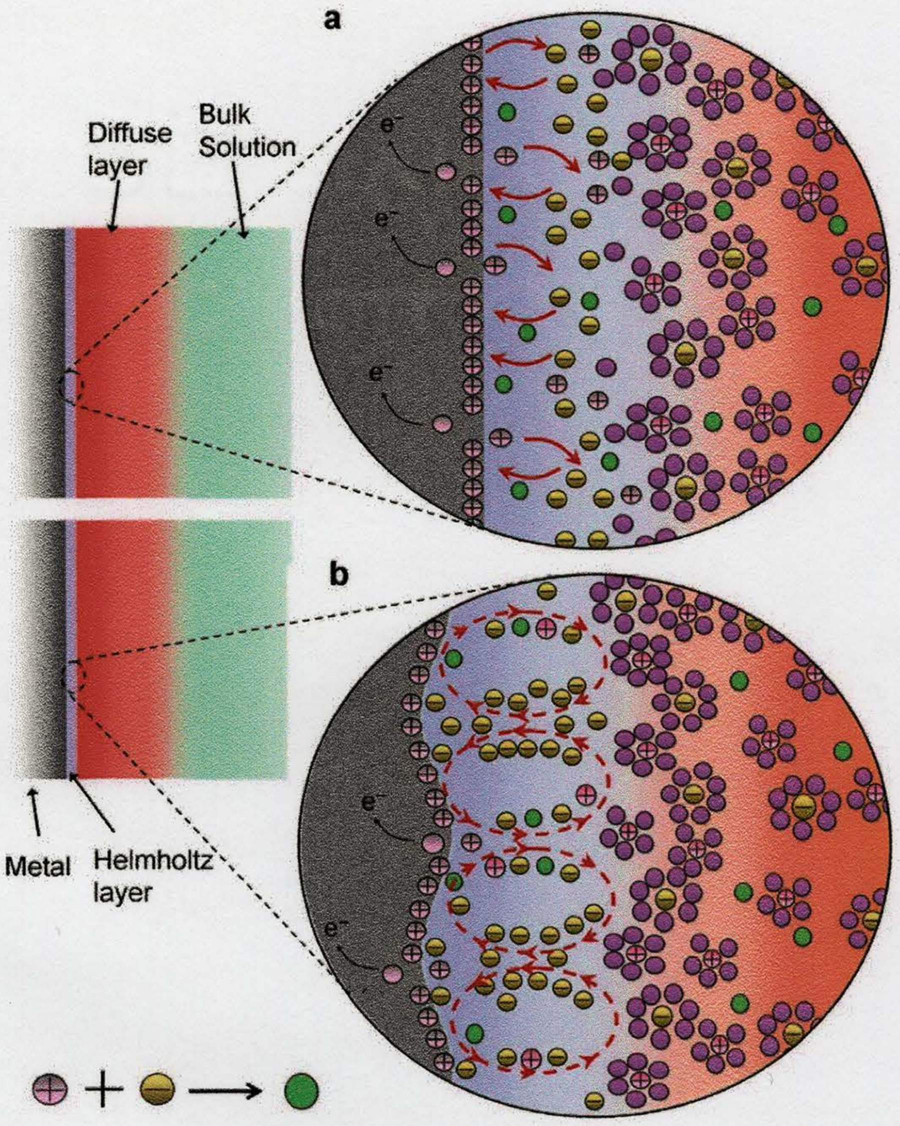

Figure 4.1. Mechanistic illustration of the Helmholtz layer under equilibrium and non-equilibrium conditions (not to scale) during the etching of the metal surface. **(a)** Undisturbed Helmholtz layer with minimal diffusion in the case of a very slow reaction. **(b)** Under vigorous reaction conditions, the layer may break up into convection cells to allow for fast electromigration of large amounts of reactants and products which leads to the dimpled morphology of the metal surface.

4.2 Formation of Dimples

Using a simple two electrode set-up, highly ordered arrays of dimples can be generated reproducibly as reported previously.[16] H_2SO_4 (95-98%, reagent grade), HF (48%), acetone and methanol (both semiconductor grade) were purchased from Fisher Scientific and used as received. Tantalum foil (99.95%, Alfa-Aesar) and tungsten wire (d = 0.25 mm, 99.95%, Alfa-Aesar) were mechanically cut and rinsed with acetone, methanol and Millipore water (18.2 MΩ.cm resistivity) and then dried under argon flow before use. A Pt/Ir wire (0.25 mm diameter) was used as the counter-electrode (cathode). The solutions were stirred using a magnetic stir-bar. All samples were thoroughly rinsed with Millipore water (18.2 MΩ.cm resistivity) and then dried under argon flow after electropolishing. All experiments were performed at room temperature (approximately 20 °C). The dimples must not be too deep in order not to disturb the convective migration pattern. Pore structures can never be formed by this mechanism. The electrolyte composition has to be varied in order to achieve reaction speeds that ensure ordering. A mixture of concentrated HF (48%) and concentrated H_2SO_4 (95-98%) was used for tantalum (1:9). As it has been established earlier, the role of the concentrated sulfuric acid in the case of tantalum chiefly consists in degrading the quality of the formed oxide, hence increasing its solubility.[35]

We have previously shown that on average the dimpled tantalum surface is covered by an oxide film of comparable thickness to a native oxide.[16] However, it was not clear whether the oxide thickness varies between the bottom of the dimples and the top of the ridges, as it would be expected if any substantial amount of oxide film was present during the electropolishing process, and possibly at the root of the pattern formation. We have now been able to perform transmission electron microscopy (TEM) on a tantalum sample (Figure 4.2) that was cross-sectioned using a focused ion beam (FIB). High-Resolution TEM was carried out with a JEOL 2010 field emission TEM/STEM, operating at an accelerating voltage of 200 kV. The thin Ta section for cross-sectional analysis TEM was prepared by FIB milling at the Nanofab facility at the University of Western Ontario. The region of interest on the specimen was in situ coated with layers of carbon and

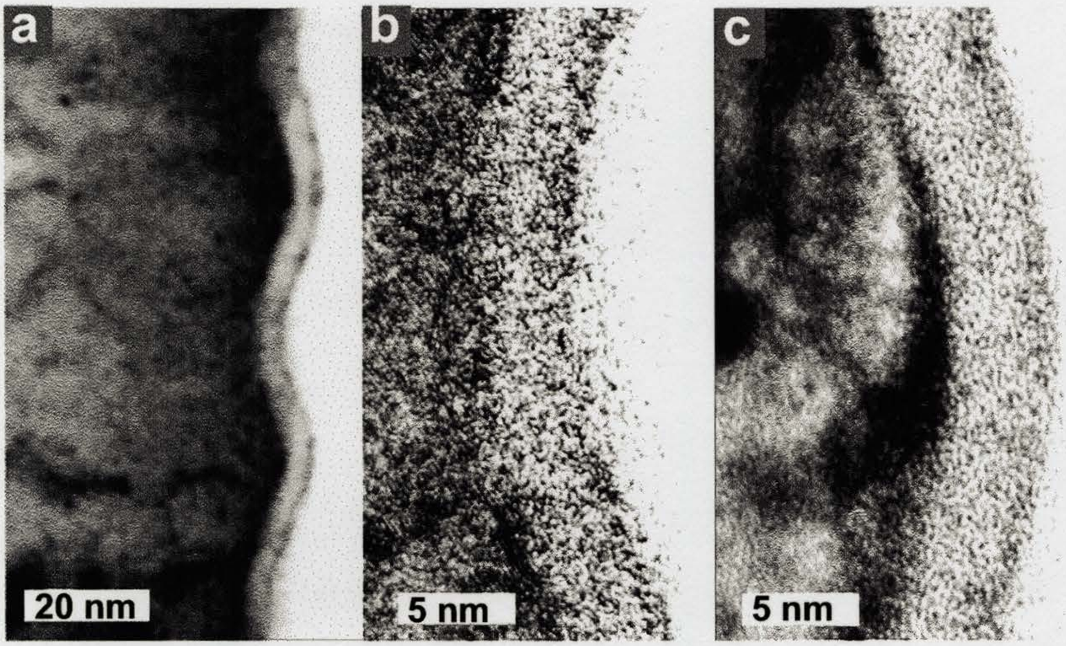

Figure 4.2. The dimple pattern is of metallic nature, as determined by cross-sectional TEM for tantalum and high resolution core-level spectra for titanium and tungsten before and after dimpling. **(a)** Cross-sectional TEM image of dimples on tantalum. **(b)** Zoom-in onto bottom part of dimple. **(c)** Zoom-in onto crest area.

platinum. The carbon layer gives a better contrast and the platinum layer protects the surface of the feature during subsequent FIB milling. The depth of the dimples is identical to what was found by AFM (about 8 nm).[15] The oxide film is shown to be amorphous and very uniform in thickness (about 4 nm) and morphology in all locations, indicating that modulations in the oxide layer do not play any role in the pattern formation process, as it would have been expected if the dimple formation process would have be analogous to porous oxide formation.[20,33,34]

4.3 Formation of Stripes

Turing predicted the ability of dissipative systems to form striped, square and hexagonal patterns,[5] out of which we have observed almost exclusively hexagonal patterns. In our system, we are constrained by the speed of oxide dissolution which has to be robustly faster than oxide formation at all points on the surface. (See discussion of zirconium in Chapter 3) Nevertheless, in the case of tungsten occasional striped patterns were observed during the etching of tungsten wires, as shown in Figure 4.3 and Chapter 3 (Figure 3.1e therein). While we have not been able find a set of experimental conditions under which stripes are reliably generated, it is noteworthy that they have only been observed during the electropolishing of thin wires (used for no reason other than materials availability for some experiments). While further study is required, this lends itself to the speculation that the change in pattern is the result of a change in boundary conditions,[3] due to the curvature in one dimension.

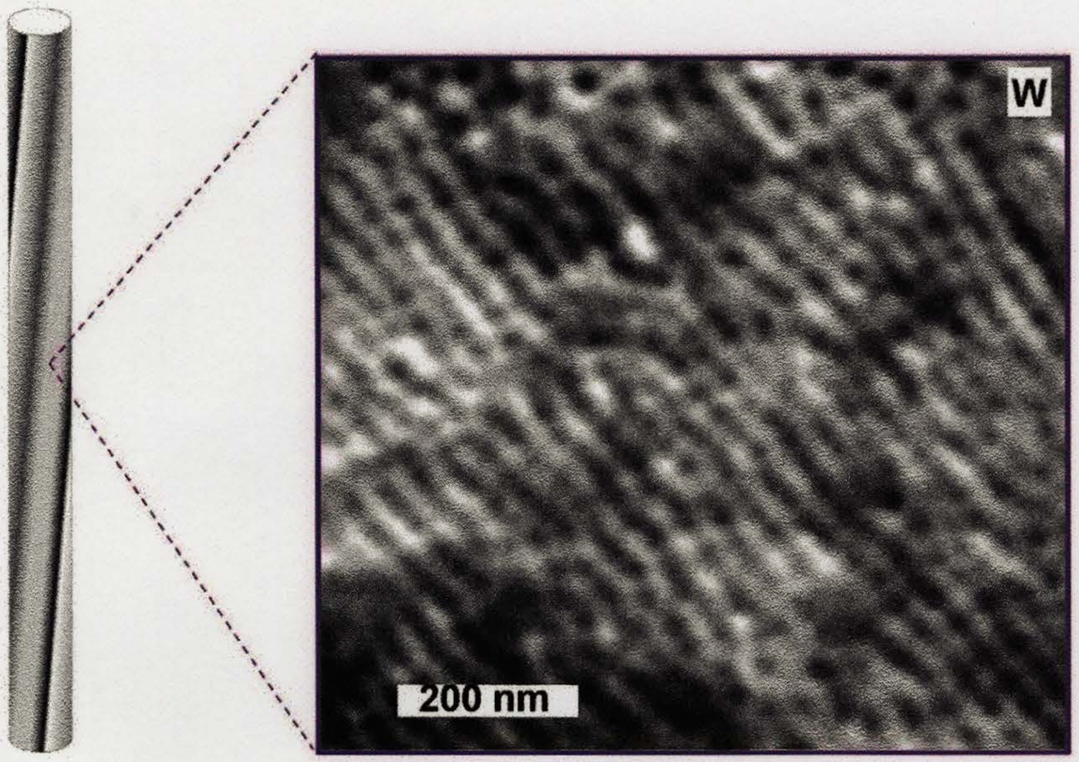

Figure 4.3. SEM image of striped pattern area as observed after electropolishing of tungsten wire.

If we go outside a narrow window of electrolyte composition and applied potential, the reaction (oxidation, dissolution) speeds change sufficiently to either cease pattern formation due to slow-down or become turbulent and less regular (Figure 4.4).

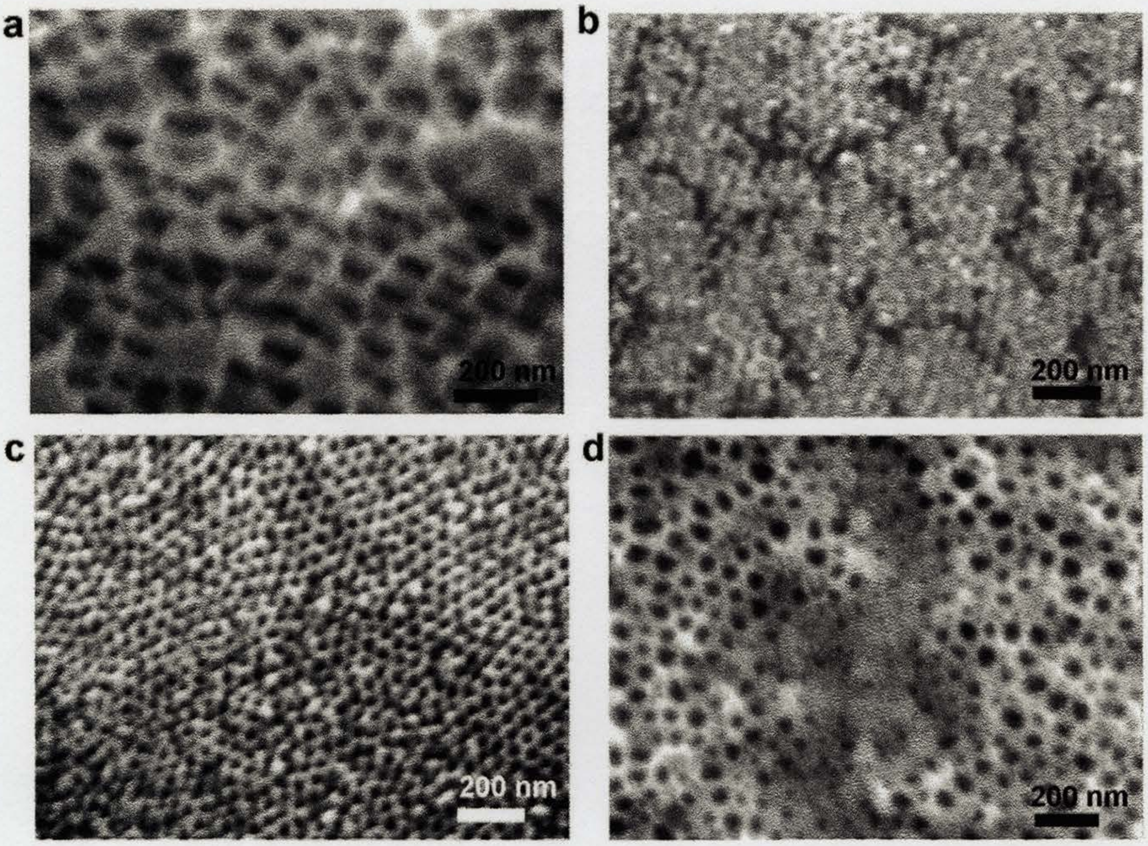

Figure 4.4. SEM images of electropolished tantalum showing the deterioration of the long-range order of dimples as one move away from the narrow electrochemical regime of ordered pattern (dimples) formation by changing the concentration or applied voltage. **(a)** 6:4 (c.H_2SO_4/ c.HF), 15 V, 30 sec **(b)** 8:2 (c.H_2SO_4/ c.HF), 15 V, 5 min **(c)** 85:15 (c.H_2SO_4/ c.HF), 15 V, 5 min **(d)** 9:1 (c.H_2SO_4/ c.HF), 25 V, 2 min.

4.4 Dimple Formation Dynamics

4.4.1 Initiation of Dimple Formation

Time scale is an important indicator of how the dimples are formed. We therefore conducted time-resolved studies (Figure 4.5), clearly elucidating the time scale required for pattern formation. We started with a very flat, unpatterned, electropolished tantalum surface, obtained by peeling off an oxide film according to a previously published process (Figure 4.5a).[36] The electrodes were connected to a power supply (Kepco BOP 20-20M) which was remote controlled by a LabVIEW program. The setup is capable of supplying a voltage pulse of variable time scales with a very short rise and decay time period (1V/μs). After only 500 ms we can observe the formation of dimples (Figure 4.5b). Since no dimples were observed after 300 ms, this marks about the timescale necessary for the electrochemical double layer to break up and order. The order of the dimples improves after a few seconds (Figure 4.5c) and stabilizes after about 1 min (Figure 4.5d). Since the electropolishing speed in our system is estimated to be around 20..50 nm/s,[16] the dimples are formed instantaneously at the onset of etching rather than as the result of an elaborate multi-step process.

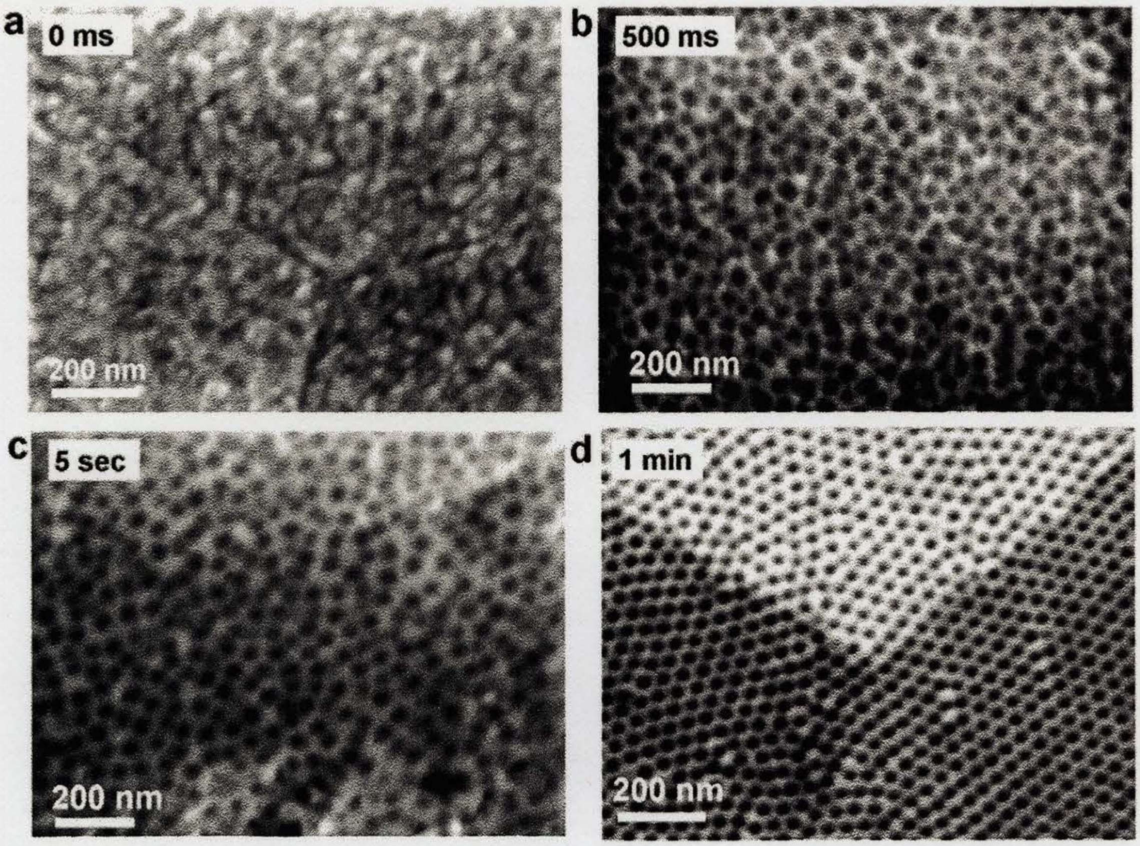

Figure 4.5. The dimple pattern appears within milliseconds, but takes several seconds to order. For all panels, a single rectangular DC pulses with 15 V ON voltage and 0 V OFF voltage was applied for different times. **(a)** Electropolished, but unordered starting surface. **(b)** Emerging dimple pattern after 0.5 s pulse. **(c)** Increasing order after 5.0 s pulse. **(d)** Well-ordered dimple pattern after 60.0 s pulse.

4.4.2 Break-up of Double Layer into Ordered Cells

We are now ready to decide the question of whether the pattern is determined by migration processes in the liquid or by surface topography. Inherently, metal surfaces are prone to instabilities during electrodissolution, which may lead to random roughness on varying length scales.[37] Mechanisms proposed in the cases of porous silicon[19] or anodic porous oxides[20,33,34] are usually based on modulation of the field strength (and hence speed of oxide formation) by defects, oxide films or other surface features. Positive feedback leads to enhanced etching at the same locations and causes pore formation. If these processes are stopped and resumed, the existing patterns are reinforced and amplified in the same location. The first indication that this is not the case in dimple formation comes from the uniform oxide thickness in the TEM cross-sectional view (Figure 4.2). It is also noticeable that grain boundaries have no impact on the order of the dimples (Figure 4.5d). Therefore the dimple formation is a very robust process that is not very sensitive to sample topography. Furthermore, while the size of the dimples remains fixed from the beginning (Figures 4.5b, c, d), the total number of dimples per unit area increases with the degree of ordering until a steady state is reached. This is characteristic of a dissipative process, but not of porous oxide formation. Final proof for this notion comes from a series of experiments where short DC pulses were applied to a fully formed dimple pattern on tantalum (Figure 4.6). In contrast to pore formation processes where pore formation is guided by field lines, the ion migration pattern in the double layer has to re-form for each pulse. If a series of short pulses is applied, e. g. 20 x 0.5 sec or 10 x 1.0 sec (Figure 4.6a and b respectively, separated by 0.5 sec each), the pattern will form in a slightly different location for each pulse due to a lack of boundary conditions, giving the dimples a somewhat gnawed appearance (Figure 4.6a, b). This shows that the double layer breaks up anew each time into a migration pattern, without memory of the previous location. The shallow dimples do not provide a strong enough template, as would be expected since not even steps along grain boundaries were able to template the growth. A longer pulse can erase the dimple pattern in the process (Figure 4.6c), whereas a sufficiently long pulse will lead to a re-formed dimple pattern (Figure 4.6d).

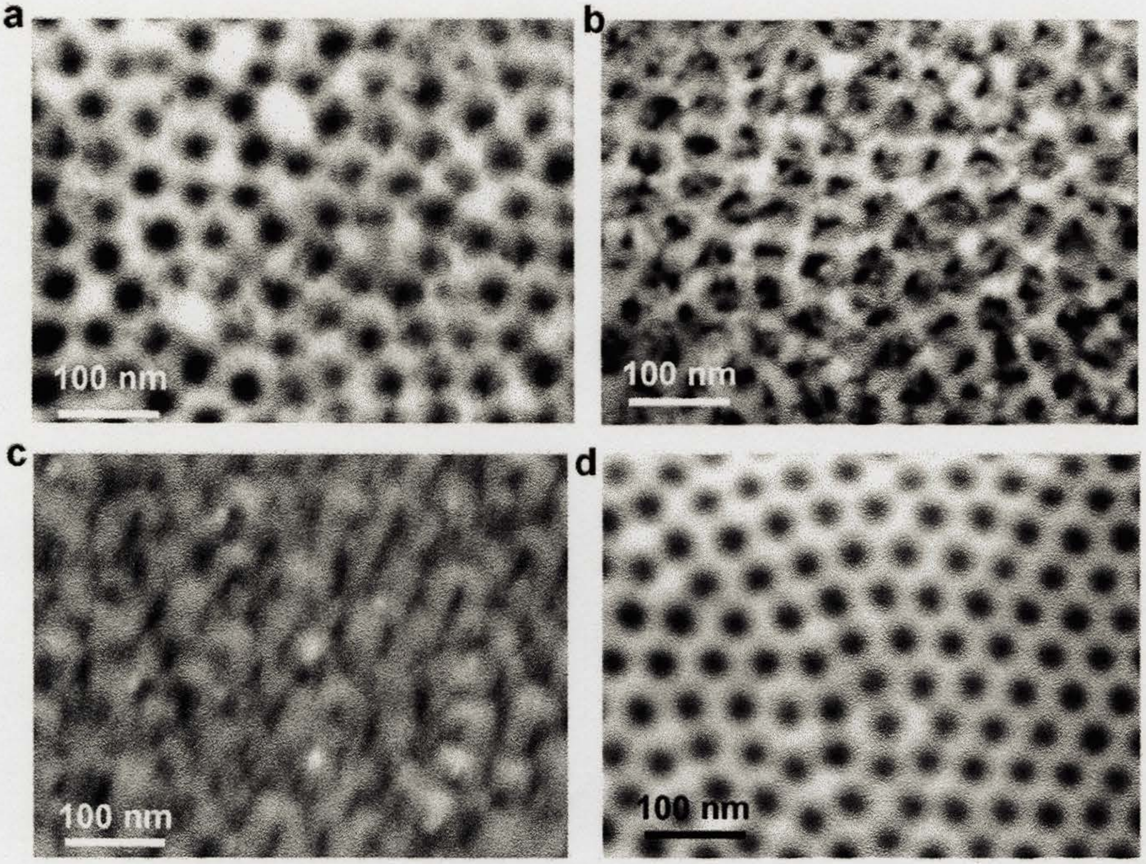

Figure 4.6. New patterns form each time the anodic potential is applied. For all panels, rectangular DC pulses with 15 V ON voltage and 0 V OFF voltage were applied for different times. **(a)** Pattern etched for 300 s ON, 30 s OFF. Then 20 pulses, each 0.5 s ON, 0.5 s OFF. **(b)** Pattern etched for 300 s ON, 30 s OFF. Then 10 pulses, each 1.0 s ON, 0.5 s OFF. **(c)** Pattern etched for 300 s ON, 30 s OFF. Then 1 pulse for 10.0 s ON. This figure shows that the pattern can be erased. **(d)** Pattern etched for 300 s ON, 30 s OFF. Then 1 pulse for 60.0 s ON. This shows that 60 s are enough to erase the previous pattern and then recreate a new pattern on the surface.

In addition to lateral ordering, it is also important to consider the depth evolution of the dimples. AFM imaging reveals that the depth of the dimples increases gradually at the same time as the order increases. (Figure 4.7) Neither AFM nor TEM nor SEM data taken by us indicate any temporal oscillation or instability in the dimple pattern once a steady state is reached within about a minute from the start of the electropolishing. This is much in contrast to most nonlinear electrochemical systems which often feature temporal oscillations.[4] Patterns originating from global coupling in an electrochemical system would result in a change of characteristic length scale with parameters of the outside system (electrode size and geometry of electrochemical cell, response time of potentiostat or power supply, etc.), whereas both Turing and electrohydrodynamic patterns have a smaller characteristic length scale that is invariant to external parameters.[4] Turing patterns can give rise to stationary spatially periodic structures,[30,31] but effectively require a permanent inhomogeneity in reaction speed. As our data demonstrates, the reaction speed is uniform across the entire surface after an initiation period of about 1 minute. (Figures 4.2a & 4.7d) Initially, the etch speed at the bottom of the dimples is slightly faster than at the ridges. If we take the lower limit of our estimate for the global electropolishing speed at around 20 nm/s, and consider the depth of the dimples after 5 seconds (Figure 4.7a, d) to be 4 nm, the ridges were etched about 100 nm deep during that time and the bottoms about 104nm deep, a speed differential of 4%. The difference in etch speed is rapidly decreasing with time until it vanishes before 60 seconds are over. While our data does not give any insight into the initiation of the pattern formation process (less than 5 seconds from the start), other than the knowledge that it takes less than 0.5 seconds for the first dimples to appear (Figure 4.5b), the dominant process for the sustenance of the dimples in electrohydrodynamic in nature.[29] The dimple formation is therefore analogous to Rayleigh-Benard convection but effectively without boundary conditions since an electrode in our experiments is typically 5 mm wide and hence contains about 100,000 convection cells across.

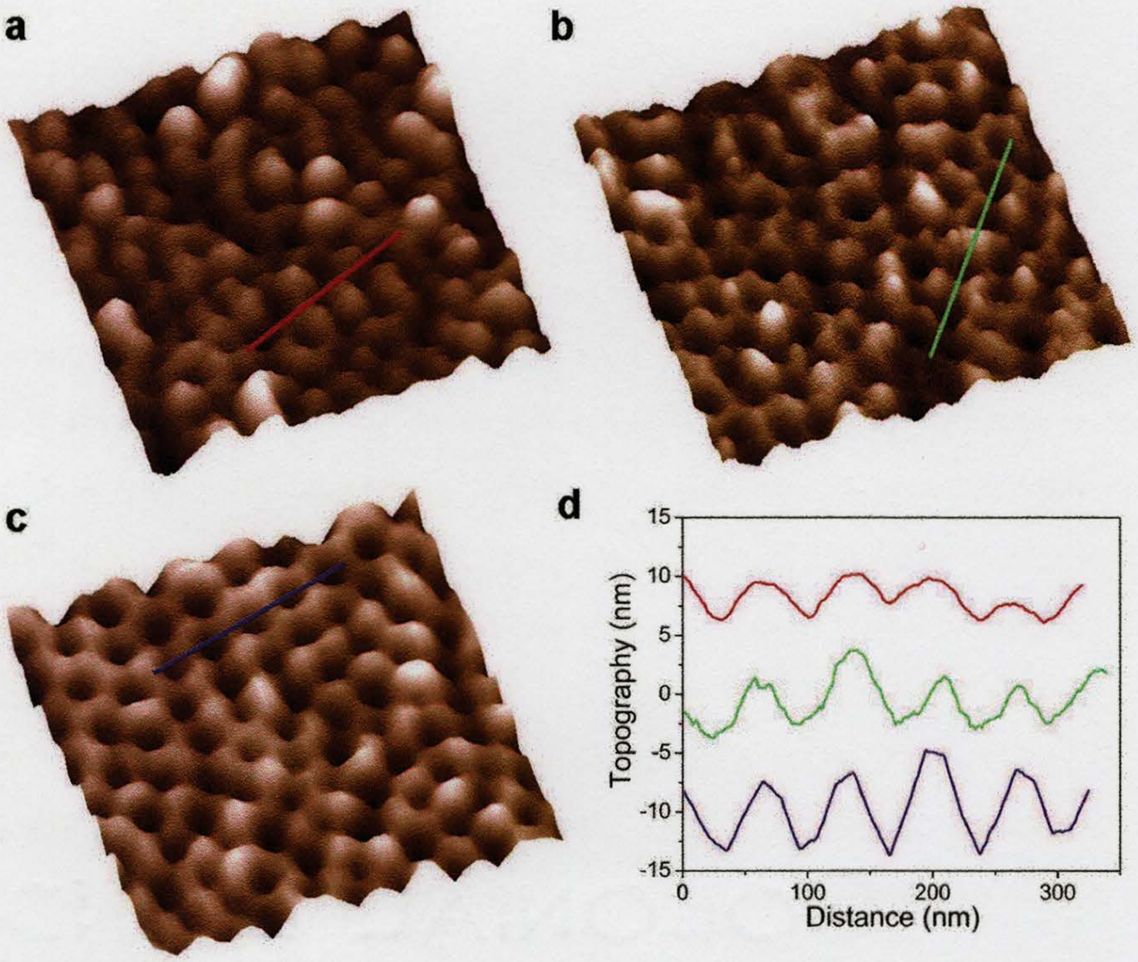

Figure 4.7. Atomic force microscopy images with 3D rendering shows the gradual increase in depth of the dimples with time on tantalum surfaces during electropolishing. **(a)** 5 seconds. **(b)** 30 seconds. **(c)** 60 seconds. **(d)** Height profiles of the dimples along the lines shown in (a), (b) and (c).

4.5 Conclusions

Overall, the evidence points towards a principally new type of nanopatterning, which is based on a dissipative process rather than self-assembly. The exact surface chemistry is irrelevant for the pattern formation process, except for driving the gradient in ionic species concentration. The pattern itself is purely a result of the physics of the nanoelectrohydrodynamical system in the Helmholtz layer. The characteristic length scale of this process is determined by the thickness of the electrochemical double layer and hence somewhat tunable by the anodic potential but independent from substrate identity, surface defects or pre-existing patterns or the composition and viscosity of the bulk electrolyte. Dimple formation has now been demonstrated with a high level of uniformity on tantalum, titanium, tungsten and zirconium.[16,18] Potentially, this mechanism is also suitable for explaining previously reported patterns on aluminum surfaces,[38] although a more detailed examination of that system would be required. Heterogeneous surface compositions will allow for area-selective pattern formation. Dissipative nanopatterning is self-limiting and results in uniformly shallow features, which can then provide templates for subsequent processing if higher aspect ratio features are desired for applications such as the formation of biocompatible surfaces for which the 50 nm length scale is very important,[39] as a template for catalyst nanoparticle formation,[40] or for the fabrication of zeptoliter size reaction vessel or sensor arrays.[41] Since the process is not tied to a specific chemistry, highly ordered dimple patterns can likely be formed on any conducting or semiconducting surface amenable to electropolishing, leading to applications in templated nanostructure growth, composite materials, electronics, catalysis, photovoltaics and biomaterials.

4.6 Experimental Section

H_2SO_4 (95-98% reagent grade), HF (48%), acetone and methanol (all semiconductor grade) were purchased from Fisher Scientific. All chemicals were used as received without further purification. Tantalum foil (Alfa-Aesar, 99.95%, 0.127 mm) was mechanically cut, rinsed with acetone, methanol and then with Millipore water (18.2 MΩ.cm resistivity) and then dried under air prior to anodization.

Time-resolved measurements were performed on flat tantalum surfaces prepared by growing oxide on electropolished (dimpled) tantalum surfaces and then peeling off the oxide layers.[26] For time resolved experiments the electrodes were connected to a power supply (Kepco BOP 20-20M) which was remote controlled by a LabVIEW program. The setup is capable of supplying a voltage pulse of variable time scales with a very short rise and decay time period (1V/μs).

Atomic force microscopy was performed in tapping mode on a Veeco Enviroscope with a Nanoscope IIIa controller and Veeco RTESP p-doped Si tips with a nominal radius of less than 10 nm. Typical scan rates were 2 micrometer per second and the images were constructed with 512 scan lines. Care was taken to ensure that the tip was not modifying the surface during the scan. A large number of images of the same sample were obtained with different tips to pinpoint the exact depth of dimples by eliminating tip convolution effects. The data was analysed using DI V5.30r3.sr3 software.

SEM imaging was performed with a JEOL JSM-7000F Scanning Electron Microscope, equipped with a Schottky type Field Emission Gun (FEG) filament. Energy dispersive X-ray (EDX) mapping was carried out using a 10 kV electron beam to obtain the distribution of O, Ni and W on the electropolished W surface. INCA 300 (EDX System, Oxford, UK) software was used for data acquisition and analysis.

High-Resolution TEM was carried out with a JEOL 2010 field emission TEM/STEM, operating at an accelerating voltage of 200kV. The thin Ta section for cross-sectional analysis TEM was prepared by focused ion beam (FIB) milling at the Nanofab facility at the University of Western Ontario. The region of interest on the specimen was coated with layers of carbon and platinum, in-situ, using the CrossBeam's gas injection system. The carbon layer gives a better contrast and the platinum layer protects the surface of the feature during subsequent FIB milling.

Author Contributions: This chapter is based on a manuscript which has been submitted for publication. The author contributions for the work presented in this chapter are as follows. S. S. participated in the experimental design, performed the experiments, analyzed the data, put together the figures and contributed to the manuscript. W.R.T.B. assisted in the experiments. P.K. participated in the experimental design and contributed to the manuscript. All authors discussed the results and commented on the manuscript.

4.7 Bibliography

(1) Ball, P. *The Self-made Tapestry: Pattern Formation in Nature* (Oxford Univ. Press, Oxford, 1999).

(2) Whitesides, G. M. & Grzbowski, B., Self assembly at all scales. *Science* **2002**, *295*, 2418-2421.

(3) Cross, M. C. & Hohenberg, P. C. Pattern formation outside of equilibrium, *Rev. Mod. Phys.* **1993**, *65*, 851- 1112.

(4) Krischer, K., Mazouz, N. & Grauel, P. Fronts, waves and stationary patterns in electrochemical systems. *Angew. Chem. Int. Ed.* **2001**, *40*, 850-869.

(5) Turing, A. M. The chemical basis of morphogenesis. *Philos. Trans. R. Soc. London* **1952**, *237*, 37-72.

(6) Sagués, F. & Epstein, I. R. Nonlinear chemical kinetics. *Dalton Trans.* **2003**, *7*, 1201-1217.

(7) Sagués, F., Sancho, J. M. & Garcia-Ojalvo, J. Spatiotemporal order out of noise. *Rev. Mod. Phys.* **2007**, *79*, 829-882.

(8) Kiss, I. Z. & Hudson, J. L. Chemical complexity: Spontaneous and engineered structures. *AIChE Journal* **2003**, *49*, 2234-2241.

(9) Li, Y. J., Oslonovitch, J., Mazouz, N., Plenge, F., Krischer, K. & Ertl, G. Turing-type patterns on electrode surfaces. *Science* **2001**, *291*, 2395-2398.

(10) Cox, M. P., Ertl, G. & Imbihl, R. Spatial Self-Organization of Surface Structure during an Oscillating Catalytic Reaction. *Phys. Rev. Lett.* **1985**, *54*, 1725-1728.

(11) Stupp, S. I., LeBohneur, V., Walker, K., Li, L. S., Huggins, K. E., Keser, M. & Amstutz, A. Supramolecular materials: Self-organized nanostructures. *Science* **1997**, *276*, 384-389.

(12) Henzie, J., Barton, J. E., Stender, C. L. & Odom, T. W. Large-area nanoscale patterning: Chemistry meets fabrication. *Acc. Chem. Res.* **2006**, *39*, 249-257.

(13) Pawin, G., Wong, K. L., Kwon, K. Y. & Bartels, L. A homomolecular porous network at a Cu(111) surface. *Science* **2006**, *313*, 961-962.

(14) Cathcart, J. V., Bakish, R. & Norton, D. R. Oxidation Properties of Tantalum Between 400° and 530°C. *J. Electrochem. Soc.* **1960**, *107*, 668-670.

(15) Pawel, R. E. & Lundy, T. S. A submicron sectioning technique for analyzing diffusion specimens of tantalum and niobium. *J. Appl. Phys.* **1964**, 35, 435-438.

(16) El-Sayed, H., Singh, S., Greiner, M. T. & Kruse, P. Formation of Highly Ordered Arrays of Dimples on Tantalum at the Nanoscale. *Nano Lett.* **2006**, *6*, 2995-2999.

(17) El-Sayed, H., Singh, S. & Kruse, P. Formation of Dimpled Tantalum Surfaces from Electropolishing. *J. Electrochem. Soc.* **2007**, *154*, C728-C732.

(18) Singh, S., Barden, W. R. T. & Kruse, P. Nanopatterning of transition metal surfaces via electrochemical dimple array formation. *submitted to Nano Lett.* (manuscript# nl-2008-01587c).

(19) Lehmann, V. *Electrochemistry of Silicon: Science, Materials and Applications.* (Wiley-VCH, Weinberg, 2002).

(20) Thompson, G. E., Furneaux, R. C., Wood, G. C., Richardson, J. A. & Goode, J. S. Nucleation and growth of porous anodic films on aluminum. *Nature* **1978**, *272*, 433-435.

(21) Masuda, H. & Fukuda, K. Ordered metal nanohole arrays made by a 2-step replication of honeycomb structures of anodic alumina. *Science* **1995**, *268*, 1466-1468.

(22) Lee, W., Ji, R., Gosele, U. & Nielsch, K. Fast fabrication of long-range ordered porous alumina membranes by hard anodization. *Nature Mater.* **2006**, *5*, 741-747.

(23) Sieber, I., Kannan, B. & Schmuki, P. Self-assembled porous tantalum oxide prepared in H_2SO_4/HF electrolytes. *Electrochem. Solid State Lett.* **2005**, *8*, J10-J12.

(24) Cai, Q. Y., Paulose, M., Varghese, O. K. & Grimes, C. A. The effect of electrolyte composition on the fabrication of self-organized titanium oxide nanotube arrays by anodic oxidation. *J. Mater. Res.* **2005**, *20*, 230-236.

(25) Rapaport, D. C. Hexagonal convection patterns in atomistically simulated fluids. *Phys. Rev. E* **2006**, *73*, 025301.

(26) Kadau, K., Germann, T. C., Hadjiconstantinou, N. G., Lomdahl, P. S., Dimonte, G., Holian, B. L. & Alder, B. J. Nanohydrodynamics simulations: An atomistic view of the Rayleigh-Taylor instability. *Proc. Nat. Acad. Sci.* **2004**, *101*, 5851-5855.

(27) Zimmermann, W. Pattern formation in electrohydrodynamic convection. *Mat. Res. Soc. Bull.* **1991**, *16*, 46-56.

(28) Dini, D., Doblhofer, K. & Ertl G. Nucleation of solution convection channels as the first step in electro-hydrodynamic pattern formation. *Phys. Chem. Chem. Phys.* **2000**, *2*, 1183-1186.

(29) Van Tassel, J. J. & Randall, C. A. Ionic gradients at an electrode above the equilibrium limit current. 2. Transition to convection. *J. Phys. Chem. C* **2007**, *111*, 3349-3357.

(30) Mazouz, N. & Krischer, K. A theoretical study on Turing patterns in electrochemical systems. *J. Phys. Chem. B* **2000**, *104*, 6081-6090.

(31) Krischer, K. New directions and challenges in electrochemistry - Spontaneous formation of spatiotemporal patterns at the electrode | electrolyte interface. *J. Electroanal. Chem.* **2001**, *501*, 1-21.

(32) Fechner, G. T. Über Umkehrungen der Polarität in der einfachen Kette, *Journal für Chemie und Physik* **1828**, *53*, 61-77 and 131-151.

(33) Yuzhakov, V. V., Takhistov, P. V., Miller, A. E. & Chang, H. C. Pattern selection during electropolishing due to double-layer effects. *Chaos* **1999**, *9*, 62-77.

(34) Guo, W. D. & Johnson, D. Role of interfacial energy during pattern formation of electropolishing. *Phys. Rev. B* **2003**, *67*, 075411.

(35) Vermilyea, D. A. Formation of anodic oxide films on tantalum on non-aqueous solutions. *Acta Metall.* **1954**, *2*, 483-486.

(36) Singh, S., Greiner, M. T. & Kruse, P. Robust inorganic membranes from detachable ultra-thin tantalum oxide films. *Nano Lett.* **2007**, *7*, 2676-2683.

(37) Pritzker, M. D. & Fahidy, T. Z. Morphological stability of a planar metal electrode during potentiostatic electrodeposition and electrodissolution. *Electrochim. Acta* **1992**, *37*, 103-112.

(38) Caicedo-Martinez, C. E., Koroleva, E. V., Thompson, G. E., Skeldon, P., Shimizu, K., Habazaki, H. & Hoellrig, G. Surface nanotextures on aluminium. *Surf. Interface Anal.* **2002**, *34*, 405–408.

(39) Cavalcanti-Adam, E. A., Volberg, T., Micoulet, A., Kessler, H., Geiger, B. & Spatz, J. Cell spreading and focal adhesion dynamics are regulated by spacing of integrin ligands. *Biophys. J.* **2007**, *92*, 2964-2974.

(40) Wu, Z. H., Mei, X. Y., Kim, D., Blumin, M. & Ruda, H. E. Growth of Au-catalyzed ordered GaAs nanowire arrays by molecular-beam epitaxy. *Appl. Phys. Lett.* **2002**, *81*, 5177-5179.

(41) Furhop, J.-H. Molecular interactions in solvent-filled yoctowells (10^{-24} L) and zeptowells (10^{-21} L). *Curr. Opin. Coll. Interf. Sci.* **2008**, *13*, 81-85.

Chapter-5

Robust Inorganic Membranes from Detachable Ultra-thin Tantalum Oxide Films.

In this chapter, we report a simple electrochemical method of making individual free standing, and uniform tantalum oxide membranes between 35 nm and 100 nm thick. These films can be separated, floated on water and transferred onto various substrates such as Si wafers, glass slides and TEM grids. Our membranes are mechanically, chemically and thermally robust, have a high dielectric constant and a high refractive index, making them potentially useful in sensors, optics, filtration and catalysis.

5.1 Introduction

Tantalum metal was discovered in 1802 by Anders Gustav Ekeberg[1] who named it after the mythological Greek figure Tantalus, whom the gods condemned to endure thirst while standing in a pool of water. Ekeberg found the chemical inertness of tantalum towards aqueous acids to be analogous to Tantalus' inability to drink from the water. The origin of this inertness is a thin protective layer of tantalum oxide (Ta_2O_5) at the metal surface. Consequently, tantalum and its oxide have found applications in chemical reactors, airplanes and corrosion protection coatings for biomedical implants, surgical instruments[2,3] and sensors.[4]

Tantalum oxide possesses several other remarkable properties. For example, Ta_2O_5 and its composites exhibit photocatalytic activity, and have been used as catalytic substrates for the photolysis of water to yield molecular hydrogen and oxygen, a reaction which can be used to harness solar energy.[5,6] Tantalum oxide also has a very high refractive index, and is being used in anti-reflective coatings for lenses and solar panels.[7] As a piezoelectric material, it can be used in surface acoustic wave devices,[8] such as band-pass filters and various types of mechanical sensors. Due to their very high dielectric constant and good compatibility with silicon, thin films of tantalum oxide are also used in thin film transistors,[9,10] ion-sensors,[11] and storage capacitors for dynamic random access memory.[12-14] Recently, thin sheets of metal oxides have found use as dielectric spacers between metal electrodes for fabricating negative refractive index materials also known as metamaterials.[15, 16] These properties have resulted in increased interest in these films and their fabrication.

High quality compact films of tantalum oxide with well-defined thickness can be grown by anodization in a variety of electrolytes.[17, 18] Dilute aqueous solutions of hydrofluoric acid, however, result in porous films due to partial dissolution of the formed oxide, with the degree of porosity depending on the fluoride ion concentration.[19] Hydrofluoric acid is the only chemical capable of attacking tantalum oxide. If tantalum is anodized in non-aqueous solutions of hydrofluoric acid, all oxide is dissolved immediately as it is formed, resulting in an electropolished tantalum surface instead of an oxide film. The fast dissolution can be attributed to the poor quality of the oxide due to high levels of incorporation of electrolyte ions.[20,21] For example, tantalum can be electropolished in a mixture of H_2SO_4 (95-98%) and HF (48%) in a 9:1 volumetric ratio.[10, 20-22] The resulting flat surface is well-suited to the growth of anodic oxide films.[10]

If a Ta_2O_5 film is desired on a substrate other than tantalum itself, a different approach such as reactive sputtering (SP),[23,24] reactive ion plating (IP),[25] pulsed laser-assisted evaporation, or chemical vapor deposition (CVD)[26-28] is required. These techniques are well established on hard substrates, but are limited by substrate damage during thin film growth, lack of vacuum compatibility in the case of soft or biological substrates, contamination due to silicon migration at elevated temperatures and carbon deposits from organo-metallic precursors. Thin films grown by these techniques are static and cannot be transferred onto other substrate surfaces or used freestanding, which is desirable for applications as sheet actuators, organized catalyst surfaces, nanolithographic templates, and separation membranes. For other materials, this limitation has recently been overcome by the synthesis of free standing organic/inorganic hybrid sheets.[29-32]

Here we report a simple and inexpensive, solution-based method for producing transferable, robust, and purely inorganic membranes of Ta_2O_5. They are chemically more inert and thermally more stable than composite organic-inorganic membranes and mechanically superior to previously-reported inorganic membranes such as porous alumina. We have fabricated and transferred uniform films as large as 2 cm by 3 cm, limited by the size of our equipment. Tantalum oxide films with a controlled thickness of as little as 35 nm and up to more than 100 nm are first grown on tantalum foil and then separated as sheets by the Lift-Off-Float-On (LOFO) technique. These sheets can be used as free standing membranes or transferred from the air-water interface to a wide variety of substrates, such as Si wafers, glass slides and TEM grids. Despite the extreme aspect ratio, these sheets remain intact throughout the transfer process. Their morphology can be tuned from ordered meso-scale dimples to nano-sized pores by adjusting the anodizing parameters, such as voltage and composition of the electrolyte solution.

5.2 Fabrication of Sheets

5.2.1 Growth of Ta_2O_5 Films

To fabricate large, uniform oxide sheets from commercially available cold-rolled tantalum foil (Alfa Aesar, 99.95%, 0.127 mm), it is first necessary to electropolish the surface (Figure 5.1a (i)). This is achieved by anodizing the tantalum foil at 15 V in a 9:1 volumetric mixture of concentrated sulfuric acid (95-98%, Fisher Scientific, reagent grade) and concentrated hydrofluoric acid (48%, Fisher Scientific, semiconductor grade; see ref. 22 for further details). We have previously reported that electropolishing of a tantalum surface under these conditions generates highly ordered dimples at the nanoscale (Figure 5.1b), 30-50 nm in diameter and around 8-10 nm deep.[22] The oxide layer on the tantalum surface at this stage is equivalent to the native oxide which forms on tantalum in air.

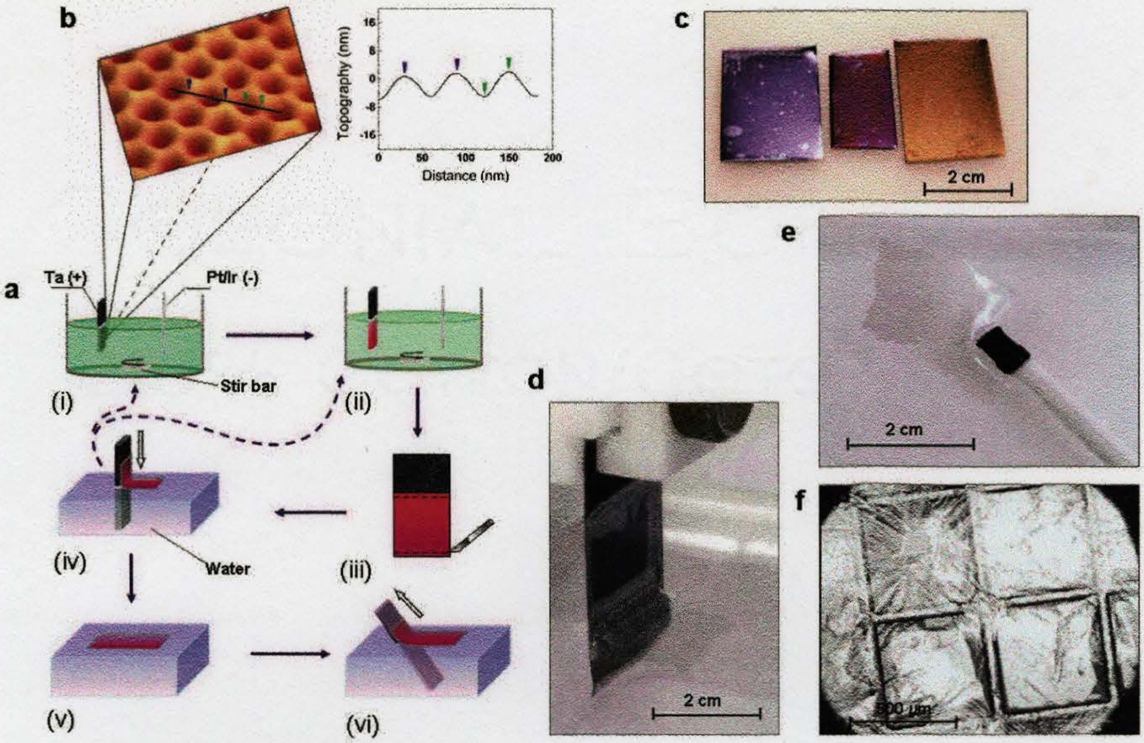

Figure 5.1. Scheme for fabricating tantalum oxide membranes. (a) Electropolishing of the tantalum surface (i); anodic growth of the oxide film (ii); scratching of oxide film at the borders to facilitate detachment (iii); detachment of the film at the air-water interface (iv); film floating on water (v); transfer of the film onto a substrate (vi). (b) AFM image with cross section showing the formation of dimples due to electropolishing. (c) Photographic image showing colors corresponding to different oxide thickness (from left to right, 5 min, 3 min, 1min growth time). (d) Photographic image of the detachment process. (e) Photographic image showing an oxide film floating on water after complete detachment. (f) Free-standing tantalum oxide membrane after transfer onto a TEM grid.

In the second step, the tantalum oxide films are grown on electropolished (dimpled) tantalum samples by anodizing them in an aqueous electrolyte containing 1M

H_2SO_4 and 2 wt% HF at constant voltage of 20 V (Figure 5.1a (ii)). Fluoride ions are required to weaken the adhesion of the anodic film to the underlying metal, so that the film can be peeled off. Even a low concentration of fluoride ions (0.1 wt% HF in 1M H_2SO_4) is sufficient for the detachment of oxide sheets, however the fluoride ion concentration affects the pore size. Due to interference of light, the films exhibit brilliant photonic colors (Figure 5.1c) which depend on their thickness, i.e. the anodization time. The thickness of the films can be estimated in situ by observing their color change during anodic oxidation. The colors of these films can also change, depending on whether they are wet or dry, due to a change in refractive index when the porous films are soaked with solvent. This property can be utilized in Bragg-Reflector sensors for the detection of various chemicals and biologically relevant molecules. Sensors of this type have already been demonstrated based on other porous oxide films and butterfly wings.[33-36]

5.2.2 Detachment of Ta_2O_5 Films

Under the conditions described above, the films can be completely detached as large, continuous sheets using the LOFO technique. Since wet films are easier to detach than dry films, the tantalum oxide samples are rinsed with deionized water before detachment. The upper and lower edges of the oxide film are then scratched with a needle to facilitate its detachment (Figure 5.1a (iii)). The lower scratch allows the penetration of water under the tantalum oxide film for lifting it from the tantalum surface. A small bend near the lower edge also helps to initiate film detachment. The upper scratch makes a well defined boundary for the film. If an appropriately scratched sample is slowly immersed (8 mm/min) into water using the dipper of a Langmuir Blodgett trough (KSV-

2000, KSV Instruments Ltd.) the film will separate (Figure 5.1a (iv) and Figure 5.1d). The separated films float as large sheets on the water surface (Figure 5.1a (v) and Figure 5.1e). These sheets can then be transferred onto glass or silicon substrates by slowly pulling the substrate up from underneath the floating film (Figure 5.1a(vi)). Alternatively, the films can be transferred onto a supporting mesh such as a TEM grid (Figure 5.1f).

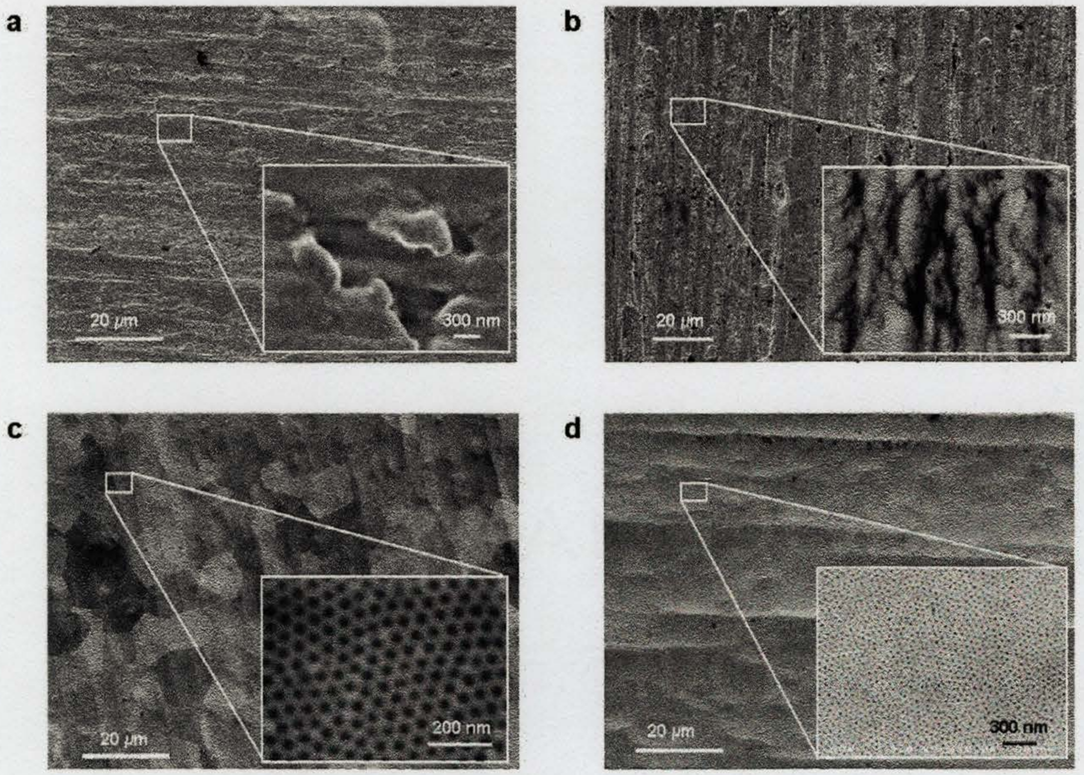

Figure 5.2. SEM images demonstrating the importance of electropolishing the tantalum surface before oxide film growth. (a) As-received cold-rolled tantalum sample surface. (b) Porous oxide film grown directly on a cold-rolled tantalum sample. (c) Tantalum surface after electropolishing,exhibiting characteristic dimples. (d) Porous oxide film grown for 5 min in 2 wt. % HF on an electropolished sample, showing the high quality of the films with pores that loosely align themselves with the dimples from electropolishing.

The ease of oxide film detachment as described in our process is somewhat surprising because compact Ta_2O_5 films are generally known to be well-controlled, with few defects and highly adherent to the underlying tantalum metal.[17,18] Even thick compact oxide films grown on dimpled surfaces have been reported to not detach.[10] We will show that the presence of fluoride ions during the anodic oxide growth step is crucial for detachment. However, the presence of fluoride ions during porous oxide growth on tantalum as reported previously by Schmuki et al.[19] is not sufficient to prepare high quality oxide films for detachment if the surface is not first electropolished. The electropolishing step is required to remove the macroscopic surface roughness of the as-received tantalum foil (Figure 5.2a), because the roughness exceeds the oxide film thickness (Figure 5.2b), leading to the separation of small, non-uniform pieces during film transfer. The electropolishing of tantalum generates a clear grain structure with a pattern of wavy lines remaining on the surface (Figure 5.2c), which are artifacts of the cold rolling process used to manufacture the tantalum foil. Even though these lines are imprinted onto the tantalum oxide films (Figure 5.2d), they do not present a problem in the fabrication of the membranes.

Detachment of the films becomes gradually more difficult as the thickness of the oxide layer increases. The most easily separable films are obtained by growing the oxide for no longer than 10 minutes in a 1M H_2SO_4, 2 wt% HF solution at 20 V. Peeling of an oxide film grown for 5 min under these conditions leaves a clean surface of the pure tantalum substrate covered with native oxide (Figure 5.3a). In contrast, anodic oxide films grown for 15 minutes or more are very difficult to detach. The texture of the surface beneath the films also changes with increasing thickness of the films. The underlying tantalum surface shows a shallower dimpled morphology after peeling of a 35 nm thick film formed after anodizing for 1 minute in (1M H_2SO_4, 2 wt% HF) solution (Figure 5.3b). The texture of surface left behind by a 5 minute film (Figure 5.3c) differs in morphology: no ordered dimples are discernible, despite a comparable overall feature size and smoothness. This substrate can be used to make further flat tantalum oxide films, without the dimpled morphology. Alternatively, the electropolishing step can be repeated at this point to regenerate the dimples. We peeled off 4 films (5 minutes oxide growth) in sequence from the same sample using this method, but there is no obvious limit to the number of detachable films other than the thickness of the tantalum substrate.

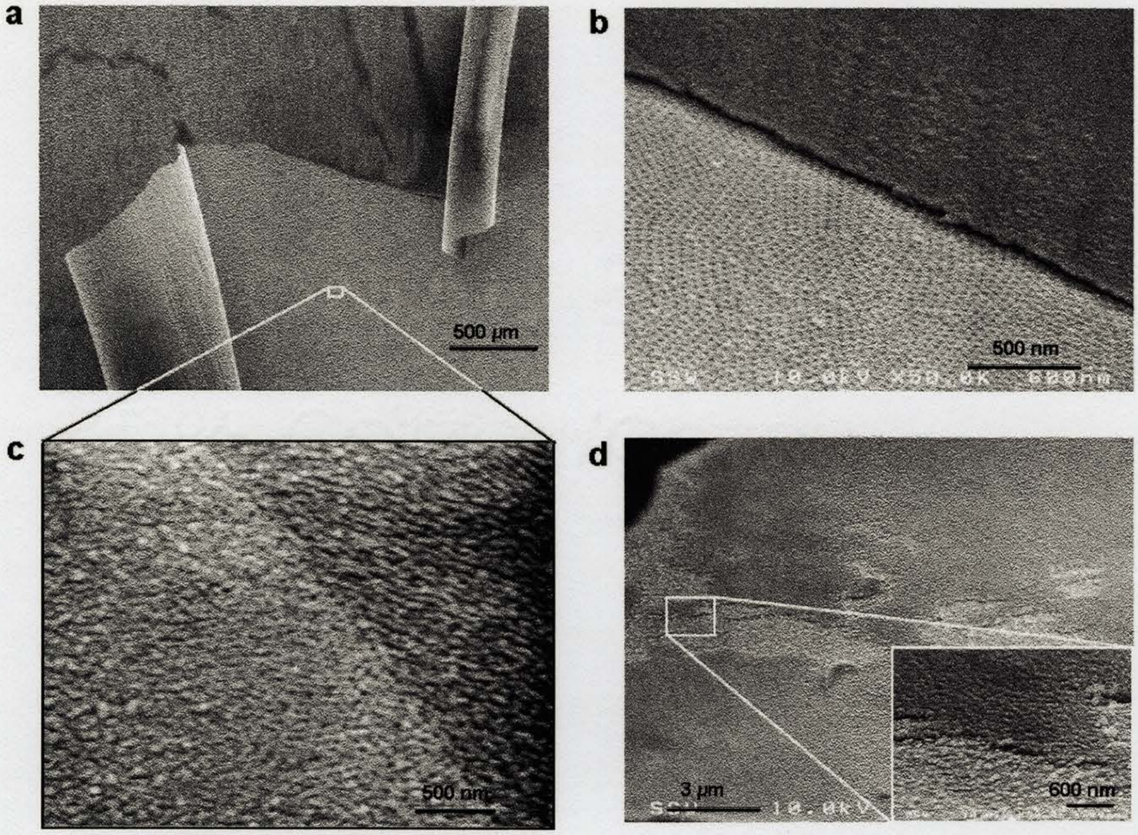

Figure 5.3. SEM images of the film peeling process. (a) Partially detached and rolled-back oxide film on the tantalum surface. (b) Boundary of an oxide film after 1 min of oxide growth on a dimpled surface, showing dimples both on the remaining oxide film and on the freshly peeled surface. (c) Irregular structure of a surface left behind after peeling a film that was grown for 5 min on a dimpled surface (close-up from area of panel a). (d) Remnant interfacial oxide after detachment of a film that was grown for 10 min on a dimpled surface.

5.2.3 Dependence of Detachment on Thickness

Oxide films grown for 10 minutes (1M H_2SO_4, 2 wt% HF, 20 V) leave undetached flakes of oxide (a few nm thick) behind on the surface, but the film still peels off uniformly (Figure 5.3d). The amount of oxide left on the surface after peeling off the films is measured with nuclear reaction analysis (NRA) using the $^{16}O(d,p)^{17}O$ nuclear reaction with a 972 keV deuterium primary beam (1 mm^2). NRA reliably gives a signal that is strictly proportional to the total oxygen content in the near surface region (approx. 0.5 μm deep) of the sample. A compact Ta_2O_5 film of a known thickness of 70.7 nm serves as a calibration standard. More about the experimental setup of the NRA system at Interface Science Western can be found elsewhere.[37] The average thickness (over 1 mm^2) of the oxide remaining on the tantalum surface after peeling increases from 2.1 nm and 2.2 nm for the 1 min and 5 min samples respectively to 3.1 nm for the 10 min sample. Clearly, the structure of the films changes with time during the oxide growth process.

A closer look at the cross-section of a 5 min film (Figure 5.4a) reveals the heterogeneous structure. A very porous layer rests on a more compact looking oxide, with a narrow stripe (dark in Figure 5.4a) at the interface to the tantalum metal which likely plays a role in detachment. The evolution of tantalum oxide films during anodic oxidation in F^- containing solutions has been studied before.[38,39] It was shown that the anodization current during oxide growth is mainly related to the migration of ionic species (F^-, O^{2-}, OH^-) from the electrolyte towards the metal/metal oxide interface and Ta^{5+} from the metal towards the oxide/electrolyte interface under the applied potential.

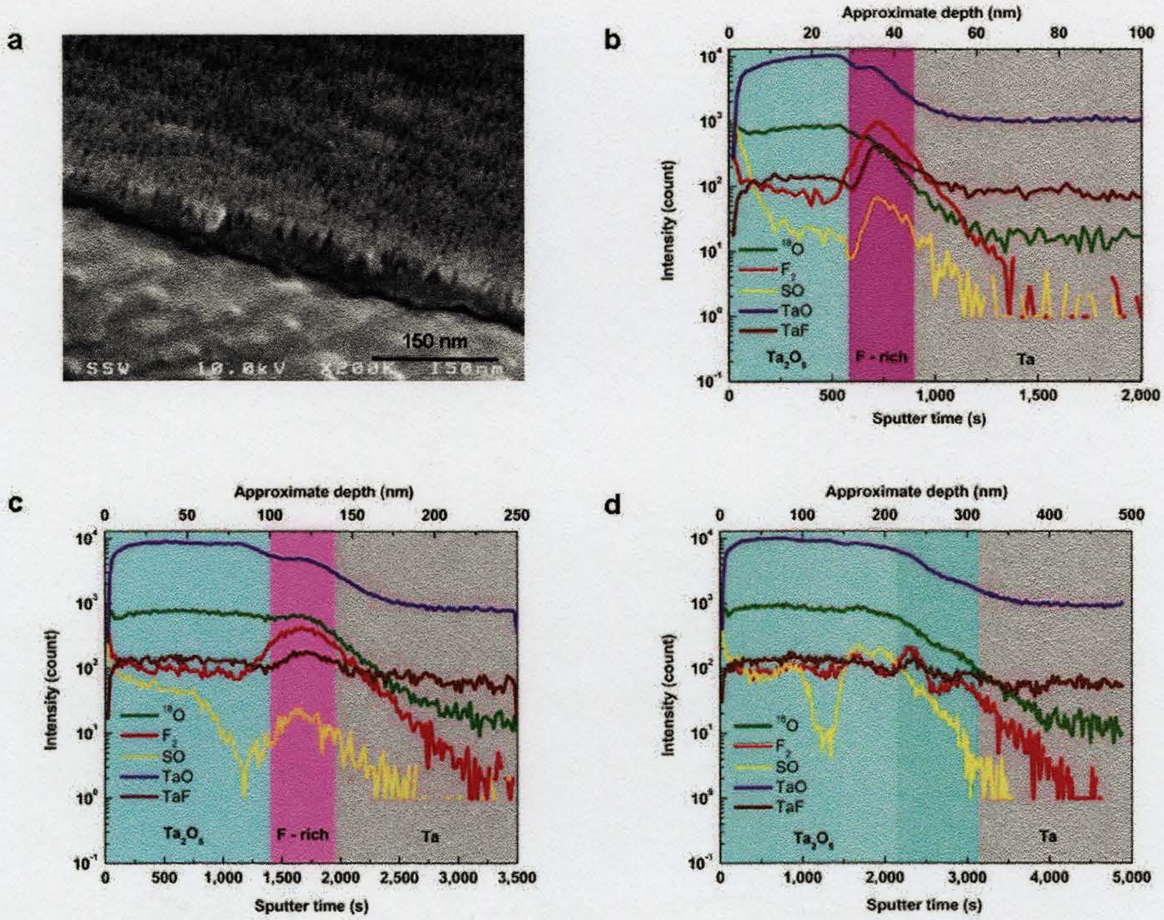

Figure 5.4. SEM micrograph of cross-sectional structure and ToF-SIMS depth profiling data of tantalum oxide films grown for different times. (a) Close-up of the edge of a partially detached 5 min oxide film. (b) Depth profile of a film grown for 1 min. (c) Depth profile of a film grown for 10 min. (d) Depth profile of a film grown for 20 min.

The higher mobility of F^- as compared to O^{2-} was shown to result in a thin tantalum fluoride rich layer at the metal/metal oxide interface. We performed depth profiling time-of-flight secondary ion mass spectrometry (TOF-SIMS) on our films to analyze the changes in film chemistry under our specific conditions. Since the $^{16}O^-$ and $^{19}F^-$ channels were saturated during part of the depth profile (Figure 5.5), we followed $^{18}O^-$ and $^{19}F_2^-$ instead. Sulfate was followed as $^{32}S^{16}O^-$, tantalum oxide is represented in Figure 5.5.4 as $^{181}Ta^{16}O^-$ and tantalum fluoride and oxyfluoride as $^{181}Ta^{19}F^-$. The results are consistent with literature reports,[38] but for the first time also illustrate the transition between detachable and non-detachable films.

5.2.4 Oxyfluoride Layer at the Interface

The depth profile of the 1 min sample (Figure 5.4b) shows a very pronounced spike in the fluoride concentration at the interface between tantalum oxide and tantalum. This is a sign of an interfacial layer rich in tantalum oxyfluoride and tantalum fluoride species, which are soluble in water, leading to the very facile detachment of the film. This picture changes for the 10 min sample (Figure 5.4c, characteristic mass spectra provided in Figure 5.5), where the fluorine peak has broadened and become shallower. Indeed, films from 10 min samples (e.g. Figure 5.3d) do not detach as easily. While tantalum fluoride and oxyfluoride continue to be present in the film, they are dispersed in an insoluble tantalum oxide matrix. Finally, a 20 min sample (Figure 5.4d) no longer has an interfacial layer with elevated fluoride concentration, even though a spike in sulfate concentration is visible in the center of the film, possibly associated with the bottom of the highly porous top layer. Fluoride and oxyfluoride species are present throughout the film, but the insoluble tantalum oxide matrix now firmly holds the anodic film on the tantalum surface.

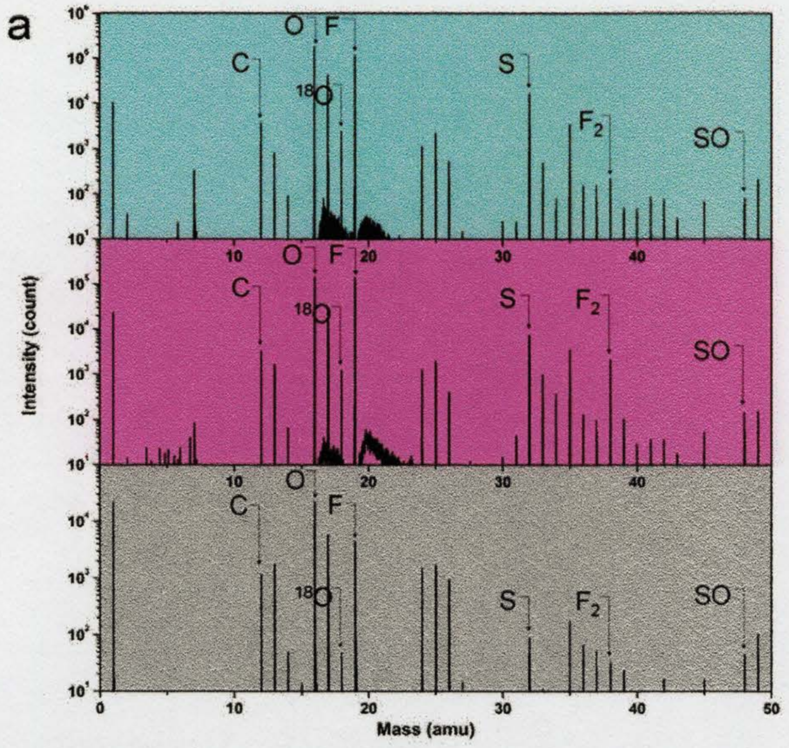
a
Intensity (count)
Mass (amu)
C
O
F
^{18}O
S
F_2
SO
0
10
20
30
40
50
10^1
10^2
10^3
10^4
10^5
10^6

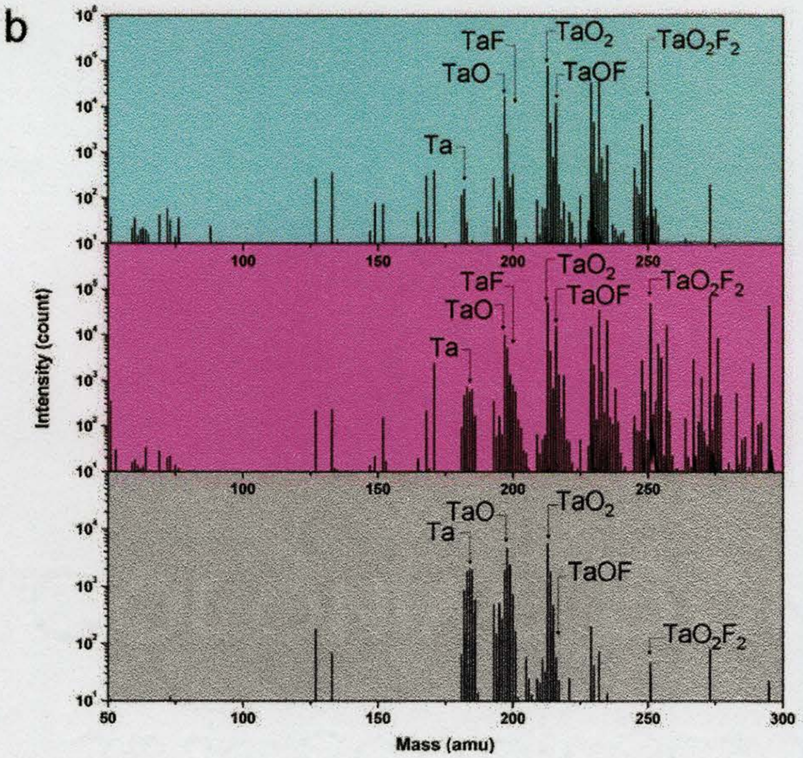
b
Intensity (count)
Mass (amu)
Ta
TaO
TaF
TaO_2
TaOF
TaO_2F_2
50
100
150
200
250
300
10^1
10^2
10^3
10^4
10^5
10^6

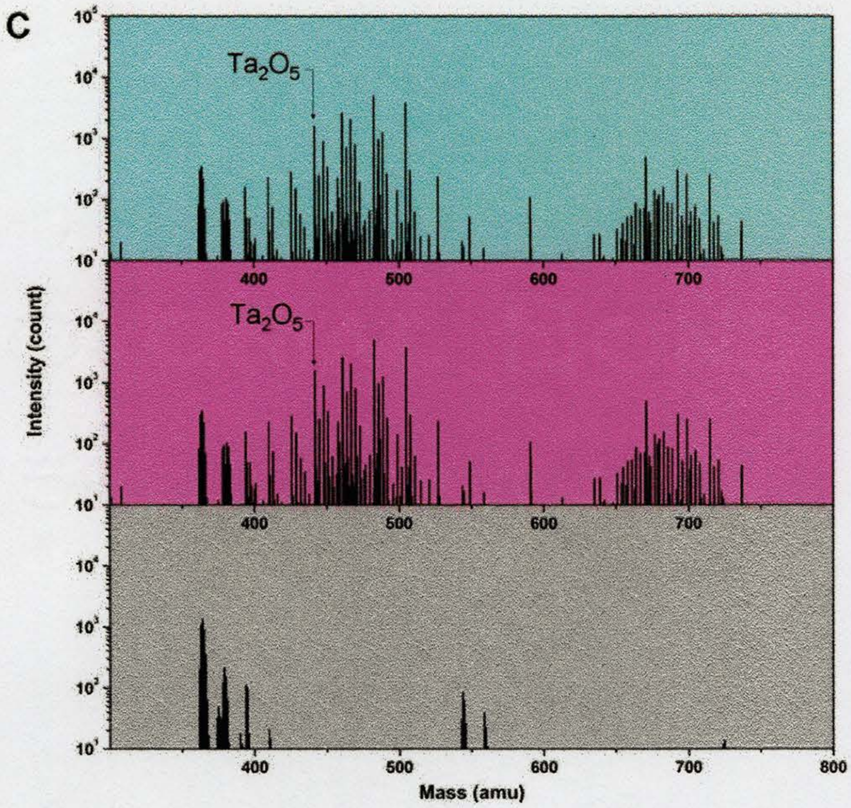

Figure 5.5. (a), (b) and (c) are SIMS spectra of inorganic tantalum oxide membranes grown on tantalum surface for 5 min at 20 V in 1M H_2SO_4, 2 wt% HF solution. Each part of the figure compares spectra from the three different regions, color coded to match Figure 4c. Green = bulk tantalum oxide film; Pink = fluorine-rich interface region leading to detachment; Grey = bulk tantalum metal. The ToF-SIMS data presented in Figures 5.4 was extracted from the full data set which is archived at the Surface Science Western analytical facility.

The lack of a distinct fluoride peak at the metal – oxide interface in the case of longer oxide growth times is not consistent with earlier findings[38] that the migration speed of fluoride ions within the films exceeds that of oxide ions. We note that even though those findings concern thicker oxide films than reported here, Shimizu et al. also employed considerably higher anodization voltages (100V) than in our study (20V). Irrespective of voltage, high concentrations of fluoride ions get incorporated into the films during the initial stages of oxide film formation. Initially, fluoride ions migrate faster than oxide ions, thus keeping up with oxide film growth. However, as the field gradient within the film decreases below a critical value of about one third of a Volt per nm due to the increase in film thickness, fluoride ions fall behind oxide ion migration as evidenced by the data presented in Figure 5.4.

The detachment of films from the tantalum surface at the air-water interface can be understood by considering the surface forces and the dissolution of tantalum fluoride in water. Penetration of water between the metal and the metal oxide film initiates the film detachment. The film detaches due to the interfacial forces at the triple contact line (air-water-substrate) and simultaneous dissolution of tantalum fluoride. We were not successful in detaching these films using low surface tension liquids such as acetone and ethanol even when they were first rinsed in water. Using a Wilhelmy plate, the surface tensions of water, acetone and ethanol are measured to be 72 mNm^{-1}, 23 mNm^{-1} and 22 mNm^{-1}, which compares well with literature values of 73.05 mNm^{-1} @ 18°C, 23.70 mNm^{-1} @ 20°C and 22.75 mNm^{-1} @ 20°C respectively.[40] Lack of solubility of tantalum fluoride in acetone and ethanol may be a contributing factor, however we note that the wetted films can be easily and completely peeled off using scotch tape. A subphase with higher surface tension (such as water) assists the detachment process, as has been reported before by Vilan et al.[41] during the separation of thin metal films from a variety of substrates. Nevertheless, it was observed that the films can float on low surface tension liquids like acetone and methanol by slowly exchanging the water underneath the films with these liquids. It should also be noted here that ultrasonication in water for 20 to 30 seconds is an alternative way of detaching the oxide films as small shards of a few square millimeters in size.

The uniform separation and transfer of large membranes illustrate their high mechanical strength. They can even roll and bend showing a certain degree of flexibility (Figure 5.3a). Previous studies[42,43] of the mechanical properties of tantalum oxide films show that porous tantalum oxide films are much more ductile (Young's modulus of 140 ± 14 GPa) than porous alumina films and can withstand up to 50% deformation before fracture. The tantalum oxide membranes reported here are stronger, thinner and have smaller size pores than porous aluminum oxide membranes, which are used as templates in a large number of applications.[44,45]

5.3 Modulating Porosity

The sheets are uniform and flat over large areas, and can contain ordered arrays of dimples 30-50 nm in diameter which are riddled with small pores perpendicular to metal/metal oxide film interface (Figure 5.6). The porosity arises from the dissolution of Ta_2O_5 by HF. The effect of fluoride ion concentration in the electrolyte solution is shown in Figure 6a-c. The pore density and pore size increase as the HF concentration increases from 0.5 wt% to 4 wt% in 1M H_2SO_4 solution. It is also observed that the pores in films grown on dimpled tantalum sheets (Figures 5.6b, c) are slightly more ordered than pores in films grown on a flat tantalum surface (Figure 5.6f), with larger pores loosely following the dimple pattern. Transmission electron microscopy (TEM) measurements (Figure 5.6 d, e) were also carried on membranes prepared on dimpled tantalum surface by anodization for 5 min in 2 wt% HF/ 1M H_2SO_4 and 0.5 wt% HF/ 1M H_2SO_4 solutions at 20 V and transferred on copper grids of mesh size 50. Membranes fabricated in 0.5 wt% HF have very small pores which do not penetrate the dimpled membrane (Figure 5.6d). On the other hand, the membranes prepared in 2 wt% solution have large diameter pores which penetrate the membrane whereas smaller size pores terminate before reaching the other end (Figure 5.6e).

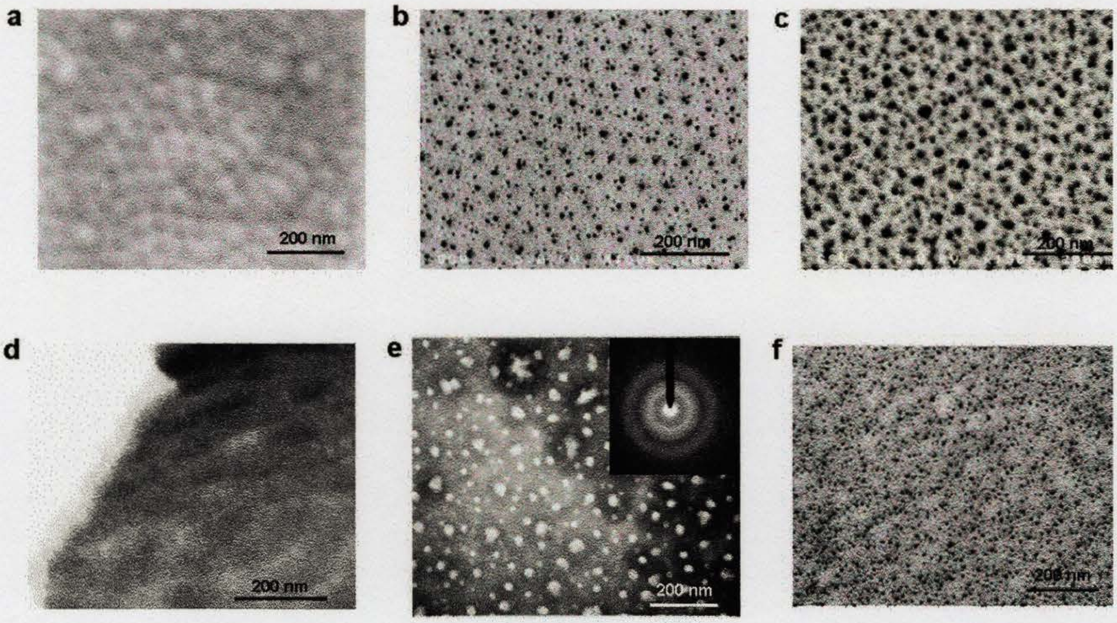

Figure 5.6. SEM and TEM images of pores in membranes grown under different conditions. (a) SEM image of an oxide film with dimples but no visible pores grown for 5 min in 0.5 wt % HF. (b) SEM image of an oxide film with small pores loosely aligned with dimples grown for 5 min in 2 wt % HF. (c) SEM image of an oxide film with large pores grown for 5 min in 4 wt % HF. (d) TEM image of an oxide film with dimples for 5 min in 0.5 wt % HF. Bright dots are probably due to shallow small pores that were invisible in SEM. (e) TEM image of an oxide film with pores grown for 5 min in 2 wt % HF. Some pores appear to penetrate the membrane. (f) SEM image of an oxide film with small pores grown for 5 min in 2 wt % HF on a previously peeled surface without dimples (such as Figure 5.3c).

5.4 Properties of Ta_2O_5 Membranes

5.4.2 Crystallinity

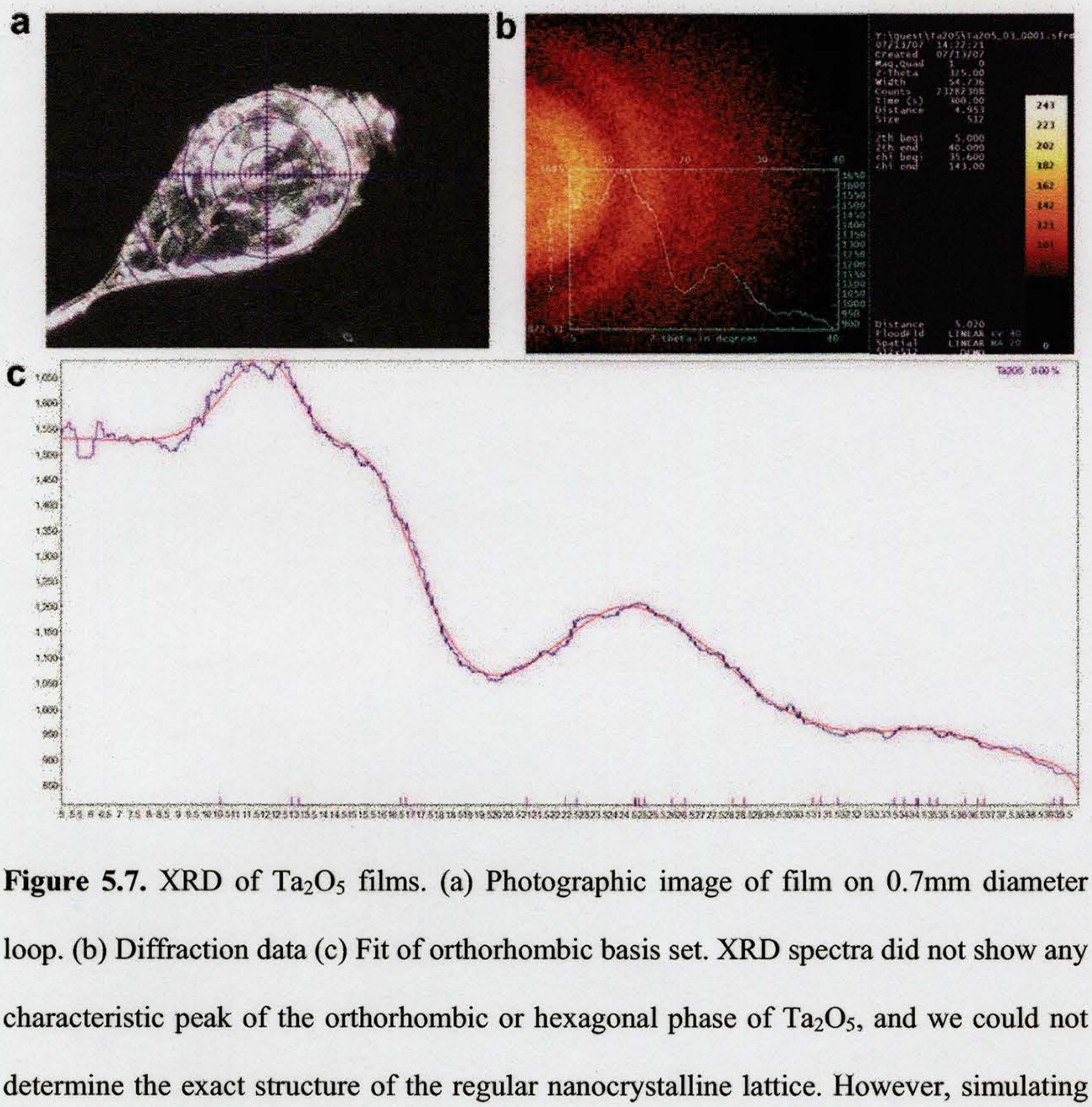

Figure 5.7. XRD of Ta_2O_5 films. (a) Photographic image of film on 0.7mm diameter loop. (b) Diffraction data (c) Fit of orthorhombic basis set. XRD spectra did not show any characteristic peak of the orthorhombic or hexagonal phase of Ta_2O_5, and we could not determine the exact structure of the regular nanocrystalline lattice. However, simulating the spectra using an orthorhombic basis set calculates the crystal size to be around 1.5 nm.

The diffuse electron diffraction pattern of the corresponding TEM image (inset of Figure 5.6e) indicates that the oxide in the membranes is amorphous. This is confirmed by X-ray diffraction (XRD), the results of which are provided as in Figure 5.7. The XRD spectra did not show any characteristic peak of the orthorhombic or hexagonal phase of Ta_2O_5, and we could not determine the exact structure of the regular nanocrystalline lattice. However, simulating the spectra using an orthorhombic basis set calculates the crystal size to be around 1.5 nm. For microelectronic applications the absence of crystallinity in Ta_2O_5 films is expected to be beneficial.[14] Annealing the membranes at around 700 °C under appropriate conditions will lead to crystallization, as has already been demonstrated for anodized tantalum oxide films.[14] Consequently, their mechanical properties and pore size[46] can be further tuned due to volume contraction.

5.4.2 Porosity

The porosity of these tantalum oxide membranes was calculated by comparing the thickness of the detached oxide membranes on a silicon substrate as measured by atomic force microscopy (AFM) with that of the total amount of oxide measured by NRA (Figure 5.8b). The oxide membranes grown at 20 V for 1, 2, 5, 8 and 10 minutes in 2 wt% HF and 1M H_2SO_4 were transferred onto Si (111) wafers and the step height of the Ta_2O_5 membrane was measured at the edge using AFM (Figure 5.8a). The porosity of the films increases with the thickness of the oxide layer and ranges from 20 Vol % to 45 Vol %. The thickness of oxide films increases at an average rate of about 8-9 nm per minute. Also the rate of dissolution increases with time because at the end the remaining oxide grows at a constant rate of 3.8 nm per minute (slope of NRA graph).

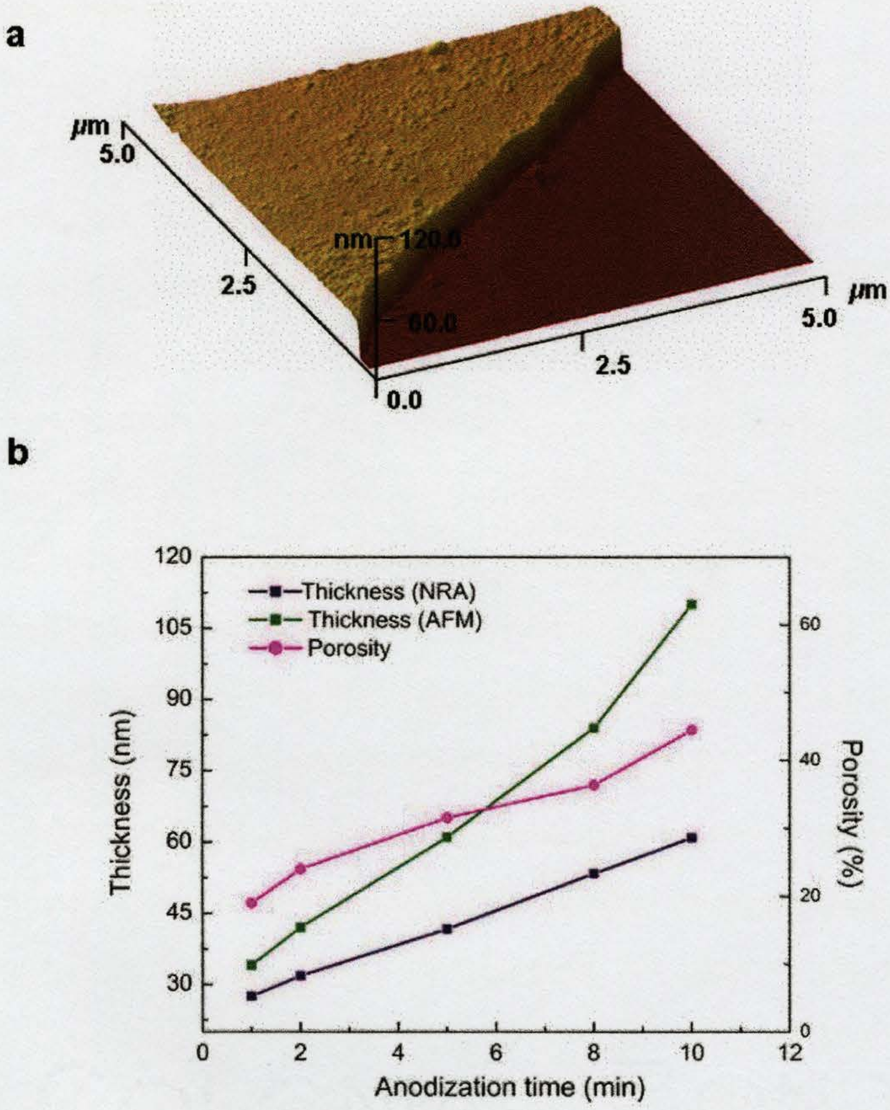

Figure 5.8. Film thickness and porosity. (a) AFM image of the edge of a tantalum oxide film growth for 5 min and transferred onto silicon, as it was used to measure film thickness. (b) Absolute thickness (*T*) of the membrane (by AFM), total amount of oxide (*O*, by NRA) and resulting porosity (*P*) as a function of anodizing time in 1M H_2SO_4, 2 wt % HF solution at 20 V. The porosity (*P*) was calculated as $P = (T - O) / T$.

5.4.3 Photonics

To better quantify the quality of our tantalum oxide membranes, we carried out refractive index measurements using iterative ellipsometry (Philips PZ-200 with HeNe laser, rotating analyzer) on five different tantalum oxide samples. Ellipsometry on porous films is nontrivial, because of possible inhomogeneities of the pores within the film,[47] the presence of adsorbates or humidity inside the pores, or in our case also the presence of F^- and SO_4^- ions inside the oxide. Tantalum substrates were anodized in a 2 wt% HF/ 1M H_2SO_4 solution at 20 V for 1, 2, 5, 8 and 10 minutes respectively and the resulting films were transferred onto glass slides. The average refractive index obtained by the iterative method for these membranes is 1.98 (± 0.02) which is slightly lower than the 2.1 reported for compact tantalum oxide.[48] The high refractive index of these membranes makes them ideal candidates for use in photonic crystals and waveguides. A detailed study is currently underway to further enhance their optical and mechanical properties as well as their surface morphology and pore size by annealing or tailoring electrochemical etching conditions.

5.5 Conclusions

In summary, we have presented a simple and inexpensive way of making self supporting, extremely thin membranes of pure tantalum oxide with remarkable control over their morphology, thickness and porosity. The principle behind the fabrication of these membranes is the utilization of differential diffusivity of anions from the electrolyte during the anodization of a metal surface to form a 'Sollbruchstelle' (predetermined breaking point) between the oxide layer and the metal. Anions that combine with the metal cations to form the insoluble membrane (e.g. O^{2-}) diffuse more slowly and dominate the outer layer, whereas anions that form the soluble Sollbruchstelle layer (e.g. F^-) quickly diffuse to the oxide layer – metal interface. The key to applying this principle lies in finding the suitable chemical system of solvent (e.g. water), insoluble membrane material (e.g. Ta_2O_5) and soluble Sollbruchstelle (e.g. TaF_5). Our method allows membrane transfer onto virtually any substrate, including biological and other soft materials, by removing the potential for physical damage resulting from most vacuum deposition procedures. Based on the exceptional properties of tantalum oxide, these porous membranes will find applications in photo-catalysis, molecular filtration membranes, Bragg like sensors and dielectric spacers. Furthermore, extension of our work to other metal oxides like niobium, titanium and hafnium would permit the fabrication of similar high aspect ratio oxide membranes, which are of great demand for catalysts, photovoltaics and electronic devices.

5.6 Experimental Section

Materials

H_2SO_4 (95-98% reagent grade), HF (48%), acetone, methanol and ethanol (all semiconductor grade) were purchased from Fisher Scientific. All chemicals were used as received without further purification. Tantalum foil (Alfa-Aesar, 99.95%, 0.127 mm) was mechanically cut, rinsed with acetone, methanol and then with Millipore water (18.2 MΩ.cm resistivity) and then dried under argon flow prior to anodization.

Electrochemical Setup for Electropolishing and Oxide Growth

Electropolishing and anodic oxide growth was performed inside a PTFE beaker using a conventional two-electrode system connected to a power supply (Agilent E3615A). A Pt/Ir wire (90/10, 0.25mm diameter, sold as STM tip wire by Nanoscience Inc.) was used 15 as the counter-electrode (cathode). The working electrode (anode) was a tantalum foil substrate connected with alligator clips and a copper wire to the power supply. The distance between the working and counter-electrodes was kept at approximately 1.5 cm. The solution was stirred using a magnetic bar. Freshly mixed electrolyte solutions typically need to settle for a few hours before the first sample is processed. All experiments were performed at room temperature (approximately 20 °C).

Instruments and Methods

The tantalum oxide membranes were separated using the dipper of KSV-2000 computer controlled Langmuir-Blodgett instrument (KSV Instruments Ltd.). Surface tensions of liquids (water, acetone, ethanol) used for the Lift-Off-Float-On technique were measured using the tensiometer (Wilhelmy plate) of the same LB trough.

Scanning electron microcopy (SEM) analysis was carried out using a Jeol 7000F FE-SEM field emission scanning electron microscope at the Brockhouse Institute for Materials Research and a Hitachi S-4500 FE-SEM at Surface Science Western. TEM measurements were carried out using a Philips CM-12 microscope on samples prepared on copper grids of mesh size 50 by Lift-off-Float-On (LOFO) technique. Atomic force microscopy was done in tapping mode on a Veeco Enviroscope with a Nanoscope-IIIa controller and Veeco RTESP p-doped Si tips with a nominal radius of less than 10 nm.

SIMS depth profiling was carried out in an ION-TOF (GmbH), ToF-SIMS IV equipped with a bismuth Liquid Metal Ion Source (LMIG). The primary analysis beam was pulsed 25 keV, Bi_3^+ with a ~ 1.5 μm spot size and a target current of ~ 0.5 pA. The Bi_3^+ primary beam was rastered over a 75 μm x 75 μm area that encompassed the area of interest. The mass resolution for this work was ~ 10,000 above 200 amu and the mass range was 0 - 1000 amu. Due to the insulating nature of the samples, a pulsed electron flood gun was employed for charge neutralization. To allow depth profiling of the thin tantalum oxide layers, a second 500 eV Cs^+ ion beam was used with a raster size of 150 μm x 150 μm. The Bi_3^+ analysis region is centred within the Cs^+ sputter crater, so as to avoid edge effects. By alternating the two ion beams with a flood gun pulse in between cycles, a depth profile is acquired. Since the species of interest included mainly F, S and

O as well as oxides and possible oxyfluorides of Ta, negative secondary ions were monitored.

X-ray diffraction (XRD) experiments were carried out on a Bruker Smart Apex-II diffractometer using a D8 3-circle goniometer, a graphite monochromater, a Molybdenum sealed tube (FF) radiation source and an Apex-II CCD detector. The XRD measurements were performed on the membrane after transferring it on a wire loop (diameter ~ 0.7mm) using LOFO technique. The detector was placed at -35° (2θ) angle and the signal integration time was 5 min. Apex-II software was used to collect the data, GADDS was used to process 2D and TOPAS was used to process 1D data.

Nuclear reaction analysis (NRA) employed the $^{16}O(d,p)^{17}O$ nuclear reaction with a 972 keV deuterium primary beam (1 mm^2) to determine the absolute oxygen content within ~0.5 μm of the surface. The deuterium beam was incident on the samples along the surface normal, and the detector was placed at 135° in the scattering plane which included the incident beam. The tantalum oxide thickness was estimated by comparing the number of protons emitted from the sample to those emitted from a calibration target of 70.7 nm (± 2 %) Ta_2O_5/Ta in an identical geometry. More about the experimental setup of the NRA system at Interface Science Western can be found elsewhere.[48]

Ellipsometry measurements were performed using a rotating analyzer Philips PZ-200 Ellipsometer operating at 632.8 nm (HeNe laser).

Author Contributions:

This chapter is based on a paper which has already been published in Nano Letters. (Singh, S.; Greiner, M. T. and Kruse, P. *Nano Lett.* **2007**, 7, 2676-2683). The author contribution for this paper is as follows. S. S. devised the method of making ultrathin membranes of tantalum oxide and conducted the electrochemical experiments. S.S. performed the SEM, TEM AFM and SIMS measurements on the samples. M.T.G. helped with the NRA experiments. Overall data analyses were conducted by the S.S. and P. K. S.S. wrote the manuscript with feedback from P.K. and M.T.G.

5.7 Bibliography

(1) Wollaston, W. H. On the identity of columbium and tantalum. *Phil. Trans. Roy. Soc. Lon.* **1809**, 1, 246-252.

(2) Findlay, D. M. *et al.* The proliferation and phenotypic expression of human osteoblasts on tantalum metal. *Biomaterials* **2004**, 25, 2215-2227.

(3) Macionczyk, F., Gerold, B. & Thull, R. Repassivating tantalum/tantalum oxide surface modification on stainless steel implants. *Surface & Coatings Tech.* **2001,** 142-144, 1084-1087.

(4) Christensen, C., Reus, R. & Siebe, B. Tantalum oxide thin films as protective coatings for sensors. *J. Micromech. Microeng.* **1999**, 9, 113-118.

(5) Sreethawong, T., Ngamsinlapasathian, S., Suzuki, Y. & Yoshikawa, S. Nanocrystalline mesoporous Ta_2O_5-based photocatalysts prepared by surfactant-assisted templating sol–gel process for photocatalytic H_2 evolution. *J. Molec. Catalysis A* **2005**, 235, 1-11.

(6) Zou, Z., Ye, J., Sayama, K., & Arakawa, H. Direct splitting of water under visible light irradiation with an oxide semiconductor photocatalyst. *Nature* **2001**, 414, 625-627.

(7) Rubio, J., Denis, J.M., Albella, J. & Martinez-Duart, M. Sputtered Ta_2O_5 antireflection coatings for silicon solar cells. *Thin Solid Films* **1982**, 90, 405–408.

(8) Nakagawa, Y., Yawata, M. & Kakio, S. Enhancement of photoelasticity assisted by surface acoustic wave and its application to the optical modulator. *Electronics and Communications in Japan (Part II: Electronics)* **2001**, 84, 46-54.

(9) Alers, G. B. *et al.* Intermixing at the tantalum oxide/silicon interface in gate dielectric structures. *Appl. Phys. Lett.* **1998**, 73, 1517-1519.

(10) Ueno, K., Abe, S., Onoki, R. & Saiki, K. Anodization of electrolytically polished Ta surfaces for enhancement of carrier injection into organic filed-effect transistors. *J. Appl. Phys.* **2005**, 98, 114503.

(11) Teravaninthorn, U., Miyahara, Y. & Moriizumi, T. The Suitability of Ta_2O_5 as a Solid State Ion-Sensitive Membrane. *Jpn. J. Appl. Phys.* **1987**, 26, 2116-2120.

(12) Kingon, A. I., Maria, J. P. & Streiffer, S. K. Alternative dielectrics to silicon dioxide for memory and logic devices. *Nature* **2000**, 406, 1032-1038.

(13) Devine, R. A. B. *et al.* Use of carbon-free Ta_2O_5 thin-films as a gate insulator. *Microelectron. Eng.* **1997**, 36, 61.

(14) Chaneliere, C., Autran, J. L., Devine, R. A. B. & Balland, B. Tantalum pentoxide (Ta_2O_5) thin films for advanced dielectric applications. *Materials Science and Engineering* **1998**, R22, 269-322.

(15) Zhang, S. *et al.* Experimental Demonstration of Near-Infrared Negtive-Index Metamaterials. *Phys. Rev. Lett.* **2005**, 95, 137404.

(16) Shalaev, V. M. *et al.* Negative index of refraction in optical metamaterials. *Optics letters* **2005**, 30, 3356-3358.

(17) Lu, Q. *et al.* Anodic film growth on tantalum in dilute phosphoric acid solution at 20 and 85 degrees C. *Electrochim. Acta* **2002**, 47, 2761-2767.

(18) Young, L. Steady-state kinetics of formation of anodic oxide films on tantalum in sulphuric acid. *Proc. Roy. Soc. Lon. Series A* **1960**, 258, 496-515.

(19) Sieber, I. & Schmuki, P. Porous tantalum oxide prepared by electrochemical anodic oxidation. *J. Electrochem. Soc.* **2005**, 152, C639-C644.

(20) Vermilyea, D. A. Formation of anodic oxide films on tantalum in non-aqueous solutions. *Acta Metall.* **1954**, 2, 483-486.

(21) Shimizu, K. *et al.* Direct observation of anodic films formed on tantalum in concentrated phosphoric and sulphuric acid solutions. *Corr. Sci.* **1998**, 40, 963-973.

(22) Sayed, H. E., Singh, S., Greiner, M. T. & Kruse, P. Formation of Highly Ordered Arrays of Dimples on Tantalum at the Nanoscale. *Nano Letters* **2006**, 6, 2995-2999.

(23) Sakai, H., Furukawa, Y., Fujiwara, E. & Tada, H. Low-voltage Organic Field-effect Transistors with a Gate Insulator of Ta_2O_5 Formed by Sputtering. *Chem. Lett.* **2004**, 33, 1172-1173.

(24) Demiryont, H., Sites, J. R. & Geib, K. Effects of oxygen content on the optical properties of tantalum oxide films deposited by ion-beam sputtering. *Appl. Optics* **1985**, 24, 490-495.

(25) Waldorf, A. J., Dobrowolski, J. A., Sullivan, B. T. & Plante, L.M. Optical coatings deposited by reactive ion plating. *Appl. Optics* **1993**, 32, 5583-5593.

(26) Zaima, S., Furuta, T., Yasuda, Y. & Iida, M. Preparation and Properties of Ta_2O_5 Films by LPCVD for ULSI Application. *J. Electrochem. Soc.* **1990**, 137, 1297-1300.

(27) Lo, G. Q., Kwong, D. L. & Lee, S. Metal-oxide-semiconductor characteristics of chemical vapor deposited Ta_2O_5 films. *Appl. Phys. Lett.* **1992**, 60, 3286-3288.

(28) Pollard, K. D. & Puddephatt, R. J. Chemical Vapor Deposition of Tantalum Oxide from Tetraethoxo(β-diketonato)tantalum(V) Complexes. *Chem. Mater.* **1999**, 11, 1069-1074.

(29) Gu, G. *et al.* V_2O_5 nanofibre sheet actuators. *Nature Materials* **2003**, 2, 316–319.

(30) Yang, H. Coombs, N. Sokolov, I. & Ozin, G. A. Free-Standing and oriented mesoporous silica films grown at the air-water interface. *Nature* **1996**, 381, 589-592.

(31) Vendamme, R., Onoue, S. Y., Nakao, A. & Kunitake, T. Robust free-standing nanomembranes of oganic/inorganic interpenetrating networks. *Nature Materials* **2006**, 5, 494–501.

(32) Wang, X., Lao, C., Graugnard, E., Summers, C. J. & Wang, Z. L. Large-Size Liftable Inverted-Nanobowl Sheets as Reusable Masks for Nanolithiography. *Nano Letters* **2005**, 5, 1784-1788.

(33) Choi, S. Y., Mamak, M., Freymann, G. V., Chopra, N. & Ozin, G. A. Mesoporous Bragg Stack Color Tunable Sensors. *Nano Letters* **2006**, 6, 2456-2461.

(34) Pan. S. & Rothberg, L. J. Interferometric Sensing of Biomolecular Binding Using Nanoporous Aluminum Oxide Templates. *Nano Letters* **2003**, 3, 811-814.

(35) Lin, V. S. Y., Motesharei, K., Dancil K. S., Sailor M. J. & Ghadiri M. R. A Porous Silicon-Based Optical Interferometric Biosensor. *Science* **1997**, 278, 840-843.

(36) Potyrailo, R. A. *et al.* Morpho butterfly wing scales demonstrate highly selective vapour response, *Nature Photonics* **2007**, 1, 123-129.

(37) Davies, J. A. & Norton, P. R. Absolute coverage measurement of adsorbed CO and D2 on platinum. *Nucl. Instrum. Methods* **1980**, 168, 611-615.

(38) Shimizu, K., Kobayashi, K., Thompson, G. E., Skeldon, P. & Wood, G. C. Anodic oxide films on tantalum: incorporation and mobilities of electrolyte-derived species. *Philos. Mag. B* **1996**, 73, 461-485.

(39) Shimizu, K., Kobayashi, K., Thompson, G. E., Skeldon, P. & Wood, G. C. The Migration of Fluoride Ions in Growing Anodic Oxide Films on Tantalum. *J. Electrochem. Soc.* **1997**, 144, 418-423.

(40) Lide, D. R. *CRC Handbook of Chemistry and Physics, 72th Ed.* (CRC Press Inc., Boca Raton, 1991).

(41) Vilan A. & Cahen, D. Soft Contact Deposition onto Molecularly Modified GaAs. Thin Metal Film Flotation: Principles and Electrical Effects. *Adv. Funct. Mater.* **2002**, 12, 795-807.

(42) Alcala, G. *et al.* Mechanical properties of amorphous anodic alumina and tantala films using nanoindentation. *Nanotechnology* **2002**, 13, 451-455.

(43) Rizkalla, H. & Wellinghoff, S. T. Inherent ductility in amorphous Ta_2O_5 films. *J. Mater. Sci.* **1984**, 19, 3895-3907.

(44) Masuda, H. & Fukuda, K. Ordered metal nanohole arrays made by a 2-step replication of honeycomb structures of anodic alumina. *Science* **1995**, 268, 1466-1468.

(45) Yamaguchi, A. *et al.* Self-assembly of a silica surfactant nanocomposite in a porous alumina membrane. *Nature Materials* **2004**, 3, 337–341.

(46) Striemer, C. C., Gaborski, T. R., McGrath, J. L. & Fauchet, P. M. Charge- and size-based separation of macromolecules using ultrathin silicon membranes. *Nature* **2007**, 445, 749-753.

(47) Herrero, A. A., Guerrero, H., Bernabeu, E. & Levy, D. Analysis of nanostructured porous films by measurement of adsorption isotherms with optical fiber and ellipsometry. *Applied Optics* **2002**, 41, 6692-6701.

(48) Ezhilvalavan, S. & Tseng, T. Y. Preparation and properties of tantalum pentoxide (Ta_2O_5) thin films for ultra large scale integrated circuits (ULSIs) application – A review. *J. Mater. Sci: Materials in Electronics* **1999**, 10, 9-31.

Chapter-6

Universal Method for the Fabrication of Detachable Ultrathin Films of Transition Metal Oxides

Ultrathin films are important nano-scale structures that are used extensively in a variety of technological contexts. However, it has traditionally been difficult and costly to fabricate detachable and purely inorganic high aspect ratio films with controlled thickness and good uniformity. Here we report a versatile method to make separable purely inorganic membranes of various metal oxides such as Nb_2O_5, TiO_2, WO_3, and Ta_2O_5 with thicknesses ranging from 30 to 150 nm. This is a conceptually unique method of fabricating ultrathin films, in which fluorine plays a dual role behind detachment of films and control over porosity due to etching. The study exposes the mechanism behind the detachment process that is largely due to the fast migration of fluoride anions relative to oxygen anions. This concept further opens up possibilities of making similar kind of detachable ultrathin membranes of other metals and semiconductors demonstrating its potential applications in material sciences

6.1 Introduction

Thin films have revolutionized many technological fields owing to their novel properties brought on by intrinsic surface effects. The ability to make ultrathin films has led to numerous advancements in technology such as microelectronics, optics, fuel cells, filtration, protective coatings, catalysis and sensing devices.[1,2,3,4] Several well established techniques such as chemical vapor deposition, reactive sputtering,[5,6] reactive ion plating,[7] and pulsed laser-assisted evaporation[8] are available to form thin films of a variety of materials. The drawback is that the films are strongly adherent to the surface and cannot be detached as free-standing membranes for uses in separation of gases, filtration of macromolecules, sheet actuators, catalyst surfaces and nano-lithographic templates.

Recently, the fabrication of free-standing ultra-thin organic/inorganic hybrid films has been reported.[9,10,11] Issues with these composite organic/inorganic films—poor thermal stability and lack of purity—have limited their use only under specified environmental conditions and have led to a significant interest in the fabrication of purely inorganic thin films. A promising avenue to solve these problems is the usage of purely inorganic materials that are robust and stable under harsh conditions. Fabrication methods based on photolithography, sol-gel techniques and surfactant assisted templating have recently shown a lot of promise for the fabrication of free-standing, purely inorganic and ultra-thin films of Si, Pt, Fe, C and CdSe.[3, 12,13] Despite these advances, the usage of these methods has been limited to research labs due to the expensive, long and specialized procedures involved in film fabrication.

Anodic oxidation of metal substrates in appropriate electrolyte solutions is one of the easiest, fastest and most energy-efficient techniques of growing metal oxide films with well-defined thickness and porosity.[14,15,16,17] However, these films are adherent to the substrate surface and are not easily separable, limiting their potential applications. Previously, we reported a simple "one pot" method for the fabrication of fully detachable, ultra-thin (35-100 nm thickness), and uniformly porous tantalum oxide membranes.[18] We found that the relatively fast migration of fluorine ions compared to other ions (such as O^{2-}), a phenomenon also studied by Shimizu and coworkers,[19,20] led to the simple film detachment. A thin oxyfluoride layer at the metal/metal-oxide interface acts as sacrificial zone and provides the predetermined breaking point (Sollbruchstelle) for the detachment of the metal oxide membranes from the underlying base metal surface.

In extension of the differential migration concept to other transition metal oxides, we now report the generic method of fabrication of detachable, porous and uniform ultra-thin films of Nb_2O_5, TiO_2, Ta_2O_5 or WO_3 with controllable thickness (from 35 to 150 nm). Whereas our previous study presented a state of the art technology and gives an indication of the principles behind the detachment process, this study generalizes the method on other metals and elucidates the details behind the mechanism, which enables tantalum oxide films to separate from the bulk metal surface. Good control over the size and degree of porosity of these free-standing membranes was achieved by varying reaction parameters such as etchant solution concentration, voltage and reaction time. Nb_2O_5, TiO_2, Ta_2O_5 or WO_3 have remarkable properties such as high melting point, high refractive index, piezoelectric behavior, hardness, high dielectric constant, excellent catalytic activity, chemical stability and corrosion resistance, which make these films relevant to applications in catalysis, optics, waveguides, electronics, supercapacitors, sensing etc.[21,22,23]

6.2 Fabrication of Nanomembranes

The general structure of our fabrication process encompasses three steps: electropolishing, oxide growth, and oxide sheet separation. Four different types of oxide sheets (Nb_2O_5, TiO_2, WO_3, and Ta_2O_5) were formed using our method. Nb_2O_5, TiO_2, WO_3, and Ta_2O_5 films were grown on electropolished Nb, Ti, W and Ta substrate surfaces by anodic oxidation in aqueous electrolytes containing either NH_4F or a mixture of HF and H_2SO_4 using a conventional two-electrode system (Figure 6.1a). The anodization conditions used for each specific metal are mentioned near its discussion.

6.2.1 Growth of Metal Oxide Films

The evolution of metal oxide films during anodic oxidation takes place by the migration of ionic species (F^-, O^{2-}, OH^-) from the electrolyte toward the metal/metal-oxide interface and M^{n+} from the metal toward the oxide electrolyte interface under the applied potential (Figure 6.1a, inset). A thin layer rich in metal oxyfluoride forms *in situ* at the metal/metal-oxide interface during anodization due to the higher mobility of F^- compared to O^{2-} under appropriate electric field as shown in zone 1 of Figure 6.1a. This

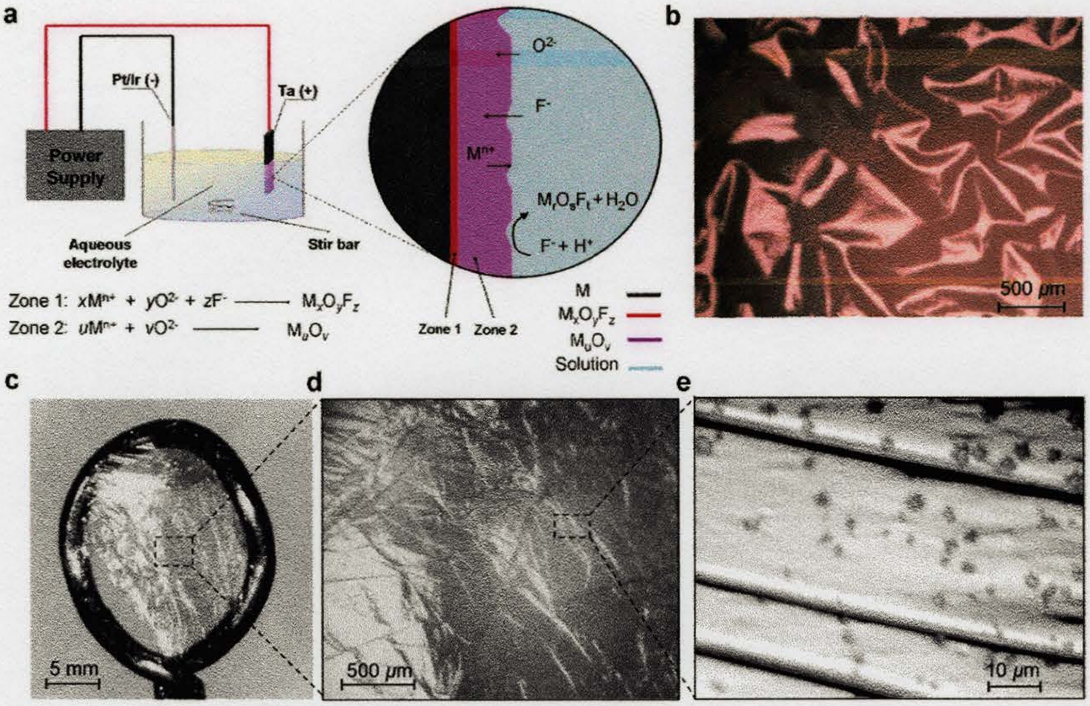

Figure 6.1. Preparation of transition metal oxide films by anodization. (a) Schematic diagram showing the anodic growth of the oxide film. (b) Optical image showing a detached 80 nm thick Nb_2O_5 membrane on filter paper. (c, d, e) Optical images of a 40 nm thick free-standing Ta_2O_5 membrane supported by a wire loop in air. The membrane is highly reflective in nature.

oxyfluoride layer provides the predetermined breaking point that we call a "Sollbruchstelle" for the detachment of the metal oxide membranes from the underlying base metal surface. A similar kind of sacrificial layer chemistry is used to make free standing membranes but the sacrificial layer is implanted before the fabrication of the film and then it is later dissolved.[24,25,26] However, in our case the sacrificial layer grows *in-situ* during the formation of oxide in the same electrolyte solution making the process simpler and straightforward. Along with detachment, the fluorine ions also etch away the oxide under acidic conditions to make it porous. Figure 6.1b-e shows typical optical images of the detached Nb_2O_5 and Ta_2O_5 membranes on filter paper and wire-loop. It should be noted that the lines in the zoomed-in images of Ta_2O_5 membrane (Figure 6.1d, e) represents the folds (with no cracks) developed during the transfer of the membrane from the air/water interface to the wire loop and demonstrates the excellent mechanical properties of these membranes.[27,28]

We performed depth profiling time-of-flight secondary ion mass spectrometry (TOF-SIMS) on the Nb_2O_5, TiO_2, WO_3 and Ta_2O_5 films to observe the changes in film chemistry as a function of depth under their specific fabrication conditions. The ToF-SIMS spectra of Nb_2O_5 (Figure 6.2a) (1 M NH_4F, 100 V, 10 s), TiO_2 (Figure 6.2b) (1 M NH_4F, 60 V, 10 s), WO_3 (Figure 6.2c) (1 M NH_4F, 50 V, 1 min) and Ta_2O_5 (Figure 6.2d) (1 M NH_4F, 20 V, 1 min) reveals the multilayer structure of our system having metal-oxide/metal-oxyfluoride/metal layers. A very pronounced spike in the fluoride concentration at the metal/metal-oxide interface confirms the presence of a thin layer (~ 5 nm) consisting of a broad range of different metal-oxyfluoride compounds such as TaF_5, TaO_2F, $TaOF_3$ etc. (in case of tantalum); Nb_2O_5, NbO_2F_2, $NbOF_3$ etc. (in case of niobium; $TiOF_3$, TiF_3 (in case of titanium) and WO_2F_2, WOF_2 (in case of tungsten). This thin layer forms because various anions (F^-, O^{2-}, OH^-) and metal cations M^{n+} combine in many different ways at the interface to give rise to this oxyfluoride compound mixture. This layer forms preferentially at the interface and not inside the metal oxide because of

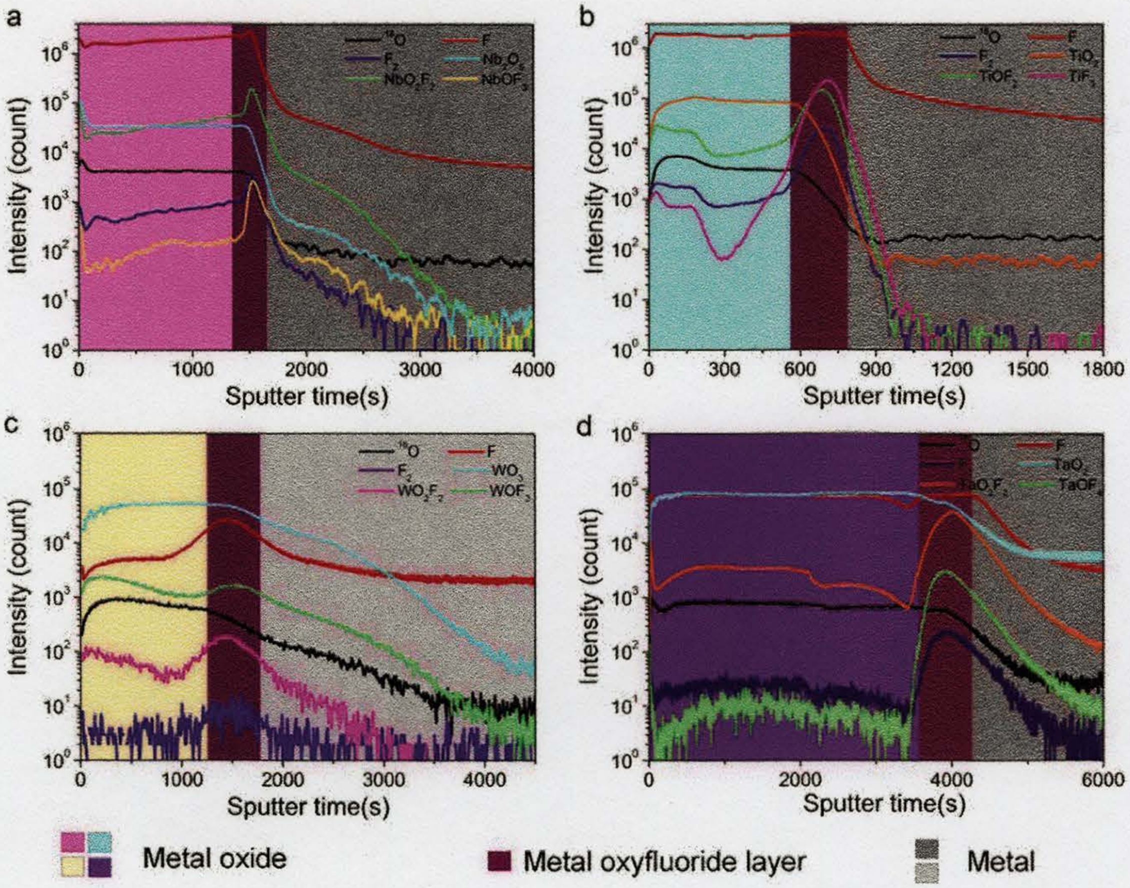

Figure 6.2. ToF-SIMS depth profiling data of detachable Ta_2O_5, Nb_2O_5, WO_3, and TiO_2. All of the depth profiles show a pronounced spike in the fluoride concentration at the metal/metal-oxide interface as shown by the dark areas. (a) Depth profile of Nb_2O_5 film grown for 10 s at 100 V. (b) Depth profile of a Ta_2O_5 film grown for 1 min at 50 V. (c) Depth profile of a TiO_2 film grown for 20 s at 60 V. (d) Depth profile of a WO_3 film grown for 1 min at 50 V.

the fast migration of F^- ions as compared to O^{2-} and OH^- under the high applied electric field (material specific but generally from 20 - 50 V). It is this very thin layer which results in poor adhesion of the metal oxide films to the underlying substrate.

6.2.2 Control Over Thickness of Membranes

The thickness of each metal oxide membrane sample can be controlled by adjusting the applied voltage and time of anodization, and is in the range of 30–150 nm under the current preparative conditions. However, the thickness of the oxide films has a substantial effect on their adhesion to the underlying metal surface. The detachment becomes progressively difficult with an increase in film thickness, requiring a larger peeling force. In general, films of thickness less than 150 nm are easiest to detach. The considerable increase in adhesion for thicker oxide films results from the decrease in fluoride ions migration due to a decrease in the magnitude of the field gradient within the film as the thickness of oxide membranes increases (see Ref. 18 and Figure 6.3). Detachment of thicker oxide films is possible under higher applied voltages but should not be too high or else the sample will burn because of dielectric breakdown. However, thicker films are in principle possible if the applied potential is gradually increased in a systematic manner.

6.2.3 Detachment of Oxide Films

Detachment behavior also varies between different metal oxide nanomembranes. The tantalum and niobium oxide sheets were separated from the bulk metal using the lift-off-float-on (LOFO) technique or ultrasonication with deionized water (Ref. 18). However, the LOFO technique only succeeds for thin tantalum and niobium oxide films but not for tungsten and titanium oxide films. Figure 6.4a, b show the LOFO process in which water seeps into the interfacial region of the freshly grown oxide on its metal substrate and dissolves the metal fluoride salts, thereby inducing separation. Even among

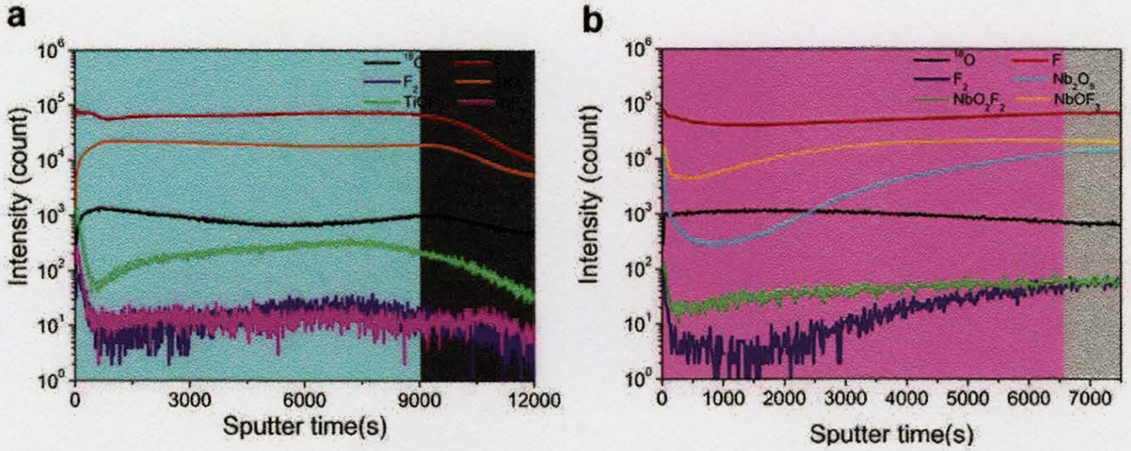

Figure 6.3. SIMS data of undetachable Nb_2O_5 and TiO_2 films grown by anodizing for longer time. (a) Depth profile of a Nb_2O_5 film grown for 1 min. (d) Depth profile of a TiO_2 film grown for 1 min at 50V in 1M NH4F solution. This data shows that it is difficult for the films to detach if they are grown for longer periods of time due to lack of oxyfluoride rich layer at the interface.

tantalum and niobium oxide, tantalum oxide membranes are easier to detach as one big sheet (up to 2 x 3 cm^2 were fabricated, limited by the size of our equipment), as compared to niobium oxide membranes. Niobium oxide membranes break up into small shards of a few mm^2 in size during separation. This might be due to the difference in mechanical properties of these different metal oxides putting tantalum on top of the list. However, the mechanical properties may be enhanced by using alloys of the particular metals.

The inorganic TiO_2 and WO_3 were very difficult to detach using the LOFO technique but can be easily peeled-off using a scotch tape (Figure 6.4d). This can be attributed to the difference in the solubility of metal oxyfluoride layer for these four kinds

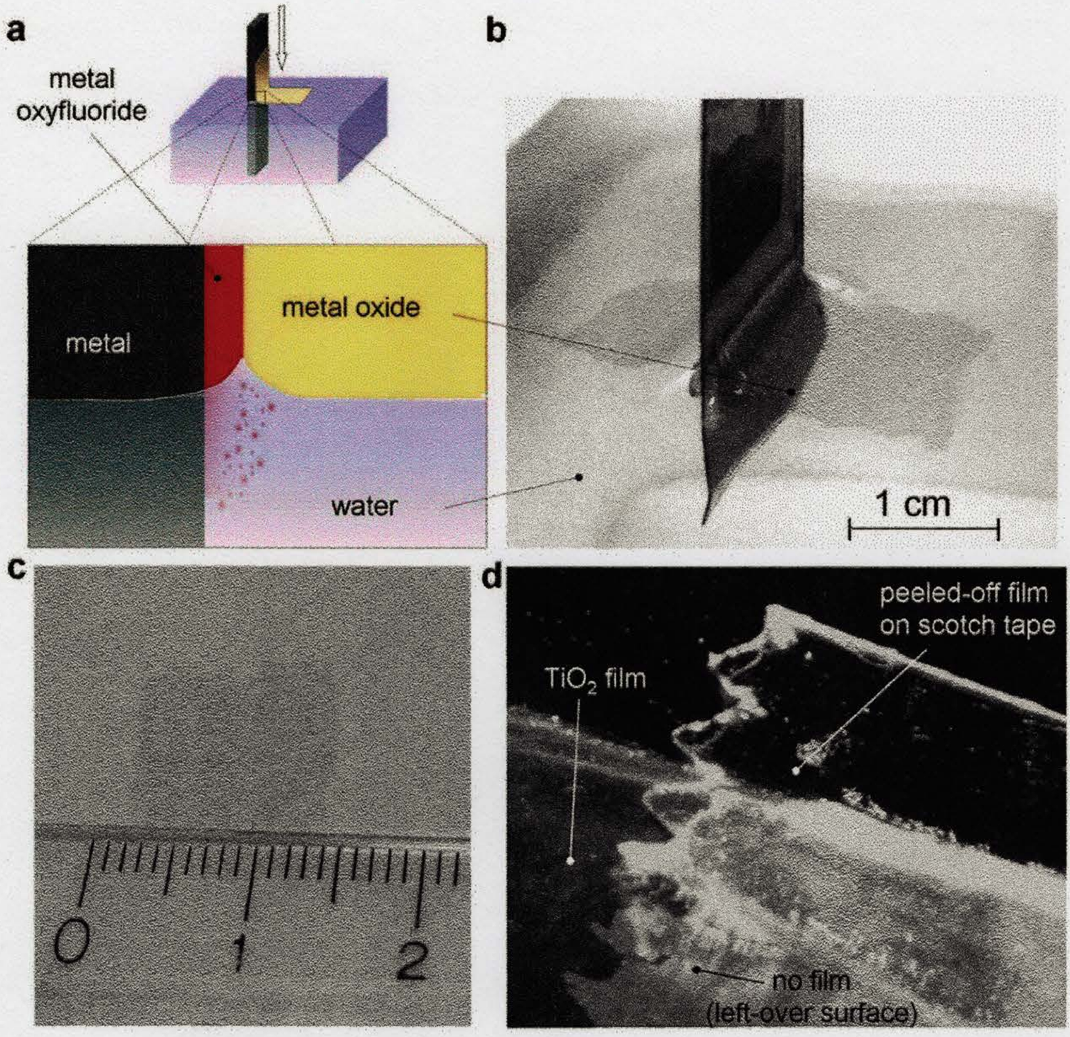

Figure 6.4. Illustration showing the film peeling process. (a) The architecture of the oxide film composition shown as separated layers. The film detaches by the dissolution of fluorine rich layer in water and floats over due to skin effect. (b) Micrograph of a partially detached and floating tantalum-oxide film over water surface. (c) Micrograph of a Ta_2O_5 nanofilm detached from the substrate and transferred on to glass slide. (d) Scotch tape peeling off a TiO_2 film (<100 nm).

of samples. Tantalum and niobium oxyfluoride species are reasonably soluble in water while their tungsten and titanium counterparts are unstable and insoluble.[29,30] A possible solution for fabricating self-supporting membranes of titanium and tungsten oxide is to detach the oxide films with an adhesive polymer followed by a rinse with solvent to regain a pure metal oxide.[31,32]

In order to further investigate the mechanism of fluorine ion migration and detachment, ToF-SIMS and X-ray photoelectron spectroscopy (XPS) measurements were performed on sequentially prepared different tantalum oxide samples. Similar affects were found in case of Ti, Nb and W oxide membranes indicating the generality of the observed phenomenon.

Analysis by XPS on the backside of peeled-off Ta_2O_5 membranes and left-over surfaces before and after rinsing them with water yielded important information on the presence and constitution of oxyfluoride layer. The XPS spectra of the underlying tantalum surface after peeling of a 40 nm thick film formed after anodizing an electropolished tantalum foil for 1 min in 1 M NH_4F solution at 20 V shows a thin layer of fluorine species on the surface (Figure 6.5a). This oxyfluoride layer can be removed by rinsing the substrate in Millipore water for 5 s confirming that this tantalum oxyfluoride layer is highly soluble in water (Figure 6.5b). On the other hand there is no significant difference in the XPS survey spectra of the backside of the detached Ta_2O_5 membrane before and after washing (Figure 6.5c and d). This means that the oxyfluoride layer is adherent to the base metal surface rather than the tantalum oxide membrane making them free of the oxyfluoride species. However, there is slight incorporation of fluorine into the membranes. This is expected, because tantalum oxides films grown by anodization are known to incorporate electrolyte anions (F^-) in the whole depth of the film.[33]

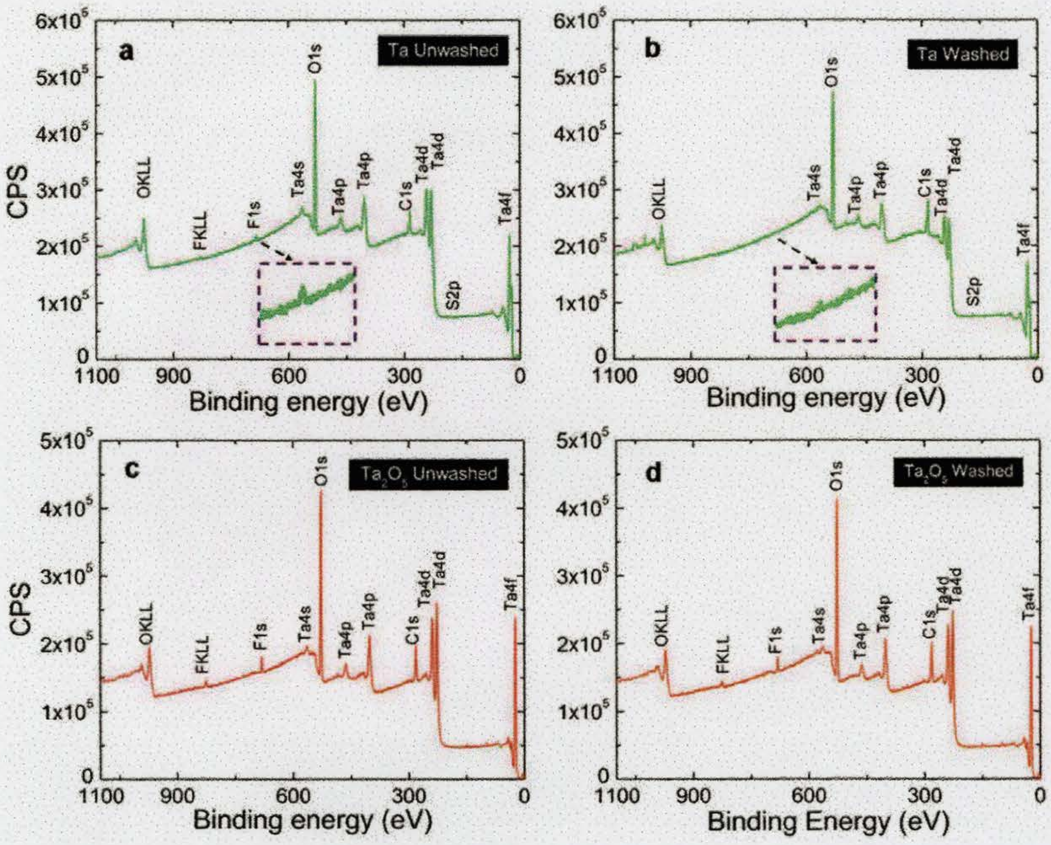

Figure 6.5. Survey XPS spectra on the left-over tantalum surface after peeling a tantalum oxide membrane grown for 1 min at 20 V in 1 M NH_4F solution (a) before washing with water (b) after washing. Survey XPS spectra of the backside of the peeled off oxide membrane (c) before washing with water (d) after washing. The data shows that the fluorine peak disappears after washing the tantalum metal but does not change after washing the oxide membrane.

We also examined the composition of the above mentioned tantalum oxide membranes using depth profiling ToF-SIMS after detaching and transferring them on to silicon surface with LOFO technique. The SIMS spectrum (Figure 6.6) shows that there is no sharp fluoride peak at the silicon/Ta_2O_5 interface confirming that the metal oxyfluoride layer dissolves in water.

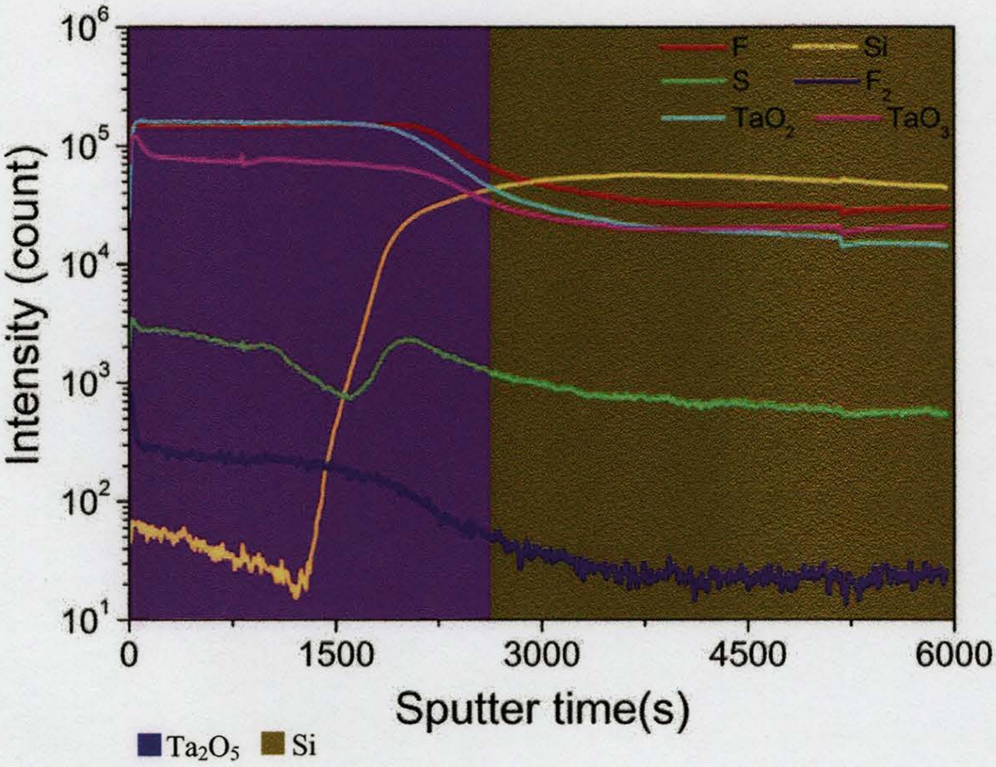

Figure 6.6. SIMS data of detached Ta_2O_5 film transferred on silicon surface using LOFO technique. The spectra shows that there is no fluorine peak at the Ta_2O_5/silicon interface indicating that the oxyfluoride species are soluble in water and gets washed away during the transfer from the water surface.

6.3 Differential Migration of Fluoride Anions

A series of experiments were performed in conjunction with ToF-SIMS depth profiling to determine the effect of concentration, voltage and time on the migration of electrolyte ions, specifically, F^- ions. Samples of tantalum metal were prepared by anodizing electropolished foils at 20 V for 1 min in 1 M H_2SO_4 electrolyte solution containing trace amounts of fluorine (<0.01 wt % HF). A second anodization step in 1 M NH_4F solution followed the first step for samples 2-4 at sample-specific voltages and anodization times. ToF-SIMS spectra were then obtained. The peak in the resulting spectrum of #1 (Figure 6.7a) indicates the presence of fluorine at the metal/metal-oxide interface. However, the oxide could not be separated implying that the amount of fluorine at the interface was insufficient to allow for detachment. The oxide layer of #2, prepared by re-anodizing the first sample at 30 V in 1 M NH_4F solution for 1 min, was also inseparable. The ToF-SIMS depth profile spectrum (Figure 6.7b) shows that the fluorine from the first experiment remains in the sample. A Ta_2O_5 layer (green shading) remains between the freshly migrated Ta oxyfluoride region and the metal/metal-oxide (located at x ~ 1400 s, Figure 6.7b) interface. Sample #3 was prepared by, after the initial step, anodization for 1 min at 60 V in 1 M NH_4F electrolyte. The ToF-SIMS spectrum (Figure 6.7c) shows a uniformly distributed region of fluorine from the oxide film surface to the metal/metal-oxide interface. In this case, the obtained film was detachable from the surface indicating that a sufficient amount of fluoride had somehow migrated to the interface. Sample #4 (Figure 6.7d) was prepared by reanodizing Sample # 1 at 60 V in 1 M NH_4F for 5 s. This film, like #3, detached.

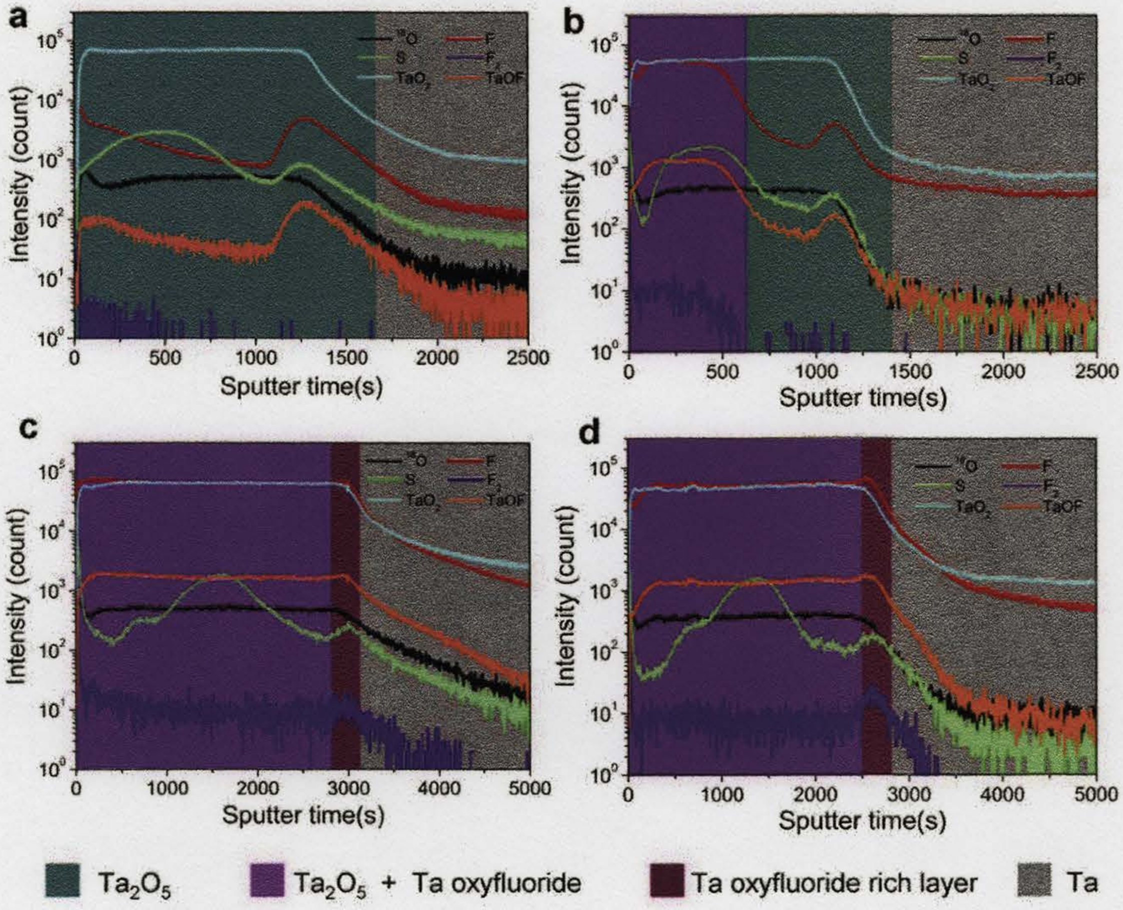

Figure 6.7. ToF-SIMS depth profile spectra of Ta_2O_5 films on tantalum substrate demonstrating the differential migration of fluoride ions under specific electric field strengths after sample-specific anodization treatments. (a) Sample #1: Inseparable Ta_2O_5 film grown for 1 min at 20 V in 1 M H_2SO_4 electrolyte (<0.1 wt % HF added). (b) Sample #2: Inseparable film grown for 1 min at 20 V in 1 M H_2SO_4 and then for 1 min at 30 V in 1 M NH_4F electrolyte. (c) Sample #3: Separable film grown for 1 min under 20 V in 1 M H_2SO_4 and then for 1 min at 60 V in 1 M NH_4F electrolyte. (d) Sample #4: Separable film grown for 1 min at 20 V in 1 M H_2SO_4 and then for 5 s at 60 V in 1 M NH_4F electrolyte.

Sample #1 had <0.01 wt % HF in solution. The ToF-SIMS spectrum (Figure 6.7a) shows that F^- is present at the interface but detachment was impossible implying that the threshold amount of Ta oxyfluoride species at the interface required for detachment was not there. Sample #2 was Sample #1 re-anodized with more F- in the electrolyte solution (from 1 M NH_4F) but the applied potential difference was not large enough to migrate the F^- ions to the interface and detachment failed. Too thick of an oxide does not let the fluorine ions pass and hence needs a high voltage. Sample #3 had more F^- in the solution and the potential difference was increased to 60 V resulting in a successful film detachment. This shows that there is sufficient F- in solution and that the driving force (electric field) was sufficient to migrate a sufficient amount of F^- to the interfacial region. Recent work of Shimizu and coworkers have shown that the fluoride anions migrate toward the metal substrate at a rate which is 1.85 times faster than that of oxygen ions under an appropriate voltage (~ 80 V).[20] Sample #4 was fabricated under the same conditions as Sample #3 but the anodization time was 5 s instead of the usual 1 min in the second anodization step. The resultant film was also separable implying that fluorine ions migrate towards the interface not by etching the oxide (as the anodization time is negligible) but by physically passing through the amorphous oxide.

Nonporous membranes were also made by growing the oxide in an electrolyte solution which does not contain fluorine species such as 1 M H_2SO_4. The films were then put in 1 M NaF solution and a potential of 60 V was applied. The films were detached if they were less than 100 nm thick. This shows that F^- migrates to the interface by passing through the amorphous oxide layer. However, the resulting films do not show any sign of porosity which is due to the lack of sufficient etching by F^- ions in the absence of adequate H^+ ions. These experiments show that fluorine concentration and applied potential should be above a minimum threshold value for the separation of metal oxide membranes from the base metal surface. However, the values can differ from metal to metal.

6.4 Porosity

The presence of fluorine ions in the electrolyte solution dictates the degree of separability and porosity of the oxide films during their fabrication. The small amount of fluorine is not only responsible for the film detachment but also causes a particularly rapid dissolution of the formed oxide thereby making the resultant oxide sheet porous.

$$M_xO_y + zF^- + yH^+ \rightarrow MF_z^- + yH_2O \tag{1}$$

The porous surface morphology of the metal oxide films is confirmed by analyzing their surface morphology using scanning electron microscope (SEM) and transmission electron microscope (TEM) images. The images in figures 6.8 and 6.10 show the porous nature of the fabricated Nb_2O_5, TiO_2, WO_3, and Ta_2O_5 films. The quality and degree of porosity depends greatly upon the type and concentration of the electrolyte solution used for anodizing. Porous Nb_2O_5 oxide sheets (Figure 6.8a-c) have disordered rough pores (Figure 6.8b) when anodized in 1 wt % HF and have circular and evenly distributed pores (Figure 6.8c) when 0.5 M NH_4F + 1 M H_2SO_4 electrolyte solution is used for anodization.

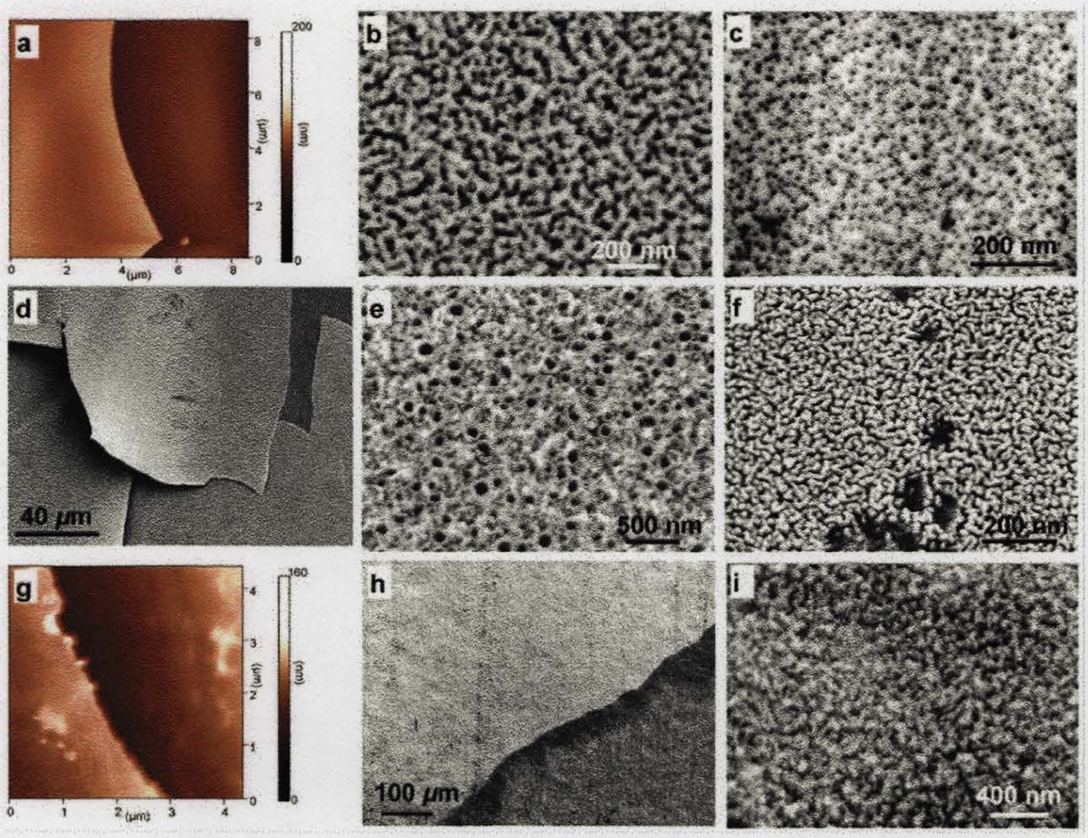

Figure 6.8. Scanning electron microscope (SEM) and atomic force microscope (AFM) micrographs of Nb_2O_5, TiO_2 and WO_3 membranes with modulated surface morphology and porosity. (a) 3D AFM image of the edge of an 80 nm thick Nb_2O_5 sheet showing an rms surface roughness of 2.6 nm in the (200 x 200) nm^2 area grown for 5 min in 0.5 wt % HF at 20 V. (b) SEM image of a Nb_2O_5 film with dimples but no visible pores grown for 5 min in 1 wt % HF at 20 V. (c) and grown for 20 seconds at 100 V in 0.5 M NH_4F + 1 M H_2SO_4 electrolyte. (d, e) SEM images of a TiO_2 film with small ordered pores grown for 5 min in 2 wt % HF at 20 V. (f) and with disordered random porous morphology grown in 1 M NH_4F for 20 s at 60 V. (g) 3D AFM image of the edge of a 60 nm thick WO_3 sheet showing an rms surface roughness of 7.2 nm in the (200 x 200) nm^2 area grown for 1min in 0.5 M NH_4F at 50 V. (h, i) SEM images of the WO_3 film as of (g).

TiO_2 films (Figure 6.8d-f) have either a tubular structure or a random surface morphology. The formation of tubular nanostructures is more favorable in solutions with a lower pH.[34,35] The surface morphology of WO_3 films is very rough and has highly disordered pores (Figure 6.8g-i). The energy-dispersive X-ray microanalysis spectra (Figure 6.9) of peeled-off Nb_2O_5, TiO_2, WO_3, and Ta_2O_5 membranes on carbon tape shows that these membranes are purely inorganic in nature with no other impurities detected. Recently, similar kind of nanostructured silicon oxide surfaces with disordered pores (~10 nm in size) prepared by anodic oxidation/etching have found an application in nanostructure-initiator mass spectrometry (NIMS) where the nanostructure of the surface helps in trapping desired molecules.[36]

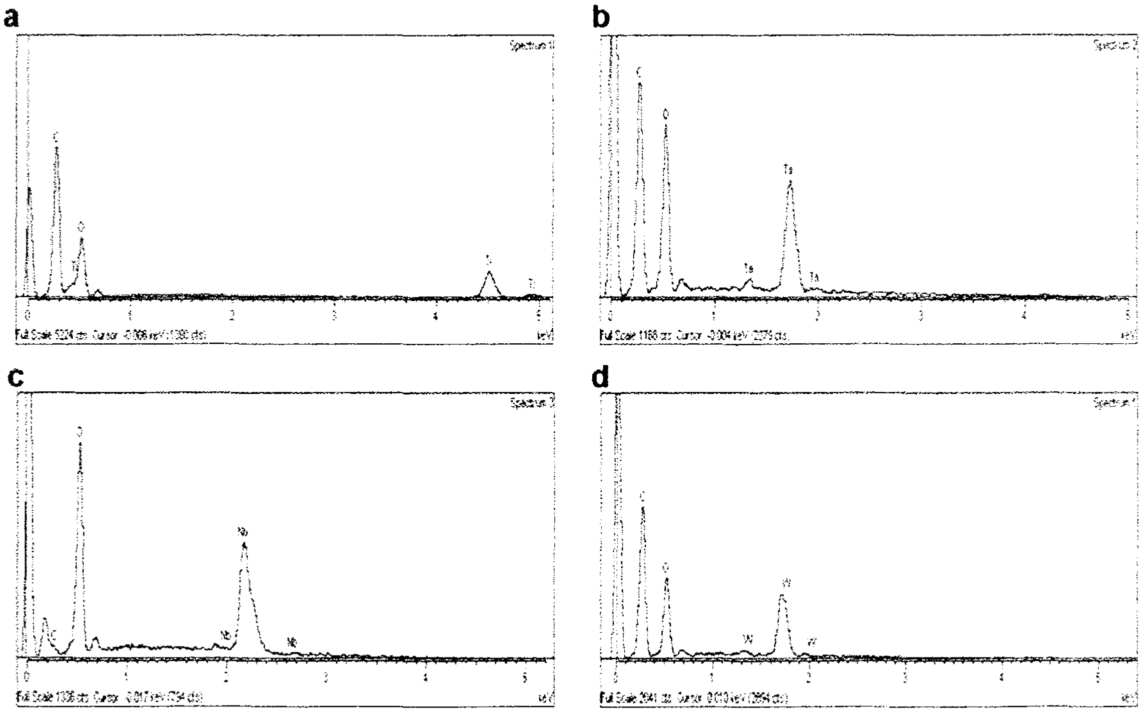

Figure 6.9. EDX spectra of Nb_2O_5, TiO_2, WO_3, and Ta_2O_5 films after peeling them on a carbon tape. This gives an idea about the purity of the oxide films.

6.4.1 Modulating Pore Size with Voltage

This section of the chapter discusses controlling the pore size and number primarily in tantalum oxide membranes. The electropolishing step generates highly ordered nano-dimples on the metal surface as outlined in a previous paper[37]. The dimpled morphology of the starting electropolished tantalum surface provides a handle in adjusting the number of pores inside each dimple of the dimpled morphology Ta_2O_5 membranes. In our previous paper we showed the control on pore size by changing the concentration of the solution. However, here we show that strength of the applied voltage provides a better handle in controlling the number and size of pores inside a dimple. The potential was kept constant during anodization and the current generally starts around 4 mA/cm^2 and gradually decreases as the oxide film grows with time. Well-controlled pores inside membranes are only observed under specific conditions as discussed below.

Smaller and more numerous pores are formed inside the dimple morphology of the membranes (Figure 6.10a and Figure 6.11a) at lower voltages (5 V) by anodizing the dimpled tantalum surface in 1 M H_2SO_4, 2 wt % HF for 5 min. As the voltage is increased to 10 V the number of pores inside each dimple decreases but their size increases (Figure 6.10b and Figure 6.11b). This ordering of pores is possible only at low voltages (~10 V) as films start to burn at higher voltages (more than 25 V) due to dielectric breakdown under the corrosive acid attack. Also, the pores start to form on the ridges of the dimples and the order deteriorates at voltages from 12 to 25 V (Figure 6.10e, f).

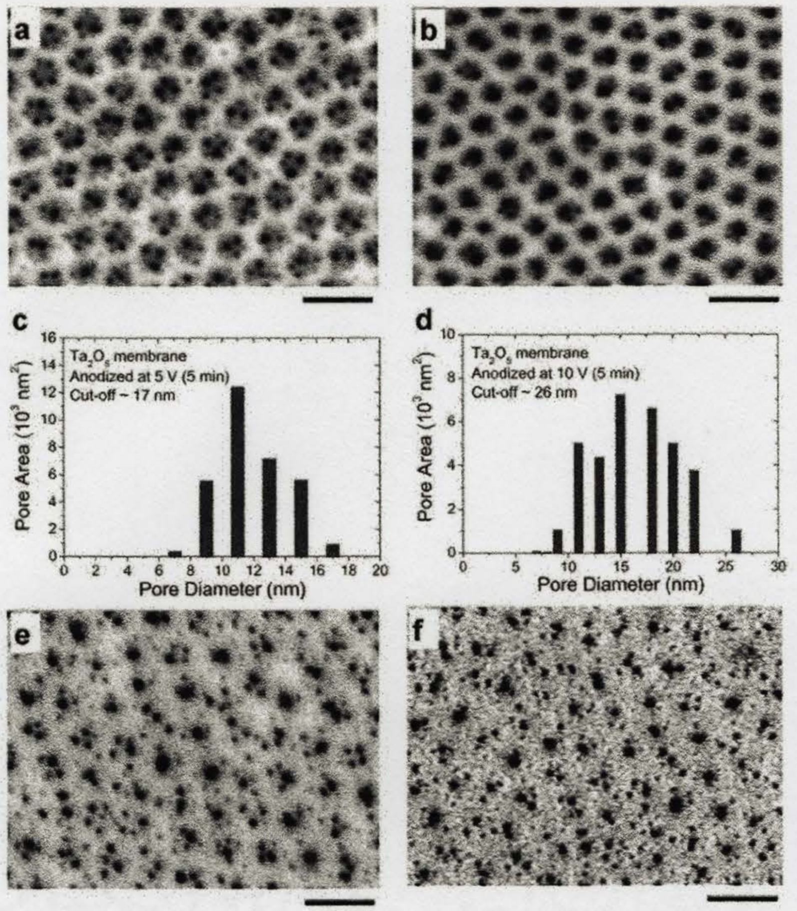

Figure 6.10. The effect of voltage on the modulation of pore size distribution in Ta_2O_5 membranes. Anodic anodization was carried out on mirror-finished tantalum substrates having highly ordered dimpled morphology (ref. 37) (a) Surface SEM micrographs of an oxide film with small pores aligned with dimples grown for 5 min in 1 M H_2SO_4 and 2 wt % HF at constant voltage of 5 V. (b) at 10 V. (c, d) The histograms that were generated using images a and b show the maximum (cut-off) pore size and porosity increase by changing the applied potential from 5 V to 10 V. (e) SEM image of an oxide film with small pores grown for 5 min in 1 M H_2SO_4 and 2 wt % HF at constant voltage of 15 V and (f) 20 V; showing the etching at the top of the ridges and the deterioration of the alignment of the pores with dimples. Scale bars correspond to 100 nm.

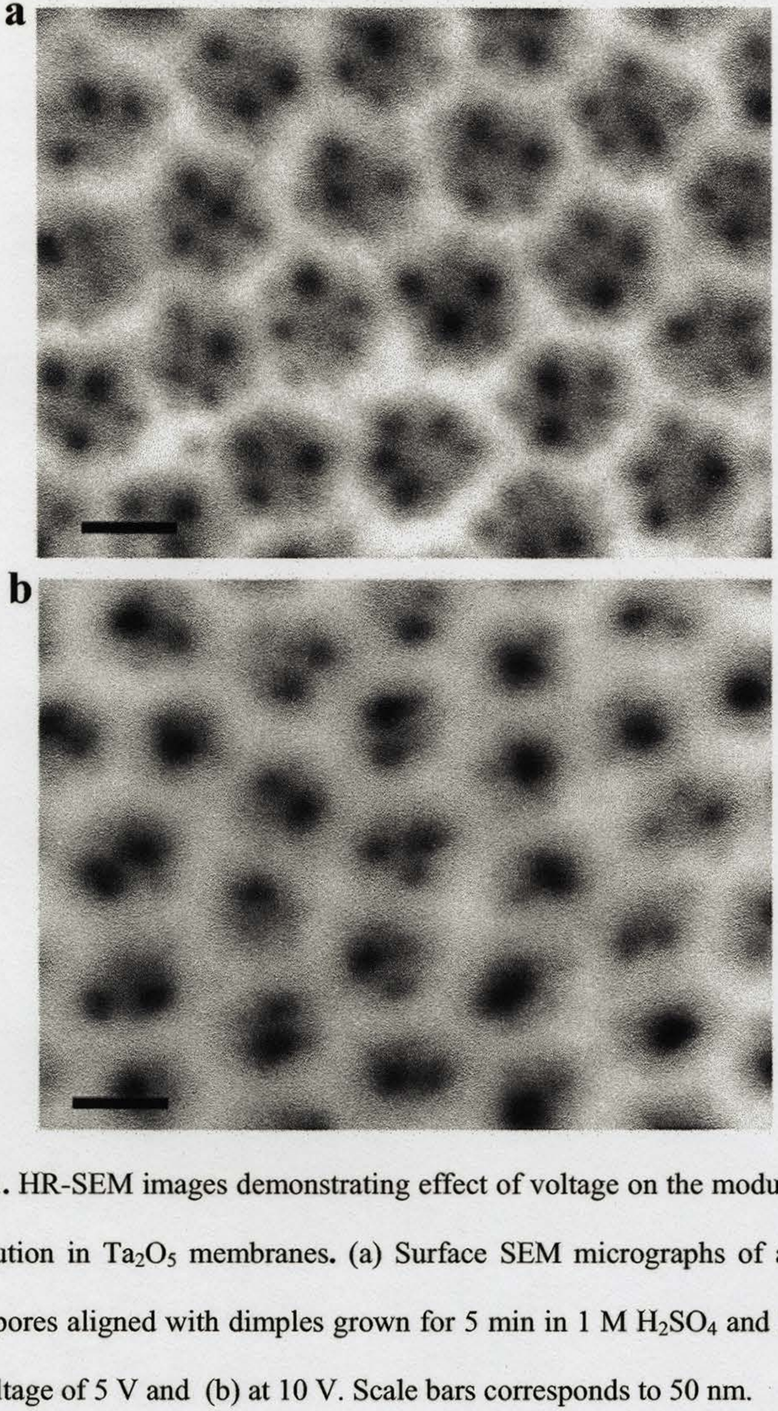

Figure 6.11. HR-SEM images demonstrating effect of voltage on the modulation of pore size distribution in Ta_2O_5 membranes. (a) Surface SEM micrographs of an oxide film with small pores aligned with dimples grown for 5 min in 1 M H_2SO_4 and 2 wt % HF at constant voltage of 5 V and (b) at 10 V. Scale bars corresponds to 50 nm.

The tunability of the number and size of the pores can be explained as localized etching that depends on the strength of the applied electric field. Low electric fields cause a localized electrolysis of water (generating H^+) and therefore a local etching (reaction equation 2) of tantalum oxide that results in smaller pores (Figure 6.11a and Figure 6.12a) due to the dissolution of the final products. High electric fields cause the electrolysis of water and the etching of the metal oxide to occur on a larger surface area that leads to the creation of bigger pores (Figure 6.11b and 6.12b).

$$Ta_2O_5 + 14F^- + 10H^+ \rightarrow 2TaF_7^- + 5H_2O \tag{2}$$

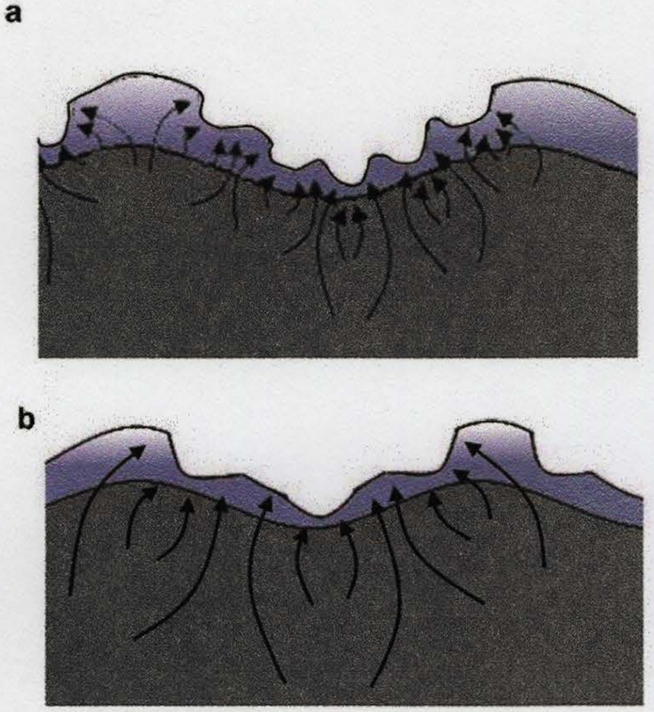

Figure 6.12. Schematic diagram showing the tunability of size and number of pores caused by variance of the strength of the applied electric field inside each dimple in Ta_2O_5 membranes. (a) Low electric field. (b) High electric field.

The electric field is more intense at the sections of the dimple with greater curvature causing the etching reaction to take place exclusively inside the dimple. As the electric field is increased from 10 V to 15 or 20 V, the etching also becomes more intense at the crest of the dimple. The pores starts to appear everywhere, but still the pores inside the dimples (Figure 6.10e, f), are larger in diameter than those on the ridges due to the high electric field inside the dimples as compared to that on the ridges. The ability to control and guide the size and number of pores in Ta_2O_5 membranes may be useful in nano-sieve filtration. Additionally, the numerous pores inside these membranes increase the surface area and could allow further chemical functionalization to further enhance their physical and chemical properties.

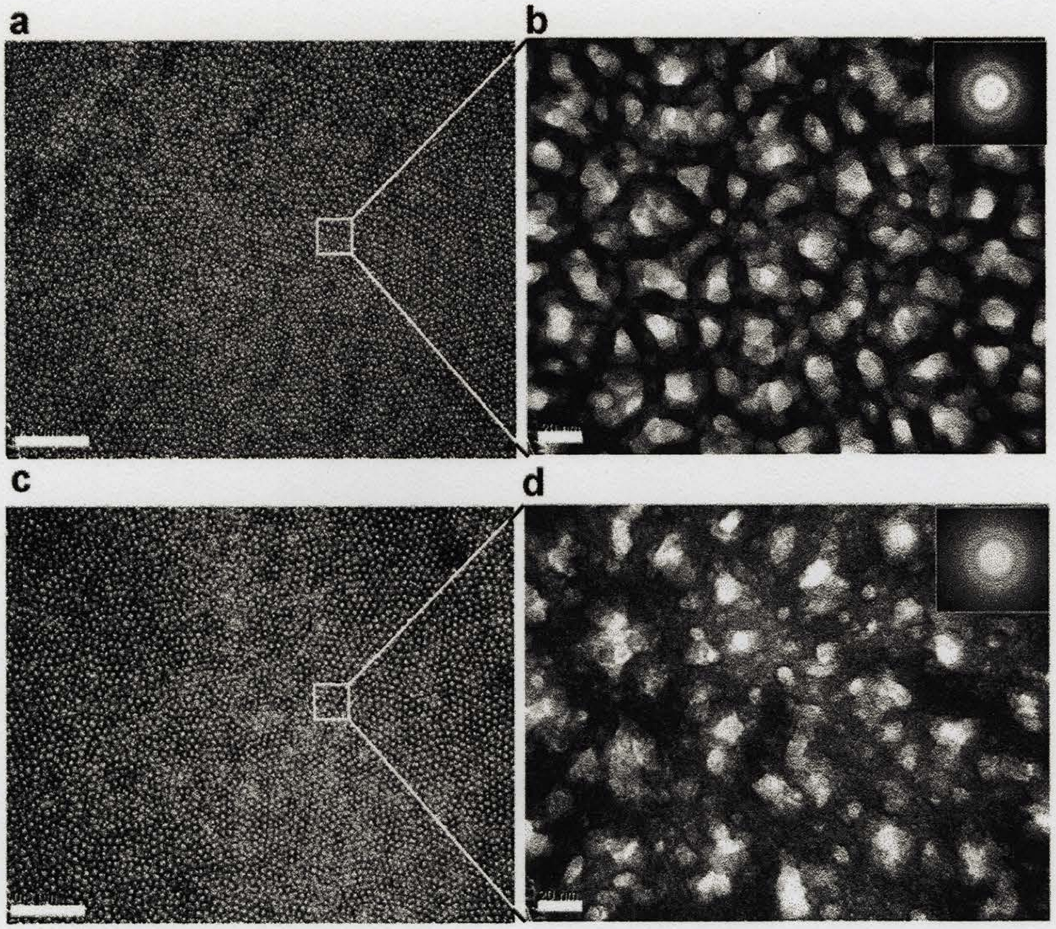

Figure 6.13. TEM-micrographs of Ta_2O_5 membranes with pores grown grown for 5 min in 2 wt % HF under (a) lower electric field (5 V) and (b) higher electric field (10 V). Pores near the center of the dimples penetrate more than pores at the ridges. Scale bars correspond to 500 nm for (a, c) and to 20nm for (b, d). Diffuse electron diffraction pattern (insets of b and d) indicates that the oxide in the membranes is amorphous

Not all of the pores penetrate the dimpled membrane as is evident from TEM micrographs taken of Ta_2O_5 membranes (Figure 6.13). However, more pores can be generated and their size further tuned by either annealing the tantalum oxide membranes to around 700 °C or chemically etching them under appropriate conditions to remove the barrier layer.[3,38,39] Annealing results in volume change (preferably contraction) of the material due to phase transformation and crystallization whereas etching will remove the material.

6.5 Conclusions

In summary, a simple and versatile method has been developed for fabricating purely inorganic, high-quality ultrathin membranes of transition metal oxides with nanoscale thickness (<100 nm). The membranes are riddled with small pores and anodization allows for fine tuning of pore size in tantalum oxide membranes via manipulation of applied potential during growth. Moreover, this study has introduced and generalized a new concept of differential migration of fluorine ions under the applied potential. So far, fluorine chemistry has traditionally generated much interest concern for safety but the discovery of more stable and effectively more controllable fluorinating agents has opened up a variety of possibilities in the pharmaceutical and silicon industry due to its usefulness in etching and lead optimization made possible by its binding efficacy, selectivity, and unique molecular properties.[40] Also in this case, fluorine is largely responsible for our success because it weakens the adhesion of the metal substrate to its protective oxide layer by migrating from the electrolyte solution to the metal/metal-oxide interface under an applied potential difference. This understanding of the fast fluorine ion migration under applied electric fields is not only an advance in fundamental science, it may also aid in technical developments, for example elucidating the role of LiF layer in organic light-emitting diodes (OLEDs).[41] Our membranes will find use as self supporting materials in the fields of catalysis, filtration, optics, sensors, and dielectric spacers.

6.6 Experimental Section

Materials

Materials: H_2SO_4 (95-98%, reagent grade), and HF (48%) used was bought from Fisher Scientific and NH_4F (40%, semiconductor grade) was purchased from Sigma Aldrich. Acetone, methanol and ethanol used were of semiconductor grade bought from Fisher Scientific. All the chemicals were used as received without any further modification.

Electrochemical Setup for Electropolishing and Oxide Growth.

The electrochemical cell was a two-electrode system consisting of a Pt/Ir (0.25 mm diameter) wire acting as the counter electrode and the cleaned metal foils as the working electrode (anode) connected to a power supply (Agilent E3615A). The distance between the working and counter-electrodes was kept at approximately 1.5 cm. During electropolishing and anodization, the solution was stirred using a magnetic stir-bar. Freshly mixed electrolytic solutions typically need to settle for a 16-20 hours before the first sample is processed. All experiments were performed at room temperature (approximately 20 °C).

Fabrication of membranes.

The titanium (Ti) foil (Alfa-Aesar, 99.99%, 0.127 mm), tungsten (W) ribbon (Alfa-Aesar, 99.95%, 0.125 mm) tantalum (Ta), (Alfa-Aesar, 99.95%, 0.127 mm) and Niobium (Nb) (Alfa-Aesar, 99.97%, 0.127 mm) samples used in this study were mechanically cut and rinsed with acetone, methanol and then with Millipore water (18.2 MΩ.cm resistivity) and then dried under argon flow before anodizing them. This was followed by electropolishing with a voltage of 15 V in a (v/v 9: 1 for Nb and Ta, v/v 8:2 for Ti and v/v 93:7 for W) mixture of concentrated H_2SO_4 (95-98% reagent grade) and HF (48%) for 5 minutes for Nb and Ta, 1 minute for Ti and 10 minutes for W. Freshly electropolished Nb, Ti, W and Ta foils were rinsed thoroughly in Millipore water and then were ultra-sonicated in water to remove any fluoride contamination and were finally dried under argon flow. These electropolished metal samples were subjected to anodization for specific times at constant voltages between 20 to 100V in either NH_4F solution or in a mixture of HF and H_2SO_4 to grow metal oxide films. The metal films can be detached from the base metal by LOFO technique for Ta_2O_5 and Nb_2O_5 films or by scotch tape for TiO_2, WO_3, Ta_2O_5 and Nb_2O_5 films.

Instruments:

SEM imaging was performed with a JEOL JSM-7000F Scanning Electron Microscope, equipped with a Schottky type Field Emission Gun (FEG) filament. Energy dispersive X-ray (EDX) spectroscopy was carried out using a 10 kV accelerating voltage. INCA 300, EDX System (Oxford, UK) software was used for the data acquisition and analysis.

Atomic force microscopy was performed in tapping mode on a Veeco Enviroscope with a Nanoscope IIIa controller and Veeco RTESP p-doped Si tips with a nominal radius of less than 10 nm. The thickness of the metal oxide membranes was assessed by measuring step height near the peeled off edges using AFM.

XPS spectra were recorded on a Kratos Axis Ultra X-ray photoelectron spectrometer with a base pressure of 1×10^{-10} mbar employing monochromatic Al Kα X-ray source (1486.71 eV) and charge neutralizer system. XPS Survey scan were taken at a pass energy of 160 eV with step sizes of 0.7 eV in an area 300 x 700 μm in size.

Quantitative SIMS analysis was carried out on a ION-TOF (GmbH), ToF-SIMS IV instrument equipped with a bismuth Liquid Metal Ion Source (LMIG). The 25 keV primary ion ($Bi3^+$) beam was pulsed and rastered over 75um x 75um area. To achieve the best mass resolution, high current bunched mode was employed. The mass resolution was ~ 10,000 above 200 amu and the mass range was 0 - 1000 amu. The detection limits are in the range of ppb-ppm, depending upon the element or species of interest. To do the depth profile analysis, a second 500eV Cs^+ beam with 4-7 nA target current was used to sputter the surface of 150um x 150um area. The analysis area is centered in the sputtered area to avoid undesirable edge effect. Since the species of interest included mainly F, S and O as well as oxides and possible oxyfluorides of metals, negative secondary ions were monitored.

High-Resolution TEM was carried out with a JEOL 2010 field emission TEM/STEM, operating at an accelerating voltage of 200kV.

Optical images were taken by a high resolution microscope (Stereo Discovery.V12, maximum magnification 400x) equipped with a quartz-tungsten-halogen white light source.

Author Contributions:

This chapter is based on a manuscript which has has been submitted for publication with the following authors on the manuscript (Singh, S.; Festin, M.; Barden, W. T.; Xi, C.; Francis, J. and Kruse, P.). The author contributions for this paper are as follows. S.S. designed and conducted the electrochemical experiments. S.S. performed the SEM, AFM, TEM measurements on the samples. M. F. and W.T.B assisted in performing the electrochemical experiments. C. X. and J. F. obtained the SIMS data. Overall data analyses were conducted by the S.S. and P.K. Also, S.S. contributed in writing the manuscript, which was discussed by all authors.

6.7 Bibliography

(1) Baker, R.W. *Membrane Technology and Applications*; Wiley: Hoboken, 2004.

(2) Xu, C., Su, J., Xu, X., Liu, P., Zhao, H., Tian, F. & Ding, Y. Low Temperature CO Oxidation over Unsupported Nanoporous Gold. *J. Am. Chem. Soc.* **2007**, *129*, 42–43.

(3) Striemer, C. C., Gaborski, T. R., McGrath, J. L. & Fauchet, P. M. Charge- and size-based separation of macromolecules using ultrathin silicon membranes. *Nature* **2007**, *445*, 749-753.

(4) Kanellopoulos, N. K. *Recent Advances in Gas Separation by Microporous Ceramic Membranes*; Elsevier: Amsterdam, 2000.

(5) Sakai, H., Furukawa, Y., Fujiwara, E. & Tada, H. Low-voltage organic field-effect transistors with a gate insulator of Ta2O5 formed by sputtering. *Chem. Lett.* **2004**, *33*, 1172-1173.

(6) Demiryont, H., Sites, J. R. & Geib, K. Effects of oxygen content on the optical properties of tantalum oxide films deposited by ion-beam sputtering. *Appl. Opt.* **1985**, *24*, 490-495.

(7) Waldorf, A. J., Dobrowolski, J. A., Sullivan, B. T. & Plante, L. M. Optical coatings deposited by reactive ion plating. *Appl. Opt.* **1993**, *32*, 5583-5593.

(8) Sankur, H. O. & Gunning, W.J. Deposition of optical thin films by pulsed laser assisted evaporation. *Appl. Opt.* **1989**, *28*, 2806-2808.

(9) Gu, G., Schmid, M., Chiu, P.-W., Minett, A., Fraysse, J., Kim, G.-T., Roth, S., Kozlov, M., Munoz, E. & Baughman, R. H. V2O5 nanofibre sheet actuators. *Nat. Mater.* **2003**, *2*, 316-319.

(10) Yang, H., Coombs, N., Sokolov, I. & Ozin, G. A. Free-standing and oriented mesoporous silica films grown at the air-water interface. *Nature* **1996**, *381*, 589-592.

(11) Wang, X., Lao, C., Graugnard, E., Summers, C. J. & Wang, Z. L. Large-Size Liftable Inverted-Nanobowl Sheets as Reusable Masks for Nanolithiography. *Nano Lett.* **2005**, *5*, 1784-1788.

(12) Raman, N. K. & Brinker, C. J. Organic template approach to molecular-sieving silica membranes. *J. Membrane Sci.* **1995**, *105*, 273–279.

(13) Jin, J., Wakayama, Y., Peng, X. & Ichinose, I. Surfactant-assisted fabrication of free-standing inorganic sheets covering an array of micrometre-sized holes. *Nat. Mater.* **2007**, *6*, 686-691.

(14) Lee, W., Ji, R., Gösele, U. & Nielsch, K. Fast fabrication of long-range ordered porous alumina membranes by hard anodization. *Nat. Mater.* **2006**, *5*, 741-747.

(15) Wehrspohn, R. B. *Ordered Porous Nanostructures and Applications*; Springer: 2005.

(16) Lu, Q., Mato, S., Skeldon, P., Thompson, G. E., Masheder, D., Habazaki, H. & Shimizu, K. Anodic film growth on tantalum in dilute phosphoric acid solution at 20 and 85 °C. *Electrochim. Acta.* **2002**, *47*, 2761-2767.

(17) Schwirn, K., Lee, W., Hillebrand, R., Steinhart, M., Nielsch, K. & Gösele, Y. Self-Ordered Anodic Aluminum Oxide Formed by H2SO4 Hard Anodization. *ACS Nano.* **2008**, *2*, 302-310.

(18) Singh, S., Greiner, M.T. & Kruse, P. Robust Inorganic Membranes from Detachable Ultrathin Tantalum Oxide Films. *Nano Lett.* **2007,** *7*, 2676-2683.

(19) Shimizu, K., Kobayashi, K., Thompson, G. E., Skeldon, P. & Wood, G. C. Anodic oxide films on tantalum: Incorporation and mobilities of electrolyte-derived species. *Philos. Mag. Part B* **1996**, *73*, 461-485.

(20) Shimizu, K., Kobayashi, K., Thompson, G. E., Skeldon, P. & Wood, G. C. The Migration of Fluoride Ions in Growing Anodic Oxide Films on Tantalum. *J. Electrochem. Soc.* **1997**, *144*, 418-423.

(21) Sreethawong, T., Ngamsinlapasathian, S., Suzuki, Y. & Yoshikawa, S. Nanocrystalline mesoporous Ta2O5-based photocatalysts prepared by surfactant-assisted templating sol–gel processfor photocatalytic H2 evolution. *J. Mol. Catal. A: Chem.* **2005,** *235*, 1-11.

(22) Nakayama, Y., Pauzauskie, P. J., Radenovic, A., Onorato, R. M., Saykally, R. J., Liphardt, J. & Yang, P. Tunable nanowire nonlinear optical probe. *Nature* **2007**, *447*, 1098-1102.

(23) Zheng, Q., Zhou, B., Bai, J., Li, L., Jin, Z., Zhang, J., Li, J., Liu, Y., Cai, W. & Zhu, X. Self-Organized TiO2 Nanotube Array Sensor for the Determination of Chemical Oxygen Demand. *Adv. Mater.* **2008**, *20*, 1044-1049.

(24) Lee, H., Lee, S.W., Goto, H., Lee, S., Lee, H., Ha, J.S., Goto, T., Cho, M.W., Yao, T. & Hong, S. Self-separated freestanding GaN using a NH4Cl interlayer. *Appl. Phys. Lett.* **2007**, *91*, 192108.

(25) Rogers, D. J., Teherani, F. H., Ougazzaden, A., Gautier, S., Divay, L., Lusson, A., Durand, O., Wyczisk, F., Garry, G., Monteiro, T., Correira, M. R., Peres, M., Neves, A., McGrouther, D., Chapman, J. N. & Razeghi, M. Use of ZnO thin films as sacrificial templates for metal organic vapor phase epitaxy and chemical lift-off of GaN. *Appl. Phys. Lett.* **2007**, *91*, 071120.

(26) Lee, T.-H., Huang, C.-H., Yang, Y. Y. & Suryasindhu, T. Nanoscale thick layer transfer of hydrogen-implanted wafer by using polycrystalline silicon sacrificial layer. *Appl. Phys. Lett.* **2007**, *91*, 203119.

(27) Alcala, G., Skeldon, P., Thompson, G. E., Mann, A. B., Habazaki, H. & Shimizu, K. *Nanotechnology* **2002**, *13*, 451-455.

(28) Rizkalla, H. Wellinghoff, S. T. *J. Mater. Sci.* **1984**, *19*, 3895-3907.

(29) Lassner, E. & Schubert, W. D. *Tungsten - Properties, Chemistry, Technology of the Element, Alloys, and Chemical Compounds*; Kluwer Academic: New York, 1999.

(30) Buslaev, Y. A., Bochkareva, V. A. & Nikolaev, N. S. The reaction of titanium dioxide with hydro fluoric acid. *Russian Chemical Bulletin* **1962**, *11*, 361-364.

(31) Meitl, M. A., Zhu, Z. T., Kumar, V., Lee, K. J., Feng, X., Huang, Y. Y., Adesida, I., Nuzzo, R. G. & Rogers, J. A. Transfer printing by kinetic control of adhesion to an elastomeric stamp. *Nature Materials* **2005**, *5*, 33 - 38.

(32) Sun, Y. & Rogers, J. A. Fabricating semiconductor nano/microwires and transfer printing ordered arrays of them onto plastic substrates. *Nano Letters* **2004**, *4*, 1953–1959.

(33) Vermilyea, D. A. Formation of anodic oxide films on tantalum in non-aqueous solutions. *Acta Metall.* **1954**, *2*, 483-486.

(34) Macak, J. M., Tsuchiya, H. & Schmuki, P. *Angew. Chem.* **2005**, *117*, 2136 – 2139; *Angew. Chem. Int. Ed.* **2005**, *44*, 2100 – 2102.

(35) Albu, S. P., Kim, D. & Schmuki, P. Growth of aligned TiO2 bamboo-type nanotubes and highly ordered nanolace. *Angew. Chem. Int. Ed.* **2008**, *47*, 1916-1919.

(36) Northen, T. R., Yanes, O., Northen, M. T., Marrinucci, D., Uritboonthai, W., Apon, J., Golledge, S. L., Nordström, A. & Siuzdak, G. Clathrate nanostructures for mass spectrometry. *Nature* **2007**, *449*, 1033-1036.

(37) El-Sayed, H., Singh, S., Greiner, M. T. & Kruse, P. Formation of Highly Ordered Arrays of Dimples on Tantalum at the Nanoscale. *Nano Lett.* **2006**, *6*, 2995-2999.

(38) Chaneliere, C., Autran, J. L., Devine, R. A. B. & Balland, B. Tantalum pentoxide (Ta2Os) thin films for advanceddielectric applications. *Mater. Sci. Eng.* **1998**, *R22*, 269-322.

(39) Yan, C. & Xue, D. Formation of Nb_2O_5 Nanotube Arrays Through Phase Transformation. *Adv. Mater.* **2008**, *20*, 1055-1058.

(40) Müller, K., Faeh, C & Diederich, F. Fluorine in Pharmaceuticals: Looking Beyond Intuition. *Science* **2007**, *317*, 1881-1186.

(41) Segal, M., Singh, M., Rivoire, K., Voorhis, T. V. & Baldo, M. A. Extrafluorescent electroluminescence in organic light-emitting devices. *Nat. Mater.* **2007**, *6*, 374-378.

Chapter-7

Conclusions and outlook

New concepts of patterning surfaces and fabricating free-standing metal oxide membranes is introduced and experimentally studied. The concept is based on the evolution of order out of chaos in nonlinear systems. In this thesis, spatio-temporal experiments were performed to investigate the evolution of hexagonal pattern formation on tantalum surfaces. The mechanism for breaking of the spatial symmetry of the electrochemical double layer in ordered migration cells similar to Rayleigh-Bernard convection cells is revealed. The principal impacts of the first part of my thesis work for the field of nonlinear pattern formation may be summarized as

- The demonstration of pattern formation on tantalum surface and establishing the fact that highly ordered surface roughness originates during electropolishing under an appropriate electrochemical window. The low fabrication cost, high-order, large surface area coverage and high reproducibility show the prospect of achieving future industrially viable nanostructured materials with this technique.
- The generalization of the method of electrochemical patterning on other metals such as titanium, tantalum and zirconium showing the presence of a universal natural phenomenon behind this kind of pattern formation.
- The experimental contribution towards the understanding of spatiotemporal self-organization phenomenon which has its roots in the nonlinear pattern formation

and fluid mechanics. The universal features governing the spontaneous pattern formation on tantalum surface were extracted and were put into the general framework of nonlinear dynamics.

- The demonstration of these ordered metal surface as nanobeakers for the placement of nanoparticles inside them.

In the 5th and 6th chapter of the thesis, a unique method of fabricating and separating purely inorganic metal oxide membranes is shown. The reasons behind the detachment of these metal oxide films are clearly illustrated. In this case the fast migration of fluorine ions compared to the oxygen ions leads to the detachment of the film from the underlying metal. To establish the fact that fluorine migrates faster a number of techniques such as XPS, SIMS etc. were used. The control over the porosity was also demonstrated. We were able to prove the feasibility of the process of fabrication of detachable transition metal oxide films for other materials such as niobium, titanium and tungsten. The second part of my thesis work was more applied in a way that it has taken the knowledge of ultrathin film fabrication a step ahead by

- Demonstrating the complete detachment of ultrathin (35-100 nm) tantalum oxide membranes using LOFO technique.
- Investigating the reasons behind the detachment of the films due to differential migration of ions.
- Showing the general applicability of the principle by demonstrating its ability to detach other metal oxide films from the underlying metal surface.

Even at this early stage in the development of 'dissipative' patterning, it is clear that advantages engendered by miniaturization may affect fabrication of tiny ordered architectures similarly to the way that self-assembly has defined the nanotechnology revolution over the past 20 years. Such methods of engineering nanostructures can be a breakthrough for making ordered structures on large surfaces and are certainly going to present some fantastic opportunities for future work. The nanopatterning systems based on dissipative processes will soon find their way into everyday research and technology, because of their low operational cost and high reproducibility.

The knowledge in this thesis on pattern formation and thin film fabrication is new compared to other methods which exist from last 10-20 years. Building on my current research results will lead to the discovery of a completely new method of formation of patterns on a wide variety of surfaces. The future research can be performed under following four main sections with each section having its own independent objective but at the same time supports the other in achieving a common goal of dissipative nanopatterning.

I. **Generalize the concept of highly ordered electrochemical pattern formation on other metal and semiconductor surfaces.** As we have demonstrated this technique on metals, the technique can be extended to other important metals such as iron, nickel and high-tech materials such as silicon, GaAs and In-P.

II. **Determine mechanisms and parameters in the formation of dimples on transition metal surfaces.** The enormous wealth in the dynamics of this hexagonal pattern formation on electrode surfaces in the narrow electrochemical windows is not yet fully captured by the experiments presented here. A main focus of the future work is to explore deeply the basic concepts behind this type of dissipative surface nanopatterning and then in simulating the nonlinear phenomenon using mathematical models. The important system parameters which generally effect the pattern formation on sample electrode surface such as concentration and type of electrolyte solution, applied potential (with programmed voltage pulses), temperature, surface tension and confined boundaries should be considered under this study. Also the metal/oxide dissolution dynamics during the initial time of few seconds should be examined thoroughly as the oscillations in the system are suspected. Other key questions to address are the effects of different types of non-linear kinetics, boundary conditions, crystallographic orientation, and domain geometry, on the selection and stabilization of patterns.

III. **Using the templated substrate surfaces to engineer functional materials.** We recently fabricated detachable ultrathin tantalum oxide membranes where the dimpled morphology of the starting tantalum surface provided a handle in controlling the porosity inside these membranes. Highly ordered porous anodic aluminum oxide (AAO) membranes have created thousands of papers in research journals and have given rise to plenty of applications in nanotechnology ranging from synthesis of nanowires, molecular sieves, to combinatorial chemistry. Nevertheless, a prepatterning process of embossing the hexagonal pattern is required before anodization to generate the final hexagonally ordered pore structure. Our method provides an easy way of pre-texturing the hexagonal pattern on the surface and therefore will allow to make free-standing membranes with highly ordered pores under appropriate electrochemical conditions. Depending on the exceptional properties of the oxide materials, these porous membranes will be used extensively for various technological applications such as molecular filtration, ordered-template for nanowires growth, photocatalysis, Bragg-like sensors, dielectric spacers etc. Also understanding of the basic mechanisms of adhesion and adhesion failure due to presence of thin metal oxyfluoride is incomplete

IV. **(Long term) Consider the general concept of using dissipative patterning processes at the nanoscale.** Along with application driven research, the processes will give enough knowledge to allow the extension of this phenomenon to other systems. In this part of the research project, one can try to look out for other non-linear systems analogous to this electrochemical system. One possible way is to replace the electric field (one of the key parameter in making pattern in electrochemical systems) with magnetic field to drive magnetic particles in making patterns on soft surfaces.

This research will be of importance not only because it falls under the "Nano-Umbrella" but because it offers a stimulating new model in terms of fundamental studies and technological innovation. The research has a great potential for expansion to other disciplines and will soon require the involvement mathematicians, physicists and material scientists for further study. From the industrial perspectives this technique of engineering nanostructures will provide a simple but powerful set of new tools for patterning surfaces and engineering nano-structures in large quantities for the advancement of science and nanotechnology.

Finally, I would like to mention that there is large number of trivial-looking nonlinear phenomena in electrochemical systems, which if explained and controlled properly will lead to a precious unexploited resource of new and highly robust patterning techniques.

Appendix A

Additional Data on Evolution of Dimpled Morphology on Tantalum Surface

In this appendix we provide additional experimental data about the spatio-temporal evolution and self-ordering of tantalum dimples during electropolishing. Even though general aspects of pattern formation at nanoscale due dissipative electrochemical processes constituted the main focus in this thesis, the results presented here further point to the possibility of involvement of chemical waves and temporal oscillations during the initial stages of pattern formation and needs further exploration. The studies shown here make it very likely that temporal oscillations exist in these systems during to the initial formation and dissolution of oxide which finally leads to ion convection cycles at nanoscale. These considerations further illustrate that we have just discovered the tip of the iceberg in this thesis and further investigations and the development of control strategies using appropriate experiments are needed to paint the complete picture.

This appendix is organized as follows. In Section A.2, the additional results of time resolved study are presented. Section A.3 presents a model for this kind of dissipative pattern formation. Finally, Section A.4 describes the formation of undesired but beautiful dendritic patterns on electropolished tantalum surfaces and discusses the methods of ceasing their formation.

Self-driven spontaneous pattern formation is a fascinating phenomenon that can be seen in everyday life ranging from complex patterns in biological systems, convective patterns in fluid dynamics, diffusion-limited nonlinear growth of snowflakes and dendritic solidification of crystals on surfaces. Nowadays, ordered pattern formation at small length scales has been extensively used in nanotechnology. One crucial challenge for existing patterning techniques, such as soft and e-beam lithography is the time and work required for patterning. Pattern formation using electrochemical methods has come to prominence due to sufficiently high fabrication speed, but the degree of regularity has always been a problem except for very few metals such as aluminum. Recently, we reported that electropolishing of tantalum metal in a single step leads to a highly ordered array of nano-dimples on its surface. Here, we report a time-resolved study which reveals the underlying mechanism behind the formation of highly ordered dimple morphology on tantalum surface. Our results show that the formation of dimples is a cooperative critical phenomenon resulting from a series of different processes. The heat generated during initial local pitting induces modulation instability in the etching rate at different surface sites and leads to ions migration coupling among dissimilar reaction spots. This ion migration coupling slowly gives rise to Rayleigh-Bernard like convection cycles in the electrochemical double layer with a characteristic length scale of around 55 nm. In addition to hexagonal pattern formation, we also observed and studied the dendritic growth of a thin layer of tantalum oxide on tantalum surface during electropolishing. The importance of sample tilt and electrolyte stirring for the achievement of desired surface quality during electropolishing is also discussed. Our findings bring a unique system of nanoscale pattern formation into a conceptual framework of autocatalytic processes and nonequilibrium pattern formation phenomenon in reaction diffusion systems. This study has further proved (Chapter-3) that if the mechanism controlling the self-ordering phenomena is applied under proper electrochemical conditions, it might be possible to pattern nanostructures on other metallic and semiconducting materials.

A.1 Introduction

The engineering of ordered nanostructures on surfaces is primarily used to fabricate small microelectronics devices[1] such as sensors and transistors, information storage,[2] “lotus-effect” based self-cleaning[3] and roughness induced biocompatible materials.[4] The most widely used approaches for creating such surface patterns are particle-beam writing,[5,6] optical lithography,[7] stamping[8] and embossing.[9] The particle-beam writing techniques are slow and expensive due to the serial nature of the processes and have been found to damage substrates due to the high energy associated with electron beams, ultraviolet light and hard X-ray radiations. Stamping and other soft lithography techniques have their own pitfalls when the master stamp template loses its structure after repeated use and becomes ineffective at imprinting its pattern.

In order to circumvent these drawbacks, globally much research is going into developing alternative more efficient, reproducible and robust methods of patterning surfaces by mimicking the ubiquity of self-organization in Nature. Various kinds of self-assembly[10,11,12,13] have shown a lot of promise but the process takes a longer time as the system has to achieve the minimum energy condition to generate the stable pattern. Ideally, for industrial applications and mass production of nanostructured materials, development of methods where the substrate can be inserted into a system, patterned under ambient conditions for a minimal amount of time and be ready to use upon extraction is the dream of the scientific community.

Dissipative patterning dictated by non–equilibrium thermodynamics is well known to make self-organized spatiotemporal Turing-type stationary structures in biological systems such as beautiful symmetrical designs on butterfly wings, spots and lines on leopard, fish and zebra skin.[14,15] The traveling wave patterns of Belousov-Zhabotinsky (BZ) reactions in appropriate chemicals is also an example of dissipative patterning and have been known and studied for a long time. These patterns are not permanent and vanish instantly as the driving force is taken away. The characteristic length scale of the patterns in all these systems have found to be between kilometres and micrometers.[16,17,18,19] The key to success in using this technique is simultaneously creating and imprinting the pattern. Recently electrochemical systems have been used to generate and imprint dissipative patterns on electrode surfaces.[20] However, very few cases have been reported using this technique to make patterns at the nanoscale.[21]

Electrochemical anodization is a well known method of growing highly ordered oxide patterns on a substrate surface (particularly aluminum and silicon) although a prepatterning step using lithography or embossing is still required to generate the final structures.[22,23] The advantage of this method is that it can pattern large surface areas reproducibly in short time, is not serial in nature, can be performed under ambient conditions and can tolerate slight variations in the electrochemical system such as separation distance between electrodes, small fluctuations in applied voltage and electrolyte concentration. Electropolishing is a special case of anodization in which the dissolution of meta/metal-oxide happens faster than the formation of metal oxide in a concentrated electrolyte solution and is widely used method to generate clean and flat surfaces.[24,25,26] However, we recently reported the fact that electropolishing not only produces a flat tantalum surface at the macro-scale but also generates a highly ordered periodic nanoscale roughness on it and then characterized the surface to a large degree.[27] Our present studies illuminate the mechanism behind this dissipative self-ordering and patterning of the tantalum surface at nanoscale during electropolishing and demonstrate the crucial steps of this phenomenon. The mechanism is revealed by performing spatiotemporal studies using sequence of short voltage pulses and studying the evolution of the pattern on the surface. The underlying principles behind this unique way of engineering nano-structures are found to have their roots in nonlinear interaction/reaction electro-hydrodynamics. The hexagonal pattern similar to Rayleigh-Benard convection cells is formed in the electrochemical double layer (EDL) due to ion migration coupling, which simultaneously gets imprinted on the tantalum surface via formation and dissolution of metal/metal-oxide. Along with hexagonal dimpled pattern formation we also studied the undesired growth of dendritic pattern of thin oxide layer on electropolished tantalum surfaces and discussed ways to inhibit their formation.

A.2 Time Resolved Study

Our time resolved study consisted of applying short constant d.c voltage pulses during electropolishing to investigate the onset of hexagonally packed dimple formation on the tantalum surface. We used a standard two-electrode electrochemical set-up to supply controlled voltage pulses of 15 V to a tantalum foil (Alfa Aesar, 99.95%, 0.127 mm) immersed in a stirred 9:1 volumetric mixture of concentrated sulfuric acid (95-98%, Fisher Scientific, reagent grade) and concentrated hydrofluoric acid (48%, Fisher Scientific, semiconductor grade). A sketch of the experimental set-up is shown in (Scheme A.1). It should be noted that most of the dimpling experiments were done in this 9:1 H_2SO_4/HF v/v electrolyte solution except if mentioned otherwise.

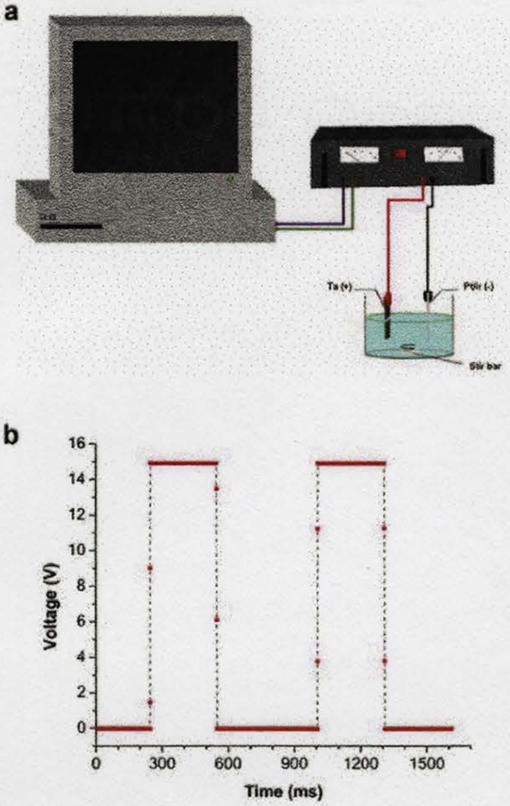

Scheme A.1. Experimental Setup

A.2.1 Evolution of Dimples on Rough Tantalum Surfaces.

Figures A.1a, b show the macroscopic surface roughness of the starting material (as-received tantalum foil). The noticeable dimple morphology on rough tantalum surface was found to form only a few seconds (~ 2 s) after turning the voltage supply on (Figure A.1d). Tantalum samples etched at small timescales retained a rough microstructure (Figure A.1c, e), which could be etched away by polishing them for longer times (> 2 minutes) (Figure A.1l). The application of constant voltage by applying a single 5 seconds long constant voltage pulse of 15 V reproducibly imprints dimples tens of nanometers in diameter, everywhere on the surface including on the sharp edges of the rough surface heterogeneities (Figure A.1f, g, h, i). Apparently, the dimples on or near the rough surface areas are not as regular in shape and mono-dispersed in size as they are on flat regions of the surface. However, the hexagonal pattern of dimples becomes perfectly ordered everywhere and the surface becomes homogeneous without any microstructure roughness with clearly visible grain structure after polishing the samples for more than three minutes (Figure A.1l, m). The dimples can even transverse grain boundaries.

We observed that the inherent microstructure heterogeneities on the commercially available cold-rolled tantalum foil (Alfa Aesar, 99.95%, 0.127 mm) were still present along with dimples if the voltage is applied for a minute (Figure A.1c-k) and eventually goes away after electropolishing the samples for 3 minutes (Figure A.l-m). These surface heterogeneities affect the order and distribution of dimples near uneven regions during the initial time periods.

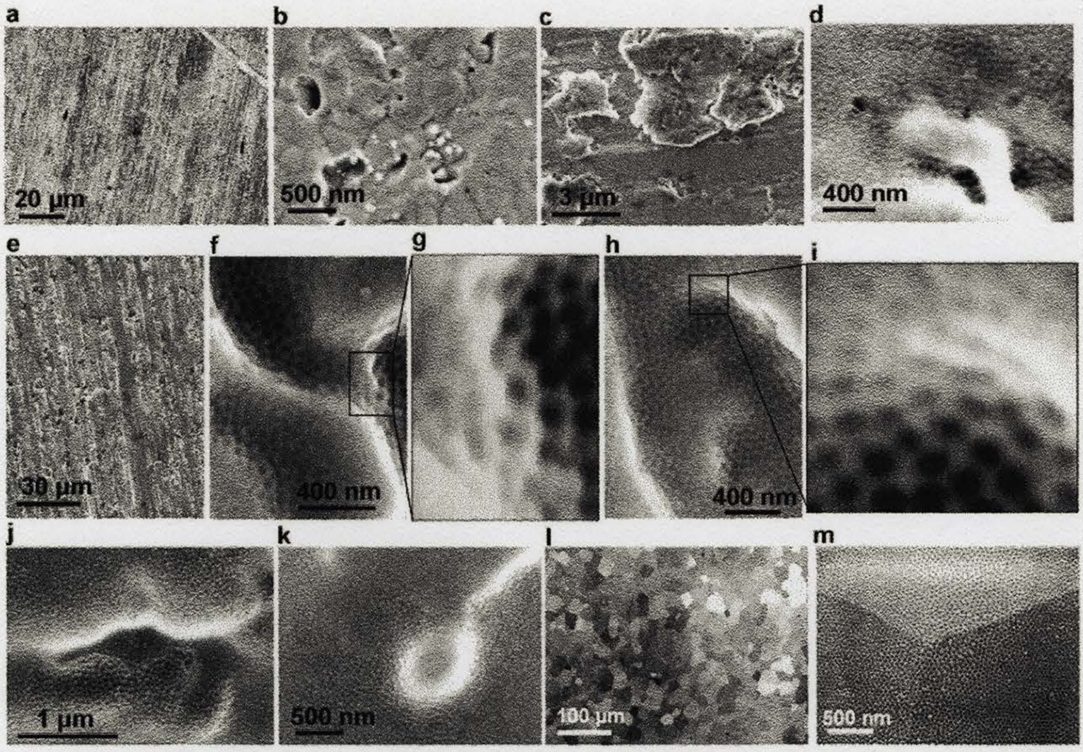

Figure A.1. SEM micrographs showing the formation of dimples on rough and flat surfaces. (a and b) As-received cold-rolled tantalum sample surface. (c and d) showing that microstructure roughness is still present along with formation of disordered dimple pattern after electropolishing the sample for 2 seconds. (f, g, h, and i) Representative SEM images of tantalum surface after electropolishing for 5 seconds showing the presence of dimples even on the edges of rough heterogeneities. (j and k) SEM images after 1 minute of electropolishing showing that rough heteroginies start to become smoother and the order of dimples is improving. (l) Tantalum surface after electropolishing for 3 minutes, exhibiting flat surface with clear grain boundaries at micrometer scale. (m) Zoomed – in image of (l) showing perfectly ordered dimples which can transverse even grain boundaries .

The microstructure roughness on as received cold-rolled tantalum foils may provide the defect sites for pit nucleation. To negate the effect of surface heterogeneities in the study of dimple formation we focus our experiments on flat tantalum surfaces. The smooth and flat tantalum surfaces for performing further time resolved experiments were prepared by growing a thin anodic oxide film on electropolished Ta surfaces and subsequently peeling the film off the substrate. The detailed procedure for manufacturing flat substrate surfaces has been described previously.[28] Briefly, the Ta surface was first electropolished with a stirred solution of concentrated H_2SO_4 (95-98%) and HF (48%) in a volumetric ratio of 9:1 for 5 minutes at 15 V. Then a thin Ta_2O_5 film was grown on these samples by anodizing them for 6 minutes in an aqueous electrolyte containing 1M H_2SO_4 and 2 wt % HF at a constant voltage of 20 V. The film was peeled off from both sides by scotch tape and ultrasonication and the resulting flat surface is well-suited for spatiotemporal study of dimple formation (Figure A.2a).

A.2.2 Evolution of Dimples on Flat Tantalum Surfaces.

The fast kinetics of formation of dimples on tantalum surface is shown in a sequence of images as a function of time in Figure A.2. During the first 300 milliseconds (ms) of applied voltage, the SEM image do not show any sign of dimple formation although the surface morphology does change (Figure A.2b). The morphology of the surface suddenly changes to visible etch pits after applying the potential for 500 ms (Figure A.2c). The local etching rate of the metal depends on the concentration of the aggressive species in the electrolyte near the surface and the local potential across the double layer. The onset of etching gives rise to metastable etch pits (Figure A.2c) which gradually start to get ordered into hexagonal arrays of dimples (Figure A.2d, e). Figure A.2f shows perfectly ordered array of dimples formed after 1 minute of electropolishing on flat tantalum surface. The fast formation of dimples on the surface in milliseconds indicates that their creation is related to the fast buildup of the electrochemical double layer (EDL).[29]

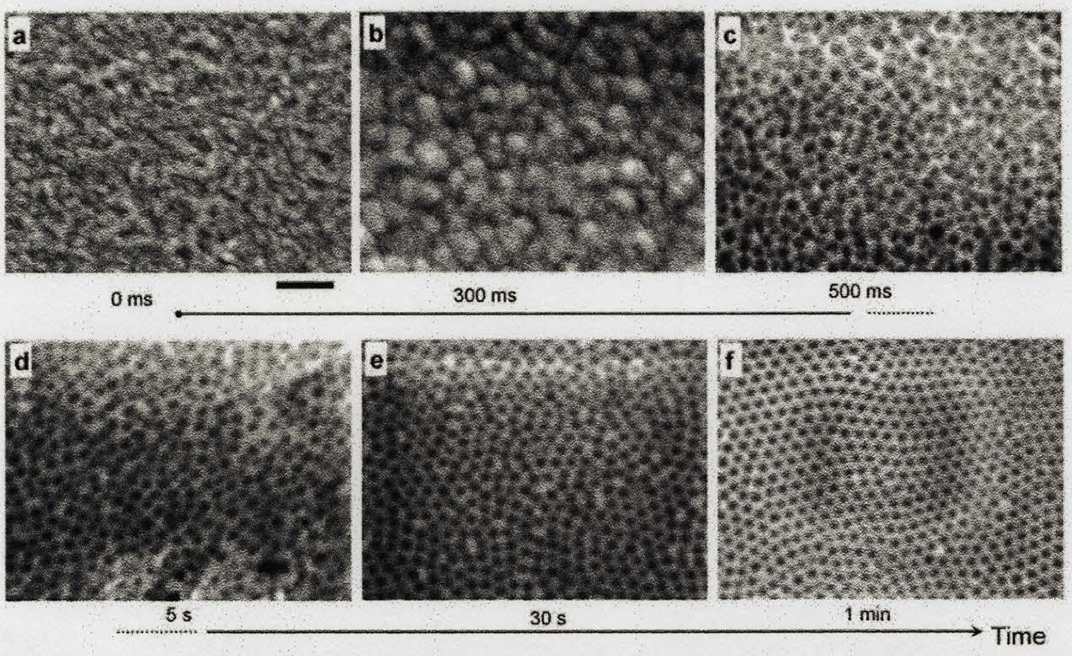

Figure A.2. Scanning Electron Microscopic images of individual electropolishing events as a function of time on a flat tantalum surface. (a) Topographic structure of a freshly peeled off surface, revealing the flat but granular structure of the surface. (b) a very small change in surface morphology after electropolishing for 300 ms (c), sudden appearance of etch pits after 500 ms (d), substantial increase in order of dimples after 5 sec e), appearance of hexagonal order after 30 sec (f), appearance of highly ordered hexagonal patterns after 1 minute. The scale bar under (a) correspond to 200 nm and is for all the images. A constant voltage of 15 V in single pulse mode was used for all these samples.

It was also noticed that the different type of surface morphology during initiation of dimpling process is dependent on the crystal orientation (Figure A.3a). We were able to observe square pattern on few of the crystal planes during initial stages of dimpling (Figure A.3b). This can be due to the initial confinement conditions imposed by the grain boundaries. However, the dimple formation slowly attains the hexagonal packaging shape - which is considered to be the most efficient geometry for filling 2-dimensional space- as the electropolishing smoothens the grain boundaries. This makes us think that other kind of patterns such as lines and squares can also be made if proper boundary conditions are imposed on the surface.

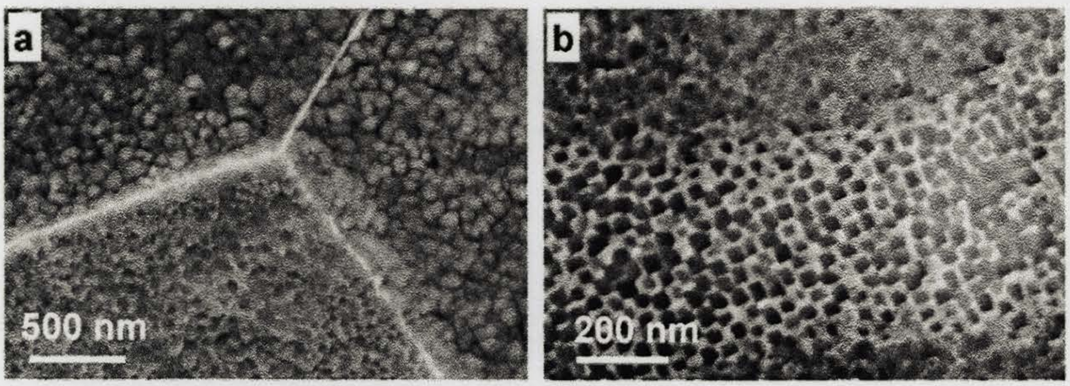

Figure A.3. SEM images showing the grain dependent faceting of tantalum surface during initial time periods (< 2 seconds) of electropolishing. (a), Image showing the intersection of different grains with varied morphology (b), a typical image showing square pattern observed on some of the grains after electropolishing flat tantalum samples for 2 seconds.

A.2.3 Slow Increase in Depth of Dimples as Compared to Fast Etching Speed.

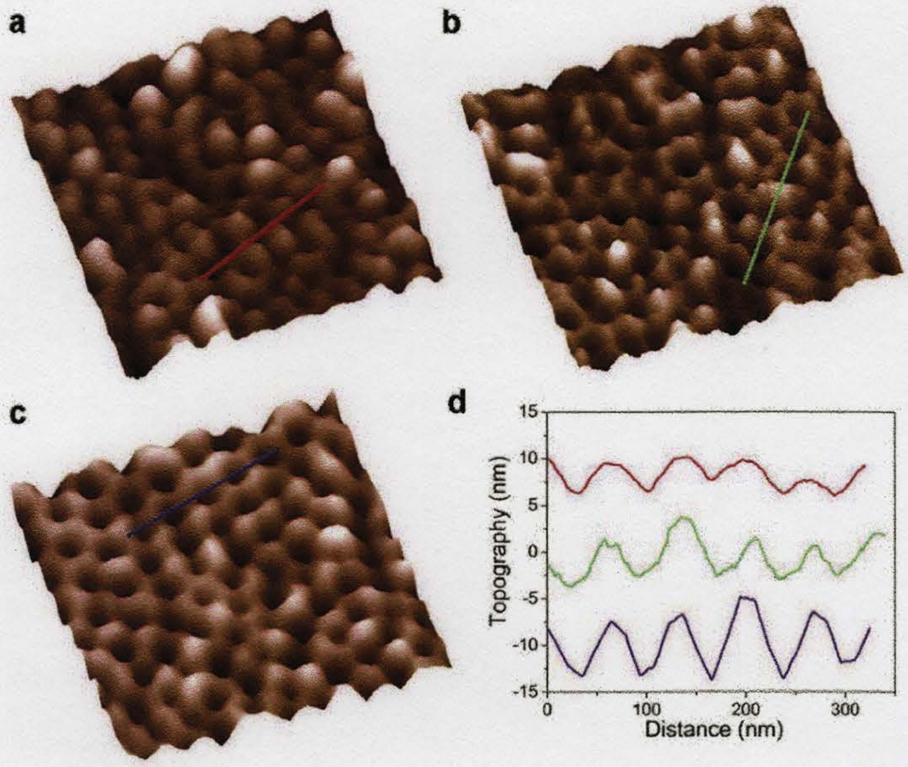

Figure A.4 (***Reproduced from Chapter-4***). Atomic force microscopy images with 3D rendering shows the gradual increase in depth of the dimples with time on tantalum surfaces during electropolishing. (a), 5 sec (b), 30 sec (c), 1 minute (d) the height profile of the dimples along the lines shown in previous three images.

Tapping mode atomic force microscopy (AFM) measurements were done to find the gradual increase in depth of dimples with time (Figure A.4). The AFM images show that the dimples are 2-3 nm deep after 5 seconds and then they become 5-6 nm deep after 30 seconds and they are around 8-10 nm deep if the images were taken after 1 minute of electropolishing. This shows that the dimple pattern imprints first and then the hexagonal order improves as the depth slowly increases. The depth of the dimples becomes constant after reaching 8-10 nm in about 1 minute. Even after 5 minutes of electropolishing there was no change in depth and order of dimples which clearly shows that the process reaches a steady state and attains a constant speed after a certain depth is achieved. It should be noted that the rate of change of depth of the dimples is not same as that of etching (20-50 nm/sec; Ref. 27). Accordingly, this supports the fact that the formation of ordered dimpled pattern on tantalum surface is not only due to etching and shows the self emergent and gradual coupling behavior of the dissipative process during electropolishing.

A.2.4 Increase in Order With Time.

We analyzed a series of SEM images to quantify the evolution and nanometer-scaled structural ordering of dimples on tantalum surface with time. Figure A.5a,b,c are the real SEM images taken after dimpling the flat tantalum surface for 5 seconds, 30 seconds and 1 minute by providing constant d.c voltage of 15 V. Figure A.5d is an artificially drawn picture of perfectly ordered dimples used for comparison. The peaks in the histograms show the periodic distance of separation of dimples from each other. The first peaks around 55 nm correspond to the distance between adjacent dimples. As the order increases with time, the peaks at longer distance starts to grow up signaling the slow evolution of long range order. The inset inside the graphs are the fast Fourier-transformed (FFT) images of Figures A.5a, b, c, d respectively. The histograms and the FFT images, clearly shows that the spatial periodicity and regularity of the hexagonally arranged nanostructures on the tantalum surface gradually increases with time during electropolishing.

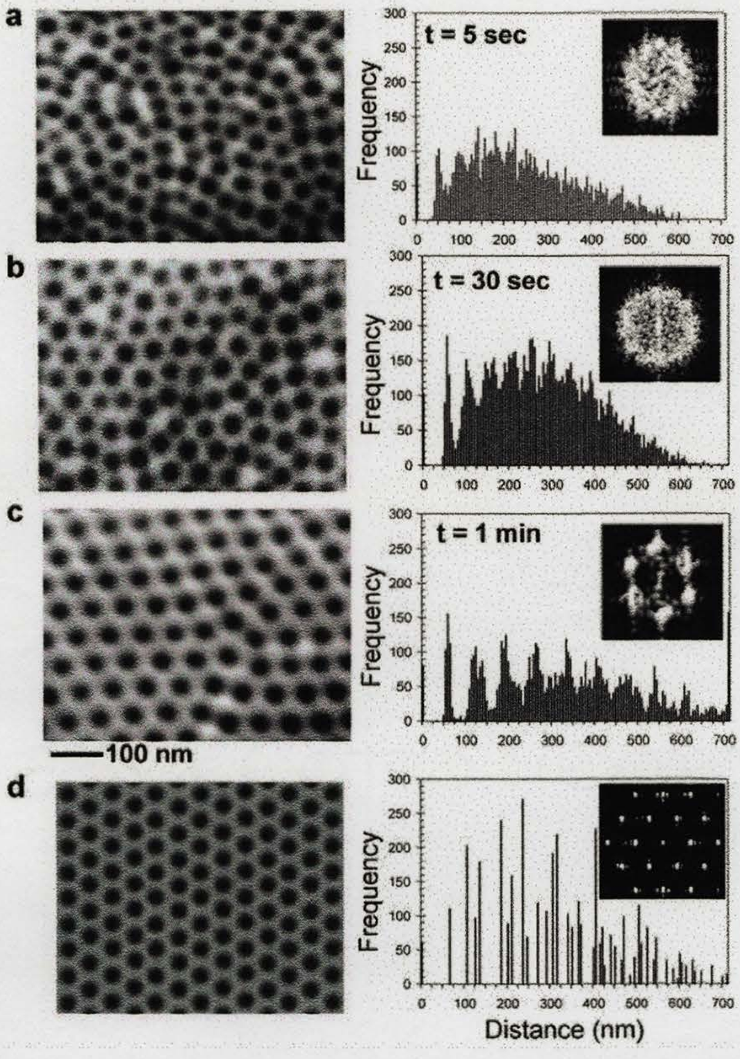

Figure A.5. Statistical analysis of time-lapse SEM images showing the increase in periodicity and regularity of dimples with time. (a) After 5 sec of electropolishing of a flat tantalum surface. (b) after 30 sec. (c) after 1 minute. (d) The artificial image of honeycomb structure drawn to compare the degree of regularity in previous three SEM images. Insets show Fourier transform of images.

A.2.5 HRTEM Images Revealing the Properties of the Dimples

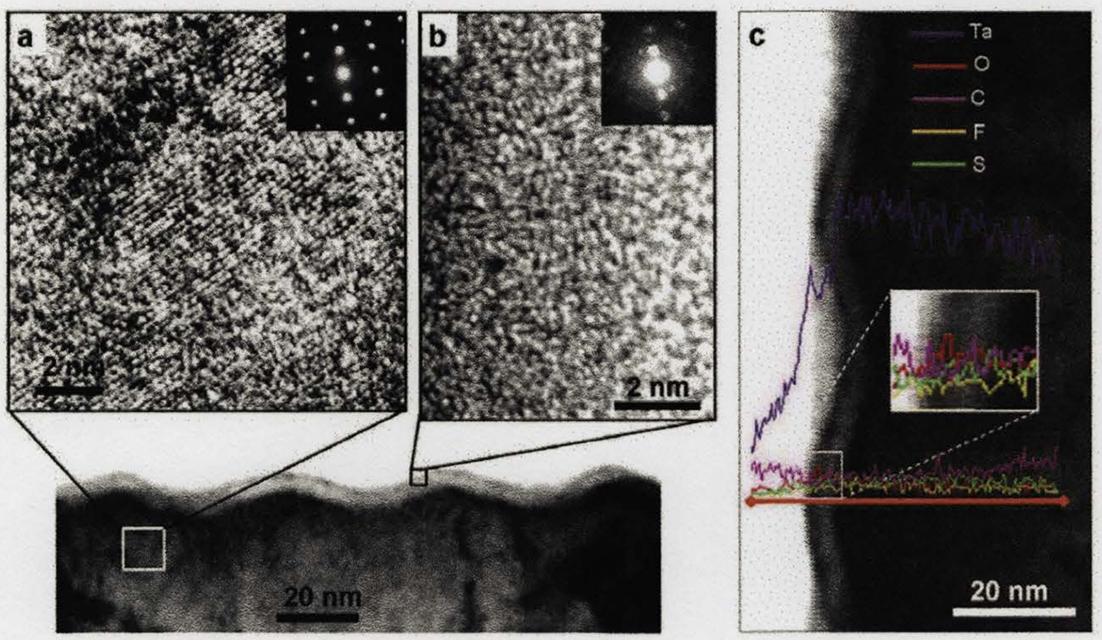

Figure A.6. HR-TEM analysis of dimples on tantalum surface (a), Electron energy-loss spectroscopy line-scan of the dimpled tantalum surface (b), HRTEM image of the base tantalum metal and the corresponding selected-area electron diffraction pattern (inset, discussed in text) is indicative of the crystalline nature of the underlying tantalum metal. (c), HRTEM image of the thin tantalum oxide layer and the corresponding selected-area electron diffraction pattern revealing its polycrystalline nature.

Representative cross-sectional transmission electron microscopy (TEM) images of dimpled tantalum surface taken after electropolishing the sample for 5 minutes are shown in (Figure A.6). The well-ordered structure with the thin tantalum oxide layer (around 4-5 nm) has a depth of around 8 -10 nm and lateral periodicity of 55 nm. The thickness of the oxide layer is approximately equal at the top and bottom of the dimple ($t_{crest} = t_{valley} = 5$ nm). HR-TEM images and diffuse electron diffraction patterns show that the base tantalum metal below the thin oxide layer is crystalline (Figure A.6a), whereas the tantalum oxide layer is polycrystalline (Figure A.6b). An energy-dispersive X-ray (EDX) line-scan through the oxide layer located at the top of the dimple (Figure A.6c) confirms the purity of the tantalum oxide nanostructure as the fingerprints of S and F species (if there are any) were below the detection limits of highly sensitive techniques such as energy filtered TEM (EFTEM) spectroscopy and electron energy-loss spectroscopy (EELS). The oxygen spectrum shows a small blip at the surface of the structure.

A.2.6 Evidence for Formation of Convective Cells Near the Metal/Electrolyte Interface.

The other important question remaining to be answered is whether the electrochemical system retains or loses its memory after been turned off and back on. In other words, if the electropolishing process is stopped and started again, will it continue from where it stopped or it starts randomly without noticing the surface morphology generated in the previous step? We conducted a systematic study with a series of experiments in which prominent surfaces features were examined in turn after providing a sequence of voltage pulses with different on and off times. These experiments further indicated that the hexagonal pattern formation is a result of imprinting of the Rayleigh-Bernard like convective cells on the metal surface.

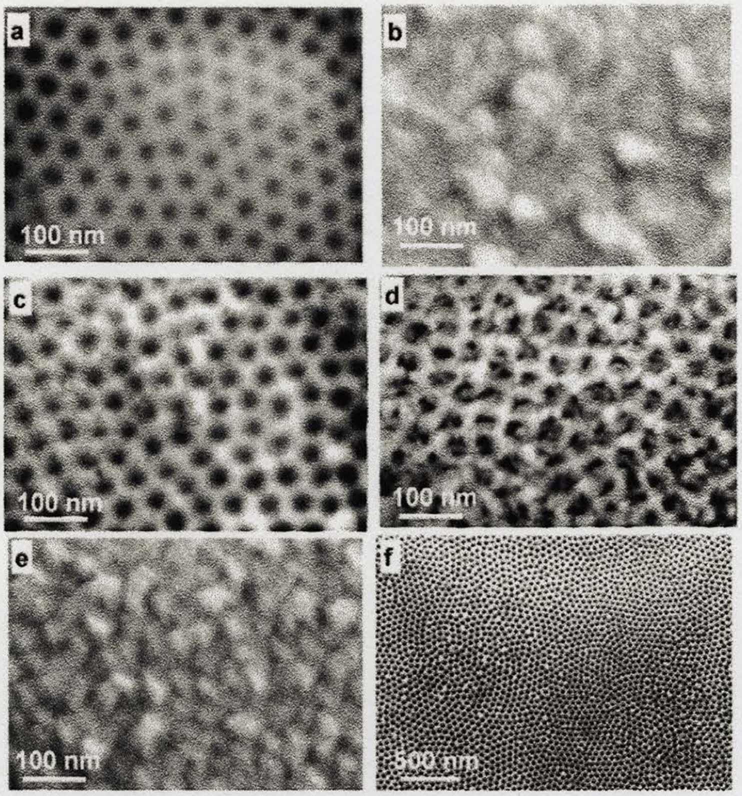

Figure A.7. The ion convective cycles breaks and then restarts at a different place as the external driving force (applied potential) is stopped and re-supplied. SEM images showing the effect of programmed voltage pulses on pattern formation and proving the Rayleigh-Benard like convection in the double layer. For all panels, rectangular DC pulses with 15 V ON voltage and 0 V OFF voltage were applied for different times. **(a)** Highly-ordered dimple pattern after 60.0 s ON, single pulse **(b)** Pattern etched by supplying 6 pulses, each 10 s ON , 0.5 s OFF. **(c)** Pattern etched for 300 s ON, 30 s OFF. Then 20 pulses, each 0.5 s ON, 0.5 s OFF. **(d)** Pattern etched for 300 s ON, 30 s OFF. Then 10 pulses, each 1.0 s ON, 0.5 s OFF. **(e)** Pattern etched for 300 s ON, 30 s OFF. Then 1 pulse for 30.0 s ON. This figure shows that the pattern can be erased. **(f)** Pattern etched for 300 s ON, 30 s OFF. Then 1 pulse for 60.0 s ON. This shows that 60 s are enough to erase the previous pattern and then recreate a new pattern on the surface.

First, a 15 V pulse was applied for 1 minute to generate highly ordered dimples on the flat tantalum surface (see Figure A.7a). Then we split the same timescale of 1 minute)into a train of 6 pulses each of 10 seconds ON time, and each separated by 500 milliseconds of OFF time. In contrast, in the case of the same voltage (15 V) applied but in a sequence of 6 pulses, the surface structure does not show any resemblance to dimples (Figure A.7b). Next, a set of 20 pulses (each pulse of 0.5 sec ON and 0.5 sec OFF) was applied to a fully formed dimple pattern on tantalum (Figure A.7c). Again, this results in the deterioration of the initial surface morphology with the formation of very small etch-pits on top of the dimples. On the other hand, the number of etch pits decreases in number but grow bigger in size if 10 pulses (each pulse of 1 sec ON and 0.5 sec OFF) are applied to a perfectly dimpled surface (Figure A.7d). The difference between these outcomes arises because the system does not recognize the previous dimple pattern on the surface after restarting; rather it evolves independently from completely new initial points and hence does not show any contribution of the previous surface morphology on the pattern formation.

Furthermore if the perfect dimples are formed by dimpling the samples for 1 minute, and then the voltage is turned off for 0.5 sec and then again turned on for 10 seconds, the pattern completely disappears from the surface (Figure A.7e). However, if the length of second voltage pulse is increased to 60 seconds in the above experiment, perfectly ordered dimple pattern morphology appears on the tantalum surface. This clearly demonstrates that electropolishing slowly establishes the convective cycles near the interface due to ion migration coupling and simultaneously imprints them on the surface during electrodissolution of the metal. The convective cycles initially are irregular and of different size and require a certain minimum amount of time to achieve perfect order. However, if the ordered convective pattern is disrupted it cannot start at the same place; every new pulse starts a new convective pattern, indicating no memory retention in this process. It is reasonable to expect that by gradually increasing the time of the second electropolishing cycle, the ordered pattern of the dimples will vanish and then will eventually reappear.

A.3 Rationale Behind Pattern Formation

Based on our spatial and time resolved experimental results, we propose the following mechanism for the formation of shallow dimple hexagonal pattern morphology on tantalum metal surface during electropolishing. The key steps in the formation of pattern on the tantalum surface during electropolishing are (a) formation of double and diffusive electrochemical layer after applying external voltage (b) transport (exchange) of ions across the double layer leading to pitting (etching) of the metal surface and generation of heat due to exothermic nature of the interfacial reactions. (c) Spatially differential migration of anions and reaction products leads to coupling and the breakup of the double layer into ordered migration cells. (d) The system attaining a constant speed of etching with highly self-organized Rayleigh-Benard like convective cycles for maximum dissipation of energy. The sequence of illustrative images shown in Figure A.8 depicts the dimple formation dynamics and various steps of the electropolishing of a Ta metal surface.

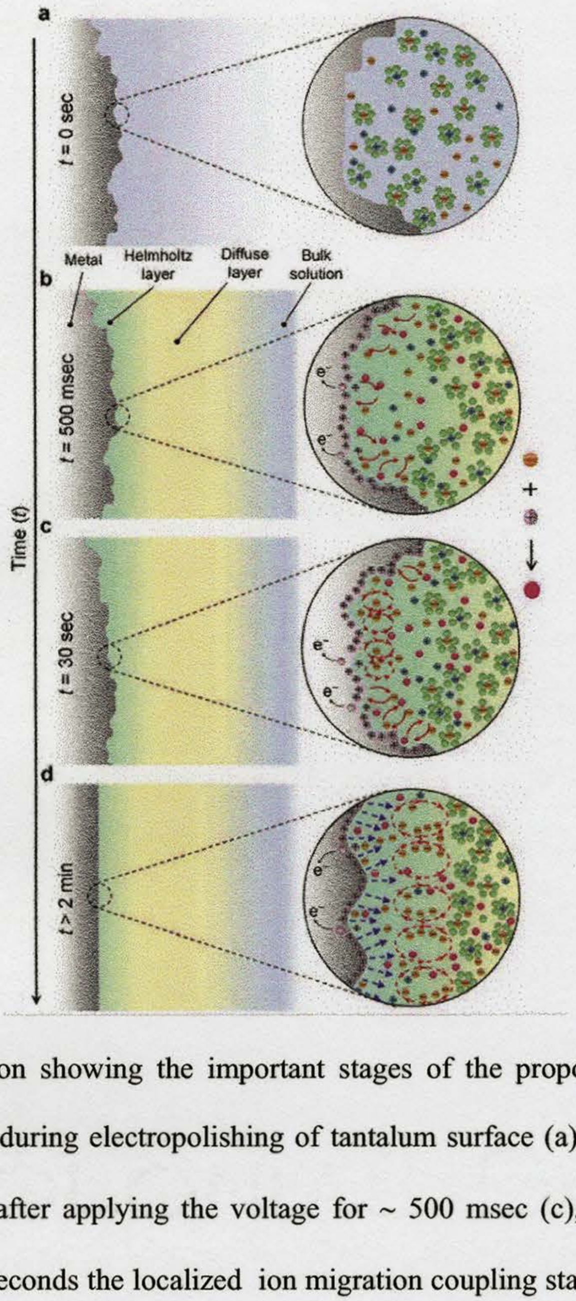

Figure A.8. Illustration showing the important stages of the proposed mechanism of formation of dimples during electropolishing of tantalum surface (a), without providing external voltage (b), after applying the voltage for ~ 500 msec (c), after applying the voltage for about 30 seconds the localized ion migration coupling starts and gives rise to pseudo-dimples on tantalum surface(d), the ion migration coupling slowly synchronizes and imprints well-ordered honeycomb packed nanostructure of dimples after applying voltage for more than 1 minute on a rough surface.

No pattern forms without providing an external strong driving force (electric field in this case). When the metal is immersed in the electrolyte solution without applying any external potential, there is no noticeable change in the surface morphology implying negligible or no electrochemical reactions have taken place (Figure A.8a). This was confirmed by dipping a tantalum piece for 12 hours in the electrolyte solutions without applying any external voltage.

The applied potential provides the external stimulus for the formation of two layers (double layer and diffusion boundary layer) adjacent to the substrate surface which play a crucial role behind the initiation of pattern formation on the electrode surface. The one close to the metal interface is the EDL and the other next to EDL is the diffusion boundary layer (DBL) (Figure8b). The EDL consists of well-packed complex arrangement of various electrostatically adsorbed ions such as polar water (H_2O) molecules and solvated ions, for example (H^+, Ta^{5+}, HSO_4^-, SO_4^{2-}, F^-, O^{2-}, and OH^-). The EDL limit the continuous electrochemical reactions at the metal surface by preventing the migration of ions due to the electrostatic shielding. The EDL behaves like a charged leaky capacitor and is also known as Helmholtz layer with small thickness (~10 nm) as compared to that of DBL (~1 μm).[29] The DBL is a thick layer located in a region of diffusely ions in contact with the EDL and bulk of solution. The external voltage U is composed of the potential drop φ_{DL} across the EDL (responsible for the interfacial process), plus the ohmic resistance R in the electrolyte between working and reference electrode multiplied by the current I, $U = \varphi_{DL} + IR$. The magnitude of the potential drop across the double layer determines the acceleration of the charged particles.

Near the metal interface where most of the chemistry is taking place, the portion of the double layer amounts to a considerable per cent by volume. The electrodissolution process starts instantly at the anode after applying the voltage with the exchange of ions in the double layer to complete the electrochemical reactions (Figure A.8b). Every electrochemical reaction produces charges that balance very quickly because no net charges can be built up in the electrolyte. Apart from the electric field which dominates the ion migration process in electrochemical systems, the other important driving force for dimple formation is heat generated due to the exothermic nature of the reactions involved in our electrochemical system. For example, the enthalpy of formation of Ta-O and Ta-F bond are 799.1 ±12.6 $kJmol^{-1}$ and 573 ±13 $kJmol^{-1}$ respectively.[30] The locally generated heat due to these reactions at the solid/liquid interface increases the kinetic energy of the species (anions and reaction products) involved and leads to their fast removal by diffusion from the metal surface to the outside of the EDL. This initial diffusion and migration of ions during the formation of etch pits gives rise to spatial instabilities which further leads to the periodic modulations in the EDL (Figure A.8c). Once things have become instable, they simply start to arrange in the way of facilitating the transport of ions across the EDL for fastest dissipation of matter and energy, which is ordered. In other words, the EDL breaks up into highly ordered migration cells similar to Rayleigh-Benard (RB) convection cycles. The resultant RB like convection pattern simultaneously gets physically imprinted on the metal surface in the form of hexagonally ordered periodic nano-dimples (Figure A.8d).

The ordered dimple pattern only forms if the speed of inward migration of ions matches with the outward diffusion. This happens in a very narrow electrochemical regime of voltage and concentration. If the magnitude of the applied voltage or the ratio of the concentrated acids in the electrolyte solution is changed to a different value, the coherence in migration and diffusion speed breaks and disrupts the regularity of the pattern. The metal oxide grows or the sample gets etched unevenly as the concentration of the electrolyte solution was changed from a 9:1 H_2SO_4:HF volumetric ratio to a 8:2 and 7:3 ratio. The 8:2 electrolyte created very disordered dimples of varying size and some dimples were not even circular. The 7:3 electrolyte showed very disordered, non-circular etch pits that did not resemble dimples at all. Similarly, if the voltage is changed by ± 2 volts the ordered hexagonal pattern ceases to form. (See chapter 4 for figures)

After slowly starting the convection cycle in the double layer, the following reaction dynamics establishes at the interface. There is slightly more reaction at the centre of the dimple due to the inward supply of fresh ions. This local nonuniformity in the supply of reactive ions in the inward flow direction of the convection cycles leads to formation/dissolution of slightly more oxide at the centre of the dimple than at the ridges and hence gradually increase the depth of the dimples. This small difference in the amount of reactions at the inward and outward points of the convective cycles inside the EDL gives rise to variant spatial surface morphology of the anode i.e. convex smooth points 'ridges' and concave curved region 'valleys'. The depth becomes constant after attaining a value of about 10 nm. Once the system reaches the stable state, there is no further change in the nano-scale hexagonal array pattern of dimples but the convection cycle of dissolution keeps going and the substrate surface is continuously etched at a constant speed. It should be noted that in Rayleigh-Benard convection the characteristic dimensions of the cell pattern is comparable to the length scale of the region in which convection is taking place. In our case, the ionic convection is taking place in the electrochemical double layer which has a dimension of few nanometers. Therefore the ionic convection cells have their lateral size of few nanometers (50-60 nm) and are comparable to the thickness of the double layer. We also again emphasize that the depth of the dimples before achieving a constant value of 10 nm does not change at the same rate as that of etching (20 – 50 nm/sec). The increase in the mechanical surface stress generated due to the dimpled surface morphology may be a factor responsible for terminating the depth to a maximum value of 10 nm and is a possible avenue for further study.

The high viscosity of the electrolyte may be another important ingredient for the ordered pattern formation. The electrolyte solution contains inorganic acids (H_2SO_4 and HF) and water. The H_2SO_4 act as a high kinematic viscosity and wetting solvent for the molecules/ions involved in the dissolution and hence ensures that the configuration of double layer is not affected due to thermal noise and bulk turbulence and eddies. Another crucial take home message from this research is that electropolishing is different than pattern formation on the surface. Actually, DBL is responsible for smoothing the surface by removing micrometer size rough bumps on the surface whereas EDL is responsible for generating the pattern on the electrode surface. The high electric field at the sharp edges of the rough surface cause high dissolution rate as compared to that of the smooth parts. This differential dissolution of metal eventually flattens the surface.

The fundamental reasons behind this kind of pattern formation are somehow similar to that for Turing-type in biological systems and Belousov-Zhabotinsky (BZ) reaction patterns in classical liquids. The pattern forms if the system is driven far away from the equilibrium through the flow of energy by applying external force. Spatio-temporal patterns originate due to periodic variations in the potential and concentration of participating molecules. In our non-equilibrium system the pattern is sustained by a constant force (in this case electric field and heat) and by a persistent dissipation of matter/energy. The initial coupling after formation of pits in milliseconds determines the surface sites at which crests and troughs of the hexagonal dimple pattern will form. So if the cycle is stopped and restarted, the spatial position of the dimples changes on the surface. In our migration-reaction-diffusion system there are different chemicals involved and the external applied potential acts as catalyst, which makes it very similar to the Belousov-Zhabotinsky reaction-diffusion system which further has its origin in Turing like patterns. Turing patterns form only with an appropriate inequality of diffusion coefficients. The chemical system in our case consists of different kind of ionic species such as O^{2-}, F^-, OH^- and Ta^{5+}. The chemical species move under the influence of the electric field depending on their net charge density. It has been previously observed and reported by Shimizu *et al*[31,32] and has been verified by us (Ref. 28) that in the electrolyte solution the fluoride anions move faster than oxygen anions through the tantalum oxide layer and forms the tantalum fluoride at the tantalum/tantalum oxide interface. In our system, F^- acts as an activator which dissolves the oxide to produce more oxide whereas O^{2-} and OH^- acts as inhibitors which tries to quench the formation of tantalum oxide by shielding the metal surface making the mechanism somewhat similar to Turing-type pattern formation.

A.4 Dendritic Patterns Made of Thin Tantalum Oxide.

The other fascinating patterns seen on the tantalum surface after electropolishing are the dendritic 'snowflake' like patterns made of tantalum oxide (Figure A.9). This kind of pattern formation has been well known during electrodeposition of metals and crystal solidification on surfaces.[14,33,34] The pattern originates on the surface because aside from electropolishing (formation and dissolution of oxide), the process is accompanied by the evolution of oxygen bubbles at the anode and hydrogen bubbles at the cathode. Most of the oxygen reacts with tantalum to make tanlum oxide which later dissolves by reacting with HF. The left over oxygen generated on the anode migrates toward the top in the form of bubbles. While migrating toward the top, oxygen bubbles produce undesired vertical traces depending on the solution agitation and sample tilt. Once the growth of the tantalum oxide starts, the previous nucleation sites (tip of the dendritic branches) act

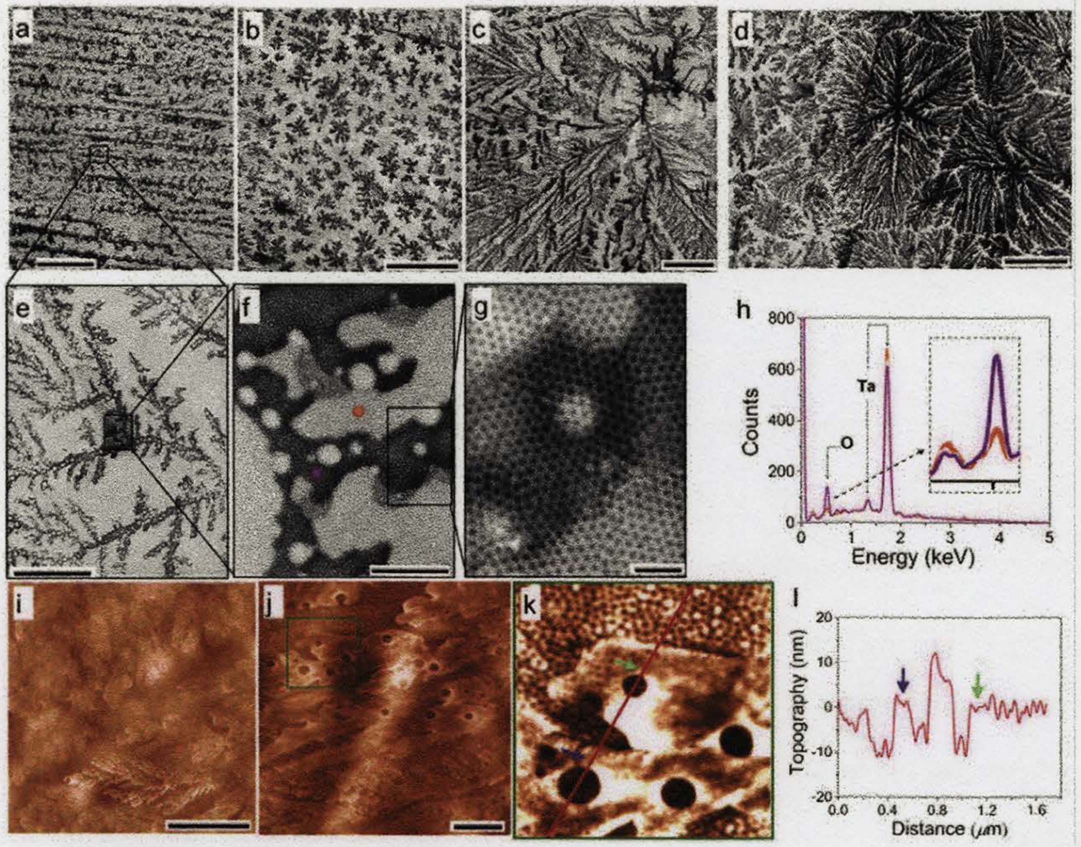

Figure A.9. SEM and AFM images showing the microstructure of tantalum oxide dendrites on dimpled tantalum surface. (a),(b),(c),(d) shows the variety of dendritic patterns observed on electropolished surfaces. (e), (f), (g) shows the zoomed over images where dimples can be seen under the oxide layer (dark black region). (h) EDX spectra corresponding to the two different spots on image (f) revealing the composition of the dendrites. (i), (j), (k) shows the AFM images of the dendrities. (l) height profile corresponding to the line drawn in image (k) shows a average thickness of 15 nm for the thin Ta_2O_5 layer. Scale bars correspond to 10 μm for (a), 20 μm for (b, c and d), 5 μm for (e and i), 1 μm for (f and j) and 300 nm for (g). A constant voltage of 15 V in single pulse mode was used for all these samples.

as initiators and hence the dendritic pattern slowly grows in two dimensions. The oxygen bubbles trace along the surface as they move up leaving the formation of dendritic patterns of thin tanlum oxide layer on the electropolished tantalum surface.

Most often these beautiful undesired patterns were observed when the metal surface was tilted or the electrolyte solution was stirred at very slow speed. The dendrite structure is made of pure tantalum oxide as was confirmed by performing SEM-EDS analysis (Figure A.9h) on the regions with and without the dendritic oxide in Figure A.9f. The two spectra differ only in the oxygen peak intensity confirming that the feature under study is only tantalum oxide and nothing else. The SEM images (Figures A.9f, g) show that the dendritic oxide area also attains dimpled morphology which actually is not true. This was confirmed by performing the AFM studies on these surfaces (Figures A.9i-k). The cross section of the AFM image shows that the dimples are covered with thin flat layer (10-20 nm; Figure A.9l) of tantalum oxide. The dimples are seen in the dark areas (where dendrites are present) of the SEM images because the SEM technique probes not only the thin Ta_2O_5 layer directly at the surface but also the deeper layers underneath (albeit with exponentially reduced sensitivity). Interestingly, the dimples below the dendritic patterns of oxide are clearly visible with SEM (Figure A.9g) showing that there is a clear interface between the dendritic tantalum oxide and the native tantalum oxide of dimples.

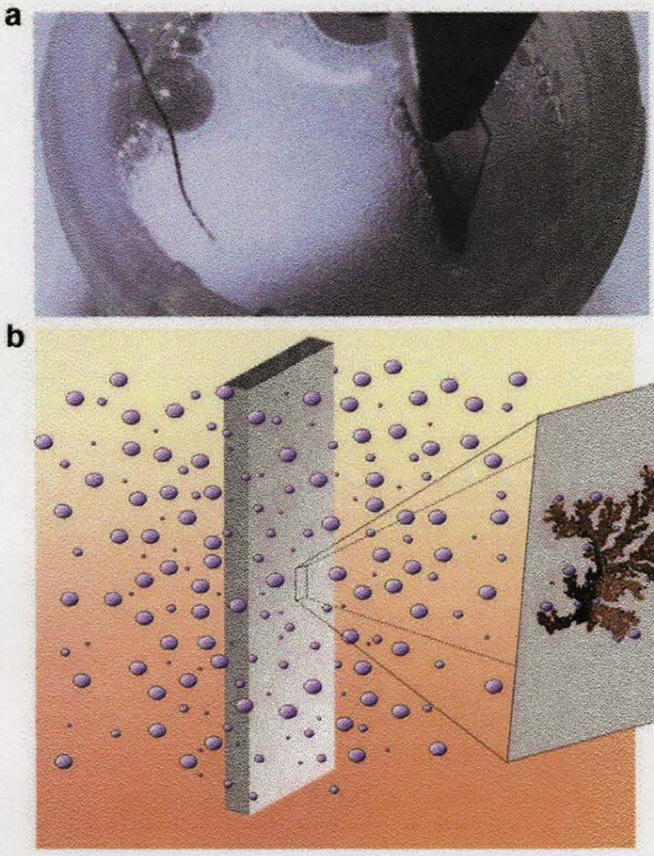

Figure A.10. (a) Photographic image showing the formation of bubbles during electropolishing. (b) Illustration demonstrating the model of the dendritic growth of oxide on the surface due to oxygen bubbles just after turning the voltage off.

The formation of this kind of dendritic tantalum oxide layer due to a huge availability of oxygen nearby and its good adherence to the surface even under highly concentrated acid solutions makes us think that the layer might be crystalline in nature as crystalline oxide are more difficult to dissolve than amorphous oxides. One other important thing to note here from the thickness of this dendritic oxide layer pattern is that it forms instantaneously or in last few seconds after turning off the voltage because the thickness (10-20nm) is of the same order of magnitude as the etching rate which is in the range between 20 to 50 nm/sec.[27] At higher voltages the gas evolution becomes stronger and the surface erosion is accompanied by pitting rather than dendritic patterns. These results further show that the last few seconds of electropolishing are very crucial moments for the achievement of the desired surface quality. However, leveled and brilliant shiny surfaces with spectacular finish similar to (Figure A.1*l*) can be obtained by adjusting the sample tilt (vertically aligned so that bubbles can easily escape) and solution agitation.

A.5 Conclusions

In summary, we have studied the spatiotemporal formation, evolution and ordering of dimples by applying programmed voltage pulses. Investigating the self-organization and etching mechanisms at the local scale and at short time intervals will pave the way towards answering many open questions regarding pattern formation on electrode surfaces in electrochemical systems. The outcome of these results also shows that it is possible to erase dimple nanostructure from the tantalum surface by applying appropriate voltage pulses, which will be helpful for biological (effect of nanostructure on adhesion of cells to surfaces) studies. In the context of the emerging field of nanotechnology, such knowledge will help to form highly ordered self-organized spontaneous nanostructures on a wide variety of substrate surfaces at the nanometer length scale. However, it should be taken into consideration that there are many processes happening in parallel and explaining this model system with mathematical tools might lead to complex equations which may be hard to solve. Furthermore, application of systematically programmed pulses and use of single crystals may allow fabrication of deeper and various other kind of regular patterns on the surface.

A.6 Experimental Section:

Materials.

H_2SO_4 (95-98% reagent grade), HF (48%), acetone and methanol (all semiconductor grade) were purchased from Fisher Scientific. All chemicals were used as received without further purification. Tantalum foil (Alfa-Aesar, 99.95%, 0.127 mm) was mechanically cut, rinsed with acetone, methanol and then with Millipore water (18.2 MΩ.cm resistivity) and then dried under air prior to anodization.

Computer controlled Experimental Setup for electropolishing.

The experimental setup is shown in (Scheme 1). The electrochemical cell consisted of a strip of tantalum foil as the working electrode (anode) and a platinum-iridium wire as the counter electrode (cathode). The electrolyte solution was agitated with mechanical stirring using a magnetic stir bar. Typically, electrolyte solutions needed to sit for 4-5 hours before they were used to etch tantalum. The electrodes were connected to a power supply (Kepco BOP 20-20M) which was remote controlled by a locally written Labview program and GPIB communication. The program had the capability to supply a voltage pulse of variable time scales with a very short rise and decay time period (1V/μs). All experiments were performed at room temperature (approximately 20°C)

Characterization

Atomic force microscopy was performed in tapping mode on a Veeco Enviroscope with a Nanoscope IIIa controller and Veeco RTESP p-doped Si tips with a nominal radius of less than 10 nm. Typical scan rates were 2 micrometer per second and the images were constructed with 512 scan lines. Care was taken to ensure that the tip was not modifying the surface during the scan. Also many images of same sample were obtained with different tips to pinpoint the exact depth of dimples by eliminating the artifacts due to tip convolution. The data was analyzed using DI V5.30r3.sr3 software

Scanning electron microscopy (SEM) analysis was carried out using a Jeol 7000F field emission scanning electron microscope (FE-SEM) at the Brockhouse Institute for Materials Research. Energy dispersive X-ray (EDX) spectroscopy was carried out using a 10 kV accelerating voltage. INCA 300, EDX System (Oxford, UK) software was used for the data acquisition and analysis.

High-Resolution TEM was carried out with a JEOL 2010 field emission TEM/STEM, operating at an accelerating voltage of 200kV. The thin Ta section for cross-sectional TEM analysis was prepared by focused Ion beam (FIB) milling on a LEO1540 FIB/SEM CrossBeam instrument at Nanofab facility (University of Western Ontario). The region of interest on the specimen was coated with layers of carbon and platinum, in-situ, using the CrossBeam's gas injection system. The carbon layer gives a better contrast and the platinum layer protects the surface of the feature during subsequent FIB milling.

Author Contributions:

The electrochemical experiments work reported here were carried out by me with some help of Warren Barden (an undergraduate student in our group). Stephen Yue Wang (currently a Masters candidate in our group) will pursue this work. Overall data analyses were conducted by the S.S.; S.S. also wrote the manuscript.

A.7 Bibliography

(1) Mossman, K. D., Campi, G., Groves, J. T. & Dustin, M. L. Altered TCR Signaling from Geometrically Repatterned Immunological Synapses. *Science* **2005**, *310*, 1191-1193.

(2) Lu, W. & Lieber, C. M. Nanoelectronics from the bottom up. *Nat. Mater.* **2007**, *6*, 841-850.

(3) Blossey, F. Self-cleaning surfaces Â— virtual realities. *Nat. Mater.* **2003**, *2*, 301-306.

(4) Curtis, A. S. G., Gadegaard, N., Dalby, M. J., Riehle, M. O., Wilkinson, C. D. W. & Aitchison, G. Cells react to nanoscale order and symmetry in their surroundings. *IEEE Trans. Nanobiosci.* **2004**, *3*, 61-65.

(5) Watt, F., Breese, M. B. H., Bettiol, A. A. & van Kan, J. A. Particle beam writing. *Materials Today* **2007**, *10*, 20-29.

(6) Mun, L. K., Drouin, D., Lavallée, E. & Beauvais, J. The Impact of Charging on Low-Energy Electron Beam Lithography. *Microsc. Microanal.* **2004**, *10*, 804–809.

(7) Ito, T. & Okazaki, S. Pushing the limits of lithography. *Nature* **2000**, *406*, 1027–1031.

(8) Chou, S.Y., Keimel; C. & Gu, J. Ultrafast and direct imprint of nanostructures in silicon. *Nature* **2002**, *417*, 835-837.

(9) Barton J. E. & Odom T. W. Mass-Limited Growth in Zeptoliter Beakers: A General Approach for the Synthesis of Nanocrystals. *Nano Lett.* **2004**, *4*, 1525-1528.

(10) Whitesides, G. M. & Grzbowski, B. Self assembly at all scales. *Science* **2002**, *295*, 2418-2421.

(11) Stupp, S. I., LeBohneur, V., Walker, K., Li, L. S., Huggins, K. E., Keser, M. & Amstutz, A. Supramolecular materials: Self-organized nanostructures. *Science* **1997**, *276*, 384-389.

(12) Henzie, J., Barton, J. E., Stender, C. L. & Odom, T. W. Large-area nanoscale patterning: Chemistry meets fabrication. *Acc. Chem. Res.* **2006**, *39*, 249-257.

(13) Pawin, G., Wong, K. L., Kwon, K. Y. & Bartels L. A homomolecular porous network at a Cu(111) surface. *Science* **2006**, *313*, 961-962.

(14) Ball, P. *The Self-made Tapestry: Pattern Formation in Nature* (Oxford Univ. Press, 1999).

(15) Kiss, I. Z. & Hudson J. L. Chemical complexity: Spontaneous and engineered structures. *AIChE Journal* **2003**, *49*, 2234-2241.

(16) Turing, A. M. The chemical basis of morphogenesis. *Philos. Trans. R. Soc. London* **1952**, *237*, 37-72.

(17) Sagués, F. & Epstein, I. R. Nonlinear chemical kinetics. *Dalton Trans.* **2003**, *7*, 1201-1217.

(18) Sagues, F., Sancho J. M. & Garcia-Ojalvo J. Spatiotemporal order out of noise. *Rev. Mod. Phys.* **2007**, *79*, 829-882.

(19) Kiss, I. Z. & Hudson, J. L. Chemical complexity: Spontaneous and engineered structures. *AIChE Journal* **2003**, *49*, 2234-2241.

(20) Li, Y. J., Oslonovitch, J., Mazouz, N., Plenge, F., Krischer, K. & Ertl G. Turing-type patterns on electrode surfaces. *Science* **2001,** *291*, 2395-2398.

(21) Cox, M. P., Ertl, G. & Imbihl, R. *Phys. Rev. Lett.* **1985**, 54, 1725-1728.

(22) Lee, W., Ji, R., Gösele, U. & Nielsch, K. Fast fabrication of long-range ordered porous alumina membranes by hard anodization. *Nat. Mater.* **2006**, *5*, 741-747.

(23) Matthias, S. & Muller, F. Asymmetric pores in a silicon membrane acting as massively parallel brownian ratchets. *Nature* **2003**, *424*, 53-57.

(24) Saito, K., Kojima, Y., Furuya, T., Mitsunobu, S., Noguchi, S., Hosoyama, K., Nakazato, T., Tajima, T. & Asano, K. Proc. The Workshop on RF-Superconductivity, *KEK* **1989**, 635.

(25) Diepers, H., Schmidt, O., Martens, H. & Sun, F.S. *Phys. Lett.* **1971**, *37A*, 139.

(26) Monti, H. Métaux Corrosion Industries, **1958,** *33*, 481.

(27) Sayed, H. E., Singh, S., Greiner, M. T. & Kruse, P. Formation of highly ordered arrays of dimples on tantalum at the nanoscale. *Nano Lett.* **2006**, *6*, 2995-2999.

(28) Singh, S., Greiner, M.T. & Kruse, P. Robust Inorganic Membranes from Detachable Ultrathin Tantalum Oxide Films. *Nano Lett.* **2007,** 7, 2676-2683.

(29) Rolf-Schuster, R., Kirchner, V., Allongue, P. & Ertl, G. Electrochemical Micromachining. *Science* **2000**, *289,* 98-101.

(30) Kerr, J. A. & Lide, D. R. *CRC Handbook of Chemistry and Physics*, 81st Ed.; CRC Press: Boca Raton, FL, 2000.

(31) Shimizu, K., Kobayashi, K., Thompson, G. E., Skeldon, P. & Wood, G. C. Anodic oxide films on tantalum: Incorporation and mobilities of electrolyte-derived species. *Philos. Mag. Part B* **1996**, *73*, 461-485.

(32) Shimizu, K., Kobayashi, K., Thompson, G. E., Skeldon, P. & Wood, G. C. The Migration of Fluoride Ions in Growing Anodic Oxide Films on Tantalum. J. Electrochem. Soc. **1997**, 144, 418-423.

(33) Gleeson J. T. Dendritic growth of electrohydrodynamic convection in a nematic liquid crystal. *Nature* **1997**, *385*, 511-513.

(34) Gránásy, L., Pusztai, T., Börzsönyi, T., Warren J. A. & Douglas J. F. A general mechanism of polycrystalline growth. *Nat. Mater.* **2004**, *3*, 645-650.

Appendix B

This appendix provides the chemical composition of the metal foils used for fabrication of highly ordered dimples on their surface. The presence of nickel perturbs the pattern formation only in case of tungsten samples. However, presence of small amounts of other elements does not show any noticeable effect in pattern formation on any of the metals.

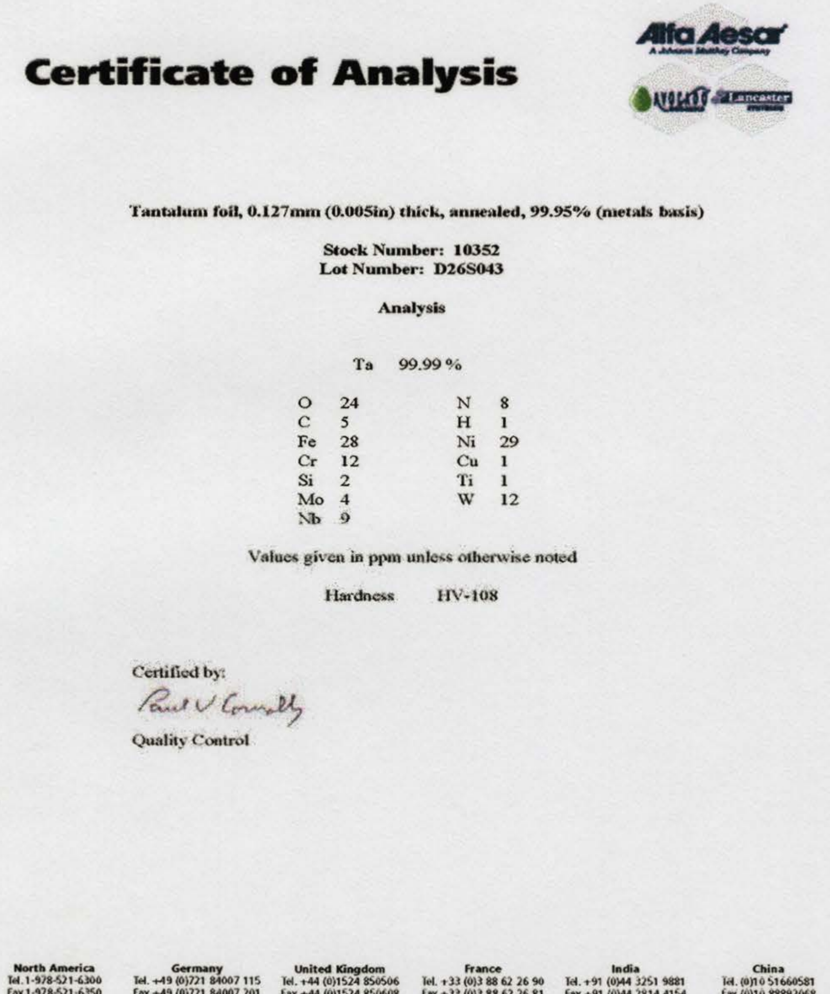

Certificate of Analysis

Alfa Aesar
A Johnson Matthey Company

Tantalum foil, 0.127mm (0.005in) thick, annealed, 99.95% (metals basis)

Stock Number: 10352
Lot Number: D26S043

Analysis

Ta 99.99 %

O	24	N	8
C	5	H	1
Fe	28	Ni	29
Cr	12	Cu	1
Si	2	Ti	1
Mo	4	W	12
Nb	9		

Values given in ppm unless otherwise noted

Hardness HV-108

Certified by:
Paul V Connolly
Quality Control

North America	Germany	United Kingdom	France	India	China
Tel. 1-978-521-6300	Tel. +49 (0)721 84007 115	Tel. +44 (0)1524 850506	Tel. +33 (0)3 88 62 26 90	Tel. +91 (0)44 3251 9881	Tel. (0)10 51660581
Fax 1-978-521-6350	Fax +49 (0)721 84007 201	Fax +44 (0)1524 850608	Fax +33 (0)3 88 62 26 81	Fax +91 (0)44 2814 4154	Fax (0)10 88892068
info@alfa.com	eurosales@alfa.com	uksales@alfa.com	frventes@alfa.com	indiasales@alfa.com	sales-china@alfa.com

Figure B.1. Certificate of analysis of tantalum foil obtained from Alfa Aesar.

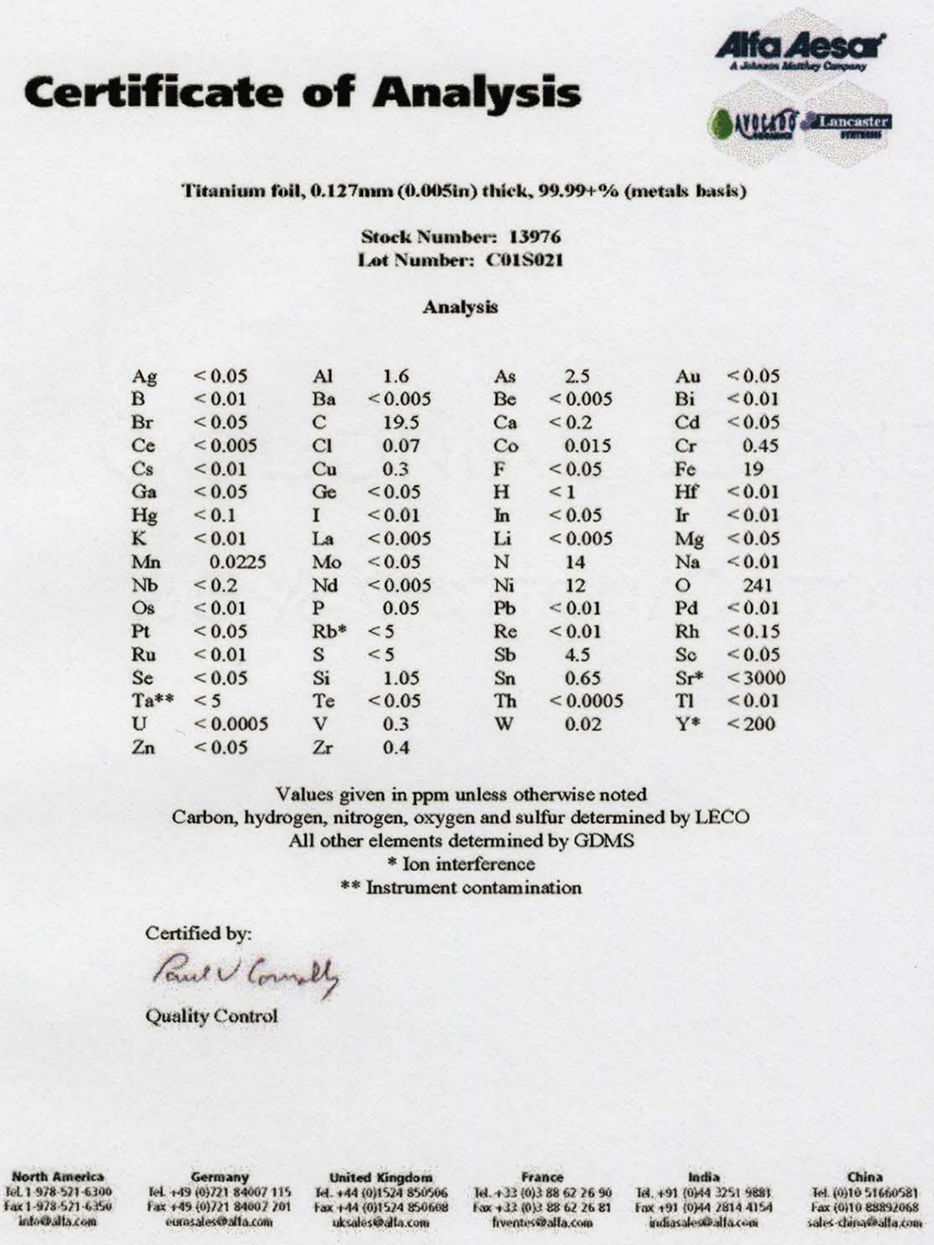

Certificate of Analysis

Titanium foil, 0.127mm (0.005in) thick, 99.99+% (metals basis)

Stock Number: 13976
Lot Number: C01S021

Analysis

Ag	< 0.05	Al	1.6	As	2.5	Au	< 0.05
B	< 0.01	Ba	< 0.005	Be	< 0.005	Bi	< 0.01
Br	< 0.05	C	19.5	Ca	< 0.2	Cd	< 0.05
Ce	< 0.005	Cl	0.07	Co	0.015	Cr	0.45
Cs	< 0.01	Cu	0.3	F	< 0.05	Fe	19
Ga	< 0.05	Ge	< 0.05	H	< 1	Hf	< 0.01
Hg	< 0.1	I	< 0.01	In	< 0.05	Ir	< 0.01
K	< 0.01	La	< 0.005	Li	< 0.005	Mg	< 0.05
Mn	0.0225	Mo	< 0.05	N	14	Na	< 0.01
Nb	< 0.2	Nd	< 0.005	Ni	12	O	241
Os	< 0.01	P	0.05	Pb	< 0.01	Pd	< 0.01
Pt	< 0.05	Rb*	< 5	Re	< 0.01	Rh	< 0.15
Ru	< 0.01	S	< 5	Sb	4.5	Sc	< 0.05
Se	< 0.05	Si	1.05	Sn	0.65	Sr*	< 3000
Ta**	< 5	Te	< 0.05	Th	< 0.0005	Tl	< 0.01
U	< 0.0005	V	0.3	W	0.02	Y*	< 200
Zn	< 0.05	Zr	0.4				

Values given in ppm unless otherwise noted
Carbon, hydrogen, nitrogen, oxygen and sulfur determined by LECO
All other elements determined by GDMS
* Ion interference
** Instrument contamination

Certified by:

Paul V Connolly

Quality Control

North America
Tel. 1-978-521-6300
Fax 1-978-521-6350
info@alfa.com

Germany
Tel. +49 (0)721 84007 115
Fax +49 (0)721 84007 201
eurosales@alfa.com

United Kingdom
Tel. +44 (0)1524 850506
Fax +44 (0)1524 850608
uksales@alfa.com

France
Tel. +33 (0)3 88 62 26 90
Fax +33 (0)3 88 62 26 81
frventes@alfa.com

India
Tel. +91 (0)44 3251 9881
Fax +91 (0)44 2814 4154
indiasales@alfa.com

China
Tel. (0)10 51660581
Fax (0)10 88892068
sales-china@alfa.com

Figure B.2. Certificate of analysis of titanium foil obtained from Alfa Aesar.

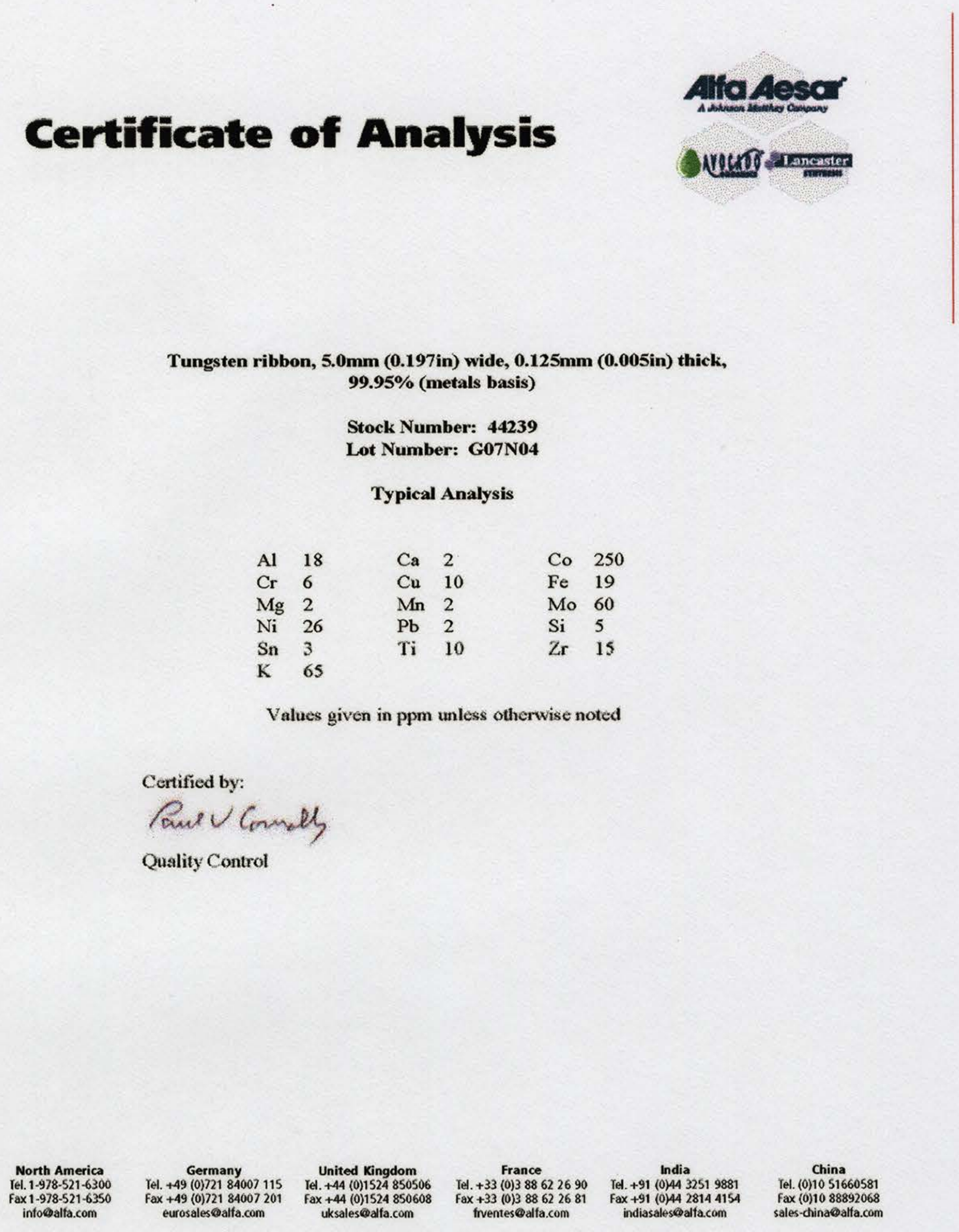

Alfa Aesar
A Johnson Matthey Company
Avocado Lancaster

Certificate of Analysis

Tungsten ribbon, 5.0mm (0.197in) wide, 0.125mm (0.005in) thick, 99.95% (metals basis)

Stock Number: 44239
Lot Number: G07N04

Typical Analysis

Al	18	Ca	2	Co	250
Cr	6	Cu	10	Fe	19
Mg	2	Mn	2	Mo	60
Ni	26	Pb	2	Si	5
Sn	3	Ti	10	Zr	15
K	65				

Values given in ppm unless otherwise noted

Certified by:
Paul V Connolly
Quality Control

North America	Germany	United Kingdom	France	India	China
Tel. 1-978-521-6300	Tel. +49 (0)721 84007 115	Tel. +44 (0)1524 850506	Tel. +33 (0)3 88 62 26 90	Tel. +91 (0)44 3251 9881	Tel. (0)10 51660581
Fax 1-978-521-6350	Fax +49 (0)721 84007 201	Fax +44 (0)1524 850608	Fax +33 (0)3 88 62 26 81	Fax +91 (0)44 2814 4154	Fax (0)10 88892068
info@alfa.com	eurosales@alfa.com	uksales@alfa.com	frventes@alfa.com	indiasales@alfa.com	sales-china@alfa.com

Figure B.3. Certificate of analysis of tungsten ribbon obtained from Alfa Aesar.

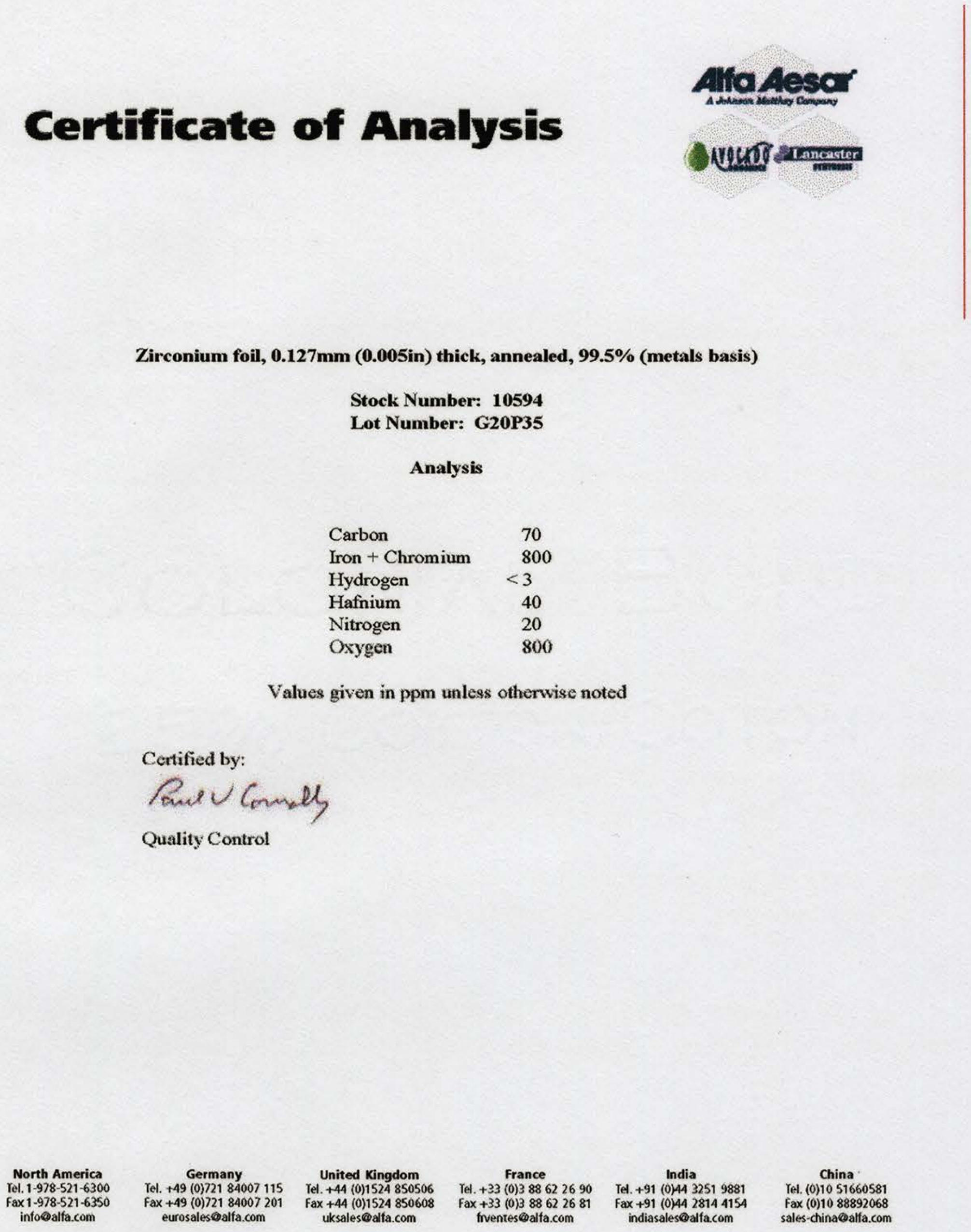

Certificate of Analysis

Zirconium foil, 0.127mm (0.005in) thick, annealed, 99.5% (metals basis)

Stock Number: 10594
Lot Number: G20P35

Analysis

Carbon	70
Iron + Chromium	800
Hydrogen	<3
Hafnium	40
Nitrogen	20
Oxygen	800

Values given in ppm unless otherwise noted

Certified by:
Paul V Connolly
Quality Control

North America	**Germany**	**United Kingdom**	**France**	**India**	**China**
Tel. 1-978-521-6300	Tel. +49 (0)721 84007 115	Tel. +44 (0)1524 850506	Tel. +33 (0)3 88 62 26 90	Tel. +91 (0)44 3251 9881	Tel. (0)10 51660581
Fax 1-978-521-6350	Fax +49 (0)721 84007 201	Fax +44 (0)1524 850608	Fax +33 (0)3 88 62 26 81	Fax +91 (0)44 2814 4154	Fax (0)10 88892068
info@alfa.com	eurosales@alfa.com	uksales@alfa.com	frventes@alfa.com	indiasales@alfa.com	sales-china@alfa.com

Figure B.4. Certificate of analysis of Zirconium foil obtained from Alfa Aesar.

Appendix C

List of Publications

Resulting from this work

- Time Resolved Study Reveals Rayleigh-Bernard Style Convection Cycles at Nanoscale in the Electrochemical Double Layer. Sherdeep Singh, Stephen Wang, and Peter Kruse, manuscript in preparation.

- Universal Method for the Fabrication of Detachable Ultrathin Films of Transition Metal Oxides. Sherdeep Singh, Warren Barden, and Peter Kruse, Submitted (2008).

- Nanopatterning of transition metal surfaces via electrochemical dimple array formation. Sherdeep Singh, Warren Barden, and Peter Kruse, Submitted (2008).

- Dissipative Nanopatterning on Electropolished Surfaces as an Alternative to Self-assembly. Sherdeep Singh, Warren Barden, and Peter Kruse, Submitted (2008).

- Robust Inorganic Membranes from Detachable Ultra-Thin Tantalum Oxide Films. Sherdeep Singh, Mark T. Greiner and Peter Kruse, *Nano Letters,* 7, (2007) 2676-2683.

- Formation of Highly Ordered Arrays of Dimples on Tantalum at the Nanoscale. Hany El-Sayed, Sherdeep Singh, Mark T. Greiner and Peter Kruse *Nano Letters*, 6 (2006) 2995 – 2999.

- Properties of Dimpled Tantalum Surfaces from Electropolishing. Hany El-Sayed, Sherdeep Singh and Peter Kruse, *Journal of Electrochemical Society*, 154, (2007) C728-C732.

Other publications

- Aurophores: Biomimetic Synthesis of Gold Nanocrystals Using Asiderophore-like Reactive Amphiphile. Ferdinand Gonzaga, Sherdeep Singh and Michael A. Brook. *Small* (2008) In Press.

- Roughening of Gold Atomic Steps Induced by Interaction with Tetrahydrofuran. Warren R. T. Barden, Sherdeep Singh, and Peter Kruse, *Langmuir*, *24* (2008) 2452 – 2458.

- Surface Chemistry of Carbon Nanotubes. Sherdeep Singh and Peter Kruse, *International Journal of Nanotechnology* 5, (2008) 900-931.

- Structure property correlations in alcohols through two-photon absorption cross-section measurements. Amit Nag, Sherdeep Singh and Debabrata Goswami *Chemical Physics Letters*, 430 *(2006) 420-423.*

- Influence of bandwidth and phase shaping on laser induced breakdown spectroscopy with ultrashort laser pulses. Tissa Gunaratne, Michael Kangas, Sherdeep Singh, Andrew Gross and Marcos Dantus, *Chemical Physics Letters,* 423 (2006) 197–201.

Curriculum vitae

Sherdeep Singh
Born on April 29th, 1982 in Punjab, India

2005 - 2008	PhD Thesis, *McMaster University, Ontario, Canada.*
2005	Visiting Research Scholar learning Ultra-fast Laser Breakdown Spectroscopy. *Michigan State University, MI, U.S.A.*
2000 - 2005	Studies in Non Linear effects at femtosecond timescale. Masters thesis and Bachelors degree at *Indian Institute of Technology (IIT) – Kanpur, India.*
1992-1999	High Schooling at *Sainik School Kapurthala, Punjab, India.*